UNIVERSITAT DE BARCELONA

Polymorphism and crystallization behaviour of triacylglycerols. From pure components to mixtures rich in oleic acid

Jorge Macridachis González

UNIVERSITAT DE BARCELONA

Departament de Mineralogia, Petrologia i Geologia Aplicada

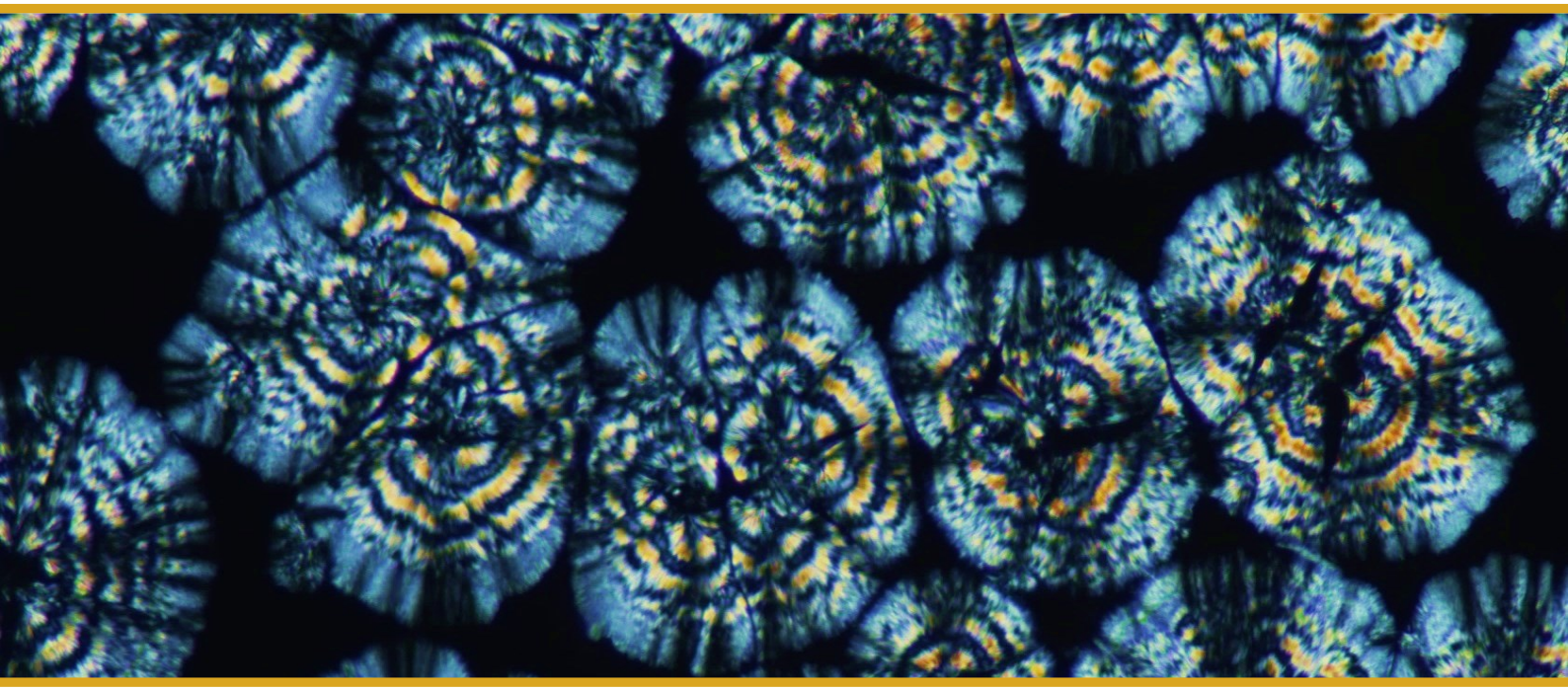

POLYMORPHISM AND CRYSTALLIZATION BEHAVIOUR OF TRIACYLGLYCEROLS. FROM PURE COMPONENTS TO MIXTURES RICH IN OLEIC ACID

Jorge Macridachis González

PhD thesis 2022

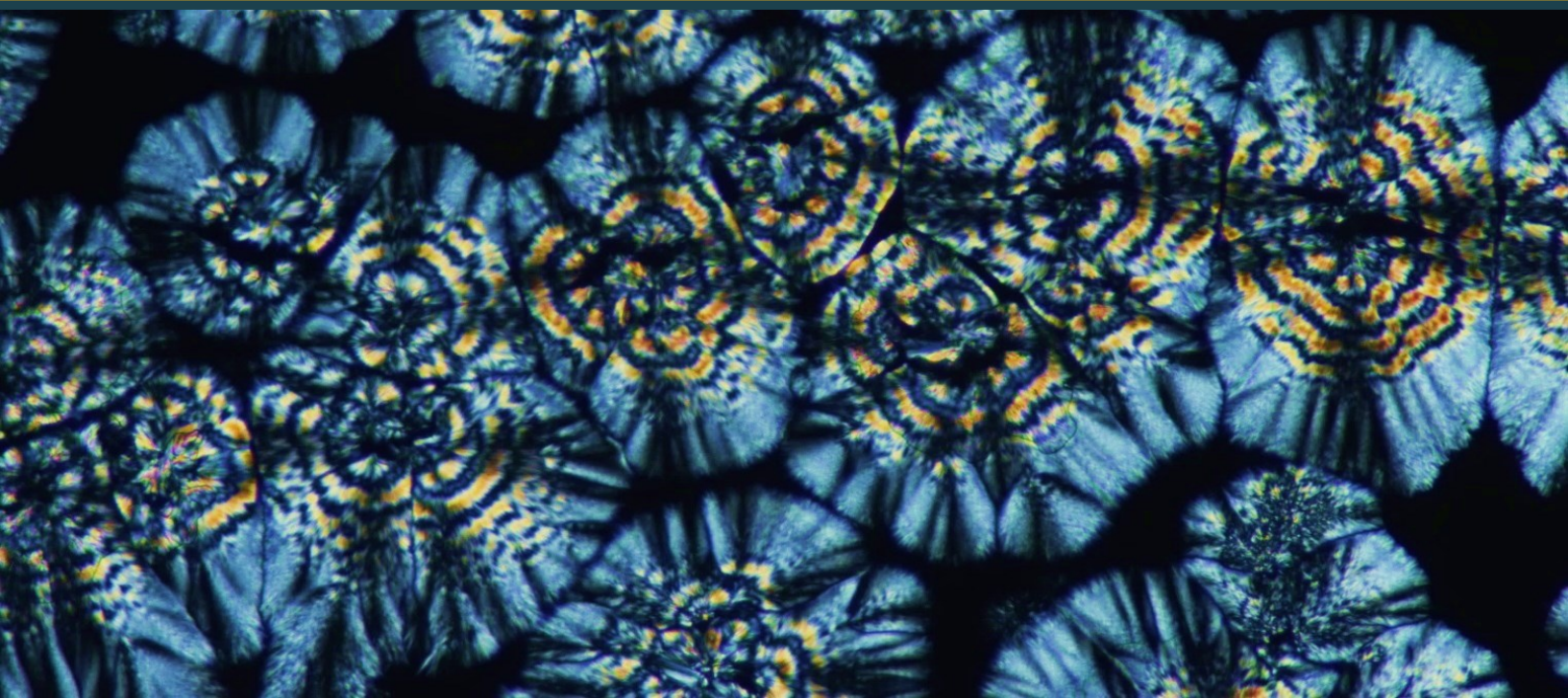

UNIVERSITAT DE BARCELONA

Departament de Mineralogía, Petrologia i Geología Aplicada

Polymorphism and crystallization behaviour of triacylglycerols. From pure components to mixtures rich in oleic acid

-2022-

Memoria presentada por **Jorge Macridachis González** para aspirar al título de doctor por la Universitat de Barcelona. Esta tesis se ha realizado dentro del **Programa de Doctorat de Ciencies de la Terra**, bajo la codirección de las **Dras. Maria Teresa Calvet Pallas y Laura Bayés García.**

El doctorando,

Jorge Macridachis González
Dpt. Mineralogia, Petrologia i Geologia Aplicada
Universitat de Barcelona

La tutora,

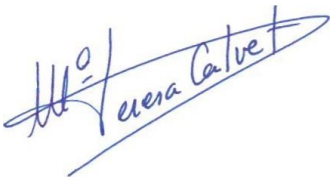

Dra. Maria Teresa Calvet Pallas
Dpt. Mineralogia, Petrologia i Geologia Aplicada
Universitat de Barcelona

Las directoras,

Dra. Laura Bayés García
Dpt. Mineralogia, Petrologia i Geologia Aplicada
Universitat de Barcelona

Dra. Maria Teresa Calvet Pallas
Dpt. Mineralogia, Petrologia i Geologia Aplicada
Universitat de Barcelona

a mi madre, Pilar,
a Ira, Pil y Ra,
a Sophie; las mujeres de mi vida,
con todo mi cariño.

ACKNOWLEDGEMENTS (AGRADECIMIENTOS)

En primer lugar, me gustaría dar las gracias a mis directoras de tesis, las Dras. Laura Bayés García y Maria Teresa Calvet Pallàs, porque el hecho de que ahora mismo esté escribiendo estas líneas es también mérito suyo. Teresa, gracias por todo lo que me has enseñado, a nivel personal y científico, por ayudar a poner un poco de orden a mis ideas y por transmitirme serenidad en los momentos oportunos. Laura, gracias por descubrirme el mundo de la cristalografía de lípidos, por ver cada resultado como un triunfo y por poner siempre en valor lo que hago. Gracias también por todas tus recomendaciones durante la tesis (y por tu lucha incansable contra, según tus palabras, no las mías, mi cabezonería). Gracias, Teresa y Laura, por vuestros ánimos, por la confianza que me habéis demostrado y por tener siempre a mano una cerilla para alumbrar el camino.

Mercedes Aguilar, gracias por hacerme reír, incluso en los malos momentos, por preocuparte, por preguntar y por estar siempre dispuesta a echarme una mano. Por supuesto, gracias también por resolver mis crisis en el laboratorio y por ayudarme a dominar al monstruo (DSC). Gracias, Mercè Font, por tu sentido del humor, por estar siempre disponible para ayudar, aconsejar y también para soltar algún que otro "zasca".

Miquel Àngel Cuevas, gracias por tu compañía hasta casi el final del recorrido. Gracias por estar ahí, como persona y como profesor. Gracias también por esos constantes mensajitos de ánimo.

A todas las personas del 129, gracias por haberme hecho sentir como en familia.

Muchas gracias, Maite Garcia Valles, por tu ayuda, por nuestras conversaciones y por traerme alguna cosilla cuando te vas de excursión (o como prefieres llamarlo, salida de campo).

Gracias, Edu, por las risas en el 125. Gracias por ser un buen compañero, un buen amigo y, sobre todo, por compartir tu extensa sabiduría sobre trabalenguas, refranes y frases populares catalanas. También quiero dar gracias por los momentos compartidos con los estudiantes que han ido "rulando" por el despacho: Mariona, Jingyao, Hugo, Alex, Martí, Sergio, Antonio…

Gracias a los miembros del Departament de Mineralogia, Petrologia, i Geologia Aplicada por su buena acogida a mi llegada y por los buenos ratos durante estos años. Gracias, Cristina

Vilanova, por tus lecciones rápidas de microscopio. Gracias, Sandra y Elisenda, por vuestra ayuda con todos los temas administrativos.

Thank you, Professor Kiyotaka Sato and Professor Satoru Ueno, for making me feel like just another Hiroshima University student at our first meeting in Belfast. Thank you also, Professor Sato, for sowing the seed of this thesis.

Muchas gracias a Xavier Alcobé y al equipo de difracción de rayos X de polvo del CCiTUB. Sin vuestra ayuda esta tesis no habría sido posible.

Gracias a Ramón Morató, de Cacao Barry, por donarnos las muestras de manteca de cacao. Muchas gracias a Jordi Soler, de Lipidos Santiga S.A., por facilitarnos las muestras de estearina de karité y hacer posible los análisis de SFC en el estudio de mezclas de manteca y estearina. Gracias, Alessandra Trujillo, por tu contribución en este trabajo.

Quiero expresar mi agradecimiento a Susana Martínez, de la secretaria de doctorat, por la cantidad de problemas y dudas que me ha ayudado a resolver durante estos años. Gracias, Alberto Sáez, por también estar ahí para ayudar y aconsejar al final de esta etapa.

Me gustaría dar las gracias a la comisión de seguimiento de esta tesis por su dedicación durante estos años. Muchas gracias también a los miembros del tribunal de tesis por el esfuerzo que conlleva aceptar y desempeñar ese papel.

Gracias al personal del punt d'informació por subir a abrirme la puerta del despacho las incontables veces que me he dejado las llaves dentro.

Muchas gracias, personal del bar de biología, por sacarme una sonrisa incluso en los momentos de "fracaso experimental máximo".

Gracias, vecinos de al lado, por compartir vuestro wifi y vuestra comida durante el confinamiento. Además de hacerlo más tolerable, permitió la escritura del primer artículo publicado durante esta tesis.

Muchas gracias a mis amigos por darme fuerza en los momentos clave. También por escucharme atentamente cada vez que hablo de mi tesis a pesar de no entender ni la mitad.

Finalmente, gracias a mis padres, Jorge y Pilar, a mis hermanas, Iratxe, Pilar y Raquel, y a los perretes de la casa, Pipa y Toxiño, por vuestro amor y apoyo constante, por entusiasmaros con cada una de mis aventuras y por sentiros siempre orgullosos de cada meta que consigo.

FUNDING

The research carried out in this thesis was financially supported by the Spanish Ministry of Science and Innovation through projects MAT2015-65756-R and PID-2019-107032RB-I00, and by the European Regional Development Fund through project MAT2015-65756-R. Additional funding from the ALBA synchrotron facility made it possible to carry out the synchrotron X-ray diffraction experiments performed during this thesis (proposals 2017022003, 2019023268, and 2020074400).

The author of this thesis benefited from a "Ayudas para contratos predoctorales para la formación de doctores 2016" fellowship from the Spanish Ministry of Science and Innovation and the European Social Fund (BES-2016-076612). The author was also financially supported during his stays in the ALBA synchrotron facility (proposals 2019023268 and 2020074400).

ABSTRACT

Quality attributes of food products such as visual appearance, melting behavior, or shelf-life are strongly determined by the crystallization behavior of natural fats and oils within. In turn, this behavior depends on the polymorphism and the sort of mixing states (eutectic phase, solid solution phase, molecular compound formation) displayed by their major triacylglycerol components. Therefore, it becomes essential that studies regarding lipid crystallization cover from pure molecular components and their mixtures to real fats and oils.

In connection with the above, this thesis focuses on gaining further fundamental knowledge about the polymorphism and crystalline behavior of lipid systems with varying degrees of complexity. Thus, the first stage of the research involved a study of pure triacylglycerols based on palmitic, lauric, and oleic acids (P, L, and O, respectively), which are typical of natural fats and oils such as lard and palm, olive, and coconut oils. During the second stage, binary and ternary mixtures including these triacylglycerols were examined to obtain an insight into their solid-state miscibility properties. Concretely, the mixtures were composed of a fully saturated triacylglycerol and one or two saturated-unsaturated triacylglycerols able to form a molecular compound. Despite the presumable crucial role of interactions including triacylglycerols forming molecular compound in the physical behavior of natural lipids and their blends, the phase behavior of triacylglycerol mixtures with such configuration is barely known. Finally, the third stage consisted of a more applied investigation of the crystalline and thermal properties of blends including natural fats. More specifically, binary blends of cocoa butter and shea butter stearin.

Regarding the investigation of pure TAGs, calorimetric and X-ray diffraction techniques were used to examine the polymorphic occurrence and transformation behavior of PPP, LLL, OPO, and PPO during the application of dynamic thermal treatments at varying cooling and heating rates. The results showed that the polymorphic occurrence on cooling, as well as the sequence and type of transformations during heating, were influenced by the rate of the thermal treatments applied. However, it was also found that the extent of the kinetic influence depended on the intrinsic properties of triacylglycerols such as the length of the fatty acid chains or the characteristic polymorphism.

The mixtures under examination during the phase behavior studies included the binary systems PPP/POP, PPP/PPO, PPP/OPO, LLL/POP, and LLL/PPO, and the ternary systems

PPP/POP/OPO, PPP/POP/PPO, and LLL/POP/PPO (keeping an equimolecular ratio of POP/OPO or POP/PPO to favor molecular compound formation). Eutectic behavior with partial miscibility was observed under metastable and stable conditions. Furthermore, the results obtained for stable binary mixtures showed that the degree of miscibility was primarily influenced by the oleic acid content of the unsaturated component, as well as the differences in the size of the triacylglycerols within the mixture. From the solid-state miscibility observed in ternary systems containing LLL or PPP, it was concluded that third components may affect the mixing interactions associated with molecular compound formation. In addition, the results suggested that the ternary interactions studied may help to explain the crystallization behavior of edible lipids like palm oil and be useful in fat structuring applications.

As a case study of real fat blends, combinations of cocoa butter and shea butter stearin at varying proportions were examined through calorimetric, X-ray diffraction, spectroscopic, and microscopic techniques. These made possible to characterize the effect of composition on the polymorphic crystallization and transformation properties, the melting profile, and the microstructural development. The results obtained for some of the parameters under study suggested that specific combinations might be considered for its application in chocolate-type confectionery products.

PREFACE

Motivation and objectives

Triacylglycerols (TAGs) are major lipidic components of edible fats and oils contained in foods like chocolate, confections, butter, or ham. In these products, properties such as the melting behavior, rheology, and shelf-life are influenced by the crystallization behavior of the lipid phases. Therefore, the design and production of high-quality fat-based products with specific functionalities rely on an in-depth understanding of the relationship between crystalline properties and the physical behavior of fats.

Natural fats and oils consist of multi-component TAG mixtures, so that their properties result from the crystalline and mixing behaviors of diverse TAGs rather than from the effect of a single component. Therefore, to understand the complex crystallization, microstructural, and thermal behavior of complex lipid systems, the study of whole fats needs to be complemented by the investigation of the fundamental properties of the major TAGs present, alone and in binary, ternary, or more complex mixtures (Rossell, 1967).

Diverse studies examined the polymorphic behavior of TAGs, as well as the influence of external factors applicable to industrial conditions (dynamic thermal treatments, annealing processes, shear, or sonication) (Bayés-García et al., 2011a, 2016; Ghazani & Marangoni, 2019a; Ueno et al., 2003). Regarding the phase behavior of TAG mixtures, many binary systems have been examined to date in metastable and/or stable polymorphs. From these, it is known that three main types of mixing behavior occur: complete solid solution, eutectic or immiscible behavior, and molecular compound formation. For example, complete miscibility was observed in POS/SOS mixtures (with S, P, and O being stearic, palmitic, and oleic acids, respectively) (Rousset et al., 1998), eutectic behavior in PPP/POP, POP/POO, SOS/POP, or POS/POP mixtures (Koyano et al., 1993; Minato et al., 1996; Sasaki et al., 2012; Zhang et al., 2007), and molecular compound formation in POP/OPO, POP/PPO, SOS/OSO, and SOS/SSO mixtures (Koyano et al., 1992; Minato et al., 1997a, 1997b; Takeuchi et al., 2002a). The mixing behavior of ternary systems including some of the mentioned components has also been reported (Gibon & Durant, 1985; Smith et al., 2013). These studies at a molecular level have shed light on the mixing interactions that rule the crystalline and melting properties of complex lipids like palm oil, cocoa butter, lard, and their blends.

At the early stage of this thesis, no studies had been carried out on ternary mixtures including two-component TAGs able to form molecular compound. However, it is worth noting that work on blends with such configuration is currently available in the scientific literature. The eutectic behavior of mixtures of LLL (with L being lauric acid), SOS, and OSO was recently reported (Yoshikawa et al., 2022). Also the ternary interactions of SOS, SSO, and OSO, and their applicability in the development of alternative fats to cocoa butter (CB), have been investigated (Watanabe et al., 2018, 2021). The phase behavior of ternary mixtures including TAGs forming molecular compound arises as a wide field of study for both basic and applied research. On the one hand, the study of these systems can provide fundamental knowledge of the molecular interactions governing the behavior of complex lipids from a broader perspective with respect to binary systems. On the other hand, the polymorphic and mixing states resulting from these interactions may be of practical value in specific applications, such as oil fractionation processes or the development of novel lipid materials by the physical blending of fats and oils.

In connection with the above, this thesis makes use of crystallographic and calorimetric techniques to analyze the binary phase behavior of specific TAG combinations, as well as the effect of adding a third component on the final miscibility of the system. Concretely, the binary and ternary mixtures under study consist of a saturated TAG (PPP or LLL) and one or two unsaturated TAGs able to form a molecular compound (POP and PPO, or POP and OPO). Therefore, as a case example, one of the aims would be to determine if a two-component eutectic mixture, such as PPP/POP, may turn into a more miscible system when combining PPP and the molecular compound POP/OPO. From this research, we expect to extract fundamental knowledge about ternary interactions naturally occurring in natural fats and their blends. We also expect to unveil TAG combinations with potential application in the design of lipid blends with tuned functionalities. An increase in the miscibility of LLL and POP/PPO with respect to the binary systems, for example, could be potentially exploited to improve the eutectic behavior of blends of cocoa butter substitutes (CBS) (rich in LLL) and CB (rich in POS, SOS, and POP).

To achieve the general purpose of this research, three specific objectives were proposed:

i) To gain a better comprehension of the crystalline behavior of the TAG components included in the mixtures. For this, the polymorphism of PPP, LLL, OPO, and PPO was examined during thermal treatments at varying cooling and heating rates.

ii) To determine the polymorphic and phase behavior of the binary mixtures PPP/POP, PPP/PPO, PPP/OPO, LLL/POP, and LLL/PPO under metastable and stable conditions.

iii) To evaluate the mixing properties of PPP/POP/OPO, PPP/POP/PPO, and LLL/POP/PPO systems, and compare the behavior observed with the previous binary systems.

As a case example of real fats blend, this thesis also includes the study of mixtures of CB and shea butter stearin (ShS). This binary system was selected based on its compatible composition (mainly S, P, and O fatty acids) with the multi-component TAG mixtures included in this thesis. In addition, the research interest in these blends lies in the current need for novel fat materials that help meet the growing worldwide demand for chocolate and related CB-based products. So far, no detailed studies have been carried out on the crystalline properties of mixtures including CB and ShS. This work aims to characterize the polymorphic properties, melting behavior, solid fat content, and microstructure of CB/ShS blends as a function of composition. From the results obtained, we expect to extract conclusions regarding the potential application of ShS to partially replace CB in end products.

Thesis structure

This thesis is structured in eight chapters, the content of which is briefly summarized below. It should be noted that the chapters describing the results consist of a brief introduction, the obtained results, a summary of these, and the main highlights in order to ease the reading and comprehension thereof.

Chapter 1: contains a general introduction, in which basic concepts about the structure, crystallization mechanisms, and polymorphism of triacylglycerols are presented. This chapter also provides a literature review about the phase behavior of lipids, with a special emphasis on triacylglycerol mixtures.

Chapter 2: describes the materials and the preparation of the samples used in this study. It also gives an overview of the experimental techniques and the methodology employed in this thesis

Chapter 3: deals with the polymorphic properties of pure PPP, LLL, OPO, and PPO, which play a part in the mixtures under study in further chapters. The chapter analyzes their polymorphic occurrence and transformation behavior as a function of kinetics or speed of the thermal treatments applied (cooling and reheating).

Chapter 4: looks at the mixing behavior of PPP and unsaturated triacylglycerols forming molecular compound. It presents and compares the stable phase diagrams of the binary systems PPP/POP, PPP/OPO, PPP/PPO, and the ternary systems PPP/POP/OPO and PPP/POP/PPO. The kinetic phase behavior of these mixtures is also covered by the chapter.

Chapter 5: presents the results obtained during the study of LLL/POP, LLL/PPO, and LLL/POP/PPO mixtures. In a similar manner to the previous chapter, the systems are analyzed after a thermodynamic stabilization process and under the influence of kinetics.

Chapter 6: focuses on the study of binary blends of cocoa butter and shea butter stearin, a system more directly connected to real applications. Their polymorphic crystallization and transformation behavior is examined under isothermal and non-isothermal conditions. In addition, the heat-resistant properties of the blends after a tempering process are also evaluated.

Chapter 7: includes a general discussion of the results obtained in this thesis.

Chapter 8: contains the conclusions derived from this thesis and includes suggestions for future work.

TABLE OF CONTENTS

LIST OF FIGURES

LIST OF TABLES

LIST OF ABBREVIATIONS

ANOVA	analysis of variance
C	capric acid
CB	cocoa butter
CBA	cocoa butter alternative
CBEx	cocoa butter extender
CBI	cocoa butter improver
CBR	cocoa butter replacer
CLM	chain-length mismatch
DAG	diacylglycerol
DSC	differential scanning calorimetry
FT-IR	Fourier transform infrared spectroscopy
KLC	kinetic liquid crystal
L	lauric acid
Li	linoleic acid
LLL	1,2,3-trilauroyl-glycerol (trilaurin)
Ln	linolenic acid
LS	long spacing
M	myristic acid
MAG	monoacylglycerol
MC	molecular compound
MMM	1,2,3-trimyristoyl-glycerol (trimyristin)
O	oleic acid
OPO	1,3-dioleoyl-2-palmitoyl-glycerol

P	palmitic acid
PLM	polarized light microscopy
p-NMR	pulsed nuclear magnetic resonance
POP	1,3-dipalmitoyl-2-oleoyl-glycerol
POS	1-palmitoyl-2-oleoyl-3-stearoyl-rac-glycerol
PPO	1,2-dipalmitoyl-3-oleoyl-rac-glycerol
PPP	1,2,3-tripalmitoyl-glycerol (tripalmitin)
S	stearic acid
SAXD	small-angle X-ray diffraction
SFC	solid fat content
ShS	shea butter stearin
SOS	1,3-distearoyl-2-oleoyl-glycerol
SR-XRD	synchrotron radiation X-ray diffraction
ss	solid solution
SS	short spacing
SSS	1,2,3-distearoyl-glycerol (tristearin)
TAG	triacylglycerol
TOPLM	thermo-optical polarized light microscopy
WAXD	wide-angle X-ray diffraction
XRD	X-ray diffraction

LIST OF SYMBOLS

d	interplanar spacing or distance
ΔG	change in the Gibbs free energy
$\Delta G^{\#}$	Gibbs free energy barrier for transformation
ΔG_n	Gibbs free energy barrier for nucleation
$\Delta G_{ss}^{\#}$	Gibbs free energy barrier for the soli-state transformation
ΔH	enthalpy change
ΔH_m	melting enthalpy
$\Delta \mu$	difference in chemical potential
ΔT	supercooling
γ	interfacial free energy of crystals
λ	wavelength
r_c	critical radius size for stable nuclei formation
θ	diffraction angle
τ_c	induction time for crystallization
τ_{ss}	induction time for the solid-state transformation
τ_{mm}	induction time for the melt-mediated transformation
T_c	crystallization temperature
T_{end}	end temperature
T_m	melting temperature
T_{onset}	onset temperature
T_{top}	peak top temperature

CHAPTER 1

GENERAL INTRODUCTION

1.1. FATS AND OILS

Lipids represent a diverse group of organic compounds generally insoluble in water but soluble in non-polar organic solvents. Within these, four main categories exist: fats and oils, phospholipids, waxes, and steroids. The terms "fat" and "oil" are used to distinguish between lipids displaying solid or liquid properties at ambient conditions, respectively. Natural fats and oils from animal and vegetable sources are complex mixtures in which triacylglycerols (TAGs) account for approximately 95% of total content. Other minor components include di- and monoacylglycerols (DAGs and MAGs), waxes, phospholipids, sterols, tocols, or pigments (Gunstone, 2013; Kodali, 2014).

The consumption of fats and oils is of paramount importance in human nutrition. Dietary lipids are the major source of caloric intake within the basic macronutrients (9 Kcal/g against the 4 Kcal/g provided by proteins and carbohydrates). Besides being a long-term energy source, they are vital for the proper operation of diverse body functions. Among other roles, lipids serve as structural elements in cell membranes and provide essential fatty acids that cannot be synthesized by the organism itself. In addition, they act as carriers of micronutrients such as fat-soluble vitamins or carotenoids (Shahidi & Senanayake, 2006).

Butter, chocolate, confections, or bakery shortenings are examples of widely consumed food products in which fats and oils are the main ingredients. Their unique properties in terms of flavor, mouthfeel, or meltability are influenced by the fat crystals formed during manufacturing processes. For this reason, controlling and tailoring the functionalities of lipid-based products require understanding how lipid crystallization and physical behavior interrelate. This has also a fundamental value to obtain lipid phases with desired characteristics during the dry fractionation of edible oils. The properties of fats and oils depend on their chemical composition, so the crystalline behavior of lipids should be analyzed from single TAG molecules and their mixtures to whole complex systems. Besides food applications, a deep knowledge of lipid crystallization is also crucial in the manufacture of diverse goods from the oleochemical, cosmetic, and pharmaceutical industries.

1.2. TRIACYLGLYCEROLS STRUCTURE

TAGs are esters of glycerol (propane-1,2,3-triol) and three fatty acids (see Figure 1.1). The positions of the fatty acids at the glycerol backbone are commonly referred to as *sn*-1, *sn*-2, and *sn*-3 according to a stereospecific numbering. Monoacid TAGs show identical fatty acids at all *sn*- positions, whereas mixed-acid TAGs present at least one different substituent. According to the presence and number of double bonds between carbon atoms (C=C), we can also distinguish between saturated, unsaturated, or saturated-unsaturated TAGs. Structure-derived properties of TAGs, such as the melting and crystallization behavior, are determined by the length of acyl chains, degree of unsaturation, and stereospecific location of the fatty acids (Marangoni, 2012).

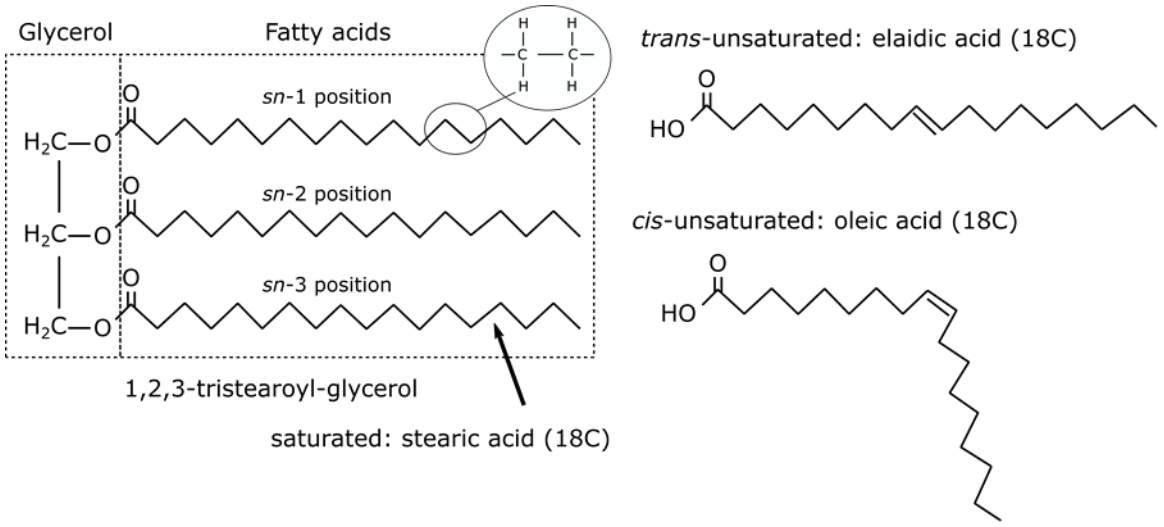

Figure 1.1. Basic structure of fatty acids and triacylglycerols.

The presence and number of C=C bonds give rise to a wide range of fatty acid structures differing in shape and properties. The straight zigzag chain of saturated fatty eases their packing in dense crystalline structures. Due to this, highly saturated fats are commonly solid under ambient conditions. Within unsaturated fatty acids, monounsaturated ones show a single C=C bond, and polyunsaturated present two or more. In addition, these are classified as *cis* or *trans* according to the isomerization of the double bonds. The *cis* configuration causes a bend in the acyl chain, which hinders molecular packing (see Figure 1.1). This results in a lower melting point, which is a typical trait of lipid components from vegetable oils. By contrast, *trans* unsaturation leads to a limited bending of the chain. Hence, the final properties are closer to

those of a saturated fatty acid. *Trans*-fatty acids are naturally present in dairy products and may occur through specific industrial processes (high-temperature treatments, partial hydrogenation) (Nagpal et al., 2021). However, *cis* double bonds are predominant in nature.

Different terminology exists to name fatty acids. Commonly, the systematic (IUPAC), trivial, or shorthand (ω, n-) nomenclatures are used. For example, the systematic name *c*-9-octadecenoic corresponds to the trivial name oleic acid (O) and the shorthand 18:1ω9. In the scientific literature regarding lipid crystallization, TAGs are frequently denoted by a three-letter code indicating the trivial names given to the constituent fatty acids. This simplifies the name of TAGs formed by common saturated fatty acids like stearic (S), palmitic (P), myristic (M), lauric (L), and capric (C), or unsaturated fatty acids like oleic and linoleic (Li). Under this nomenclature, fatty acids are named starting by that located at the *sn*-1 position of the glycerol group. Thus, the mixed-acid saturated-unsaturated TAG denoted as SOS would correspond to 1,3-distearoyl-2-oleoyl-glycerol. It is worth noting that, in asymmetric TAGs, the different fatty acid substitution at *sn*-1 and *sn*-3 positions leads to the formation of optically active stereoisomers (R and S enantiomers). In turn, an equal mixture of stereoisomers is called a racemic mixture. To distinguish a racemic mixture of TAGs, the (*rac*) notation is included in the corresponding three-letter code (*rac*-TAG). However, the notation is often omitted when fatty acids with lower degree of unsaturation and/or shorter chain length are named in the first place. This is the case of POS (1-palmitoyl-2-oleoyl-3-stearoyl-rac-glycerol), PPO (1,2-dipalmitoyl-3-oleoyl-rac-glycerol), or POO (1-palmitoyl-2,3-dioleoyl-rac-glycerol) (with P, S, and O having 16, 18, and 18 carbon atoms, respectively), which are relevant racemic mixtures in edible lipids like cocoa butter (CB), lard, or palm oil (Nagai et al., 2020; Takagi & Ando, 1995). Given the importance of racemic mixtures in nature, the asymmetric PPO evaluated in this thesis consisted of an equimolecular blend of R-PPO (1,2-dipalmitoyl-3-oleoyl-sn-glycerol) and S-OPP (1-oleoyl-2,3-dipalmitoyl-sn-glycerol).

1.3. CRYSTALLIZATION OF TRIACYLGLYCEROLS

Crystallization is the conversion of a liquid phase into a solid with its components (ions, atoms, or molecules) following an ordered structural pattern. As depicted in Figure 1.2A, this occurs via nucleation and crystal growth from a supersaturated mother phase. In lipid crystallization, the supersaturation or supercooling conditions are generally induced by decreasing the temperature of the initial phase below the melting point of the highest melting component. The driving force for crystallization is the difference in chemical potential ($\Delta\mu$) or Gibbs free energy per molecule (ΔG) in the liquid and in the crystal phase. In lipids crystallized from the neat liquid, $\Delta\mu$ relates to the degree of supercooling (ΔT), or the difference between the melting and the crystallization temperature (T_m-T_c), by

$$\Delta\mu = \Delta H_m \cdot \Delta T / T_m$$

where ΔH_m is the enthalpy of melting (Himawan et al., 2006).

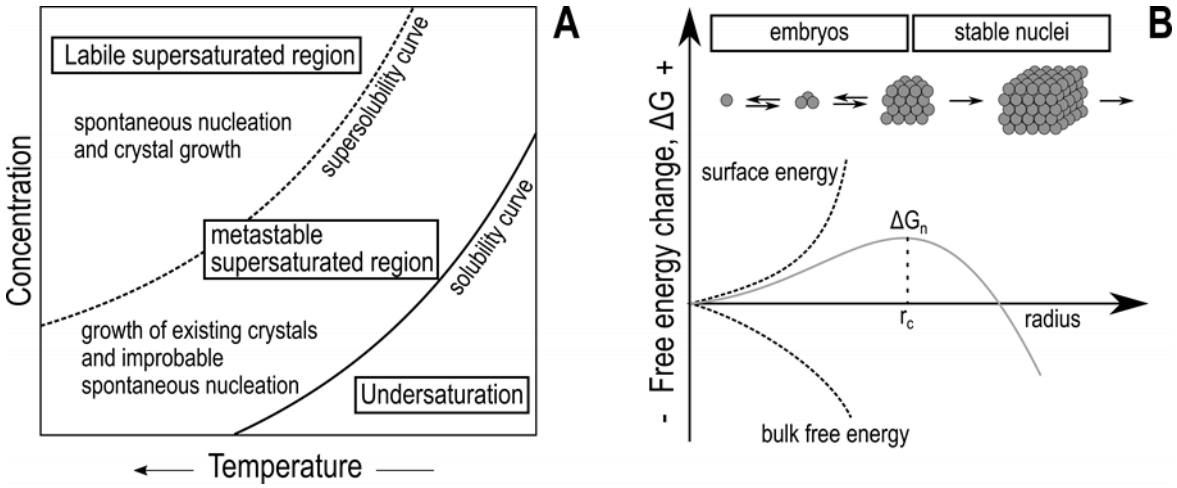

Figure 1.2. A) Schematic solubility/supersolubility diagram. B) Energy diagram of the nucleation process.

1.3.1. Nucleation

According to the classical nucleation theory, under supercooled conditions, lipid molecules aggregate into small clusters called "embryos" that continuously form and dissolve until a stable nucleus develops. During crystallization, the formation of solid-liquid interfaces results in a positive contribution to the free energy, whereas the opposite effect arises from increasing the crystalline volume (Marangoni & Wesdorp, 2013a). As shown in the diagram of Figure 1.2B, this leads to a Gibbs free energy barrier that needs to be overcome for the nucleation to occur (ΔG_n). Only the nuclei above a critical size or radius (r_c) at the point of maximum energy grow irreversibly to form larger crystal structures in order to minimize their free energy. For the same reason, smaller clusters tend to dissociate. As the degree of supercooling increases, the critical size needed to form stable nuclei decreases. Thus, more crystals (a larger number of nucleation sites) are formed when fast cooling treatments are applied.

Nuclei formation occurs via primary and secondary nucleation processes (Mullin, 2001). In addition, two types of primary nucleation exist: homogeneous and heterogeneous.

During primary homogeneous nucleation, two molecules interact to form dimers and further molecules keep accumulating until a stable nucleus occurs (Badan Ribeiro et al., 2015). This process requires a high degree of supercooling and takes place in the absence of foreign particles. By contrast, the primary heterogeneous nucleation is catalyzed by the presence of nucleation sites from matter such as dust particles, impurities, or rough surfaces. Interactions at the interface of the solid particle and the supersaturated liquid favor some degree of local order of lipid molecules, which act as template during crystallization and cause a decrease in the energy barrier for the formation of stable nuclei (Metin & Hartel, 2005). For this reason, heterogeneous nucleation takes place at lower supercooling than homogeneous nucleation. Complete purity of lipid solutions is highly unlikely, so heterogeneous nucleation is more industrially relevant than homogeneous nucleation.

Secondary nucleation consists of the formation of new nuclei from the crystals grown during primary nucleation. This results from the detachment of small portions of the crystals, generally favored by collisions either between crystals or between crystals and surfaces (stirrers, vessel walls) (Douaire et al., 2014). In many industrial applications, especially when shear is involved, secondary nucleation becomes predominant at the latest stages of lipid crystallization (Gregersen et al., 2017; Tran & Rousseau, 2016). Moreover, this type of nucleation is often deliberately

induced by adding crystal seeds into a liquid mother phase. These accelerate the crystallization or act as templates for the development of crystals with a specific structure (Hachiya et al., 1989).

1.3.2. Crystal growth

Once the first nuclei occur, nucleation and crystal growth take place in a simultaneous manner. During the growth of crystalline surfaces, lipid molecules from adjacent liquid layers aggregate into stable nuclei in order to form three-dimensional networks. This process continues as long as a driving force for crystallization exists. The rate of crystal growth is strongly influenced by the time needed for the new TAG molecule to adopt the right orientation and incorporate at the correct site in the growing crystal (Knoester et al., 1968). This relates in part to the nature of the liquid-crystal surface and the competition of different lipid molecules for the same growing sites. In addition, the degree of supercooling also determines the rate of crystal growth. Lower temperatures result in a higher viscosity, which limits the molecular diffusion from the liquid to the crystalline phase (Timms, 2003).

1.3.3. Crystal morphology and microstructure

As illustrated in Figure 1.3, the crystallization of TAGs results in a complex structural hierarchy of fats from the nano- to the macro-scale. At the initial stages of nucleation and crystal growth, TAG molecules stack by pairs (Bennema et al., 1988) and then associate forming lamellar structures with a characteristic longitudinal and lateral packing of the fatty acid moieties. The specific lamellar arrangement depends on TAGs polymorphism, which will be discussed in a further section. Once formed, lamellae align epitaxially to form crystalline domains, which correspond to the thickness of a single crystallite or crystalline nanoplatelet (Acevedo & Marangoni, 2010). Nanoplatelets aggregate then into clusters, which set the limit from the nanoscopic to the microscopic world. Finally, the clusters join into flocs or agglomerates to form the three-dimensional fat crystal network. In addition to van der Waals forces, fat adhesion through sintering (development of solid bridges) may contribute to the strength and preservation of this network (Johansson & Bergenståhl, 1995; Marangoni et al., 2012; Walstra, 2001). The mechanical properties (texture, firmness, spreadability), physical stability, and behavior on eating (melting, mouthfeel) of fats depend on the structural behavior at the different length scales. In turn, the structural arrangement along the whole hierarchy is determined by the lipid

composition and external factors such as the speed of thermal treatments, the application and intensity of shear, or the long-term storage (Acevedo & Marangoni, 2015).

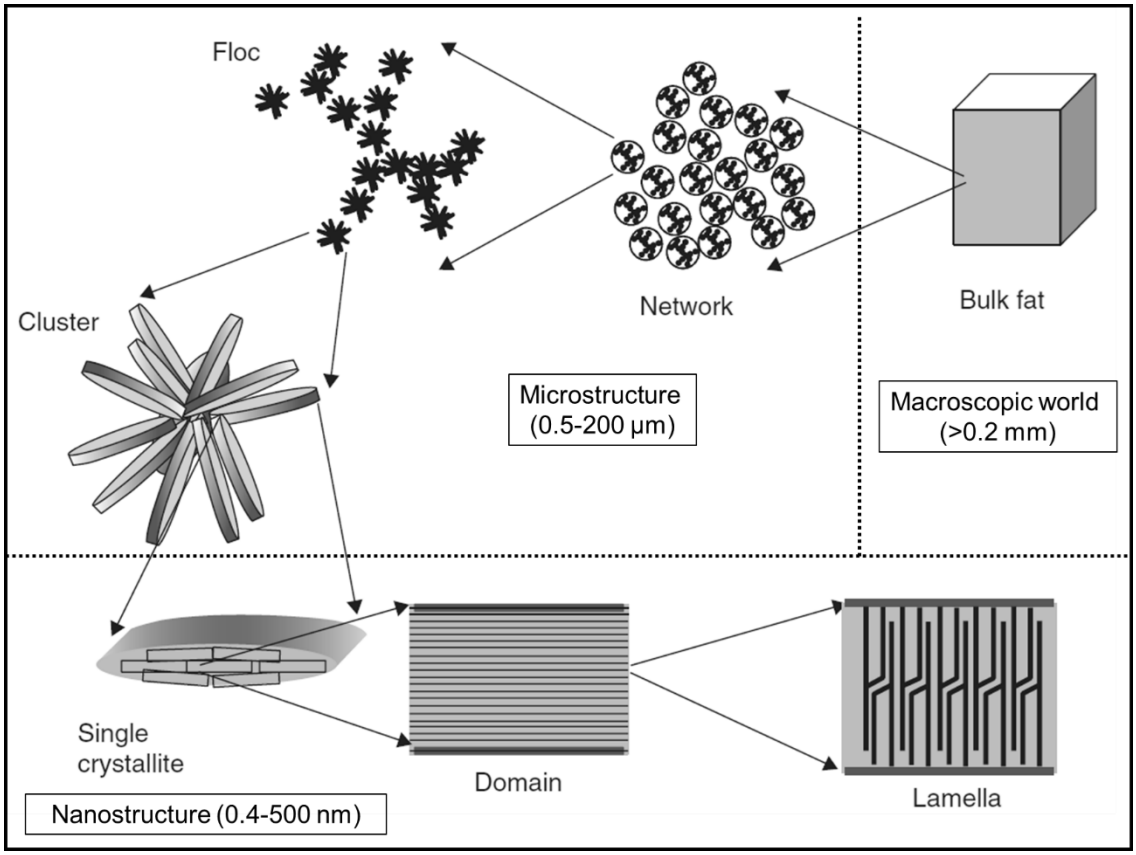

Figure 1.3. Structural hierarchy of fats. Adapted with permission from Peyronel et al. (2010), Copyright (2010) Elsevier.

The microstructural level of fats is defined by the number, size, shape, and spatial distribution of the crystals and clusters formed (Narine & Marangoni, 2005). As previously stated, the speed of thermal treatments influences the nucleation rate by means of supercooling. This implies the formation of many small crystals when lipid melts are cooled at high rates, and fewer crystals with higher dimensions during slow cooling processes (Maleky et al., 2012). Regarding the shape and morphology, TAGs tend to crystallize in the form of spherulites (see Figure 1.4). The formation of this characteristic morphology relies on the occurrence of high supersaturated conditions. Spherulites consist of aggregated nanoplatelets growing radially from the nucleation site. Their progression occurs through a secondary nucleation mechanism for each layer at the surface of individual lamellae (Rousset, 2002), which is affected by the magnitude of the driving force (Himawan et al., 2006). A low driving force (i.e., low supercooling) slows the secondary

nucleation and favors the development of the front surface layer by layer. This leads to highly branched structures with well-defined spherical bodies. By contrast, a high driving force eases the simultaneous nucleation at different layers before one is completed, giving rise to more diffuse spherulitic structures. The specific size, shape, density, and fineness of spherulites depend on the crystallization temperature and the cooling conditions. Due to this, different microstructures such as grainy, fibrous, feathery, or lamellar may be observed under the microscope for the same TAG component (Kellens et al., 1992). In addition, other structures different from spherulites occur during lipid crystallization. For example, small needle-shaped crystals may form during fast cooling processes (Yang & Hrymak, 2011). These are, actually, precursors of spherulitic structures (Rousset, 2002). However, the thermal processing allows them to grow separately and adopt random orientations.

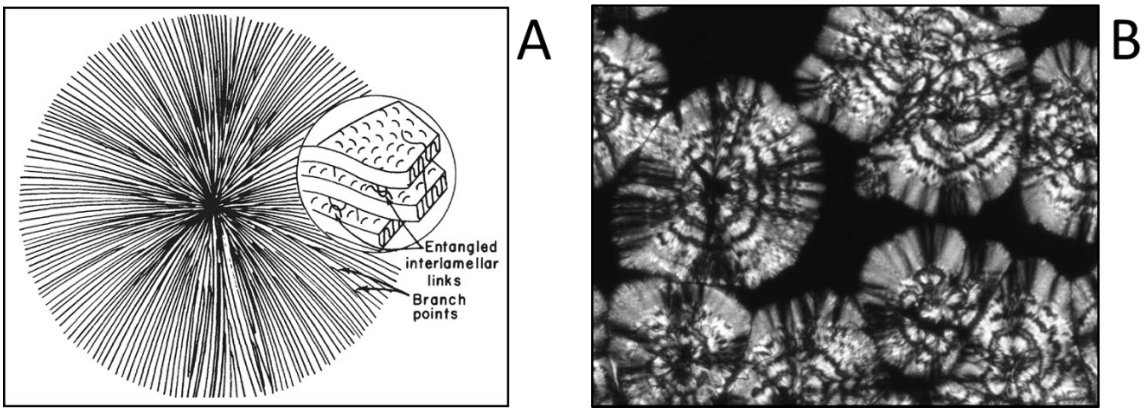

Figure 1.4. A) Scheme of a spherulitic structure growing radially from its center. Reprinted with permission from Hoffman et al. (1976): Springer Nature, *Treatise on solid state chemistry. Volume 3. Crystalline and noncrystalline solids* by Hannay, N. B, Copyright (1976). B) Polarized micrograph of typical TAG spherulites.

Controlling the size and shape of the crystals defining the microstructure is required to assure the final quality of foodstuffs or the efficiency of diverse industrial processes. As a case example, in semisolid products like margarine, crystals smaller than 30 μm are preferred to avoid an undesirable sandy mouthfeel (Foubert et al., 2007; Herrera et al., 1998). By contrast, large dense spherulites are advantageous to reduce the entrapment of liquid and ease the filtration process during oil fractionation processes (Smith, 2001).

1.4. POLYMORPHISM OF TRIACYLGLYCEROLS

TAGs are polymorphic since different crystalline structures may occur for the same molecular species. The polymorphic behavior that results from individual TAGs and their mixing interactions define physical properties of fats such as the melting point.

During polymorphic crystallization, intra- and intermolecular interactions are optimized to favor an efficient packing of TAGs (Larsson et al., 2006). This is achieved via the lateral and longitudinal stacking of repetitive sequences of hydrocarbon chains in a specific manner. As shown in Figure 1.5, the major molecular factors influencing the polymorphic structures of TAGs can be summarized in four (Sato, 2001a): i) aliphatic chain packing resulting from hydrocarbon chain-chain interactions; ii) glycerol configuration, in which dipole-dipole interactions presumably play a key role; iii) methyl end stacking, which determines the final length of the structures in the long-chain axis; and iv) olefinic group interactions, which are relevant when unsaturated fatty acids are included in the molecules.

The packing of TAGs along the long-chain axis defines the chain-length structure and relates to the thickness of a unit lamella. The specific length results from the number of leaflets or sublayers formed by single hydrocarbon chains, which depends on the fatty acid composition of TAGs. Thus, identical fatty acid moieties at *sn*-1, *sn*-2, and *sn*-3 positions lead to double chain-length structures (2L) (Helmholdt et al., 2002; Jensen & Mabis, 1963; Larsson, 1964). By contrast, dissimilar fatty acids increase steric hindrance and may prevent their packing in the same lamellar plane. As a result of chain sorting, triple chain-length structures (3L) arise (Goto et al., 1992; Kodali et al., 1987; Sato et al., 1989). Even though lengths of four and six leaflets may be found in some asymmetric mixed-acid TAGs (Kodali et al., 1989; Sato et al., 2001), double and triple chain-length structures are the most common. During the analysis of fat crystals by powder X-ray diffraction (XRD), the chain-length structure results in long spacings (LS) or small-angle XRD (SAXD) reflections. These denote the distance between methyl end groups of TAGs, which varies with the length of the acyl chains and their angle of tilt with respect to the methyl end plane.

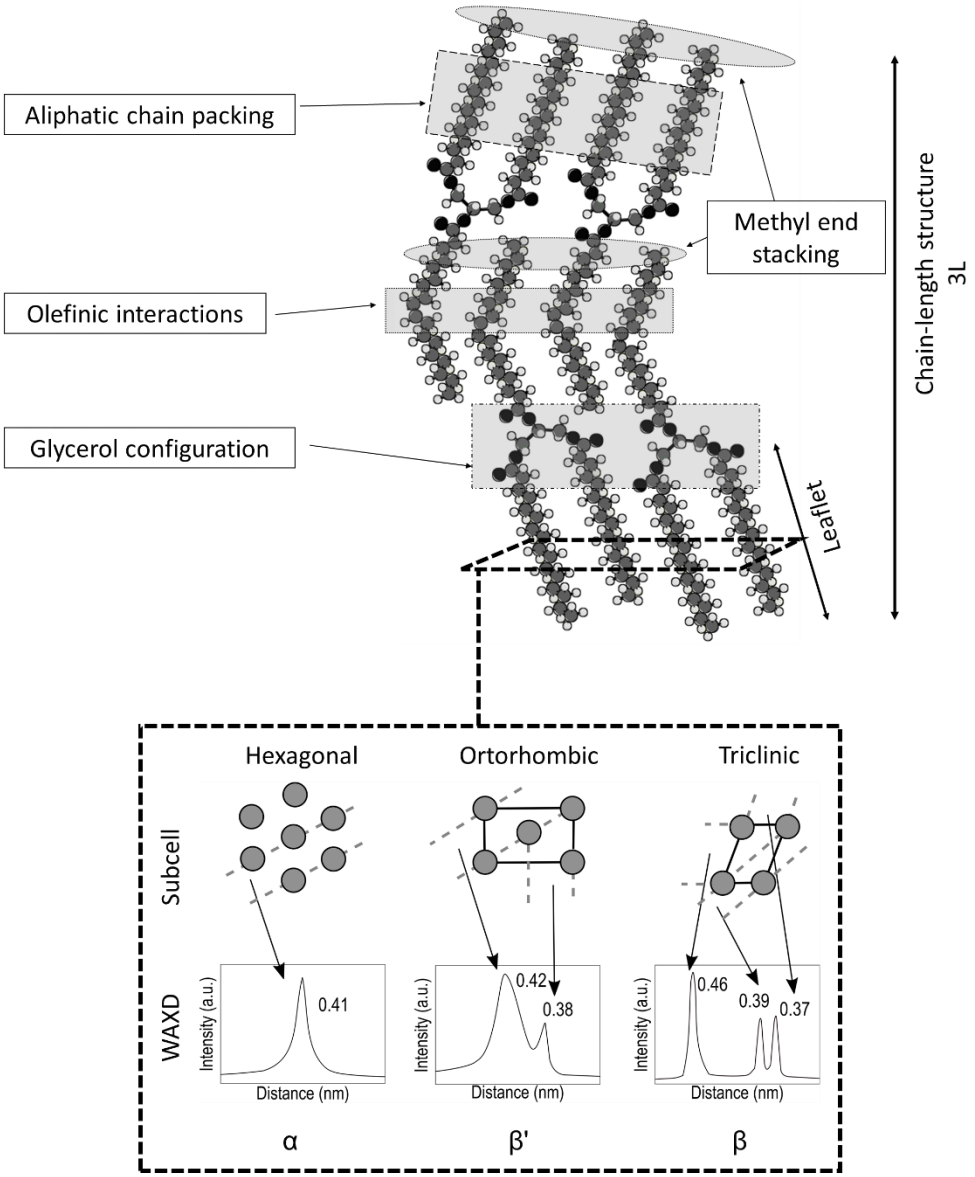

Figure 1.5. Scheme of the longitudinal and lateral packing of TAGs.

The cross-sectional packing mode of the zigzag hydrocarbon chains shapes the subcell structure, which is characteristic of each polymorphic form (D'Souza et al., 1990). In XRD patterns, the distances between subcell planes are defined by the short spacings (SS) or wide-angle XRD (WAXD) reflections (see Figure 1.5). According to the type of subcell structure, three basic polymorphs occur in TAGs: α, β', and β (Larsson, 1966). α presents a hexagonal subcell (H), in which the acyl chains are normal to the methyl end plane and have some degree of rotational freedom (Small, 1986). This results in a disordered and loosely packed crystalline structure. β' has an orthorhombic perpendicular subcell (O⊥), in which the acyl chains are tilted

and those nearby are located at different planes. In the triclinic parallel subcell ($T_{//}$) of β, the presence of tilted acyl chains in the same plane favors a tight molecular packing.

α, β', and β are identified through typical short spacings in XRD patterns: α has a single one at 0.41-0.42 nm, β' has two at 0.42 and 0.38 nm, and β typically has a strong one at 0.46 nm and two less intense at 0.39 and 0.37 nm. However, it must be made clear that these spacings vary subtly among different molecules. Depending on the molecular configuration, distinct α, β', and β forms can occur for a single TAG (Hagemann et al., 1975; Norris, 1977) or some of them may not crystallize. For example, β is typical of symmetric TAGs but uncommon in asymmetric TAGs (Lutton et al., 1948; Minato et al., 1997b; Sato et al., 2001; van de Streek et al., 1999). Besides α, β', and β, additional polymorphs may be formed. This is the case of sub-α, which shows a pseudohexagonal subcell with characteristic short spacings at 0.41-0.42 and 0.37-0.38 nm (Akita et al., 2006). In mixed-acid saturated-unsaturated TAGs, also γ and δ forms have been identified (Lutton, 1951; Sato et al., 1989).

The density, enthalpy, and thermodynamic stability increase from α to β' to β. This means that the Gibbs energy decreases in the same direction (see Figure 1.6). One could expect that the crystallization of more stable forms will be favored before less stable ones due to a higher driving force. However, when more than one polymorph can crystallize, the occurrence is governed by their respective nucleation rates (Sato, 2001b). In turn, these are determined by the magnitude of ΔG_n, which decreases from the β to the α form due to a lower interfacial tension (Himawan et al., 2006). This behavior relates to the Ostwald step rule concerning the polymorphic behavior of organic and inorganic substances (Ostwald, 1897). It states that under high supercooling or supersaturation conditions, the least thermodynamically stable polymorph occurs first and transforms sequentially into the next one in order of increasing stability. However, this does not consider how external factors, such as temperature fluctuations, the application of shear, or the addition of seed crystals, influence the polymorphic crystallization kinetics (Sato, 2001b). As an example, extensive work on pure TAGs showed that the polymorphic occurrence can be controlled by tailoring the speed of cooling treatments through ΔT (Baker et al., 2014a, 2014b; Bayés-García et al., 2011a, 2013a, 2013b, 2016).

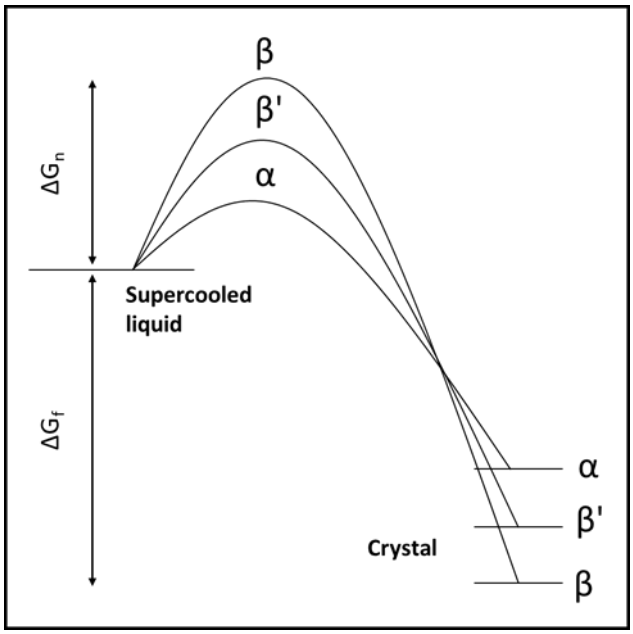

Figure 1.6. Scheme of the differences in activation free energy of nucleation (ΔG_n) and free energy of formation (ΔG_f) of α, β', and β forms of TAGs. Adapted with permission from Sato et al. (2013). Copyright (2013) John Wiley & Sons.

When enough time is provided or the temperature is increased, polymorphs undergo transformations driven by a negative ΔG. Except for the reversible α → sub-α transition, the transformations from less stable to the most stable form take place in a monotropic manner. This refers to the fact that only one polymorph is stable over the entire temperature range. Polymorphic transformations occur mostly in two ways: through a reorganization of the crystalline structure (solid-solid transformation) or by the melting and subsequent recrystallization (via melt-mediation). Additionally, polymorphic transitions through intermediate liquid crystal phases were confirmed in diverse unsaturated TAGs (Bayés-García et al., 2016; Ueno et al., 1997). This behavior relates to the fact that TAG melts retain some degree of structural order in the liquid state. This occurs even at temperatures considerably far above their melting point. However, the specific organization of TAGs in the liquid crystal phase is still unclear and different models have been proposed (Figure 1.7). The smectic model of Larsson (1972) states that TAGs arrange in bilayers forming pseudolamellar structures. This was supported by XRD and carbon-13 nuclear magnetic resonance (^{13}C-NMR) studies on monoacid saturated TAGs (Callaghan, 1977; Hernqvist, 1984). By contrast, the nematic model postulated by Cebula et al. (1992) denies the formation of bilayers and assumes that TAGs with a "chair-type" conformation arrange parallel in a disordered manner. This conformation implies that the

acyl chains at *sn*-1 and *sn*-3 positions of the glycerol group are packed alongside each other in an opposite direction to that at *sn*-2 position. According to the discotic model developed by Corkery et al. (2007), TAGs would form Y-conformers and then stack loosely into short flexible cylindrical rods. A further theoretical study by the same authors supported the Y-shaped configuration of TAGs in the liquid state but discarded the formation of discotic phases (Pink et al., 2010).

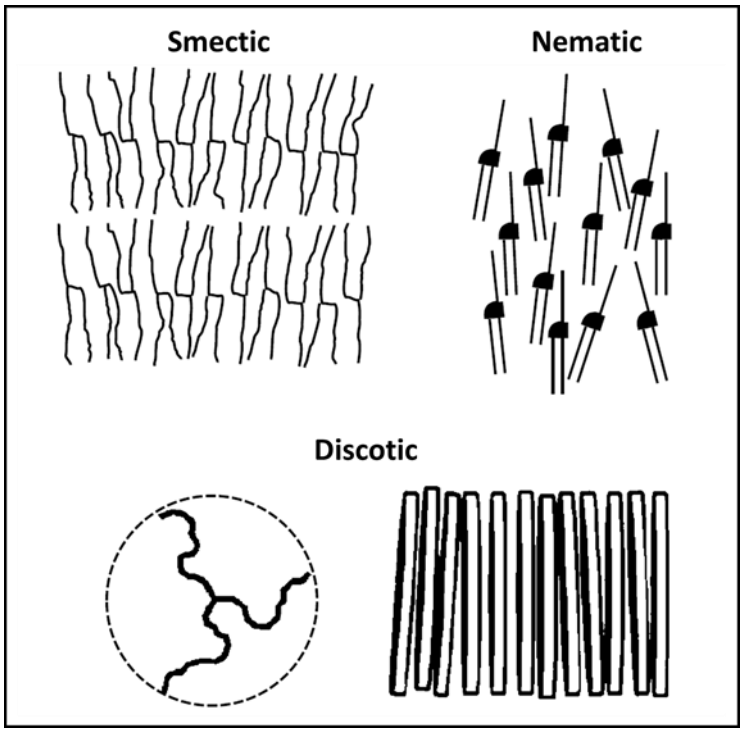

Figure 1.7. Structure models of triacylglycerol liquid crystals. Adapted with permission from Hondoh et al. (2018). Copyright (2018) John Wiley & Sons.

Diverse studies have evaluated the crystallization and transformation behavior of TAGs, especially under the influence of thermal treatments at static temperatures and/or with dynamic temperature variations. Hence, vast knowledge has been gathered about the polymorphic properties of TAGs at varying fatty acid composition, degree of unsaturation, and symmetry. To provide some examples, we summarize below the polymorphic forms, including the respective chain-length structures, of common palmitic and oleic acid-based TAGs. Some of them will be further examined throughout this thesis.

The presence of the same fatty acid substituent at *sn*- positions in monoacid TAGs leads to a relatively simple polymorphism. In this sense, α-2L, β'-2L, and β-2L forms have been reported

for PPP and OOO (Bayés-García et al., 2013a; Elisabettini et al., 1995; Lutton, 1955). A more complex polymorphic behavior is shown by mixed-acid saturated-unsaturated TAGs. For example, in the symmetric OPO, α-2L, β'-2L, and two distinct β forms have been identified (Minato et al., 1997b). The chain-length structure of β_2 has not been determined but that of β_1 is known to be triple. This diversity in longitudinal packing among polymorphs relates to differences in the density of the corresponding crystalline structures. The looser molecular packing in less stable forms allows the formation of double structures with palmitic and oleic acids sharing a leaflet. However, the larger steric hindrance at increasing density of packing prevents the same behavior in β. The formation of triple chain-length structures by chain sorting favors the separation of saturated and unsaturated chains in different layers. As a result, the structure is stabilized. In contrast to OPO, the asymmetry of POO prevents the formation of the β form. In this TAG, α-2L, β'_2-3L, and stable β'_1-3L forms have been identified (Zhang et al., 2007). In addition, it was demonstrated that a transient kinetic liquid crystal (KLC) phase may occur during the conversion of α into β'_2 (Bayés-García et al., 2016).

The number and diversity of polymorphs increases in POP, which may crystallize in α-2L, γ-3L, δ-3L, β'_2-2L, β'_1-2L, β_2-3L, and β_1-3L (Bayés-García et al., 2013b; Sato et al., 1989). The occurrence of metastable γ and/or δ forms is a characteristic trait of TAGs with a single unsaturated fatty acid located at the *sn*-2 position (Arishima et al., 1991; Takeuchi et al., 2000). By contrast, the polymorphism of the asymmetric PPO is simpler and strongly depends on stereochemistry. While R-PPO and S-OOP enantiomers crystallize in α-2L and β-3L forms, α_2-2L, α_1-3L, β'_2-2L, and β'_1-3L forms have been identified in the racemic mixture (Mizobe et al., 2013; Norris, 1977). This polymorphism results from the greater affinity of PPO molecules for the opposite enantiomer, which leads to the formation of a racemic compound.

1.5. PHASE BEHAVIOR OF LIPIDS

A phase is a state of matter, such as a mixture of TAG crystals, in which the physical and chemical properties are homogeneous. In addition, it remains separated from other phases by a physical boundary. For a specific system, the phases formed and their changes depending on parameters like temperature, pressure, or chemical composition are described by the phase behavior.

Fats are basically a crystalline network containing entrapped liquid oil. Therefore, liquid and solid phases are naturally present under ambient conditions. These result from the heterogeneous mixture of TAGs within, each one with own melting and polymorphic properties. Provided that no great differences in molecular weight and volume exist, TAGs are ideally miscible in the liquid state (Wesdorp, 1990; Wesdorp et al., 2013). Thus, a single liquid phase is normally found in a fat material. By contrast, diverse solid phases may arise depending on the phase behavior and polymorphism of different TAG combinations. The whole set of phases in the fat defines its textural properties and melting profile (Co & Marangoni, 2020).

1.5.1. Phase behavior of triacylglycerol mixtures

The phase behavior of complex real fats cannot be understood without analyzing first the physicochemical properties of TAGs in multi-component systems. So far, most studies on this matter have focused on the mixing interactions of two-component blends at equilibrium conditions. This equilibrium is normally induced through thermal incubation processes, which in some cases may last for several months or even for more than one year (Bayés-García et al., 2015a). Once stable conditions have been achieved, the behavior of TAG phases as a function of temperature and composition is generally mapped in binary phase diagrams.

TAGs ideally miscible in the liquid state may lead to three types of mixing phases in the solid state: solid solution (ss), eutectic, and molecular compound (MC) formation. As shown in the phase diagrams of Figure 1.8, the mixing states result in different behaviors of phase boundaries at solid-solid and solid-liquid interfaces. Within these: i) the liquidus curve is the barrier between a liquid phase and a region with solid and liquid phases; ii) the solvus separates single solid phases from two solid phases; iii) the solidus sets the limit between a solid phase and a region with liquid and solid phases; and iv) the eutectic line joins the intersections between solvus and solidus at the extremes of the diagram.

TAGs with equivalent thermal stability and isomorphic crystalline structures show complete solid miscibility. This is due to the ability of each TAG to integrate into the crystal phase of the other without causing a significant disturbance in crystal packing (Lusi, 2018). As a result, miscible phases often present thermal and crystallographic properties halfway between those of the pure components. Conversely, dissimilar TAGs result in distinct phases or eutectic mixtures. In these, the eutectic point or equilibrium of the two solid phases and the liquid occurs at a

specific composition and temperature below the melting point of the components. In addition, some miscibility is generally observed near the pure TAG compositions. The behavior of the liquidus curve and the degree of solid solubility in eutectic systems is largely determined by structure-derived properties of TAGs like the type of subcell packing, chain-length structure, and melting behavior (Floeter et al., 2018; Minato et al., 1996; Timms, 1984). Lastly, strong interactions between TAGs with a specific molecular composition and symmetry may lead to the formation of a molecular compound with structural and thermodynamic properties differing from those of the individual TAGs (Koyano et al., 1992; Minato et al., 1997a, 1997b). Contrary to solid solutions, molecular compounds follow a stoichiometric ratio (typically 1:1 in TAGs). Therefore, the typical phase diagram shows juxtaposed eutectic mixtures of the molecular compound and each TAG bounded by the mixture at equimolecular composition.

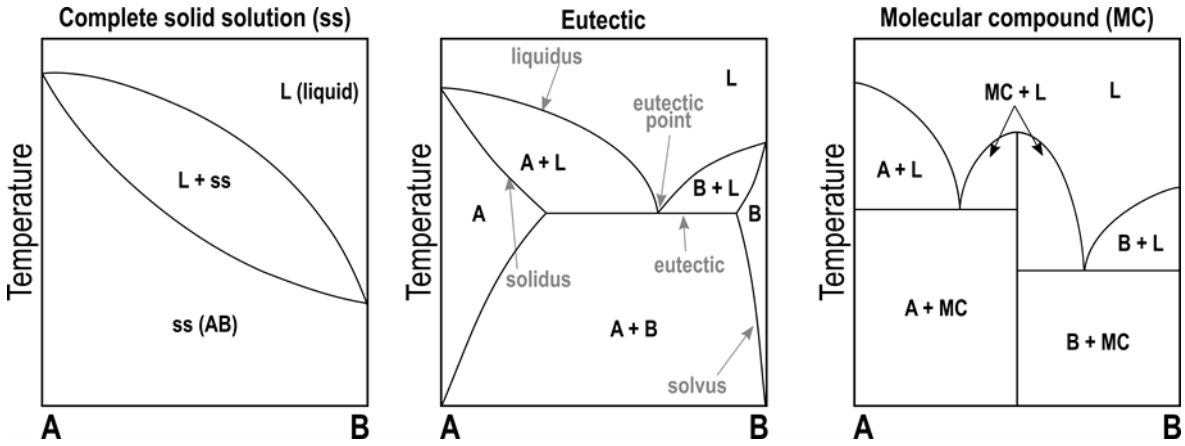

Figure 1.8. Typical phase diagrams exhibited by binary mixtures of TAGs.

From an industrial point of view, a deep knowledge of the phase behavior of TAGs is critical to understand the physical behavior of natural fats and oils, designing fat blends with desired functionalities, and optimizing the separation of specific TAG phases during lipid fractionation processes (Sato, 2001b). It is worth noting that, during industrial processes, fats are far from equilibrium conditions due to the application of external forces (pressure, temperature gradients) (Floeter et al., 2018). This means that diverse metastable phases occur before reaching stability in terms of solid miscibility and polymorphic state. Moreover, such phases may show a long shelf-life and be preferred for specific applications. This is the case of β' crystals of coconut oil, which eventually transform into β (Rossell, 1985), or the typical β_2 polymorph (Form V) of chocolate, which is a metastable solid solution phase of the major TAGs of CB. According to

this, the polymorphic and phase behavior of TAG mixtures should be analyzed not only under stable conditions but also in the metastable state during the application of dynamic thermal treatments.

TAGs symmetry, glycerol configuration, degree of unsaturation, and chain-length mismatch determine the polymorphic and binary phase behavior. Some studies have addressed the phase equilibrium of TAGs following a computational approach. For example, Wesdorp (1990) developed a model to predict the thermodynamic properties of pure TAGs, which has been reviewed by later work (Seilert et al., 2021). The same author performed a theoretical analysis of the experimental diagrams of binary and ternary mixtures of TAGs published to date. Despite this, most of the current knowledge about the mixing properties of TAGs comes from the implementation of experimental techniques. More specifically, thermal analysis techniques, such as differential scanning calorimetry (DSC), and structure determination techniques, such as X-ray diffraction. In the next sections, we provide a summary of the main results obtained by previous work for TAG mixtures with varying molecular configurations. For more details, we refer the interested reader to the review article by Macridachis et al. (2020).

1.5.1.1. *Mixtures of saturated triacylglycerols*

The miscibility of monoacid saturated TAGs is largely influenced by the length of the component fatty acids and polymorph-dependent properties, such as density of packing and molecular mobility at the methyl end region.

Complete miscibility in α and β' forms, and eutectic behavior in β forms, were reported for mixtures of 1,2,3-tripalmitoyl-glycerol and 1,2,3-distearoyl-glycerol (PPP/SSS) (Lutton, 1955; MacNaughtan et al., 2006). However, it is well recognized that solid solution formation in this system is kinetically favored by fast cooling treatments and that two α phases rich in either PPP or SSS occur when cooling at 20 °C·min^{-1} and below (Himawan et al., 2007; Kellens et al., 1991a). In a further study, Takeuchi et al. (2003) used synchrotron radiation X-ray diffraction (SR-XRD) to examine the binary systems 1,2,3-trilauroyl-glycerol/1,2,3-trimyristoil-glycerol (LLL/MMM), LLL/PPP, and LLL/SSS. As PPP/SSS mixtures, LLL/MMM mixtures cooled at a high rate formed solid solutions in the α form. During a subsequent heating process, α (ss) transformed into β' (ss), after which phase separation led to the occurrence of different β forms. By contrast, LLL/PPP and LLL/SSS showed eutectic behavior with limited miscibility in metastable and

most stable forms. The variable behavior among systems resulted from the different lengths of L, M, P, and S fatty acids (12, 14, 16, and 18 carbon atoms respectively). α and β' solid solutions were favored in PPP/SSS and LLL/MMM mixtures due to a low difference of 2 carbon atoms in the length of fatty acids and a low steric hindrance in loosely packed metastable forms. Higher differences in the number of carbon atoms would result in larger gaps during methyl end stacking in LLL/PPP and LLL/SSS mixtures. The subsequent increase in the Gibbs free energy of mixing would prevent the mutual solubility of the components independently of the subcell structure. In addition to the miscibility properties, the authors also found that the eutectic point shifted from a more symmetric to a very asymmetric composition in the LLL/MMM → LLL/PPP → LLL/SSS direction. This was due to the larger mismatch in the number of carbon atoms of the component fatty acids, which increased the difference in melting point of TAGs. Eutectic behavior with eutectic compositions near the pure low-melting component, which is often referred to as monotectic, is typical of binary mixtures including TAGs that differ in melting point by more than ~20 °C (Timms, 1984).

Research carried out in binary mixtures of monoacid and mixed-acid saturated TAGs showed their tendency to eutectic behavior. It was also found that the mixed-acid component has a major influence on the polymorphic behavior during crystallization, transformation, and melting events. For TAG mixtures based on P and S under stable or near stability conditions, Knoester et al. (1972) delimited wider miscibility regions in eutectic diagrams when asymmetric TAGs were included. The kinetic phase behavior study of SSS/PSS, PPP/PSS, and PPP/PSP mixtures showed that the occurrence of β in monoacid TAGs during crystallization or polymorphic transformation was hindered by β'-stable mixed-acid TAGs (Bhaggan et al., 2018a, 2018b; Bouzidi & Narine, 2012b). Besides the composition, the thermal treatments applied also influenced the polymorphic behavior of the mixtures and the final shape of the kinetic phase diagrams. As an example, α crystals of PPP and PSS were formed when cooling PPP/PSS mixtures at rates from 10 to 1 °C·min^{-1}. During reheating, these transformed into distinct β' forms and the final melting behavior depended on the next β' → β transformation of PPP. When heating at 5 °C·min^{-1}, PPP/PSS mixtures system showed a minimum eutectic at a composition with 30% PSS content, and β-stable mixtures were only observed below this value. Decreasing the heating rate to 1 °C·min^{-1} favored the occurrence of β at 40% PSS content and below, which shifted the eutectic point to the 50PPP/50PSS composition.

Regarding mixtures of mixed-acid TAGs, Narine's group carried out a systematic study on symmetric/asymmetric binary systems differing in the chain-length mismatch (CLM) (Boodhoo et al., 2008, 2009a, 2009b; Bouzidi et al., 2010). The term CLM refers to the difference in the number of carbon atoms of the fatty acids contained within the same TAG component. Specifically, DSC and laboratory-scale XRD techniques were used to evaluate the phase behavior of PSP/PPS, MSM/MMS, LSL/LLS, and CSC/CCS mixtures heated at 5 °C·min^{-1} after cooling at 3 or 1 °C·min^{-1}. The kinetic phase diagrams constructed for the PSP/PPS system (CLM=2) showed a singularity in the equimolecular composition. This consisted of a clear change in slope in the liquidus curve, which delimited two distinct eutectic regions at each side. Such behavior was attributed to the formation of a molecular compound. Increasing the CLM to 6 in LSL/LLS resulted in similar mixing properties. By contrast, eutectic behavior was found in MSM/MMS (CLM=4) and CSC/CCS (CLM=8) mixtures. It was concluded that the formation of molecular compound in blends of saturated TAGs may be favored by the presence of TAGs with different symmetry and a specific chain-length mismatch. However, further research is needed to clarify the specific structural features allowing such a mixing state.

1.5.1.2. *Mixtures including unsaturated triacylglycerols*

Mixing phase behavior studies regarding TAGs with *trans*-unsaturated fatty acids are scarce in the scientific literature (Wesdorp et al., 2013; Zhang et al., 2020). Hence, only blends of TAGs with *cis*-unsaturated fatty acids are considered in this section. These are the most relevant ones in natural lipids and in actual industrial processes.

Mixtures of monoacid saturated and monoacid unsaturated TAGs, such as PPP/OOO and SSS/OOO, display eutectic behavior (Costa et al., 2011; Lutton, 1955; Rossell, 1967). This results from the steric hindrance arising between saturated and unsaturated fatty acid chains, which impedes their close packing to form a single structure. Similar behavior occurs in blends of monoacid saturated and mixed-acid saturated-unsaturated TAGs. For example, PPP/POP mixtures subjected to thermodynamic stabilization showed a very asymmetric eutectic composition near pure POP, and a solubility of POP in PPP of around 40-50% (Minato et al., 1996). The liquidus curve followed a similar trend in PPP/POO mixtures in most stable polymorphs. However, the greater disturbance during crystallization at increasing number of olefinic groups reduced the content of mixed-acid TAGs dissolved in PPP to around 15%

(Gibon & Durant, 1985; Lu et al., 2019). Although binary systems with this configuration are generally immiscible in metastable forms, the crystallization of solid solution phases can be promoted by rapid quenching of TAG melts. This was confirmed for binary and ternary mixtures including monoacid saturated and mixed-acid saturated-unsaturated TAGs based on palmitic and oleic acid (Gibon & Durant, 1985).

Molecular compound formation in unsaturated TAGs was firstly reported by Moran (1963). Further work by Engström (1992) confirmed that β-2L molecular compounds occurred in the combinations of SOS/SSO, SOS/SPO, SOS/PPO, and POP/PPO. By using SR-XRD, Sato's group showed that, besides β-2L molecular compounds, also metastable α-2L and/or β'-2L molecular compounds occur in SOS/SSO, SOS/OSO, POP/PPO, and POP/OPO systems (Koyano et al., 1992; Minato et al., 1997a, 1997b; Takeuchi et al., 2002a). The same group also investigated the role of chain-chain interactions, glycerol conformation, and methyl end stacking in the structural stabilization of molecular compound structures by Fourier transform infrared spectroscopy (FT-IR) (Minato et al., 1997c; Yano et al., 1993; Yano & Sato, 1999).

The formation of molecular compounds may be more easily understood by considering the molecular structure models of pure component TAGs and analyzing the stabilizing or destabilizing molecular interactions between them (Bayés-García et al., 2015a; Minato et al., 1997a, 1997b; Zhang et al., 2007), as depicted in Figure 1.9. In this regard, it is worth mentioning the close structural properties between molecular compounds ascribed to the pairs SOS/SSO and POP/PPO, and SOS/OSO and POP/OPO (Minato et al., 1997c), which allow foreseeing an equivalent nature of the molecular interactions that are involved in their stabilization.

It is assumed that the glycerol group of TAGs in the solid phase adopts a "tuning fork" conformation in symmetric TAGs (achiral) and a "chair" conformation in asymmetric TAGs (chiral) (Craven & Lencki, 2012). As previously indicated, in the "tuning fork" conformation, the acyl chains at *sn*-1 and *sn*-3 positions pack alongside each other and in the opposite direction of that at *sn*-2 position. In the "chair" configuration, the chain at *sn*-2 is alongside that at *sn*-1 (or *sn*-3), whereas the one at sn-3 (or *sn*-1) remains alone. The structure of $MC_{POP/OPO}$ would be stabilized by an opposite turn of the neighboring glycerol groups and separated saturated and unsaturated leaflets. Steric hindrance would be the driving force for crystal packing in a double chain-length structure. In such configuration, the close contact between glycerol and methyl end groups in stable β-3L structures of POP and OPO, and the subsequent excess energy for

molecular packing, would also be avoided. The occurrence of $MC_{POP/PPO}$ might be more difficult to explain since the unbalanced content in palmitic and oleic fatty acids may inevitably lead to the presence of adjacent palmitoyl and oleoyl chains in both leaflets. However, the destabilizing effect of palmitic-oleic interactions could be compensated if a structure with both TAGs in a "tuning fork" configuration is assumed. The disposition of glycerol groups in a parallel arrangement and with an opposite turn, together with affinity interactions in the palmitoyl leaflet, might be decisive in the stability of $MC_{POP/PPO}$. The strong specific interactions associated with molecular compound formation were confirmed by the crystallization of $MC_{POP/OPO}$ and $MC_{POP/PPO}$ from neat liquid and from diluted *n*-dodecane solutions (Bayés-García et al., 2011b; Ikeda-Naito et al., 2014; Ikeda et al., 2010).

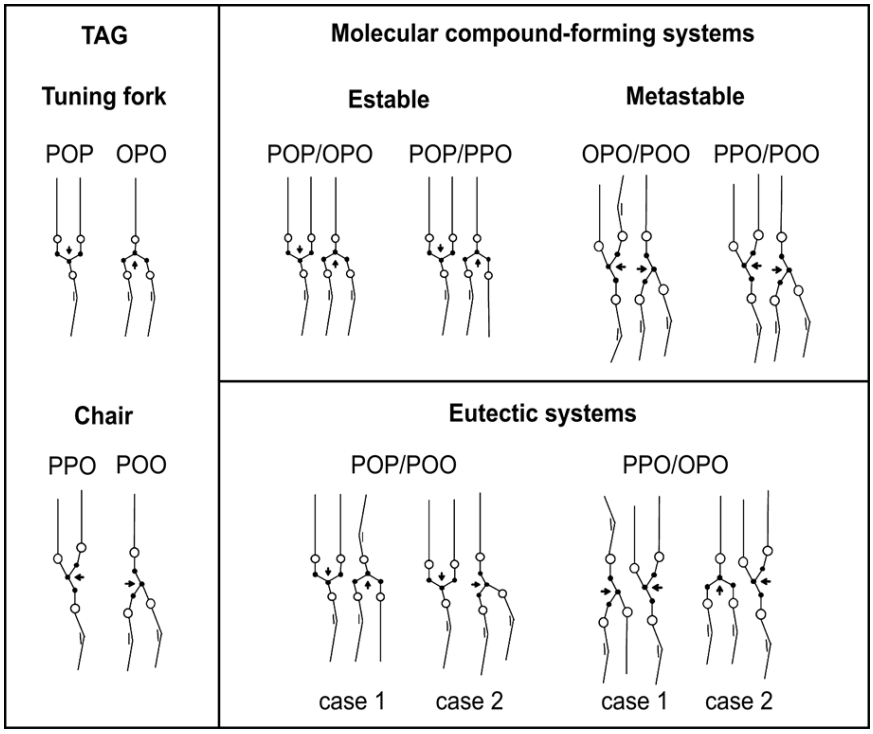

Figure 1.9. Proposed structural models for mixed-acid saturated-unsaturated TAGs and their binary mixtures. Adapted with permission from Bayés-García et al. (2015). Copyright (2015) American Chemical Society.

Chain-chain interactions and glycerol conformation also played a major role in the singular mixing behavior reported for the OPO/POO and PPO/POO systems during a 17-month period of thermodynamic stabilization. In both cases, molecular compound formation occurred in the metastable state but the systems tended to eutectic behavior over time (Bayés-García et al., 2015a). It was assumed that the occurrence of a metastable OPO/POO molecular compound

was favored by a stable oleoyl leaflet and the parallel disposition of neighboring glycerol groups, with that of OPO adopting a "chair" conformation. However, the eventual change to a more stable "tuning fork" glycerol conformation during thermodynamic stabilization would increase steric hindrance, thus explaining the metastable nature of the molecular compound. The metastability of PPO/POO molecular compound was hardly explained just by means of the proposed molecular structure. However, SR-XRD data on the 50PPO/POO mixture cooled and subsequently heated at 2 °C·min^{-1} suggested that the crystallization and transformation behavior was governed by competitive S-OPP/R-PPO, S-OOP/R-POO and (R-)S-OPP/(R-)S-OOP interactions. Thus, the racemicity exhibited by both TAGs could be the underlying cause of the metastability of $MC_{PPO/POO}$.

Contrary to the previous systems, the fatty acid disposition in PPO/OPO and POP/OOP systems led to eutectic behavior under stable and metastable conditions (Bayés-García et al., 2015a; Zhang et al., 2007). PPO/OPO exhibited a eutectic point near the pure OPO composition. Stable POP/POO mixtures displayed a peritectic-type phase diagram with each component solubilizing around 20% of the other in its solid phase. Similar behavior was found in stable SOS/*sn*-OOS mixtures, with only slight differences ascribed to the distinct polymorphism of TAGs containing palmitic and stearic fatty acids (Zhang et al., 2009). Thus, the immiscibility of these systems was presumably driven by incompatible interactions involving glycerol groups and hydrocarbon chains with no apparent influence on whether the chiral TAG is present in its optically active or racemic form.

The formation of complete solid solution in mixtures of mixed-acid saturated-unsaturated TAGs was revealed in SOS/SLiS mixtures in α-2L and γ-3L forms (Takeuchi et al., 2002b). Additionally, Rousset et al. (1998) reported complete miscibility of POS and SOS in the β_2 form. This system is directly related to CB, the polymorphic behavior of which is determined by a solid solution of its major TAGs POS, SOS, and POP. However, eutectic behavior can be found at specific compositions of this ternary system by cause of POS/POP interactions (Ghazani & Marangoni, 2019b; Koyano et al., 1993; Smith et al., 2013). The complete miscibility of TAGs is restricted to molecules with almost identical structural properties, so most combinations display eutectic behavior with partial miscibility. Nevertheless, the miscibility can be promoted through specific TAG interactions. In fact, the engineering of solid solutions with tunable functionalities is of practical importance in many food applications, for example the development of alternative fats to CB. In this connection, Watanabe et al. (2018) demonstrated that mixtures with constant

50% SOS and 50% SSO + OSO content crystallize in a β-2L form consisting of a solid solution of $MC_{SOS/SSO}$ and $MC_{SOS/OSO}$. Equivalent behavior was revealed in blends of CB, rich in saturated-unsaturated-saturated TAGs (Sat-Unsat-Sat), and interesterified fractions of fully hydrogenated canola oil rich in Sat-Sat-Unsat and Unsat-Sat-Unsat TAGs (Watanabe et al., 2021). It was also found that replacing 50% CB content by those fractions in dark chocolate preparations led to optimal properties in terms of hardness and fat bloom stability.

1.5.2. Phase behavior of complex lipid mixtures

The diverse TAG composition of a natural fat may lead to the simultaneous occurrence of different types of mixing behavior. Due to this, the characterization of the true phase behavior of blends of natural lipids is far more difficult than in multi-component TAG systems. In practice, blends of two fats can be treated as pseudo-binary systems, for which three types of phase behavior are recognized: complete solid solution, eutectic, and monotectic (Figure 1.10A).

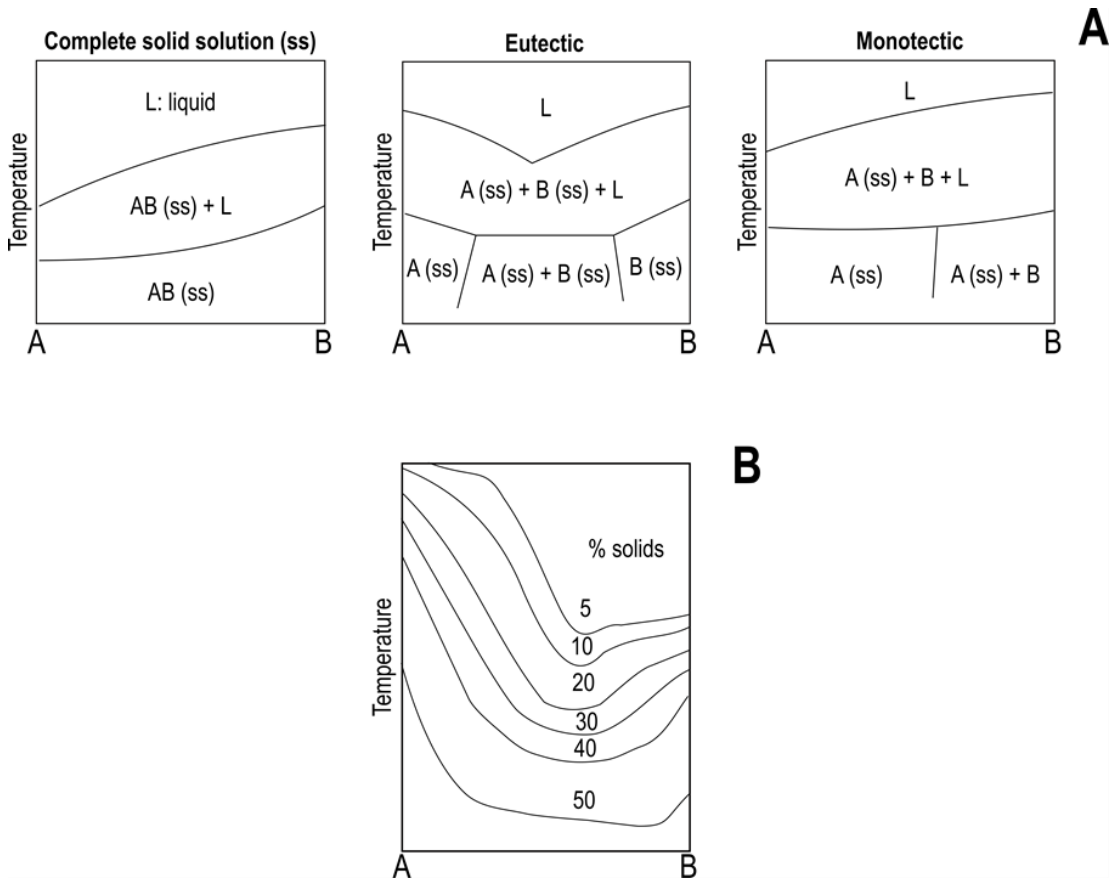

Figure 1.10. A) Pseudo-phase diagrams of binary blends of fats. Adapted with permission from Timms (1984), Copyright (1984) Elsevier. B) Typical isosolid diagram depicting eutectic interaction.

The principles ruling the mixing phase behavior of fats resemble those of pure TAGs. However, three aspects distinguish the binary blends of complex fats: i) the heterogeneous composition makes them exhibit broad melting point ranges rather than clearly defined melting points; 2) regarding eutectic systems, no precise eutectic points are encountered in pseudo-phase diagrams, but a eutectic minimum can be observed in the liquidus curve; and iii) in contrast to binary mixtures of pure TAGs, the region delimited by the liquidus and solidus lines do not provide information about the solid-liquid ratio of the system (Timms, 2003).

The macroscopic properties and physical stability of lipid-based products depend on the equilibrium of liquid and solid phases in the fat at specific temperature ranges (Silva et al., 2021). Thus, the study of the pseudo-phase diagrams alone may not be enough in real fat blending applications. In this respect, the determination of isosolid diagrams provides a clearer view of the compatibility and melting profile of fat blends (Figure 1.10B). For its construction, the isosolid points along the whole range of compositions are calculated from the proportion of solid fat or solid fat content (SFC) determined at varying temperatures by pulsed nuclear magnetic resonance (p-NMR). Additionally, isosolid and pseudo-phase diagrams may be combined to construct isosolid phase diagrams (Gordon et al., 1979).

The study of the phase equilibrium of complex lipids mixtures is essential for the development of new processes and products, for the improvement of those already existent, and for adding value to diverse byproducts from fruits, crops, and seeds (Maximo et al., 2014). This has led to extensive research aimed to unveil the mixing phase behavior of natural fats and oils from varied sources. For example, eutectic behavior was found in mixtures of CB with fractionated hydrogenated palm kernel oil (Williams et al., 1997), anhydrous milk fat (Sabariah et al., 1998), or shea butter (Rodriguez-Negrette et al., 2019). Mixtures of palm kernel oil with the stearin and olein fractions of palm oil also showed eutectic interaction (Liu et al., 2019; Zhou et al., 2010). The monotectic behavior gives rise to the undesirable oil migration occurring in blends of hard fats and nut oils. Examples of monotectic systems are the blends of CB with hazelnut and almond oils (Ziegler, 2009). Blends of beef tallow and canola oil (Meng et al., 2011), or coconut oil and palm oil stearin (Liu et al., 2018), also led to monotectic pseudo-phase diagrams. As in pure TAG mixtures, the occurrence of complete solid solutions is uncommon in fat mixtures. This behavior was suggested for blends of high and middle melting fractions of milk fat (Marangoni & Lencki, 1998).

Based on the above literature review, it can be deduced the importance of understanding the polymorphic and phase behavior of lipids from single TAG components to whole fat systems. In line with this, the present study seeks to gain deeper knowledge about the crystalline behavior of lipid blends involving both pure TAGs and real fats.

Regarding pure TAG mixtures, this thesis presents the results obtained during the phase behavior study of binary and ternary mixtures of monoacid saturated TAGs (PPP, LLL) and mixed-acid saturated-unsaturated TAGs able to form molecular compound (POP and PPO, or POP and OPO). The TAGs included in the mixtures were selected based on their importance in common raw materials used in the food industry. It is well known that the formation of molecular compound may occur naturally in diverse fats or be a consequence of the physical blending of different lipid materials. So far, the phase behavior of TAGs forming molecular compound and a third component has been largely unexplored. This study is a further step towards the characterization of the mixing interactions that determine the polymorphism and physical properties of complex lipid systems. In addition, the fundamental knowledge obtained from comparing the phase behavior of fully saturated TAGs and mixed-acid saturated unsaturated TAGs, either alone or forming molecular compound, could be of practical value for specific food applications. In this regard, a prior step to the study of TAG mixtures involved examining the polymorphic behavior of the individual components under the influence of dynamic thermal treatments.

As an example of a binary blend of real fats, we also examined the crystalline and thermal behavior of combinations including CB and shea butter stearin (ShS). The importance of this type of study relies on the need to find suitable fat-structured materials that help meet the high worldwide demand for CB-based products. In addition, this research closely relates to our study of multi-component TAG mixtures, since the polymorphic properties of CB/ShS blends are expected to be determined by a reduced number of components. More specifically, by the ternary system formed by POS, SOS, and POP.

CHAPTER 2

MATERIALS AND METHODS

2.1. MATERIALS AND SAMPLE PREPARATION

2.1.1. Materials

The sample materials used in this thesis included pure TAG components and natural fats.

1,2,3-tripalmitoyl-glycerol (PPP), 1,2,3-trilauroyl-glycerol (LLL), 1,3-dipalmitoyl-2-oleoyl-glycerol (POP), 1,3-dioleoyl-2-palmitoyl-glycerol (OPO), and 1,2-dipalmitoyl-3-oleoyl-rac-glycerol (PPO) with purity ≥ 99% were purchased from Larodan (Solna, Sweeden) and used as received.

Cocoa butter was donated by *Cacao Barry* (Gurb, Barcelona, Spain), and shea butter stearin was kindly supplied by *Lipidos Santiga S.A.* (Santa Perpetua de Mogoda, Barcelona, Spain).

2.1.2. Sample preparation

The mixing behavior studies included in Chapter 4 and Chapter 5 required the preparation of diverse binary and ternary mixtures of pure TAGs.

The binary mixtures PPP/OPO, PPP/POP, PPP/PPO, LLL/POP, and LLL/PPO were prepared in a similar manner. TAG components were mixed at different molar mass intervals in amber glass vials. These were then introduced in a water bath at 85 °C, a temperature far above the melting point of the high-melting component, and stirred repeatedly using a vortex mixer. To ensure the homogeneity of the mixtures, the heating-stirring step was performed for several minutes. Finally, the vials containing the mixtures were purged with N_2 to prevent oxidation and then stored at -20 °C until use.

In the ternary mixtures PPP/POP/OPO, PPP/POP/PPO, and LLL/POP/PPO, the mixed-acid saturated-unsaturated TAGs were maintained at a constant 1:1 ratio at all compositions to favor molecular compound formation. Thus, equimolecular POP/POP and POP/PPO mixtures were prepared in the first place by melting the components at 50 °C and stirring for several minutes. Then, different molar mass fractions of the same were blended with the trisaturated TAGs by following the same procedure as in binary systems. It is important to note that, given the constant ratio of unsaturated TAGs, and for simplification of the nomenclature, POP/OPO and POP/PPO in the mixtures will be indicated by their respective molecular

compounds. This means that, for example, the 50LLL/25POP/25PPO mixture will be referred to as 50LLL/50$MC_{POP/PPO}$.

Generally, blends containing from 0 to 100% of the components at 5-10% molar mass concentration intervals were prepared. In the case of PPP/POP mixtures, only specific compositions of interest were evaluated in order to compare the results with those obtained by previous work.

To study the phase behavior of the mixtures in most stable polymorphs, these were subjected to a long-term thermodynamic stabilization process in a cooled incubator. One of the main factors that contribute to hinder and prolong the stabilization of TAG systems is the low molecular diffusion rate in the solid state. In addition, the length of stabilization processes may be increased when incubation temperatures are far below the melting point of the components. This may cause the initially occurring metastable phases to enter in a "frozen" state which may persist for years (Wesdorp et al., 2013). For this reason, a two-step thermal incubation was carried out for TAG mixtures. The samples were first held for a few days at a temperature below the melting point of the higher melting component but above that of the lower melting component. This was done to favor the stabilization of the first one (monoacid saturated TAG). Then, the temperature was lowered below the melting point of the lower melting component (mixed-acid saturated-unsaturated TAG) and the samples were kept under such conditions for several months. The incubation temperatures were based on the melting temperatures reported by previous studies for the components of the mixtures. The specific length of the incubation process and the temperatures used for each mixture system are detailed in the chapters containing the corresponding results (see Tables 4.1 and 5.1).

The study on real fats included in Chapter 6 involved the preparations of mixtures of CB and ShS. The components were blended in amber glass vials at specific weight ratios and melted at 70 °C. To ensure homogeneity, the molten samples were stirred using a vortex mixer for several minutes. Five compositions with 95, 80, 70, 50, and 30% of CB were prepared. The samples were purged with N_2 to prevent oxidation after which they were stored at -20 °C until use.

2.2. EXPERIMENTAL TECHNIQUES

2.2.1. Differential Scanning Calorimetry

DSC is a thermoanalytical technique used to determine phase transitions in diverse organic and inorganic materials subjected to a specific time-temperature program. When a substance undergoes a phase transition, heat is released or adsorbed depending on whether the process is exothermic or endothermic, respectively. The DSC technique consists of measuring this change in the heat flow with respect to a reference material, which should no undergo phase transitions under the experimental conditions studied. For this reason, air is commonly used as a reference.

A DSC analysis results in a thermogram, which plots the heat flow as a function of either temperature or time. It depends on whether the DSC experiment is carried out at dynamic temperature conditions (cooling and heating treatments) or a static temperature (isothermally). The occurrence of exothermic events, such as crystallization, and endothermic events, such as melting, gives rise to peaks at opposite sides of a horizontal heat flow baseline.

Typical parameters used to describe the crystallization and melting phenomena observed in a thermogram include the onset, peak top, and end temperatures (T_{onset}, T_{top}, and T_{end}, respectively), and the enthalpy (ΔH). T_{onset} is the temperature at which the formation or melting of the first crystals begin, whereas T_{top} is the temperature at which the crystallization or melting processes are completed and T_{end} corresponds to the baseline recovery. T_{onset} and T_{end} are calculated from the intersection of the tangent lines at the front and back sides of the DSC peak, respectively, and the extrapolated baseline. The ΔH associated with the melting or crystallization corresponds to the area delimited by the baseline and the DSC peak.

The physical phenomena of lipids that can be studied by DSC include glass transitions, melting profiles, heats of fusion, and percent crystallinity (Peyronel & Campos, 2012). It is also useful to determine the occurrence and type of polymorphic transitions. Due to this, the DSC technique proved to be a rapid, sensitive, and reproducible method to fingerprint the thermal behavior of natural fats and oils (Bayés-García et al., 2017, 2021).

2.2.1.1. *Experimental methodology*

Thermal analysis of the samples (polymorphic crystallization, transformation, and melting events) were performed using PerkinElmer DSC Diamond and DSC 8000 calorimeters operating under the same conditions. The measurements were carried out at atmospheric pressure and under a nitrogen flow of 20 $cm^3 \cdot min^{-1}$. The melting temperature and enthalpy of indium and n-decane standards were used for the calibration of the instruments. An empty DSC pan was used as reference.

Lipid samples were weighed (4.0-4.4 mg) into 50 μL aluminum pans and hermetically sealed. Then, sample and reference pans were subjected to a dynamic thermal treatment consisting of cooling from the melt and/or heating at different rates. For each thermal treatment, at least three independent samples (n=3) were measured.

The thermograms resulting from the DSC analyses were processed by Pyris software to obtain T_{onset}, T_{top}, and T_{end} (°C), and ΔH ($J \cdot g^{-1}$) of the main phenomena observed. The calibration of the equipment was performed at 2 °C·min^{-1}, so a correction was applied to the samples subjected to other rates (PerkinElmer, 1982). The corrected values ($T_{correct}$) were obtained through the equation

$$T_{correct} = T_{obs} - C \cdot (dT/dt)_a + C \cdot (dT/dt)_b$$

where T_{obs} corresponds to the temperature value observed, C is a constant (0.085), $(dT/dt)_a$ is the rate of the analysis, and $(dT/dt)_b$ is the calibration rate. To attain a 95% confident interval of the measurements, the standard error was estimated using the Student's method approximation.

Depending on the purpose of the analysis and the nature of the sample (pure TAGs, TAG mixtures, or fat mixtures), different thermal protocols were used.

To examine the thermal behavior of TAG mixtures subjected to thermodynamic stabilization, the samples were held for 1 minute at 0 or 10 °C and then heated at 2 °C·min^{-1} until complete melting.

The thermal behavior of pure TAGs, TAG mixtures, and real fat mixtures was examined during the application of dynamic thermal treatments at varying cooling and heating rates. The samples were first held at a temperature far above the melting point of the higher melting

component. These were then cooled to a specific temperature and subsequently heated until complete melting. The end temperature of cooling treatments and the cooling/heating rates used varied according to the type of sample. The specific thermal protocols are detailed in the chapters concerning the results.

In Chapter 6, significant differences in the crystallization and melting temperatures between cocoa butter, shea butter stearin, and their blends were determined at p-value < 0.05 through a one-way analysis of variance (ANOVA) with a post-hoc Tukey's test. For this, SPSS Statistics 25.0 software was used.

2.2.2. X-Ray Diffraction

X-ray diffraction (XRD) is one of the most powerful techniques for analyzing the atomic or molecular structure of crystalline materials. It can be distinguished between single-crystal XRD and powder XRD. The first one is preferred for an accurate determination of crystalline structures. However, in many materials, the difficulty of growing single crystals with enough size or quality to be analyzed limits the applicability of this technique. Powder XRD is used for the study of polycrystalline or powdered samples, in which tiny crystals of varying sizes are arranged in random orientations. This is the standard technique to analyze lipid crystals. However, single-crystal XRD has been successfully used to solve stable and metastable polymorphic structures of some lipid components, including TAGs (Goto et al., 1992; Jensen & Mabis, 1963; van Langevelde et al., 2000).

Depending on the source of the X-rays, two techniques are differentiated: laboratory-scale XRD and synchrotron radiation X-ray diffraction (SR-XRD).

The radiation in laboratory-scale X-ray diffractometers is normally generated in a vacuum tube containing two principal elements: a filament or cathode, and a target or anode. The filament, often made of wolframium, is heated to produce electrons, which then are accelerated towards the target anode by applying a voltage. The emission of X-rays is caused by the deceleration undergone by the electrons when hitting the target anode. Depending on the target material (copper, iron, molybdenum, chromium), a group of wavelengths dominates the X-rays generated. This radiation is then filtered to reduce the range of wavelengths and produce a monochromatic beam.

Synchrotron light is the electromagnetic radiation emitted by charged particles, generally electrons, which have been accelerated to nearly the speed of light through high-powered magnetic fields. The electrons are injected into a storage ring, where they are forced to follow a circular orbit for many hours. Synchrotron radiation is generated when electromagnetic devices located at different points of the ring cause a change in the trajectory of the electrons. This leads to a loss of energy, which is released in the form of light with a wide energy spectrum (from infrared light to X-rays). The light is then directed to the beamlines surrounding the ring, each one designed to conduct a concrete type of investigation. The high intensity of synchrotron light allows the real-time observation of processes like phase transitions or chemical transformations. The excellent signal-to-noise ratio also permits the clearer determination of macromolecular structures by X-ray diffraction. However, the special large facilities needed to generate the light impedes the use of SR-XRD as an experimental technique of routine.

When a beam of monochromatic X-rays strikes a crystal at an angle θ with respect to a set of crystalline planes, it is scattered in all directions by the atoms within the crystal lattice. In some directions, constructive interferences take place, which lead to the formation of detectable diffracted X-rays. According to Bragg's law, constructive interference occurs when the length of the path traveled by X-rays reflected from adjacent planes at a distance *d* differs by an integer multiple (n) of the wavelength (λ) (Figure 2.1). This is expressed by the Bragg's law as

$$\lambda n = 2d \sin\theta$$

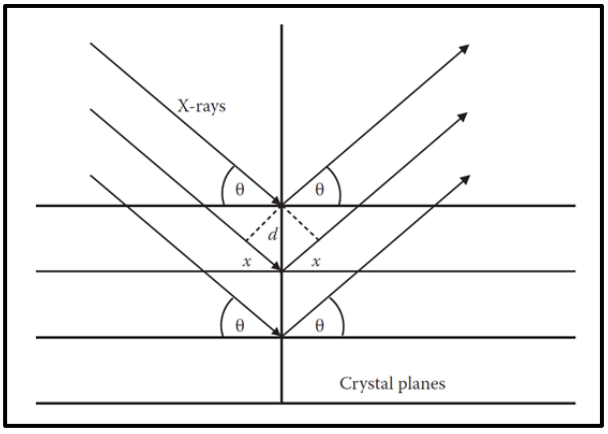

Figure 2.1. Scheme of the path length traveled by X-rays reflected from parallel planes. Reprinted with permission from Marangoni & Wesdorp (2013b). Copyright (2013) Taylor & Francis Group, LLC.

When this equation is satisfied, peaks or reflections occur in the X-ray spectra or diffraction pattern. These are characterized by the X-ray counts (intensity) and 2θ position, which corresponds to the angle between the incident and reflected X-ray beams. Since λ is a known parameter, the *d*-spacing or interplanar distance responsible for a specific reflection can be determined from θ through Bragg's law. According to the scattering angle, the reflections are classified into small-angle (SAXD) and wide-angle XRD reflections (SAXD). In lipids, SAXD reflections (long spacing values) provide information about the chain-length structure and the arrangement of interlamellar planes. WAXD reflections (short spacing values) are characteristic of the subcell structure. The combination of SAXD and WAXD data is the basis of the polymorphic identification during the X-ray diffraction study of lipid materials.

2.2.2.1. *Experimental methodology*

The same thermal processing implemented in DSC was applied to laboratory-scale XRD and SR-XRD experiments in order to attain polymorphic identification. When cooling and heating rates equal or exceeding 5 °C·min^{-1}, SR-XRD was always the technique of choice.

Laboratory-scale XRD measurements were carried out in the facilities of the scientific and technical services of the UB (CCiTUB). For these, a PANalytical X'Pert Pro MPD powder diffractometer equipped with a hybrid monochromator and a PIXcel detector was used. The equipment operated with Debye-Scherrer transmission and temperature control was achieved through an Oxford Cryostream Plus 220V. The samples were introduced in a 1 mm diameter Lindemann glass capillary, which was rotated about its axis in the course of the experiment to minimize preferential crystalline orientation. The step size was 0.013° from 1° to 28° 2θ, and the measuring time 150 s per step. Diffraction data were analyzed with X'Pert Highscore V2.2e software.

SR-XRD measurements were carried out at beamline BL11-NCD-SWEET at the ALBA synchrotron (Cerdanyola del Vallès, Barcelona, Spain) at 12.4 keV. SR-SAXD data was collected on a Pilatus 1M detector with a pixel size of 172 X 172 μm^2. SR-WAXD data was collected on a LX255-HS Rayonix detector with a pixel size of 40 X 40 μm^2. An aluminum cell with Kapton film windows was used to hold 2mm-thick sample during the measurements, whose temperature was controlled by a Linkam stage. The q-axis calibration was obtained by measuring silver behenate for SR-SAXD and Cr_2O_3 for SR-WAXD. SR-XRD spectra were acquired at 20 s or

30 s intervals, depending on the cooling and heating rates applied. The program pyFAI was used to integrate the 2D SR-WAXD into the 1D data; the SR-SAXD data were processed with in-house software. Data analysis was performed using Igor Pro V6.3.7.2 software.

2.2.3. Polarized Light Microscopy

Polarized light microscopy (PLM) is a contrast-enhancing technique used to observe materials with an optically anisotropic character. The polarizing microscope includes two polarizing filters. The first one, which is located between the light source and the sample, is used to produce a beam of light waves oscillating in a single plane (linearly polarized light). The second one, also known as analyzer, is located between the sample and the ocular lens. When the polarizer and analyzer are at an angle of 90° to each other, the light generated by the first one is extinguished. This is the so-called "dark position", which leads to the visualization of a black background. However, if the sample contains anisotropic elements, these will become visible. When the beam light originated by the first polarizer passes through an anisotropic material, it splits into two orthogonal waves traveling at different speeds. This phenomenon is known as birefringence or double refraction. The emitted waves are recombined when reaching the analyzer, which gives rise to a high contrast image. Lipid crystals are birefringent, so they usually appear as bright features which may present different tones. These are the so-called interference colors. By contrast, liquid oil and non-crystalline lipid material contribute to the dark background due to their optical isotropy.

PLM provides direct information about the size and shape of the crystals and aggregates forming the fat crystal network of a sample. By using complementary techniques, such as XRD or Raman spectroscopy, the morphological features may be associated with specific polymorphs. However, different processing conditions result in varying microstructures for the same polymorph (Kellens et al., 1992; Marangoni & McGauley, 2003), so PLM is not intended as an identification technique. Coupling a hot/cold stage to the microscope permits emulating the time-temperature protocols applied during DSC and/or XRD experiments. Therefore, the microstructural changes occurring in the sample during crystallization, melting, and polymorphic transformation events may be visually monitored. This technique can be referred to as thermo-optical polarized light microscopy (TOPLM). In addition, the combination of PLM and image analysis techniques can also be used to study nucleation and crystal growth processes, as well as

the mass-spatial distribution (fractal dimension) of fat crystal networks (Narine & Marangoni, 1999).

2.2.3.1. *Experimental methodology*

The Microscopic study of samples subjected to dynamic thermal treatments was carried out by using a Nikon Eclipse 50iPol Microscope with a Linkam THMSG-600 stage attached. The system was coupled to an LNP liquid nitrogen cooling system and a TMS94 temperature controller. To visually analyze the sample behavior detected by DSC and XRD analyses, images were captured at different time intervals using a Nikon Digital Camera DXM1200F and Linksys 32 software.

Samples evaluated at static temperature conditions were analyzed by a Nikon Eclipse LV100N POL polarized light microscope linked to a Nikon DS-Ri2 camera. Images of the samples were taken with the NIS-Elements BR 5.20.02 software data capture system. The temperature of the sample was controlled by adjusting the room temperature.

For the microscopic analyses, 1.5 μL of molten lipids were pipetted into a glass slide, after which a coverslip was placed on top of the sample. The same was then lightly tapped in order to remove air bubbles. The specific thermal protocols applied during TOPLM (pure TAGs) and PLM (CB, ShS, and their blends) experiments are indicated in the chapters concerning the results. In all cases, the experiments were performed in duplicate.

2.2.4. Pulsed Nuclear Magnetic Resonance

The proportion of solid fat or solid fat content (SFC) of a fat sample at a specific temperature or set of temperatures can be measured by pulsed nuclear magnetic resonance (p-NMR). This technique analyzes the response of hydrogen nuclei (protons) placed in a magnetic field and subjected to a short pulse of radiofrequency energy. Applying this pulse to a sample, such as a fat, generates a measurable magnetization signal with an amplitude proportional to the number of protons contained. Once the pulse stops, the protons undergo a relaxation phenomenon towards the original state. This causes a decay in the magnetization signal, which is faster for the protons in the solid phase than in the liquid phase.

The SFC can be estimated by sampling at two suitable time points of the magnetization decay (Campos, 2005). Depending on these, the SFC is determined through the direct or indirect method. The direct method measures the response of the protons in the solid and liquid phases (~11 μs after the pulse) and the response corresponding only to the liquid phase (~70 μs) (ISO, 2008). These are used to calculate the response attributed only to the solid phase. Thus, the SFC will be defined by the ratio, expressed as a percentage, between the signal in the solid phase and the signal in the solid and liquid phases. Through the indirect method, the SFC is estimated by comparing the signal from the liquid phase with the signal obtained for the same sample when fully melted at a higher temperature. The temperature effect on the instrument sensitivity is eliminated by measuring a liquid reference, usually triolein (OOO) or olive oil, at the same temperatures. Since this method is based on the weight of the samples, the inadequate filling of the measurement NMR tubes leads to inaccurate results. The insensitivity to the sample preparation technique and the simpler measurement protocol of the direct method makes it the preferred choice for SFC routine analysis (Zhang et al., 2015).

2.2.4.1. *Experimental methodology*

The SFC determination was carried out in the facilities of *Lipidos Santiga S.A.* SFC analysis were carried out by using a Bruker NMR Minispec MQ20 analyzer. This technique was applied during the study of fat blends consisting of CB and ShS. Therefore, the specific procedure followed was the direct method described in the ISO 8292-1:2008 (ISO, 2008) standard for the SFC determination of β-stable fats.

Before p-NMR measurements, NMR tubes containing 2 ml of sample were introduced into a water bath and subjected to a multi-stage tempering process. This involved holding the samples at 0 °C for 90 min, then at 26 °C for 40 hours, and again at 0 °C for 90 °C. Finally, these were kept for 60 min at each measurement temperature before determining the SFC. The SFC curves were obtained from the SFC data obtained for two replicates at 10, 20, 25, 30, 25, 40, and 45 °C. The measurements were made in parallel, which means that different NMR tubes were tempered and measured at each temperature for the same sample.

SFC curves were fitted by the quadratic interpolation method described by Timms (1979) to determine the isosolid points and build a diagram of temperature against sample composition.

Thus, for each composition, the three first measuring temperatures (T_1, T_2, and T_3) and corresponding SFC values (S_1, S_2, and S_3) were used to estimate parameters a, b, and c in equation

$$S_i = aT_i^2 + bT_i + c$$

In this manner, we could determine T for each solid fat percentage desired within the range from S_1 to S_3. The first measurement was then discarded, and the process was repeated (S_2, S_3, and S_4) until all the SFC range was covered. When the same S_i was included in different ranges and more than one T resulted, the mean value was taken.

CHAPTER 3

EFFECT OF DYNAMIC THERMAL TREATMENTS ON THE POLYMORPHIC BEHAVIOR OF MONOACID SATURATED AND MIXED-ACID SATURATED-UNSATURATED TRIACYLGLYCEROLS

3.1. INTRODUCTION

As previously stated in the general introduction of this thesis, natural fats and oils are multi-component systems in which TAG molecules represent the major fraction. Therefore, the physical properties of lipid-based products from the pharmaceutical, cosmetic, and food industries are strongly determined by the TAG crystals formed during manufacture processes (Larsson et al., 2006). This means that an adequate control of industrial operations to obtain products with specific quality standards relies on an in-depth knowledge about the crystallization behavior of TAGs, which in turn passes through a good understanding of three main aspects: the molecular and crystal structures, solidification, and transformation properties, and the rheological and textural behavior resulting from the fat crystal networks formed (Sato, 1999).

Specific solidification properties of TAGs such as crystallization rate, crystal size, morphology, and network crystallinity are all interrelated and strongly influenced by polymorphism (Sato, 2001b). For example, β forms are associated with the formation of large crystals, which confer the desirable snap of chocolate products and flakiness in pie crust applications (Aini & Miskandar, 2007; Danthine & Deroanne, 2003; Ghotra et al., 2002). However, their occurrence may result in sandy texture and poor spreadability in end products such as margarine and shortenings, in which the fine crystal networks formed by the smaller β' crystals provide smoother mouthfeel, higher aeration, and improved creaming properties (de Man, 1998; de Man & de Man, 2001).

Therefore, one of the main challenges of industrial crystallization processes is setting the conditions to achieve the most suitable polymorphic forms to each specific application and prolonging their shelf-life to the maximum possible extent. For this, the first step is obtaining fundamental knowledge about the crystalline properties and polymorphic behavior of individual TAGs. From here, the elucidation of the polymorphic and mixing behavior of major TAG species in complex lipids and their blends, as well as their relationship with physical properties and functionalities, will be eased.

The occurrence of a specific polymorph rather than others during crystallization is primarily defined by a process of competitive nucleation. Based on German literature gathered until the end of the XIX century regarding the crystallization from the melt and solution of diverse organic and inorganic materials, Ostwald postulated its rule of stages (Ostwald, 1897), which is

still used as a guideline for understanding polymorphic crystallization and transformation phenomena of many substances (Bernstein, 2002). According to this rule, least stable forms tend to occur first during crystallization, which then evolve towards a more stable configuration. When different phase transformations can take place from a metastable form into a more stable one, often the polymorph with closest Gibbs free energy occurs and this behavior repeats until the lowest-energy (stable) polymorph is formed.

The behavior described above fits well with the observations made in diverse materials, including minerals (Bots et al., 2012; van Driessche et al., 2012), inorganic polymers (Hikosaka et al., 1994; Keller et al., 1994), or biomolecular crystals (Sazaki et al., 1996; Vekilov, 2010). However, this rule may not apply when systems are subjected to the influence of external factors and further studies are needed in such cases to obtain an accurate insight into the crystallization and polymorphic characteristics (Sato et al., 2013). In the specific case of lipids, research has focused on the effect of factors involved in actual industrial processes, such as the addition of indigenous or foreign materials (Badan Ribeiro et al., 2015; Smith et al., 2011) and the application of shear (Tran & Rousseau, 2016), sonication (Martini, 2013), or different thermal processing conditions (Bayés-García et al., 2018).

The great significance of thermal treatments in crystallization processes carried out on an industrial scale has led to a growing research interest in the kinetic influence of cooling and heating treatments on the crystalline properties of pure TAGs (Baker et al., 2014a, 2014b; Bayés-García et al., 2011a, 2013a, 2013b, 2016; Sato et al., 1989; Sato & Kuroda, 1987; Takeuchi et al., 2000; Ueno et al., 1997), their mixtures (Bhaggan et al., 2018a, 2018b,; Boodhoo et al., 2009a; Nakanishi et al., 2018; Nakanishi & Ueno, 2020; Rousset et al., 1998; Rousset & Rappaz, 1996), and more complex fats (Barba et al., 2013; Bayés-García et al., 2017; Campos et al., 2002; Danthine et al., 2015; Foubert et al., 2008; Kaufmann et al., 2012; Ray et al., 2013; Rigolle et al., 2016).

For instance, the isothermal crystallization study carried out by Sato & Kuroda (1987) on pure PPP between 35 and 65 °C confirmed the longest induction time for crystallization (τ_c) of the β form, intermediate of β', and shortest of the α form. Similar results were obtained by Koyano et al. (1989) when examining the kinetics of melt crystallization of POP and SOS, which also confirmed their higher rate of crystallization via melt-mediation as compared to simple melt-cooling at the same crystallization temperatures. In a further SR-XRD study by Ueno et al.

(1997), it was confirmed that, in addition to the characteristic polymorphic forms of SOS (α, γ, β', β_2, and β_1), liquid crystalline phases of smectic nature may occur during α transitions. Aiming to construct suitable phase development models, Rousset & Rappaz (1996, 1998) combined DSC and PLM techniques to investigate the morphology, nucleation, and growth kinetics of POP, POS, and SOS, the three major TAGs of CB, and the binary system POS/SOS. Bayés-García et al. (2011, 2013a, 2013b, 2016) performed a detailed study of the kinetic-dependent polymorphic crystallization and transformation pathways of pure mixed-acid saturated-unsaturated TAGs based on S, P, O, and Li fatty acids when subjected to cooling and heating treatments at varying rates. Later on, this fundamental research helped the authors attribute the overall polymorphic behavior of extra virgin olive oil to the combination of TAGs OOO, POO, OOLi, POLi, PPO, and SOO (Bayés-García et al., 2017).

Regarding complex lipid systems rich in monounsaturated TAGs, the stop-and-return DSC method introduced by Foubert et al. (2008) has been proved as a useful tool in the study of the crystallization mechanisms of fats such as CB, shea butter, and related mixtures (Danthine et al., 2015; Ray et al., 2013; Rigolle et al., 2016). In this method, the crystallization of the sample at a specific temperature is interrupted at different times. Then, the phase development is examined through differences in the melting profiles obtained during subsequent heating processes. As to non-isothermal crystallization studies, Campos et al. (2002) used anhydrous milk fat and lard as model fats to clarify the critical role of the cooling speed on the main factors (polymorphic occurrence, solid fat content, and microstructure) determining mechanical properties and hardness of lipidic materials.

In the present chapter, we describe the polymorphic crystallization and transformation behavior of the pure monoacid saturated TAGs PPP and LLL, and the mixed-acid saturated-unsaturated TAGs OPO and PPO when cooled from the melt and reheated at varying rates. All of them are relevant in edible industrial lipids and their polymorphic and thermal properties have been a matter of interest in many studies available in the scientific literature. Thus, one of the aims of DSC and X-ray diffraction data here reported is to review and complement experimental data delivered by previous authors. In addition, a first insight into the individual properties of these TAGs will help a better comprehension of the mixture systems under study in this thesis, which are discussed in Chapters 4 and 5.

3.2. POLYMORPHIC BEHAVIOR OF PURE TRIACYLGLYCEROLS

The crystallization, transformation, and melting behavior of pure monoacid saturated and mixed-acid saturated-unsaturated TAGs was evaluated during thermal treatments consisting of cooling from the melt to -80 °C, holding for one minute at isothermal conditions, and subsequently heating until complete melting. The cooling and heating rates applied depended on the specific TAG and ranged from 0.1 to 15 °C·min^{-1}. The thermal behavior was examined by DSC, whereas the polymorphic identification was performed through laboratory-scale XRD and SR-XRD. Unless otherwise indicated, T_{onset} will be used to define the temperature of the thermal events. In addition, TOPLM experiments were carried out under the same thermal conditions to monitor the microstructural changes occurring in TAG samples during the polymorphic events. The specifics about the experimental methods were included in Chapter 2.

3.2.1. Monoacid saturated triacylglycerols

Fully saturated monoacid TAGs are not usually major components in edible fats and oils but may determine the crystallization and melting behavior due to their high-melting properties. More concretely, these TAGs tend to crystallize first, and the solid material formed promotes the heterogeneous nucleation of lower-melting components. This so-called "seeding effect" is of practical value for the design of faster crystallization processes and PPP has proved to be suitable as a crystallization modifier of natural fats like palm oil, in which this TAG is naturally present (Basso et al., 2010), and oleic-rich blends including vegetable oils from diverse sources (Vereecken et al., 2009, 2010a, 2010b).

The isothermal crystallization and phase transformation kinetics of PPP under isothermal conditions has been deeply investigated (Kellens et al., 1990; Sato & Kuroda, 1987). Additionally, the DSC study carried out by Himawan et al. (2007) on PPP subjected to cooling and subsequent heating treatments at varying rates from 0.1 to 20 °C·min^{-1} shed some light on the influence of kinetics over the polymorphic occurrence and transformation behavior of this TAG. However, no studies have directly focused on the influence of varying thermal treatments on the polymorphic and thermal properties of LLL. Fats rich in this TAG such as coconut oil may be used in the formulation of structured lipids alternative to palm- and cocoa butter-based fat

materials. Thus, fundamental studies on this TAG become a matter of interest for further industrial applications.

This section reports on the polymorphic and thermal behavior of PPP and LLL when subjected to different thermal treatments consisting of i) cooling and reheating at a high rate of 15 °C·min^{-1}, ii) cooling and reheating at an intermediate rate of 2 °C·min^{-1}, and iii) cooling and reheating at rates of 0.5 or 0.1 °C·min^{-1}.

The relatively simple polymorphism of these TAGs, which present α, β', and β forms of double chain-length structure, results from the equivalent fatty acid substituents at the three *sn*-positions of the glycerol group. Long and short spacing values of PPP and LLL forms identified in this work and in previous studies used as references are shown in Tables 3.1 and 3.2, respectively.

Table 3.1. Long and short spacing values of main PPP polymorphic forms detected in the present (A) and previous work (B) (Kellens et al., 1990).

		sub-α-2L	**α-2L**	**β'-2L**	**β-2L**
A	Long spacing (nm)	4.5	4.5	4.2	4.1
	Short Spacing (nm)	0.41, 0.38	0.41	0.43, 0.42, 0.38	0.46, 0.39, 0.37
B	Long spacing (nm)	4.6	4.6	4.2	4.1
	Short Spacing (nm)	0.41, 0.38	0.41	0.42, 0.38	0.46, 0.39, 0.37

Table 3.2. Long and short spacing values of main LLL polymorphic forms detected in the present (A) and previous work (B) (Takeuchi et al., 2003).

		α-2L	**β'-2L**	**β-2L**
A	Long spacing (nm)	3.5	3.2	3.1
	Short Spacing (nm)	-	0.43, 0.42, 0.38	0.46, 0.39, 0.38
B	Long spacing (nm)	3.5	3.2	3.1
	Short Spacing (nm)	0.42	0.42, 0.38	0.46, 0.39, 0.38

The occurrence of several β' forms with different subcell packing and melting points has been suggested in monoacid saturated TAGs (Kellens et al., 1991a; Simpson & Hagemann, 1982) but it is still unclear if in some cases these changes were related to subtle differences in crystalline perfection and crystallinity rather than to significant changes in the molecular arrangement. Precht & Frede (1977) described the occurrence of two β forms in LLL. A further SR-XRD

study showed that the β_2 to β_1 transition of LLL results in a sharpening of characteristic β WAXD peaks and a subtle variation in their angular positions of less than 0.25 ° (Allais et al., 2003). Recent work on monoacid TAGs based on S, P, M, and L fatty acids (with 18, 16, 14, and 12 carbon atoms in their chain, respectively) showed that distinct thermal treatments and starting polymorphs (α or β') led to diverse β forms with similar subcell structure during polymorphic transformations (Takeguchi et al., 2020). Since further research is still needed for a better characterization of different β' and β sub-modifications in monoacid TAGs, these forms will be simply referred to as β' and β in this section.

3.2.1.1. 1,2,3-Tripalmitoyl-glycerol (PPP)

3.2.1.1.1. Cooling from the melt and reheating at a high rate of 15 °C·min^{-1}

DSC and SR-XRD data obtained when PPP was cooled from the melt to -80 °C and subsequently heated at 15 °C·min^{-1} is shown in Figure 3.1.

Upon cooling, a single exothermic signal was detected at T_{onset} of 41.2 °C by DSC. Diffraction peaks at 4.5 nm in the small-angle region (SAXD) and 0.41 nm in the wide-angle region (WAXD) of SR-XRD patterns allowed to confirm the crystallization of the α-2L form. No additional polymorphic events occurred during the cooling step according to DSC data but a weak reflection with *d*-spacing of 0.38 nm was detected in SR-WAXD almost at the end of cooling. This was due to the change from a hexagonal to a pseudo-hexagonal subcell typically shown by TAGs with diverse composition, symmetry, and degree of unsaturation during α → sub-α transitions at sub-zero temperatures (Kellens et al., 1990; Mykhaylyk & Martin, 2009).

When reheating, the sub-α → α-2L transformation was followed by the melting of α-2L, which in DSC was spotted at 44.5 °C. Afterward, a broad exothermic peak corresponding to several polymorphic events appeared at 48.4 °C. Despite the complexity of the phenomena, SR-SAXD and SR-WAXD patterns enabled the identification of the corresponding polymorphic transformations. Thus, at 58 °C the intensity of the α-2L peak at 4.5 nm decreased at the expense of a new one at around 4.2 nm in SR-SAXD, whereas the occurrence of a new peak at 0.38 nm in SR-WAXD indicated the crystallization of β'-2L. SAXD peaks corresponding to α-2L and β'-2L were no longer seen when reaching 62 °C, and emerging peaks at 0.46, 0.39, and 0.37 nm confirmed the transformation of the metastable β'-2L form into β-2L, which finally melted at 63.2 °C.

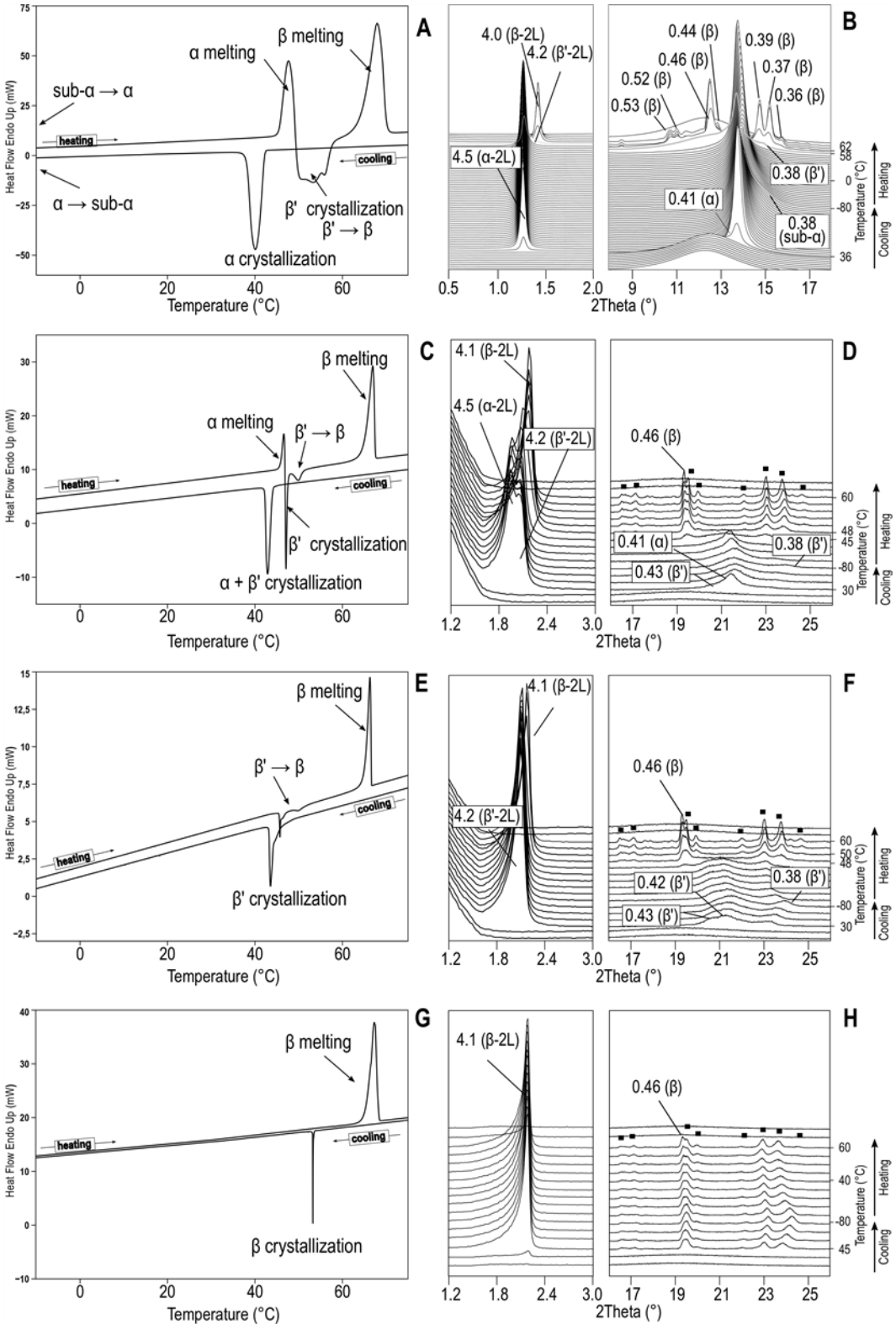

Figure 3.1. DSC thermograms (left) and XRD data (right) of PPP when cooled and subsequently heated at different rates. (A, B) Cooling and heating at 15 °C·min^{-1}, (C, D) cooling and heating at 2 °C·min^{-1}, (E, F) cooling and heating at 0.5 °C·min^{-1}, and (G, H) cooling at 0.1 °C·min^{-1} and heating at 2 °C·min^{-1}. ■ denotes characteristic WAXD peaks of PPP β form. *d*-spacing values are given in nm.

The fast-heating conditions applied did not permit clarifying the polymorphic transformation pathway followed by PPP during the β'-2L transformation due to overlapping of DSC thermal signals. The monitoring of β'-2L development and transformation by SR-XRD was also hindered by the 5 °C difference between patterns. Figure 3.2 depicts the TOPLM micrographs taken during the heating treatment of α crystals at 15 °C·min^{-1}. The liquid medium originated in the sample due to the α-2L melting was still present after β'-2L crystals were obtained and during the microstructural related to the β'-2L → β-2L transition. Despite the lack of confirmation, the conversion of β'-2L into β-2L through the melt would agree with previous XRD, DSC, and microscopy studies on the transformation behavior of PPP β' isothermally crystallized. During heating processes at 1 °C·min^{-1}, β' transformed into β via melt-mediation at temperatures ranging from 52 to 60.5 °C depending on the perfection in molecular packing allowed by the crystallization conditions (Kellens, Meeussen, & Reynaers, 1992, 1990; Stewart, Chong, & Stapley, 2017). In line with this, one explanation for the short-life shown by β'-2L in SR-XRD patterns may be the low stability induced by a rapid and less perfect molecular packing under fast heating. This would favor the quick transformation of β'-2L into β-2L soon after recrystallizing from the α-2L melt. It cannot be ruled either that some β-2L formed directly from the α-2L melt when reaching elevated temperatures close to that of β'-2L melting.

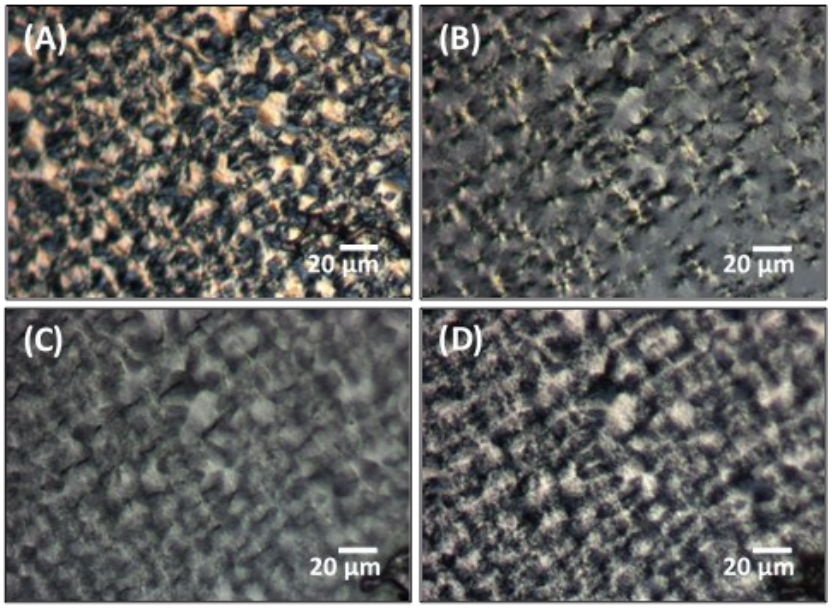

Figure 3.2. Polarized micrographs of PPP obtained during heating at 15 °C·min^{-1} soon after a melt cooling process at the same rate. (A) α spherulites at 38 °C; (B) α melting at 46 °C; (C) β' crystals + liquid at 51 °C; and (D) β crystals + liquid at 60 °C.

3.2.1.1.2. Cooling from the melt and reheating at intermediate and low rates

PPP cooled at 2 °C·min^{-1} showed the concurrent crystallization of β'-2L and α-2L at 43.7 °C (Figures 3.1C and 3.1D). When reheating at the same rate, a set of close events involving a first endothermic peak followed by two consecutive exothermic peaks were detected by DSC. The strengthening of the peak at 4.2 nm at the expense of that at 4.5 nm in the SAXD region at 45 °C indicated that α-2L melted first and β'-2L crystallized. The second exothermic event at around 47 °C was due to the β'-2L → β-2 solid-solid transformation. At a close temperature, the SAXD reflection had shifted towards a *d*-spacing of 4.1 nm and highly intense typical β WAXD peaks emerged (denoted by ■). Finally, stable β-2L form melted at around 65 °C.

For PPP cooled at 0.5 °C·min^{-1} (see Figures 3.1E and 3.1F), laboratory-scale XRD confirmed the sole occurrence of β'-2L (reflections at 0.43, 0.42 and 0.38 nm). During reheating, the solid-state transformation of this form into β-2L before complete melting resulted in the double exothermic event starting at 45.7 °C in the corresponding thermogram. When lowering the speed of cooling to 0.1 °C·min^{-1}, single exothermic and endothermic events related to the crystallization and melting of β-2L occurred throughout the whole thermal treatment (Figures 3.1G and 3.1H).

The results here confirmed by XRD are in agreement with previous data on PPP obtained by Himawan et al. (2007). Based on the Δ*H* and the characteristic temperatures of DSC peaks obtained during cooling, the authors suggested that the occurrence of α was promoted at cooling rates from 20 to 2.5 °C·min^{-1}, under which concurrent crystallization of α-2L and β'-2L took place. Moreover, only when cooling rates of 0.2 °C·min^{-1} and below were applied, enough time was provided to allow the nucleation and subsequent growth of the β-2L phase.

It should be noted that the occurrence of the intermediate β'-2L form of PPP during α-2L → β-2L transformations has been overlooked in several studies solely based on thermal analysis (Himawan et al., 2007; Lu et al., 2019). Our results show that the latter occurs during thermal processing when applying from intermediate to fast heating rates. They also evidence the important complementary role of powerful identification techniques, such as XRD, to obtain a more accurate picture of the polymorphic behavior of lipid systems.

3.2.1.2. 1,2,3-Trilauroyl-glycerol (LLL)

3.2.1.2.1. Cooling from the melt and reheating at a high rate of 15 °C·min^{-1}

Figures 3.3A and 3.3B show the experimental data obtained for LLL when cooled and subsequently heated at 15 °C·min^{-1}.

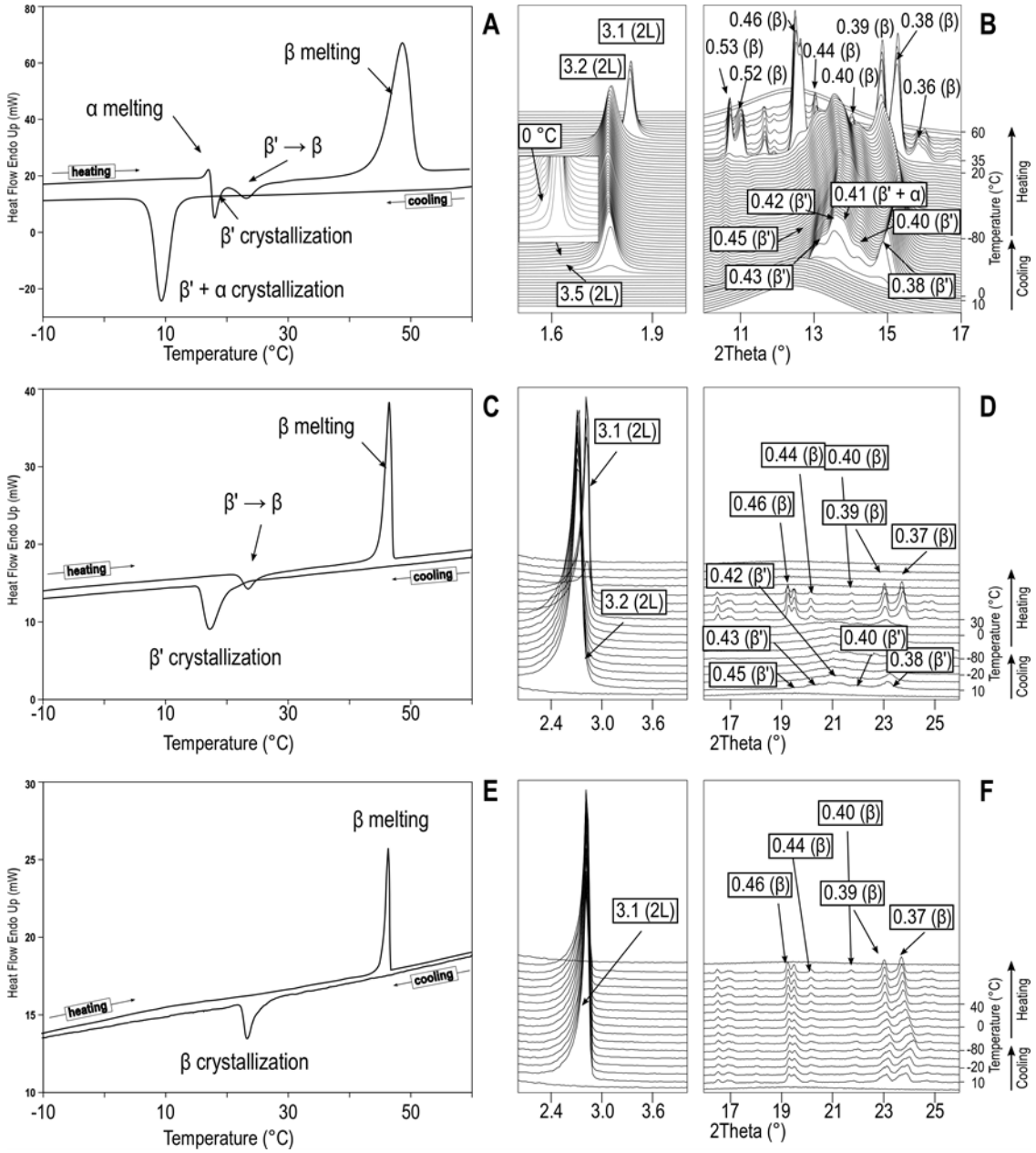

Figure 3.3. DSC thermograms (left) and XRD data (right) of LLL cooled and subsequently heated at different rates. (A, B) Cooling and heating at 15 °C·min^{-1}, (C, D) cooling and heating at 2 °C·min^{-1}, and (E, F) cooling and heating at 0.5 °C·min^{-1}. *d*-spacing values are given in nm.

On cooling, a single exothermic event at around 8 °C was detected by DSC. In SR-XRD patterns obtained at 10 °C, the occurrence of SAXD reflection at 3.2 nm and WAXD reflections at 0.43, 0.42, and 0.38 nm confirmed the crystallization of this TAG in the β'-2L form. In addition, a weak reflection at 3.5 nm arose in SAXD patterns when reaching 0 °C (see the amplified image). We assumed that also some α-2L crystallized (Takeuchi et al., 2003; Yoshikawa et al., 2020).

In a similar manner to PPP, the transformation behavior of LLL when reheated at 15 °C·min^{-1} was characterized by the transition of polymorphic forms to the next one in order of increasing stability until the whole sample was molten. The α-2L melting peak at 15.7 °C in DSC was followed by an exothermic event attributed to β'-2L recrystallization. Then, another exothermic event occurred at 22 °C which, according to SR-WAXD reflections at 0.46, 0.39, and 0.38 nm, clearly discernible at 35 °C, corresponded to the β'-2L to β-2L transition. The proximity of the former polymorphic events, which were partially overlapped in the corresponding heating curve, hindered the clear distinction of the polymorphic transformation pathway followed by β'-2. However, taking into consideration the much higher temperature of 35 °C ascribed to the β'-2L melting of this form (Takeuchi et al., 2003), it can be assumed that the β'-2L → β-2L transformation took place via the solid-state.

It can be noticed the quite distinguishable α-2L → β'-2L and further β'-2L → β-2L transformation peaks shown by LLL in DSC if compared with the greatly convoluted ones displayed by PPP at the same heating rate (see Figure 3.1). This evidences a higher shelf-life of β'-2L of LLL than that of PPP, which may be in part explained by the different polymorphic solidification pathways shown by each TAG. In LLL, most of the crystallized mass was in the β'-2L polymorph at the end of the cooling process at 15 °C·min^{-1}, whereas in PPP this form was obtained from the α-2L melt and, therefore, its occurrence was influenced by the corresponding rate of transformation. Previous work on PPP and SSS showed that β' to β transitions are more favored when β' is obtained from the least stable α than when directly obtained through melt cooling (Kellens et al., 1991b; Kellens & Reynaers, 1992a). The less-dense molecular packing of β' crystals obtained through a rapid polymorphic transformation would lead to an accelerated transformation into the most stable form. As previously mentioned, this may have contributed to the short-lived β'-2L form identified for PPP at these conditions.

In addition, the influence of the length of aliphatic chains over phase transitions of TAGs with even-numbered fatty acids should not be disregarded. A previous work on monoacid saturated TAGs pointed to an inverse relationship between the number of carbon atoms in aliphatic chains of fatty acids and the kinetic stability of β' forms obtained via α-melt mediation during heating processes (Aronhime, 1988). This would eventually lead to a single thermal signal associated with the β' crystallization and next β' → β in large molecules even at reduced heating rates, in which the separation of DSC phenomena is normally improved. The latter certainly contributes to the difficult, often neglected, identification of short-life β'-2L forms of SSS and PPP during α to β transitions shown by previous work (Bouzidi & Narine, 2012a; Garti et al., 1989; Himawan et al., 2007).

3.2.1.2.2. Cooling from the melt and reheating at intermediate and low rates

Figures 3.3C-F depict thermal and structural data obtained for LLL when lower cooling and heating rates were applied during the thermal processing.

The cooling treatment at 2 °C·min^{-1} resulted in the crystallization of the whole mass of the monoacid TAG in β'-2L, which during reheating at the same rate transited to β through the solid-state before the final melting.

When the rate was decreased to 0.5 °C·min^{-1}, single peaks in the corresponding cooling (23 °C) and heating (46 °C) thermograms, and XRD patterns indicating an invariable packing in the triclinic parallel subcell, evidenced that only β-2L was present during the whole thermal treatment. However, subtle changes in WAXD data when reaching 40 °C showed that subcell packing was modified during the heating process. The broad β-2L reflections at 0.46, 0.39, and 0.37 nm were noticeably sharper before the whole sample became liquid. No substantial changes were detected in SAXD patterns. The higher definition of WAXD peaks suggested an increase in the crystallinity of β-2L. As discussed earlier, this behavior has been associated with the transition from a less stable to a more stable β-2L form ($\beta_2 \rightarrow \beta_1$) (Allais et al., 2003).

3.2.1.3. Summary of monoacid saturated triacylglycerols

Tables 3.3 and 3.4 summarize the overall crystallization, transformation, and melting behavior found during the study of PPP and LLL, respectively. As shown, in both TAGs the occurrence of the least stable polymorph was favored by the application of a high cooling rate, whereas decreasing the speed promoted the nucleation and growth of more stable forms. During reheating, polymorphs obtained under the different conditions transformed into the next one in order of increasing thermodynamic stability.

The crystallization behavior shown by these TAGs did not comply with the Ostwald step rule, which states that least stable polymorphs, with closest thermodynamic properties to the parent phase, tend to form first during crystallization, and then transform sequentially into the next one until achieving the most stable configuration (Chung et al., 2009; Ostwald, 1897). This is in line with previous research on pure TAGs, their mixtures, and more complex lipids subjected to the influence of external factors (Bayés-García et al., 2018; Sato, 2001b).

Table 3.3. DSC data of the polymorphic crystallization and transformation behavior of PPP when cooled and subsequently heated at different rates.

	Cooling at 15 °C·min^{-1}		**Heating at 15 °C·min^{-1}**			
	a (c)	*a → sub-a*	*sub-a → a*	*a (m)*	*β′ (c)/ β′ → β*	*β (m)*
T_{onset} (°C)	41.2 ± 0.4	n.d.	n.d.	44.5 ± 0.4	48.4 ± 0.6	63.2 ± 0.5
ΔH (J·g^{-1})	-118 ± 16			80 ± 11	-144 ± 23	189 ± 22
	Cooling at 2 °C·min^{-1}		**Heating at 2 °C·min^{-1}**			
	a + β′ (c)		*a (m)*	*β′ (c)*	*β′ → β*	*β (m)*
T_{onset} (°C)	43.7 ± 0.7		45.5 ± 0.7	46.6 ± 0.8	47.4 ± 0.8	64.6 ± 0.7
ΔH (J·g^{-1})	-125 ± 4		33 ± 2	-91 ± 5[a]		203 ± 6
	Cooling at 0.5 °C·min^{-1}		**Heating at 0.5 °C·min^{-1}**			
	β′ (c)		*β′ → β*	*β (m)*		
T_{onset} (°C)	44.5 ± 0.3		45.7 ± 0.3	65.3 ± 0.2		
ΔH (J·g^{-1})	-137 ± 9		-19 ± 4	206 ± 6		
	Cooling at 0.1 °C·min^{-1}		**Heating at 2 °C·min^{-1}**			
	β (c)		*β (m)*			
T_{onset} (°C)	53.4 ± 1.4		65.7 ± 0.5			
ΔH (J·g^{-1})	-185 ± 7		211 ± 6			

(c): crystallization; (m): melting; n.d.: not determined. [a]ΔH corresponds to the global enthalpy of the overlapped phenomena.

Table 3.4. DSC data of the polymorphic crystallization and transformation behavior of LLL when cooled and subsequently heated at different rates.

	Cooling at 15 °C·min^{-1}		**Heating at 15 °C·min^{-1}**				
	a + *β′ (c)*	*a* → *sub-a*	*sub-a* → *a*	*a (m)*	*β′ (c)*	*β′* → *β*	*β (m)*
T_{onset} (°C)	8.2 ± 0.3	n.d.	n.d.	15.7 ± 0.7	16.7 ± 0.8	21.9 ± 0.8	47.1 ± 0.9
ΔH (J·g^{-1})	-101 ± 4			3 ± 0.3	-54 ± 2[a]		186 ± 6
	Cooling at 2 °C·min^{-1}		**Heating at 2 °C·min^{-1}**				
	β′ (c)		*β′* → *β*	*β (m)*			
T_{onset} (°C)	17.8 ± 1.2		23.9 ± 1.0	46.8 ± 0.9			
ΔH (J·g^{-1})	-129 ± 4		-47 ± 1	191 ± 5			
	Cooling at 0.5 °C·min^{-1}		**Heating at 0.5 °C·min^{-1}**				
	β (c)		*β (m)*				
T_{onset} (°C)	23.4 ± 0.2		46.5± 0.2				
ΔH (J·g^{-1})	-143 ± 5		189 ± 4				

(c): crystallization; (m): melting; n.d.: not determined. [a]ΔH corresponds to the global enthalpy of the overlapped phenomena.

The overall behavior observed is explained by considering that the polymorphic-dependent crystallization of TAGs under varying temperature conditions is determined by the rate of nucleation, which in turn is ruled by two main factors: the activation free energy of nucleation (ΔG_n) and the degree of supercooling (ΔT or T_m-T_c) (Sato & Kuroda, 1987). ΔG_n is defined by

$$\Delta G_n = K\gamma^3/(\Delta\mu)^2$$

where K is a constant, γ is the interfacial free energy of crystals, which is generally higher at increasing polymorphic stability (α → β' →β), and Δμ represents the difference in chemical potential or Gibbs free energy per molecule between the liquid and the solid-state. As illustrated by the diagram of Figure 3.4A, at a fixed T_c below T_m of the least stable form, the magnitude of Δμ is largest for the stable β form, intermediate for β' and smallest for the least stable α form, and directly proportional to the rate of crystal growth (Hondoh et al., 2018; Wagh & Martini, 2017). However, at reduced T_c, the difference in Δμ between polymorphic forms is minimized and the nucleation rate is primarily dictated by γ (Himawan et al., 2006; Hondoh et al., 2018). Therefore, the formation of α forms is generally promoted at lower T_c, as confirmed by DSC and XRD data obtained when cooling PPP and LLL at the highest rate. Then, a decrease in ΔT by reducing the cooling rate (increase in T_c) will break this tendency and favor the occurrence of more stable polymorphs depending on the influence of kinetic factors (Figure 3.4B).

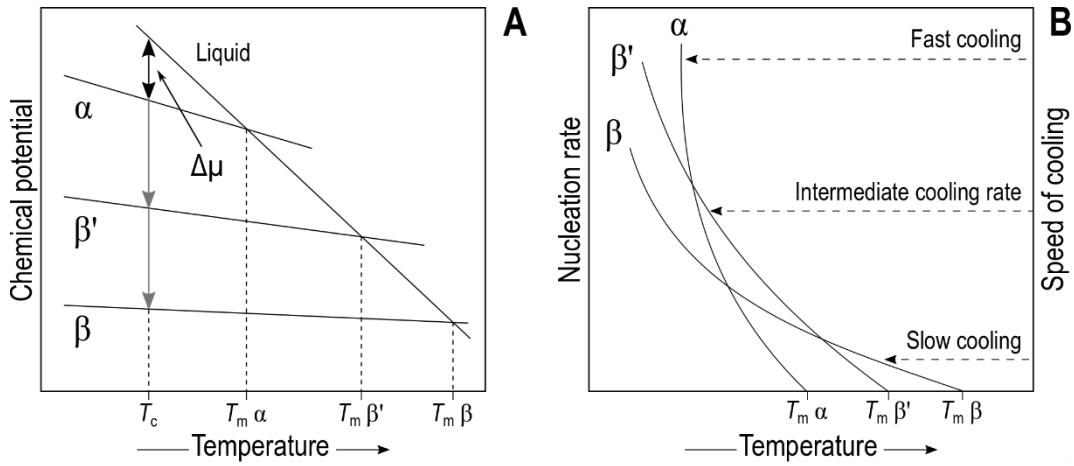

Figure 3.4. (A) Driving force for the polymorphic crystallization (Δμ) from the liquid. (B) Scheme of the polymorphic nucleation rate as a function the cooling speed. Adapted with permission from Sato & Ueno (2011), Copyright (2011) Elsevier.

The above mentioned translated into the occurrence of more stable PPP and LLL polymorphs at decreasing cooling rate. The effect was especially noticeable in LLL, which crystallized in the β'-2L form when cooling at 2 °C·min^{-1} and β-2L at the low rate of 0.5 °C·min^{-1}. By contrast, PPP still showed α-2L crystals at 2 °C·min^{-1} and a cooling rate below 0.5 °C·min^{-1} was needed for the β-2L form to occur. In a previous study, SSS showed to crystallize exclusively in the α-2L form when cooling rates from 25 to 1 °C·min^{-1} were applied, whereas β-2L crystals became predominant when lowering the rate to 0.1 °C·min^{-1} (Bouzidi & Narine, 2012b). According to Himawan et al. (2007), the different polymorphic occurrence between TAGs at the same cooling rate would not be due to differences in the driving force of crystallization, since once T_m is passed during the cooling process, the degree of supercooling as a function of time increases at the same extent independently of the sample composition. Therefore, the divergent polymorphic occurrence displayed by PPP and LLL must be attributed to their distinct chemical nature.

Previous work underscored the strong influence exerted by the methyl end terrace configuration on the polymorphic occurrence of TAGs under the application of dynamic thermal treatments. In mixed-acid saturated-unsaturated TAGs, the enabled crystallization of POP in α-2L as compared to SOS was attributed to the length of the constituent saturated fatty acid chains (Koyano et al., 1989). In POP, the similar length between the straight palmitic acid and the bent oleic acid results in a low perturbation of the lamellar packing. The longer stearic

acid moieties of SOS would protrude in the interlamellar space, and the instability induced may favor the occurrence of the more stable γ-3L even at T_c below the melting point of α-2L (SOS).

In the sequence of fully-saturated TAGs SSS, PSS, and PPS the increasing number of missing $–CH_2$ groups in aliphatic chains was directly related with a higher structural disturbance at the methyl end region and subsequent favored crystallization of polymorphic forms of decreasing stability (Bouzidi & Narine, 2012a). Specifically, at the low cooling rate of 0.1 °C·min^{-1}, PPS still showed predominant α crystals, whereas β' ones prevailed in PSS. However, in monoacid saturated TAGs such as CCC, LLL, PPP, and SSS the contact between methyl end group regions may not completely explain the distinct polymorphic occurrence at equivalent kinetic conditions, since all of them present a common almost flat methyl terrace (de Jong & van Soest, 1978) (see as an example the molecular structure of LLL in Figure 3.5). Thus, the reasons for this behavior remain unclear but our results evidence a direct relationship between longer hydrocarbon chains and a more hindered molecular packing in ordered and dense structures.

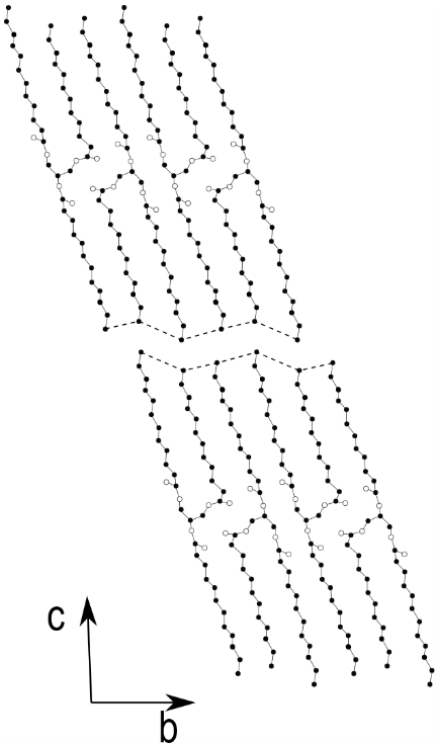

Figure 3.5. Lamellar structure of LLL. The almost flat terrace formed by methyl end groups is indicated by dotted lines. Adapted with permission from Larsson (1972). Copyright (2006) John Wiley & Sons.

3.2.2. Mixed-acid saturated-unsaturated triacylglycerols

Mixed-acid saturated-unsaturated TAGs represent the major fraction of most common animal and vegetable lipids with edible purposes. For example, OPO is the dominant molecular species in lard (Marikkar et al., 2013) and contributes to the softening of lipid-based food products due to a melting point near 22 °C. With increased palmitic acid content, PPO is not only a determinant TAG in higher-melting fractions of semi-solid fats such as lard and palm oil (Basiron, 2005; Noorzyanna et al., 2017), but also exerts a relevant role in the crystallization behavior of extra virgin olive oil (Bayés-García et al., 2017). In addition, a particularity of this TAG is its β' stability, which is desired for the development of shortenings and spreadable lipid products. The ability of both OPO and PPO to form binary molecular crystal compounds with POP stable at ambient temperature becomes another property with potential exploitation in fat structuring applications.

Tables 3.5 and 3.6 depict the main polymorphic forms and corresponding *d*-spacing values of OPO and PPO. As shown, the combination of saturated and unsaturated fatty acids in the same TAG molecule results in a more complex polymorphism as compared to monoacid TAGs. Basically, diverse β' and β forms with well-differentiated molecular packing can be found. Moreover, chain shorting due to steric hindrance between palmitic and oleic acid is responsible for the occurrence of triple chain-length structures in these TAGs. In the case of PPO, symmetric factors are also responsible for the impeded packing in the triclinic subcell structure typical of the β form.

Table 3.5. Long and short spacing values of OPO polymorphic forms detected in the present (A) and previous work (B) (Bayés-García et al., 2011a).

		sub-α-2L	**α-2L**	**β'-2L**	**β_2[1]**	**β_1-3L**
A	Long spacing (nm)	5.2, 5.0	5.1	4.3	5.6 (2.8)	6.4 (3.2)
	Short Spacing (nm)	0.41, 0.37	0.41	0.44, 0.42, 0.39	0.46	0.46, 0.38, 0.37
B	Long spacing (nm)	5.4, 5.2	5.3	4.4	-	6.7
	Short Spacing (nm)	0.42	0.42	0.43, 0.40	-	0.46, 0.38, 0.37

[1]Undefined chain-length structure

Table 3.6. Long and short spacing values of PPO polymorphic forms detected in the present (A) and previous work (B) (Mizobe et al., 2013).

		sub-α_2-2L	sub-α_1-3L	α_2-2L	α_1-3L	β'_2-2L	β'_1-3L
A	Long spacing (nm)	4.1	3.9	4.9 → 4.1	7.6 (3.9)	4.2	6.4 (3.2)
	Short Spacing (nm)	0.42,0.38	0.42, 0.38	0.41	0.41	0.42, 0.39	0.42, 0.38
B	Long spacing (nm)	-	-	4.98 → 3.92	7.8	4.2	6.7
	Short Spacing (nm)	-	-	0.41	0.41	0.41, 0.38	0.41, 0.38

→ denotes a change in the lamellar organization of the initially formed crystals.

Previous work examined the polymorphic behavior of OPO during thermal treatments consisting of cooling at rates from 0.5 to 15 °C·min^{-1} and subsequent heating at a constant rate of 15 °C·min^{-1} (Bayés-García et al., 2011a). To shed more light on the kinetic crystallization and transformation properties of this TAG, this section presents the thermal and structural data obtained when subjecting OPO to three different thermal protocols including different speeds of heating: (i) cooling and reheating at 15 °C·min^{-1}, (ii) cooling and reheating at 2 °C·min^{-1}, and (iii) cooling and reheating at 0.5 °C·min^{-1}.

Little is known about the influence of dynamic thermal treatments on the crystallization and transformation behavior of PPO, since previous work on this TAG was mainly addressed to highlight polymorphic differences between the pure enantiomeric forms and the racemic compound formed by these at a 1:1 ratio (Mizobe et al., 2013; Norris, 1977). To go a step further, we used DSC, laboratory-scale XRD, and SR-XRD to investigate the kinetic effect on the polymorphic behavior of racemic PPO when subjected to dynamic thermal treatments at rates ranging from 0.1 to 15 °C·min^{-1}.

3.2.2.1. 1,3-dipalmitoyl-2-oleoyl-glycerol (OPO)

3.2.2.1.1. Cooling from the melt and reheating at a high rate of 15 °C·min^{-1}

The main polymorphic events identified by XRD during the thermal processing of OPO at different conditions, together with the ΔH and T_{onset} estimated for the corresponding DSC thermal signals, are depicted in Table 3.7.

Table 3.7. DSC data of the polymorphic crystallization and transformation behavior of OPO when cooled and subsequently heated at different rates.

	Cooling at 15 °C·min^{-1}		**Heating at 15 °C·min^{-1}**				
	a (c)	*a* → *sub-a*	*sub-a* → *a*	*a (m)*	*β′ (c)*	*β′* → *β*$_1$	*β*$_1$ *(m)*
T_{onset} (°C)	-14.4 ± 0.3 -21.5 ± 0.4	-45.1 ± 0.4	-32.3 ± 1	-20.2 ± 0.8	-18.7 ± 0.8	-6.6 ± 0.7	16.2 ± 1.2
ΔH (J·g^{-1})	-44 ± 1	-10 ± 1	11 ± 1	2 ± 0.3	-28 ± 1	-30 ± 1	138 ± 11
	Cooling at 2 °C·min^{-1}		**Heating at 2 °C·min^{-1}**				
	β$_1$ + *β*$_2$ + *β′ (c)*		*β′* → *β*$_1$ + *β*$_2$	*β*$_2$ *(m)*	*β*$_1$ *(c)*	*β*$_1$ *(m)*	
T_{onset} (°C)	-6.4 ± 0.7		-3.5 ± 1.2	n.d.	13.9 ± 0.4	18.8 ± 0.7	
ΔH (J·g^{-1})	-82 ± 2		-41 ± 2		-8 ± 2	144 ± 5	
	Cooling at 0.5 °C·min^{-1}		**Heating at 0.5 °C·min^{-1}**				
	β$_1$ + *β*$_2$ + *β′ (c)*		*β′* → *β*$_1$ + *β*$_2$	*β*$_2$ *(m)*	*β*$_1$ *(c)*	*β*$_1$ *(m)*	
T_{onset} (°C)	-4.0 ± 0.9		-2.9 ± 0.3	8.8 ± 0.6	10.6 ± 0.6	19.3 ± 0.3	
ΔH (J·g^{-1})	-122 ± 6		-8 ± 2	10.2 ± 3	-27 ± 4	149 ± 3	

(c): crystallization; (m): melting; n.d.: not determined.

When OPO was cooled at a rate of 15 °C·min^{-1}, two convoluted exothermic events were first detected in the corresponding DSC thermogram (weak and strong peaks at -14.4 and -21.5 °C, respectively, in Figure 3.6A). These were associated with the crystallization of α-2L by SR-XRD through diffraction peak at 5.1 nm in SAXD and peak at 0.41 nm in WAXD patterns (Figure 3.6B). At decreasing temperature, the peak at 5.1 nm split into two reflections at 5.2 and 5.0 nm. In addition, a new one appeared at 0.37 nm in WAXD patterns. From this, we concluded that the small exothermic peak occurring in the cooling thermogram at -45.1 °C corresponded to the α → sub-α transition.

When reheating at the same rate, the broad DSC exothermic peak at -32.3 °C and the next sharper one at -20 °C indicated the reverse sub-α → α-2L transformation and the upcoming melting of α-2L. Soon after, a strong exothermic event occurred at -18.7 °C which, according to the emerging SR-WAXD peaks at 0.44 and 0.39 nm around the same temperature, was due to the crystallization of β'-2L. At increasing temperature, the intensity of the SAXD peak at 4.3 nm, associated with β'-2L decreased in intensity until its disappearance at around 3.5 °C. Simultaneously, characteristic peaks of triple chain-length structure at 6.3 and 3.1 nm (002 reflection) were observed, and new reflections at 0.55, 0.53, 0.46, 0.39, 0.38 and 0.37 nm occurred in WAXD patterns. Thus, we identified the exothermic peak observed in DSC at around -7 °C as the β'-2L → β$_1$-3L solid-solid transformation. Finally, the most stable form of OPO melted at about 16 °C.

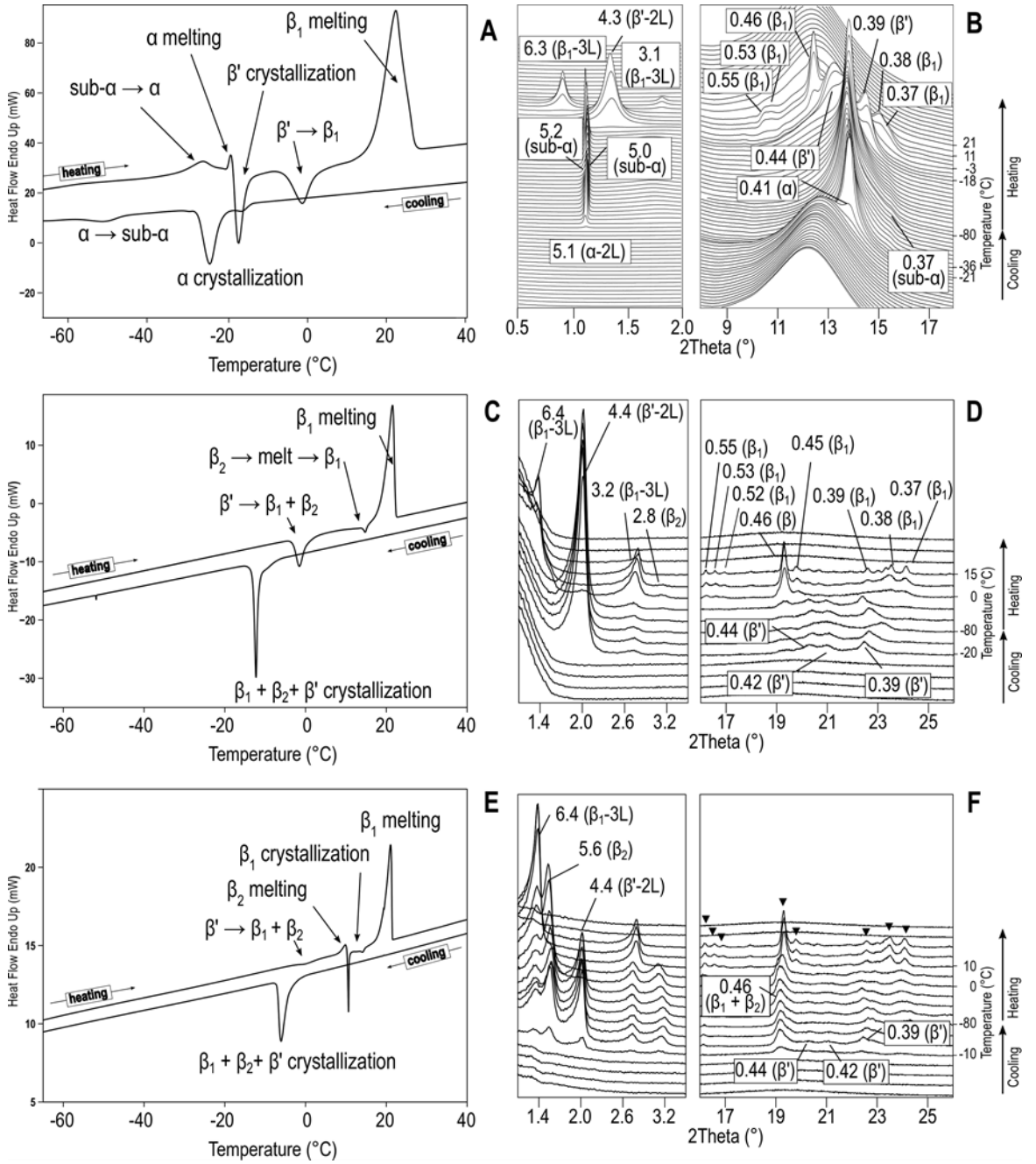

Figure 3.6. DSC thermograms (left) and XRD data (right) of OPO cooled and subsequently heated at different rates. (A, B) Cooling and heating at 15 °C·min^{-1}, (C, D) cooling and heating at 2 °C·min^{-1}, and (E, F) cooling and heating at 0.5 °C·min^{-1}. ▼ denotes characteristic WAXD peaks identified for OPO β_1 form. *d*-spacing values are given in nm.

3.2.2.1.2. Cooling from the melt and reheating at intermediate and low rates

At lower cooling rates of 2 °C·min^{-1} and 0.5 °C·min^{-1}, the corresponding DSC thermograms showed exothermic peaks at -6 °C and -4 °C, respectively (Figures 3.6C and 3.6E). In both cases, laboratory-scale XRD patterns obtained at -20 °C confirmed the concurrent crystallization of

β_1-3L, β_2, and β'-2L forms (Figures 3.6D and 3.6F). β'-2L could be easily identified by the SAXD peak at 4.4 nm and WAXD peaks at 0.44, 0.42, and 0.39 nm. Due to the structural similarities between β_2 and β_1-3L, the simultaneous presence of these forms could only be discriminated by 002 reflections detected at 2.8 and 3.2 nm, respectively (Minato et al., 1997b). In addition, the relative intensity of these (and the corresponding 001 ones at 5.6 and 6.4 nm) in XRD patterns at the end of cooling showed the promoted crystallization of β forms, particularly β_2, with respect to β'-2L when the rate was decreased from 2 °C·min^{-1} to 0.5 °C·min^{-1}.

The transformation and melting behavior of β'-2L, β_1-3L, and β_2 crystals when heated at 0.5 and 2 °C·min^{-1} were highly similar. First, a solid-state transformation of β'-2L into β_2 and β_1-3L took place, followed by the melting of β_2 and further crystallization of β_1-3L just before its melting. In the heating thermogram at 2 °C·min^{-1}, the exothermic peak at -3.5 °C corresponded to the β'-2L → β_1-3L + β_2 transformation, as confirmed by the concurrent decrease in intensity of WAXD peaks at 0.44, 0.42, and 0.39 nm and increase in those characteristic of the two β forms in XRD patterns at 0 °C. On further heating, the SAXD reflection associated to β_2 (2.8 nm) was no longer seen at 15 °C, indicating that the exothermic peak registered at around 14 °C corresponded to its transformation into the stable β_1-3L. The β_2 melting peak was not clearly discerned by DSC at this heating rate, but endothermic and exothermic events at 9 and 11 °C, respectively, displayed by OPO heated at 0.5 °C·min^{-1}, confirmed the melt-mediated nature of the β_2 to β_1-3L transition.

From the results obtained, we may conclude a great dependence of the polymorphic transformation behavior of OPO β' on the heating rate applied. A β'-2L → β_1-3L + β_2 transformation occurred when low and intermediate rates were used, whereas the direct β'-2L → β_1-3L transformation was kinetically favored at the highest rate (15 °C·min^{-1}). Moreover, by considering results obtained in previous work, we can also highlight the key role of thermal history and polymorphic occurrence during cooling on the transformation behavior of OPO when reheating. The β'-2L form obtained through the α-2L melt when heating at 5 °C·min^{-1} also transformed directly into β_1-3L, but concurrent β_2 and β_1-3L were obtained at the same heating rate when β'-2L was obtained by melt cooling (Minato et al., 1997b). Complementarily, SR-XRD experiments confirmed that the β'-2L → β_2 transformation during heating treatments at 15 °C·min^{-1} was inhibited when also β_1-3L crystals were obtained in the crystallization process (Bayés-García et al., 2011a). Accordingly, the β'-2L → β_1-3L + β_2 transformation confirmed in the present work during heating treatments at 2 and 0.5 °C·min^{-1} might have been favored by

both the lower rates applied and the concurrent presence of small amounts of β_1-3L and β_2 in the crystallized mass at the end of the cooling step. The latter might have exerted a template effect in the course of the β'-2L melt recrystallization.

3.2.2.2. 1,2-dipalmitoyl-3-oleoyl-rac-glycerol (PPO)

The polymorphic crystallization and transformation behavior of PPO was evaluated during a thermal processing consisting of cooling and reheating at varying rates from 0.1 to 15 °C·min^{-1}. Thermal data of the main polymorphic events identified are gathered in Tables 3.8 and 3.9.

3.2.2.2.1. Cooling from the melt at 15 °C·min^{-1} and reheating at different rates

The first DSC exothermic event shown by PPO when cooling at 15 °C·min^{-1} (peak at T_{onset} of around 16 °C in Figure 3.7A) was ascribed to the crystallization of α_2-2L through diffraction peaks detected at 4.9 and 0.41 nm in SR-SAXD and SR-WAXD patterns at 9 °C, respectively (Figure 3.7B). Soon after, the decrease in *d*-spacing value of the SAXD peak to 4.1 nm suggested a difficult packing of this TAG, probably due to steric interactions between saturated and unsaturated acyl chains. Previous work on SOS and SLnS (with Ln being linolenic acid) confirmed that configurational changes in α_2-2L phases of unsaturated mixed-acid TAGs during cooling can be favored by the presence of empty regions in the lamellar structures formed at the early stages of the crystallization (Mykhaylyk et al., 2007; Mykhaylyk & Martin, 2009).

The new SR-SAXD peak with *d*-spacing value of 3.9 nm detected at -1 °C indicated that also α_1-3L crystallized. In DSC, this was linked to the shoulder by the side of the α_2-2L crystallization peak (see the amplified image in Figure 3.7A). On further cooling, the exothermic event observed at -15 °C translated into the shifting of the SR-SAXD peak at 0.41 nm towards a *d*-spacing of 0.42 nm and the growth of a new one at 0.38 nm. These changes corresponded to an α → sub-α transition which, according to the complete disappearance of the reflection at 0.41 nm, took place for both α_2-2L and α_1-3L. The last exothermic peak at around -64 °C (and the endothermic one at -56 °C during the heating process) indicated the occurrence of a low-temperature reversible polymorphic event, the nature of which was not resolved by SR-XRD.

Table 3.8. DSC data of the polymorphic crystallization and transformation behavior of PPO when cooled at 15 and 2 °C·min^{-1}, and subsequently heated at different rates.

	Cooling at 15 °C·min^{-1}	
	$a_2 + a_1$ *(c)*	$a \rightarrow$ *sub-a*
T_{onset} (°C)	14.7 ± 0.2	-15.1 ± 0.7
ΔH (J·g^{-1})	-74 ± 2[a]	

	Heating at 15 °C·min^{-1}			
	sub-a → *a*	$a_2 \rightarrow m \rightarrow a_1$	$a_1 \rightarrow m \rightarrow \beta'_2$	β'_2 *(m)*
T_{onset} (°C)	-5.1 ± 0.3[b]	13.6 ± 0.3	17.2 ± 0.1	29.2 ± 0.4[b]
ΔH (J·g^{-1})	n.d.	76 ± 2[a]		<1

	Heating at 5 °C·min^{-1}				
	sub-a → *a*	$a_2 \rightarrow m \rightarrow a_1$	a_1 *(m)*	$\beta'_2 + \beta'_1$ *(c)*	$\beta'_2 \rightarrow m \rightarrow \beta'_1 \rightarrow m$
T_{onset} (°C)	-5.4 ± 0.3[b]	13.0 ± 0.9	18.0 ± 0.8	19.9 ± 0.7	29.1 ± 1.0
ΔH (J·g^{-1})	n.d.	2 ± 0.4	70 ± 0.3	-110 ± 3	114 ± 3

	Heating at 2 °C·min^{-1}						
	sub-a → *a*	$a_2 \rightarrow a_1$	a_1 *(m)*	$\beta'_2 + \beta'_1$ *(c)*	β'_2 *(m)*	β'_1 *(c)*	β'_1 *(m)*
T_{onset} (°C)	n.d.	n.d.	18.1 ± 0.8	19.1 ± 0.8	27.2 ± 1.0	28.6 ± 0.9	29.8 ± 1.0
ΔH (J·g^{-1})			50 ± 2	-89 ± 4	4 ± 1	-2 ± 1	106 ± 4

	Heating at 0.5 °C·min^{-1}						
	sub-a → *a*	$a_2 \rightarrow a_1$	a_1 *(m)*	$\beta'_2 + \beta'_1$ *(c)*	β'_2 *(m)*	β'_1 *(c)*	β'_1 *(m)*
	n.d.	n.d.	18.0 ± 0.3	18.5 ± 0.3	27.5 ± 0.3	28.4 ± 0.3	30.2 ± 0.3
			14 ± 5	-34 ± 6	3 ± 1	-9 ± 2	120 ± 10

	Cooling at 2 °C·min^{-1}	
	$a_2 + a_1$ *(c)*	$a \rightarrow$ *sub-a*
T_{onset} (°C)	16.9 ± 0.3	n.d.
ΔH (J·g^{-1})	-77 ± 2	

	Heating at 15 °C·min^{-1}			
	sub-a → *a*	$a_2 \rightarrow m \rightarrow a_1 \rightarrow m \rightarrow \beta'_2 \rightarrow m$		β'_2 *(m)*
T_{onset} (°C)	n.d.	17.6 ± 0.3		27.8 ± 0.5
ΔH (J·g^{-1})		77 ± 3		<1

	Heating at 5 °C·min^{-1}				
	sub-a → *a*	$a_2 \rightarrow m \rightarrow a_1$	a_1 *(m)*	$\beta'_2 + \beta'_1$ *(c)*	$\beta'_2 \rightarrow m \rightarrow \beta'_1 \rightarrow m$
T_{onset} (°C)	n.d.	13.7 ± 0.6	18.0 ± 0.6	20.0 ± 1.0	29.2 ± 0.3
ΔH (J·g^{-1})		<1	70 ± 5	-108 ± 0.3	112 ± 1

	Heating at 2 °C·min^{-1}						
	sub-a → *a*	$a_2 \rightarrow m \rightarrow a_1$	a_1 *(m)*	$\beta'_2 + \beta'_1$ *(c)*	β'_2 *(m)*	β'_1 *(c)*	β'_1 *(m)*
T_{onset} (°C)	n.d.	13.4 ± 0.2	17.8 ± 0.3	18.6 ± 1.0	26.7 ± 0.6	28.1 ± 0.5	29.5 ± 0.5
ΔH (J·g^{-1})		<1	47 ± 2	-86 ± 5	4 ± 1	-2 ± 0.4	108 ± 3

	Heating at 0.5 °C·min^{-1}						
	sub-a → *a*	$a_2 \rightarrow a_1$	a_1 *(m)*	$\beta'_2 + \beta'_1$ *(c)*	β'_2 *(m)*	β'_1 *(c)*	β'_1 *(m)*
T_{onset} (°C)	n.d.	n.d.	18.0 ± 0.4	18.4 ± 0.4	27.3 ± 0.3	28.2 ± 0.3	30.2 ± 0.3
ΔH (J·g^{-1})			16 ± 1	-38 ± 2	1 ± 0.1	-5 ± 0.4	130 ± 5

(c): crystallization; (m): melting; n.d.: not determined. [a]ΔH corresponds to the global enthalpy of the overlapped phenomena. [b]This value corresponds to T_{top}.

Table 3.9. DSC data of the polymorphic crystallization and transformation behavior of PPO when cooled at 0.5 and 0.1 °C·min^{-1}, and subsequently heated at different rates.

	Cooling at 0.5 °C·min^{-1}	
	$\beta'_2 + a_2 + a_1$ *(c)*	$a_1 \rightarrow sub\text{-}a_1$
T_{onset} (°C)	17.2 ± 0.3	n.d.
ΔH (J·g^{-1})	-91 ± 2	

	Heating at 15 °C·min^{-1}			
	$sub\text{-}a_1 \rightarrow a_1$	$a_1 \rightarrow m \rightarrow \beta'_2$	$\beta'_2 \rightarrow m \rightarrow \beta'_1$	β'_1 *(m)*
T_{onset} (°C)	n.d.	17.7 ± 0.6	21.5 ± 0.4	25.5 ± 0.4
ΔH (J·g^{-1})		86 ± 1[a]		

	Heating at 2 °C·min^{-1}				
	$sub\text{-}a_1 \rightarrow a_1$	a_1 *(m)*	$\beta'_2 + \beta'_1$ *(c)*	$\beta'_2 \rightarrow m \rightarrow \beta'_1$	β'_1 *(m)*
T_{onset} (°C)	n.d.	17.9 ± 0.3	18.8 ± 0.3	26.6 ± 0.3	29.7 ± 0.3
ΔH (J·g^{-1})		33 ± 6	-59 ± 8	108 ± 3[a]	

	Heating at 0.5 °C·min^{-1}					
	$sub\text{-}a_1 \rightarrow a_1$	a_1 *(m)*	$\beta'_2 + \beta'_1$ *(c)*	β'_2 *(m)*	β'_1 *(c)*	β'_1 *(m)*
T_{onset} (°C)	n.d.	18.3 ± 0.4	19.1 ± 0.5	27.5 ± 0.5	29.2 ± 0.5	30.3 ± 0.5
ΔH (J·g^{-1})		13 ± 1	-38 ± 5	7 ± 1	n.d.	111 ± -1

	Cooling at 0.1 °C·min^{-1}
	$\beta'_2 + \beta'_1$ *(c)*
T_{onset} (°C)	22.7 ± 0.3
ΔH (J·g^{-1})	-122 ± 6

	Heating at 2 °C·min^{-1}		
	β'_2 *(m)*	β'_1 *(c)*	β'_1 *(m)*
T_{onset} (°C)	24.7 ± 0.6	28.2 ± 0.7[b]	29.8 ± 0.6
ΔH (J·g^{-1})	4± 0.2	n.d.	115 ± 9

	Heating at 0.5 °C·min^{-1}	
	$\beta'_2 \rightarrow m \rightarrow \beta'_1$	β'_1 *(m)*
T_{onset} (°C)	25.5 ± 0.4[b]	30.1 ± 0.3
ΔH (J·g^{-1})	n.d.	125 ± 4

(c): crystallization; (m): melting; n.d.: not determined. [a]ΔH corresponds to the global enthalpy of the overlapped phenomena. [b]This value corresponds to T_{top}.

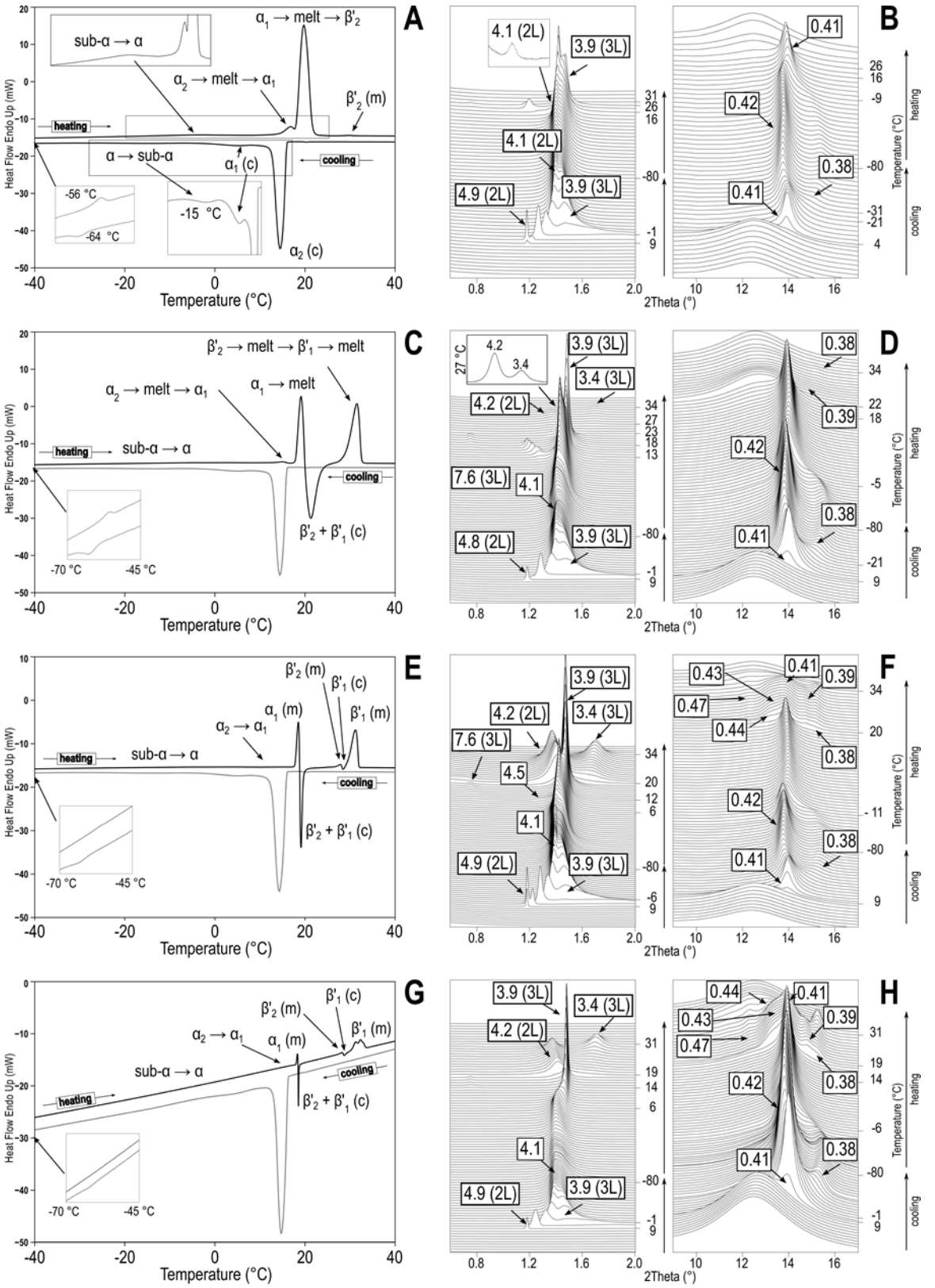

Figure 3.7. DSC thermograms (left) and SR-XRD patterns (right) of PPO cooled at 15 °C·min^{-1} and subsequently heated at (A, B) 15 °C·min^{-1}, (C, D) 5 °C·min^{-1}, (E, F) 2 °C·min^{-1}, and (G, H) 0.5 °C·min^{-1}. (c): crystallization; (m): melting. *d*-spacing values are given in nm.

When reheating at the same rate, the sub-α → α transition (see SR-WAXD patterns at around -9 °C) was monitored by DSC through a small perturbation in the baseline at 5 °C (see the heating curve in Figure 3.7A). Several degrees above, the reversibility of the changes in lamellar ordering undergone by α_2-2L during cooling was confirmed through the shifting of the SR-SAXD peak at 4.1 nm again towards a *d*-spacing of 4.9 nm. The further vanishing of this reflection and strengthening of that at 3.9 nm was indicative of the α_2-2L → α_1-3L transformation. In DSC, this polymorphic event corresponded to the melting peak observed at 13.6 °C, the overlapping of which with the next α_1-3L melting signal (T_{onset}=17.2 °C) hampered the identification of an intermediate crystallization event. No reflections were observed in SR-WAXD patterns when reaching 26 °C. However, given the weak reflection at 4.1 nm displayed by SR-SAXD patterns, it is reasonable to infer that the last DSC event observed at around 29 °C was due to the melting of some β'_2-2L crystals formed from the α_1 melt.

A similar sequence of polymorphic transformations (sub-α_2 + sub-α_1 → α_2 + α_1 → melt → α_1) occurred at the beginning of the heating process when a rate of 5 °C·min^{-1} was applied (see corresponding DSC and SR-XRD data in Figures 3.7C and 3.7D, respectively). However, the α_1-3L melting peak in DSC was succeeded by a strong crystallization event (T_{onset}=20 °C; ΔH=-110 J·g^{-1}) before the complete melting of the sample. The emerging reflections at 0.39 and 0.38 nm in SR-WAXD patterns, and 4.2 and 3.4 nm in SR-SAXD patterns above 20 °C indicated that both β'_2-2L and β'_1-3L forms were formed from the α_1-3L melt. Above 27 °C, the β'_1-3L SAXD reflection increased in intensity at the expense of the β'_2-2L one. Thus, the melting peak detected by DSC at 29 °C resulted from the convolution of the melt-mediated β'_2-2L → β'_1-3L transformation and the subsequent β'_1-3L melting.

The kinetic influence on the polymorphic transformation behavior of PPO during heating became patent through qualitative and quantitative changes in DSC and SR-XRD data when lower rates of 2 and 0.5 °C·min^{-1} were applied. The corresponding data is shown in Figures 3.7E-H.

When heating at 2 °C·min^{-1}, the SR-SAXD peak of α_2 at 4.1 nm shifted to a *d*-spacing value of 4.5 nm, which vanished before reaching its initial value of 4.9 nm. In PPO heated at 0.5 °C·min^{-1}, no SAXD reflections different from that at 4.1 nm occurred before the α_2-2L to α_1-3L transition. This means that a lower degree of structural changes is needed for this transformation to occur at decreasing rates. In both cases, the low energy attributed to this

transformation hampered the identification of the corresponding thermal signals in the DSC curves.

At both heating rates, SR-SAXD reflections at 4.2 and 3.4 nm were stronger than those observed when heating at 15 and 5 °C·min^{-1}. In addition, peaks at 0.47, 0.44, 0.43, 0.41, 0.39, and 0.38 nm were noticeable in the corresponding WAXD patterns. Therefore, a higher amount of β'_2-2L and β'_1-3L was formed from the α_1-3L melt. This was the result of the much higher time provided for the molecular arrangement in a novel structure when reducing the speed of heating. In addition, the next melt-mediated $\beta'_2 \rightarrow \beta'_1$ transformation and β'_1-3L melting could be clearly discerned by DSC through the successive endothermic → exothermic → endothermic events ranging from around 27 to 33 °C. Due to the similar subcell of the two β' forms, the β'_2-2L to β'_1-3L transition was more easily followed in SR-SAXD patterns. However, the WAXD peak at 0.39 nm vanished and that at 0.38 nm strengthened near 31 °C when heating at 0.5 °C·min^{-1}. This led us to conclude that the first reflection must correspond to β'_2-2L and the second to β'_1-3L.

3.2.2.2.2. Cooling from the melt at 2 °C·min^{-1} and reheating at different rates

Figures 3.8A and 3.8B depict the DSC thermogram and SR-XRD patterns, respectively, corresponding to PPO cooled at a rate of 2 °C·min^{-1} and subsequently heated at 15 °C·min^{-1}.

The melt crystallization of α_2-2L (peak at 16.9 °C in the cooling thermogram) was confirmed by the occurring SR-SAXD peak at 4.9 nm when reaching 15 °C, which again shifted towards a higher angle (→ 4.0 nm) at decreasing temperature. Interestingly, its intensity decreased at the same time that the α_1-3L reflection emerged at around 12 °C. This suggests that α_2-2L crystals may have acted as precursors of the initial formation of α_1-3L ones. Below the former temperature, the considerably higher area of the reflection at 3.9 nm compared to that at 4.0 nm suggested that α_1-3L became predominant in the crystallized mass.

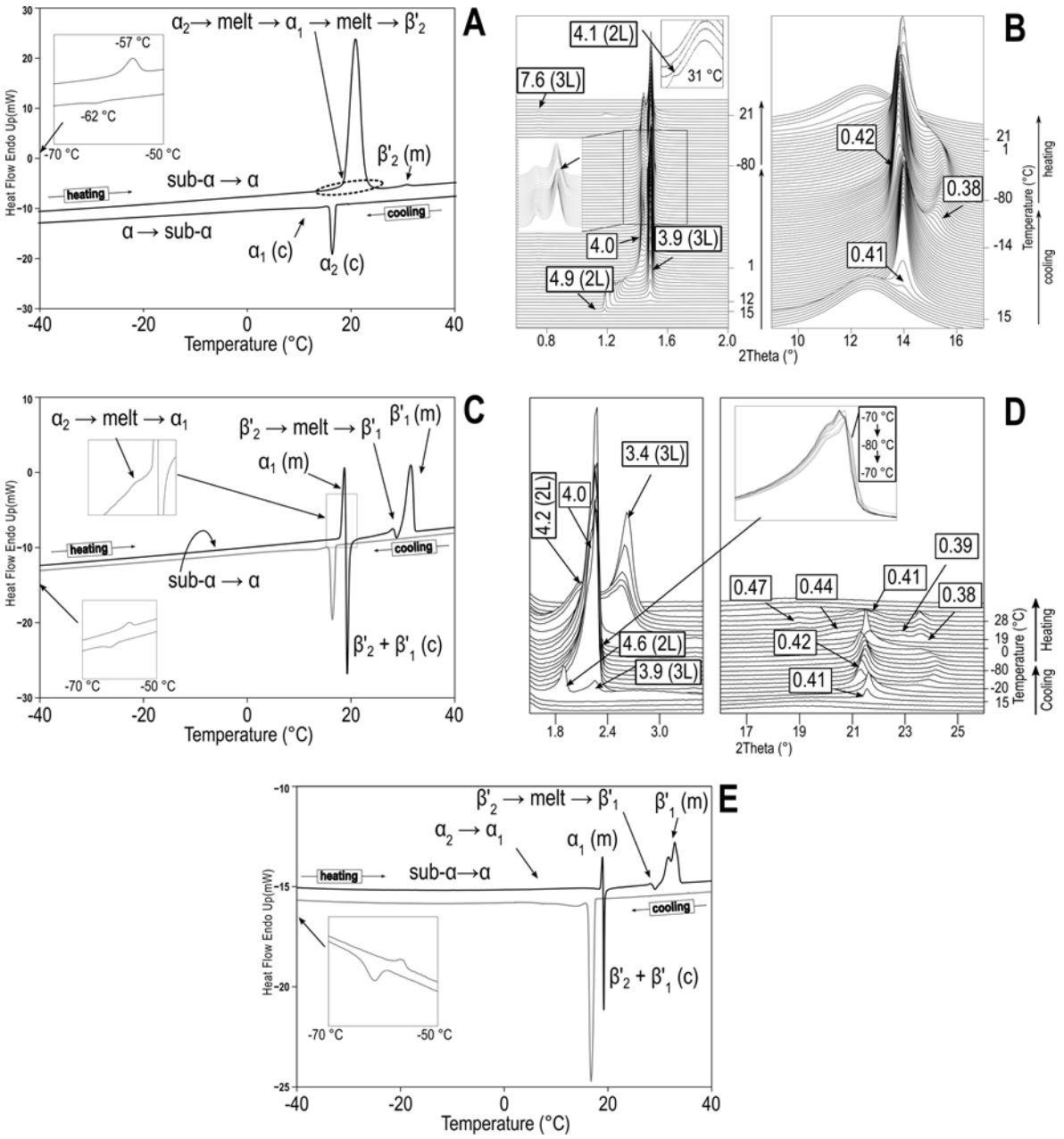

Figure 3.8. DSC thermogram and SR-XRD patterns of PPO cooled at 2 °C·min^{-1} and subsequently heated at (A, B) 15 °C·min^{-1} and (C, D) 2 °C·min^{-1}. (E) Depicts the DSC thermogram of PPO cooled at 2 °C·min^{-1} and reheated at 0.5 °C·min^{-1}. (c): crystallization; (m): melting. *d*-spacing values are given in nm.

The above mentioned would be in line with previous observations of a Ph.D. dissertation on the atypical thermal behavior of α forms of the monounsaturated asymmetric TAGs PPO, SSO, PSO, and SPO during polymorphic crystallization and transformation (Norris, 1977). The Δ*H* values determined for the single DSC crystallization peaks detected during cooling were substantially smaller than those attributed to the melting endotherms of the α forms (α_2+ α_1)

produced. Although not confirmed by complementary techniques, the author assumed that probably some α_2-2L → α_1-3L transformation occurred in the cooling process and that the absence of specific DSC signals for this event was due to slow uncompleted transitions. In our case, SR-XRD patterns seem to confirm that the occurrence of α_1-3L takes place from a quick transformation of the initial α_2-2L formed. This behavior resembles that observed by Taguchi et al. (2021) during the isothermal crystallization of PPO at 13 °C. Some α_2-2L formed at the earlier stages of the process and, after 40 seconds, the occurrence of α_1-3L was initiated by the incorporation of supercooled melt into the initially formed crystals.

After the solidification of α forms and the subsequent α → sub-α transitions, the low-temperature DSC event detected at -64 °C when cooling PPO at 15 °C·min^{-1} was also observed at this rate when reaching -62 °C (weak exothermic peak in amplified image). In this case, a subtle shifting of SR-SAXD reflections attributed to sub-α could be distinguished in the range of temperatures between 70 and 80 °C (pointed by an arrow in the amplified image of Figure 3.8B). This ultimately confirms this event as a subtle modification of the existing structures rather than the occurrence of new crystalline phases. Such behavior was not observed in the study of PPP and LLL, which suggest that, again, the difficult lateral packing of palmitic and oleic acid moieties may have contributed to a non-stop molecular readjusting even at a very low temperature. Moreover, the complicated crystalline packing observed may have been accentuated by the asymmetric distribution of fatty acids at the *sn-* positions of the glycerol group. This would be supported by the identification of a similar low-temperature polymorphic event in SSO (Baker et al., 2014a) and the absence thereof in POP and SOS (Baker et al., 2014a; Bayés-García et al., 2013b). We did not observe equivalent behavior during the study of OPO, but it has also been confirmed in OSO (Baker et al., 2014b).

When heating at 15 °C·min^{-1}, no DSC peak could be ascribed to the further melting of α_2-2L, and only the strong one associated with that of α_1-3L was visible in the heating thermogram (peak at around 18 °C in Figure 3.8A). We previously saw the very low energy of DSC events associated with the α_2-2L melting compared to that of α_1-3L in PPO previously cooled at the highest rate of 15 °C·min^{-1} (see Figure 3.7A). It seems plausible that in PPO cooled at 2 °C·min^{-1}, which showed a clear predominance of α_1-3L over α_2-2L at the end of the crystallization stage, the α_2-2L melting during reheating resulted in a weaker thermal signal overlapped with that of α_1-3L melting. Despite the great amount of liquid after the vanishing of SR-XRD reflections

associated with α forms, the SR-SAXD peak with *d*-spacing value of 4.1 nm observed at 31 °C confirmed that some β'_2-2L formed from the α_1-3L melt before complete melting.

As shown by Figures 3.8C and 3.8E, DSC curves of PPO obtained when heating at 2 and 0.5 °C·min^{-1} were almost identical to those obtained at the same rate when previously cooled at 15 °C·min^{-1} (see Figures 3.7E and 3.7G). Consequently, equivalent polymorphic transformation behavior was confirmed by laboratory-scale XRD (patterns of the PPO sample heated at 2 °C·min^{-1} are depicted in Figure 3.8D).

In summary, the sub-α → α transition was followed by the α_2-2L → α_1-3L transformation and the next α_1-3L melting. After the crystallization of β'_2-2L and β'_1-3L a melt-mediated β'_2-2L → β'_1-3L transformation occurred before the whole sample was molten. One may notice that the weak endothermic event associated with the α_2-2L → melt → α_1-3L was visible in the heating thermogram obtained at 2 °C. This was not observed when PPO was previously cooled at 15 °C·min^{-1} (Figure 3.7E). Actually, the endothermic event linked to the transition of α_2-2L was only spotted by DSC when applying cooling/heating rates of 15 °C·min^{-1}/15 °C·min^{-1}, 15 °C·min^{-1}/5 °C·min^{-1}, and 2 °C·min^{-1}/2 °C·min^{-1} (Figures 3.7A, 3.7C, and 3.8C). The low stability of PPO in the α_2-2L form became patent through the quite small Δ*H* values estimated for its melting under these conditions, below 2 J·g^{-1} (see Table 3.8). It is worth underscoring that reducing the speed of thermal treatments usually results in a noticeable decrease in the height of DSC peaks. This may explain the failure to identify the event at intermediate-low heating rates.

3.2.2.2.3. Cooling from the melt at 0.5 and 0.1 °C·min^{-1} and reheating at different rates

Figure 3.9 depicts DSC and XRD data of PPO when cooled at 0.5 °C·min^{-1}and subsequently heated at different rates of 15 and 0.5 °C·min^{-1}.

The cooling curve displayed by PPO resembled those obtained when higher rates were applied (crystallization peak with a shoulder at around 17 °C). However, the SR-SAXD peak at 4.1 nm and SR-WAXD peaks at 0.41 and 0.39 nm detected when reaching 18 °C confirmed that some PPO molecules arranged in the β'_2-2L polymorph at the early stage of crystallization. Then, SR-SAXD reflections belonging to α_2-2L (4.8 nm) and α_1-3L (7.6 and 3.9 nm) appeared several degrees below. It should be mentioned that the SR-SAXD reflection of α_2-2L soon vanished and that at 3.9 nm underwent a considerable increase in intensity. This was indicative of a complete α_2-2L → α_1-3L transformation at this low cooling rate.

A stronger change in the crystallization behavior of PPO occurred when decreasing the rate to 0.1 °C·min^{-1} (see corresponding DSC and XRD data in Figure 3.10). The crystallization temperature raised to 23 °C and WAXD patterns obtained at 20 °C indicated that only β' forms were formed. Moreover, according to the intensity ratio shown by reflections at 4.2 and 3.4 nm in the SAXD region, the occurrence of β'$_1$-3L crystals was noticeably favored before β'$_2$-2L ones.

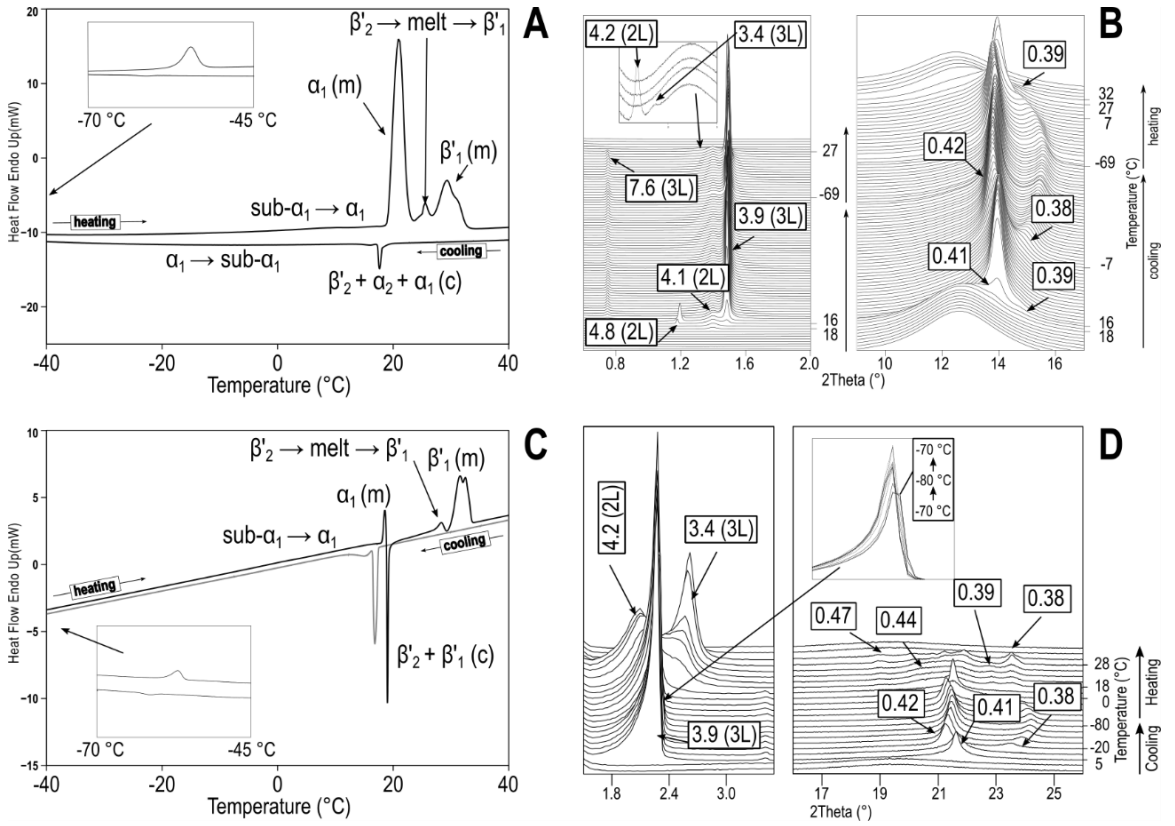

Figure 3.9. DSC and XRD data of PPO heated at (A, B) 15 °C·min^{-1} and (C, D) 0.5 °C·min^{-1} after previous cooling at 0.5 °C·min^{-1}. (c): crystallization; (m): melting. *d*-spacing values are given in nm.

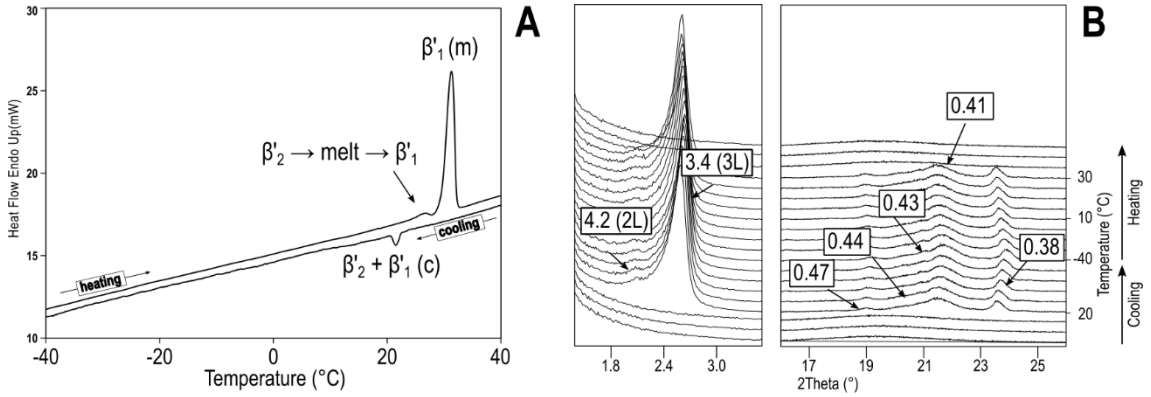

Figure 3.10. DSC thermogram (A) and SR-XRD patterns (B) of PPO cooled at 0.1 °C·min^{-1} and subsequently heated at 2 °C·min^{-1}. (c): crystallization; (m): melting. *d*-spacing values are given in nm.

On the subsequent heating, PPO exhibited similar polymorphic transformation behavior independently of the rate applied, which was consistent with that observed in the samples cooled at higher rates. In PPO cooled at 0.5 °C·min^{-1}, the α_1-3L → melt → β'_2-2L → melt transformations occurring when heating at 15 °C·min^{-1} could be more easily monitored by DSC as compared to PPO cooled at 15 and 2 °C·min^{-1} (see Figures 3.7A and 3.8A). This was presumably due to the occurrence of some β'_2-2L during cooling, which eventually led to a more energetic thermal signal when melting in the heating process (peak at 28.3 °C in Figure 3.9A). In the same manner, the β'_2-2L → β'_1-3L transformation also showed to be eased at increasing β'_2-2L in the sample. This was confirmed by SR-XRD (see amplification in Figure 3.9B) through the occurrence of the weak short-life SR-SAXD signal at 3.4 nm when reaching 27 °C, and by DSC through the final melting peak detected at 30.1 °C. The same for the samples cooled at 0.1 °C·min^{-1}, in which the melt-mediated transformation of β'_2-2L into the stable β'_1-3L was clearly revealed by DSC.

Figure 3.11 depicts the TOPLM micrographs obtained when heating PPO at 0.5 °C·min^{-1} after cooling at the same rate. At this low rate, the β'_2-2L → β'_1-3L transition could be directly monitored through the increase in brightness of the spherulitic clusters of PPO between 25 °C (with predominant β'_2-2L crystals according to XRD data) and 29 °C (β'_1-3L). Furthermore, the size of the spherulites slightly decreased and the edges became noticeably sharper at the higher temperature. This was visual evidence of a noteworthy increase in the density of molecular packing undergone by PPO molecules when arranged in the most stable polymorph.

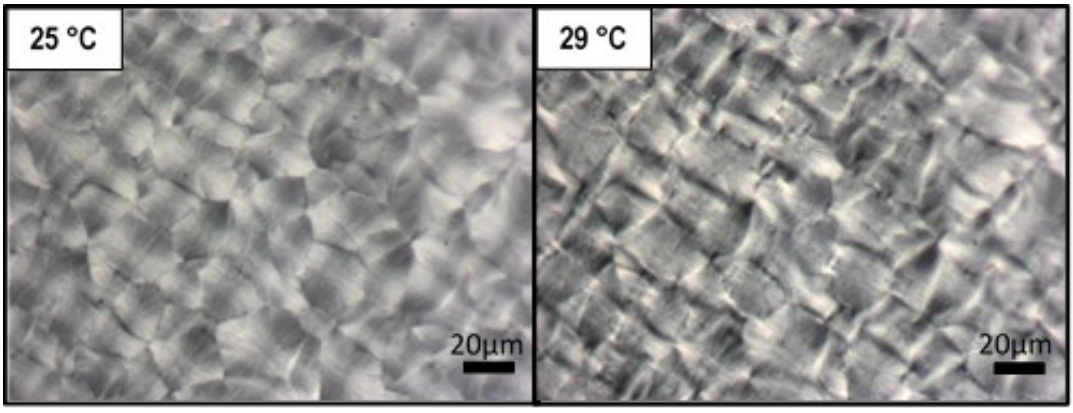

Figure 3.11. Microstructural changes of PPO during the β'_2 → β'_1 transformation at a heating rate of 0.5 °C·min^{-1}.

Regarding the melting behavior of the most stable form of PPO during reheating processes, it is worth mentioning the similarities found between the sample cooled at 0.5 °C·min^{-1} and those cooled at higher rates (15 and 2 °C·min^{-1}). In all cases, heating thermograms obtained at 2 °C·min^{-1} showed single DSC peaks near 30 °C associated with the β'_1-3L melting, whereas two convoluted melting peaks occurred at 0.5 °C·min^{-1} (see Figures 3.7G, 3.8C and 3.9C). The presence of two different polymorphic forms at the lowest rate could not be confirmed by XRD techniques. According to previous work, PPO presents a stable β'_1 with triple chain-length structure in both its enantiomeric forms (R and S) and racemic mixture (compound), with the latter exhibiting a slightly lower melting point (36.8 and 35.5 °C, respectively) (Norris, 1977). In addition, it was found that in equimolecular S-OPP/R-PPO mixtures, not all PPO molecules contribute to the formation of a racemic compound during crystallization, but some remain packed with their equivalent enantiomer (Mizobe et al., 2013). Therefore, the double endothermic event observed at the end of the heating treatment at 0.5 °C·min^{-1} could be due to a successive melting of β'_1-3L of the racemic compound and the pure enantiomers. The lower heating rate might have improved the separation of both phenomena in the heating curves.

3.2.2.3. Summary of mixed-acid saturated-unsaturated triacylglycerols

This section summarizes the main observations made on OPO and PPO. In addition, their behavior is compared against that of other TAGs with dissimilar structures already published in the literature. Figures 3.12 and 3.13 summarize the overall crystallization and polymorphic transformation behavior exhibited by OPO and PPO when subjected to cooling and subsequent heating treatments at varying rates. Again, the crystallization behavior of TAG molecules showed to deviate from the Ostwald rule of stages when different thermal treatments were applied.

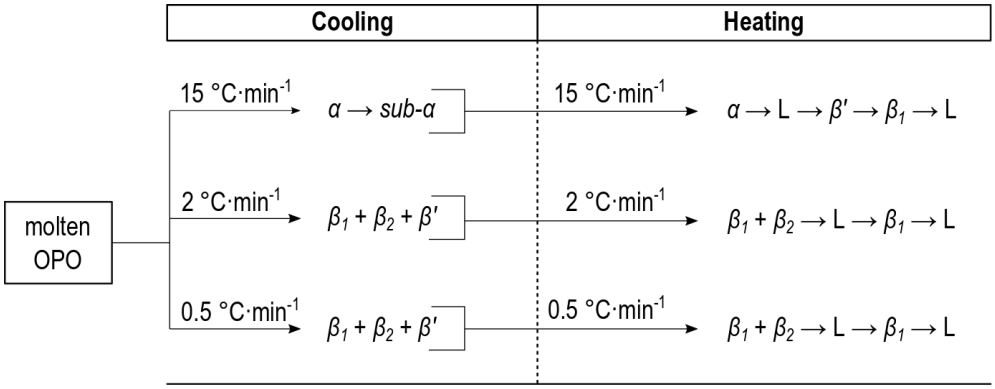

Figure 3.12. Diagram of the polymorphic crystallization and transformation pathways shown by OPO under different cooling and heating conditions.

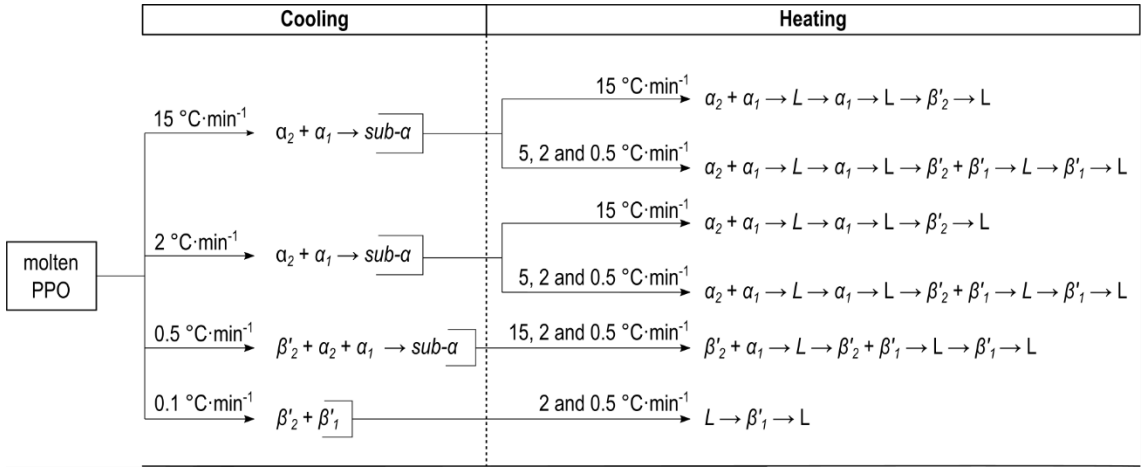

Figure 3.13. Diagram of the polymorphic crystallization and transformation pathways shown by PPO under different cooling and heating conditions.

The fast cooling (15 °C·min^{-1}) of molten OPO resulted in the single crystallization of the α-2L form, whereas at lower rates (2 and 0.5 °C·min^{-1}) the crystallization process was characterized by the concurrent occurrence of more stable polymorphs (β'-2L, β_2, and β_1-3L). This behavior is in line with that previously reported for related mixed-acid saturated-unsaturated TAGs. In POO, the α crystallization predominated when cooling at 15 or 2 °C·min^{-1}, but decreasing the rate to 0.5 °C·min^{-1} resulted in the concurrent crystallization of its β'_2 and β'_1 forms (Bayés-García et al., 2016). As for POP, the γ form was favored before the least stable α when cooling rates from 1 °C·min^{-1} and below were applied (Bayés-García et al., 2013b). In SLiS, γ was obtained from the melt at a faster cooling rate of 5 °C·min^{-1} (Takeuchi et al., 2000). Finally, cooling treatments at 1 °C·min^{-1} and below promoted the occurrence of β' and hindered that of α and γ in SOS (Baker et al., 2014a).

The change in subcell packing as a function of the crystallization conditions was not so obvious in PPO. The occurrence of α forms was strongly favored at fast and intermediate cooling rates. SR-XRD data suggested that the initial formation of α_2-2L may be a necessary condition for the development of α_1-3L. A low heating rate of 0.5 °C·min^{-1} led to the occurrence of some β'-2L, but short-life α_2-2L crystals still formed and α_1-3L ones predominated at the end of the process. Only when the rate was decreased to 0.1 °C·min^{-1}, the formation of α forms was avoided and β'_1-3L crystals were obtained. Thus, a much greater reduction of the kinetic factors is needed to achieve a molecular arrangement different from the hexagonal subcell in PPO.

The favored crystallization of α_2-2L may be in part explained by the properties of PPO in the liquid state. As mentioned in the introduction section, it is understood that molten lipids exhibit some degree of molecular order even at temperatures far above their melting point (Hernqvist, 1984). In such conditions, the strength of dipole-dipole interactions between carbonyl groups (C=O) of the glycerol backbones and Van der Waals forces between aliphatic chains of TAGs may be enough to enable molecular aggregation in lamellar-like structures (Hondoh et al., 2018). It has been suggested that the first occurring α forms of monounsaturated TAGs such as SOS, SLnS, and PPO consist of transient mesophases inheriting the structural arrangement of smectic-A liquid crystalline phases (with hexagonal in-plane order) (Mykhaylyk et al., 2004, 2007; Mykhaylyk & Martin, 2009; Seddon, 1998). Also, that these undergo structural modifications in the course of crystallization processes due to an incompatible packing of saturated and unsaturated fatty acid chains (Mykhaylyk et al., 2007). In SR-XRD patterns of PPO, this is linked to the shifting of the initial α_2-2L SAXD reflection at 4.9 nm to a final value of around 4.1 nm.

However, the reversibility of this change during fast heating treatments (see Figures 3.7B and 3.7D) questions the transient nature of this phase.

The relatively simple polymorphic properties of PPO with respect to other monounsaturated TAGs also influence the more prevalent α forms obtained during crystallization. The lateral packing of PPO molecules may lead to either α and β' forms. In between these, TAGs with different symmetry such as POP, POS, or SOS present intermediate γ and/or δ forms. When discussing the polymorphism of PPP and LLL TAGs, we already mentioned that the polymorphic-dependent crystallization is influenced by the activation free energy of nucleation and the degree of supercooling. In addition, we know that the energy barrier to overcome for the crystallization of a specific form becomes higher as the density of molecular packing increases. Therefore, it is comprehensible the much lower reduction in the degree of supercooling needed to induce a change of subcell packing in PPO. We have seen how in the diunsaturated OPO, the occurrence of α is prevented and that of β' promoted when cooling at 2 °C·min^{-1} and lower rates. The same was reported for POO, POLi, and SOO (Bayés-García et al., 2016). One may assume that the formation of β' of PPO is more sterically hindered by cause of the two saturated fatty acid moieties within the molecule. In addition, we should also consider the influence of stereochemical factors on the behavior displayed by PPO. Mizobe et al. (2013) demonstrated that, contrary to the racemic mixture, pure R(S)-PPO enantiomers pack in β' during cooling processes at 2 °C·min^{-1} and α crystals only occur in very fast cooling processes.

Regarding the transformation behavior of PPO during reheating processes, the effect of kinetics was evident in the increased quantity of each polymorph obtained during transitions when lower rates were applied. The higher time for polymorphic transitions to occur provided by slow heating led to a higher number and better-defined polymorphic transitions in the heating curves obtained at 2 and 0.5 °C·min^{-1} than at 15 °C·min^{-1} (see Figures 3.7 and 3.8). In addition to the stronger DSC signals attributed to melting and recrystallization events, the promoted transition to more stable forms was recognized by SR-XRD through a remarkable increase in the intensity of β'_2-2L and β'_1-3L reflections.

Despite the above mentioned, the different heating conditions applied did not influence the overall polymorphic transformation pathways and the sequence of transformations (see Figure 3.13). PPO polymorphs obtained during crystallization at different rates, when reheating transited to the next one in order of increasing stability (sub-$\alpha \rightarrow \alpha_2 \rightarrow \alpha_1 \rightarrow \beta'_2 \rightarrow \beta'_1$) via melt-

mediation. This contrasts with the complex polymorphic transformation behavior revealed by other mixed-acid saturated-unsaturated TAGs. In SOO, POO, and POLi, the α-2L polymorph always transformed into the more stable β'_2-3L form via melt-mediation when high heating rates were applied (15 °C·min^{-1}), whereas reducing the rate (2-0.5 °C·min^{-1}) resulted in solid-state transformations or transitions via KLC phases (Bayés-García et al., 2016). The solid-state transformation of α-2L of POP into the γ-3L form, the following one in order of increasing stability, was only promoted when rates below 2 °C·min^{-1} were applied (Bayés-García et al., 2013b). Interestingly, α-2L transformed directly into β'-2L through the melt during fast heating at 15 °C·min^{-1}. Similar behavior was observed in the γ-3L → β-3L transformation, which only at the very low rate of 0.1 °C·min^{-1} occurred in the solid-state through the intermediate δ-3L.

It becomes evident the great dependence of the polymorphic transformation pathways followed by TAGs on the specific thermal treatments applied. One way to explain this is by means of the Gibbs free energy of activation involved in the structural changes during phase transitions ($\Delta G^{\#}$) (changes in lamellar and subcell packing) and the induction times (τ) required for the different polymorphic transformations to occur (simple melting, via melt-mediation, through the solid-state, via KLC phase) (see Figure 3.14).

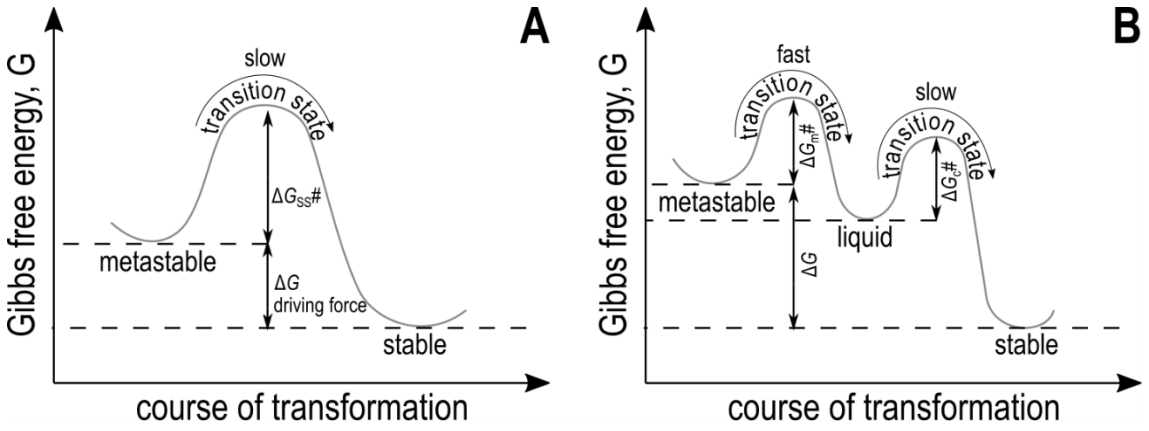

Figure 3.14. Energy diagrams of (A) solid-state and (B) melt-mediated polymorphic transformations.

According to the above, the heating rate influences the transformation behavior by means of the time provided for the transition from a metastable phase to a more stable one. It is expected that the transformation time will be greater as the rate is decreased. Thus, solid-state transformations (with higher $\Delta G^{\#}$ and τ) are often more favored during slow heating. Under such conditions, it will be easier that the time provided for the transformation equals or exceeds

τ_{ss} (induction time for the solid-state transformation). By contrast, the shorter time available when heating at high rates usually results in melt-mediated transformations. We have seen that, unlike the mixed-acid saturated-unsaturated TAGs previously described, different heating rates did not substantially change the transformation behavior of PPO. By considering the similar chain of melt-mediated polymorphic transitions observed during the heating treatments, it can be presumed τ_{ss} was higher and τ_{mm} (melt-mediated transformation) lower than the time of transformation allowed by the heating rates evaluated.

In addition to the type of transition, kinetics may determine the occurrence or not of specific forms. As exemplified earlier by means of the α-2L form of POP, sufficiently high heating rates might not provide enough time to overcome the energy barrier for a metastable form to transform into the next one in order of increasing stability (γ-3L), and further ones may be obtained instead (β'-2L) (Bayés-García et al., 2013b). This explains the direct β'-2L → β_1-3L transformation without passing through β_2 shown by OPO cooled and reheated at 15 °C·min^{-1} in the present chapter (see Figure 3.6A). The same applies to PPO heated at 15 °C·min^{-1} soon after cooling at the same rate, which after the α_1-3L → β'_2-2L transformation melted without further crystallization of the stable β'_1-3L (Figure 3.7A). However, the involvement of the thermal history on the transformation behavior of TAGs cannot be disregarded. We confirmed that β'_1 does occur even at fast heating rates when some β'_2 is obtained in the previous cooling process (see Figure 3.9A).

The intrinsic structural properties may also have a key role in the transformation behavior of TAGs. In contrast with the β'_2-2L → melt → β'_1-3L transformation of PPO at heating rates from 0.5 to 15 °C·min^{-1}, β'_2-3L→ β'_1-3L transition of SOO, POLi, and POO when heated at the same rates took place through the solid-state (Bayés-García et al., 2016). A higher degree of structural changes occurs when a transformation implies a conversion from a double to a triple chain-length structure (or vice versa) than in transformations that do not require changes in the longitudinal packing. Thus, one may expect $\Delta G_{ss}^{\#}$ to be noticeably higher when starting and final polymorphs differ in chain-length structure. This helps explain the favored melt-mediated transformation of PPO, whose polymorphs in order of increasing stability show sequential double and triple chain-length structures. The effect of palmitic acid at two *sn*- positions of the glycerol group should also be considered. The lower flexibility of the chain packing associated with the straight zigzag configuration of saturated fatty acids (Small, 1984) may lead to greater $\Delta G_{ss}^{\#}$ values in PPO than in di- or triunsaturated ones such as those previously mentioned. This

would be in line with the also hindered solid-state transitions found in the symmetric monounsaturated POP even at a heating rate of 0.1 °C·min^{-1} (Bayés-García et al., 2013b).

On basis of the above, one may conclude that the steady transformation behavior shown by PPO during heating treatments at different rates was primarily determined by structural factors and that very low heating rates, below those applied in the present work, may be needed to induce remarkable changes in the polymorphic transformation pathways of this TAG.

3.3. CHAPTER CONCLUSIONS

The present chapter comprises the DSC and X-ray diffraction study of pure TAGs contained in natural fats and oils widely used in the pharmaceutical, cosmetic, and food industries. The manufacture of many products from these often involves crystallization and reheating processes in which temperature gradients need to be tailored. The polymorphic crystallization and transformation properties of pure components under dynamic thermal conditions enable an initial approach to the behavior of complex fat systems. On this basis, we monitored the thermal and structural properties of PPP, LLL, OPO, and PPO during melt cooling and subsequent heating processes at different rates.

All TAGs exhibited a common trend during crystallization processes at varying rates of cooling. Least stable forms (α) occurred when the highest cooling rate was applied and slower cooling processes promoted the crystallization of more stable polymorphs, often in a concurrent manner. Therefore, the Ostwald rule of stages showed to be invariably broken during melt cooling when the influence of kinetic factors was sufficiently reduced (increase in T_c). However, this rule was mostly followed during the subsequent reheating treatments at different rates, in which TAGs polymorphs transformed sequentially into the next one in order of increasing stability.

PPP and LLL displayed distinct polymorphic occurrence when subjected to the same cooling treatments, and therefore, to the same supercooling versus time history. In LLL, the shorter length of aliphatic chains allowed the crystallization of more stable polymorphs under less intense thermal treatments. This property may be of interest for specific applications aiming to achieve stable β crystals through shorter crystallization processes. In PPP, we confirmed that, despite its great kinetic instability, β' occurs during α to β transitions even at high heating rates.

The polymorphic behavior of OPO agreed with the kinetic-dependent crystallization and transformation reported for mixed-acid TAGs in previous studies. The application of different heating rates did not change the polymorphic transformation pathways (solid-state, melt-mediated) but did affect the sequence of metastable phases obtained before achieving the thermodynamically stable one. In combination with the available data in the scientific literature, our results showed that the occurrence of different β forms relies on the heating rate but also

on the specific polymorphic forms attained during previous melt cooling processes. This evidences the crucial role of thermal history on the transformation behavior of TAGs.

The polymorphic crystallization and transformation properties of PPO differed from other mixed-acid saturated-unsaturated TAGs. During crystallization, very low cooling rates were needed to achieve a molecular packing different from the typical hexagonal subcell. The fatty acid composition, asymmetry, and racemic nature of PPO were main influencers of such behavior. When reheating, slower processes yielded higher transformation rates, but no substantial changes occurred in the transformation pathways or the sequence of polymorphic transformations at the different conditions applied. These were invariably via melt-mediation. The absence of solid-state transformations even at the lowest cooling rate evidenced large activation free energies to overcome during these transitions, probably enhanced by the complex longitudinal packing of PPO polymorphs (with consecutive double and triple structures) and a restricted chain packing induced by the two palmitic acid moieties.

CHAPTER 4

PHASE BEHAVIOR OF 1,2,3-TRIPALMITOYL-GLYCEROL AND OLEIC-RICH TRIACYLGLYCEROLS FORMING MOLECULAR COMPOUND

4.1. INTRODUCTION

The number of TAG species present in complex fats and oils may reach more than one hundred (Gresti et al., 1993). This means that the properties of complex lipid systems cannot be understood as an effect of individual pure molecules, but as the synergistic effect of specific TAG combinations. On this basis, the only way to achieve a clear picture of the structure-interaction-function relationships of lipids goes through studying the phase behavior of mixture systems including their most representative TAGs.

So far, our knowledge on the mixing properties of TAGs comes from the study of two-component systems. From these, we know that molecular interactions between lipids lead to three main types of mixing behavior: complete miscibility, eutectic behavior, and molecular compound formation. Stable solid solutions at all concentration ratios only occur in mixtures of TAGs with very isomorphic crystal structures, as seen for the POS/SOS system in the β phase (Rousset et al., 1998). Typically, a different fatty acid composition, degree of unsaturation, and symmetry favor the steric repulsive interactions that cause the formation of eutectic phases. This is the most prevalent type of behavior, which is exemplified in systems as diverse as SSS/PPP, SSP/PSP, SOS/SOO, POP/POO, PPO/OPO, or PPP/OOO (Bayés-García et al., 2015a; Costa et al., 2011; Knoester et al., 1972; Zhang et al., 2007, 2009). However, specific aliphatic interactions may promote the formation of molecular compounds with own structural and thermodynamic properties in some TAG combinations. This was confirmed in the oleic-rich mixtures POP/OPO, POP/PPO, SOS/OSO, and SOS/SSO (Koyano et al., 1992; Minato et al., 1997a, 1997b; Takeuchi et al., 2002a), and suggested in the fully saturated ones PSP/PPS and LSL/LLS (Boodhoo et al., 2009a; Bouzidi et al., 2010).

The crystallization and mixing behavior of TAG systems matter in two main industrial applications: the processing and design of end products made by fat crystals and the separation of specific lipid materials during the fractional crystallization of natural resources (Sato, 2001b). The quality of some lipid-based materials can be explained by the polymorphic and mixing behavior of a reduced number of molecules. For example, the snap, gloss, and heat resistance of chocolate products is primarily determined by CB crystals (Manning & Dimick, 1985; Sato & Koyano, 2001). These are in turn the result of the polymorphic and mixing behavior of SOS, POS, and POP, which account for 80-90% of the total TAG content (Sasaki et al., 2012). In more heterogeneous lipid sources, understanding the behavior of the whole fat and their

fractions goes through unveiling the specific interactions of each TAG with the others (Smith, 2001). For example, PPP is the main high-melting component of palm oil (5%). Within the medium-melting TAGs, the monounsaturated POP (24%) predominates followed by POS and PPO. Finally, POO (20%) and other highly unsaturated low-melting components contribute to the softening of the bulk. The overall behavior of this fat relies, therefore, on how all these components interlink.

We already stated that most of the phase behavior studies on TAG mixtures correspond to binary systems, even though changes in the mixing properties may be expected from the presence of a third component. The work of Gibon & Durant (1985) on palmitic- and oleic acid-based TAG contained in palm oil included binary systems such as PPP/POO, PPP/PPO, or PPO/POO and the ternary mixtures PPP/POP/POO and PPP/PPO/POO. A complex polymorphic and mixing behavior in the metastable state resulted from the application of fast thermal treatments, but no attention was paid to the mixing interactions under thermodynamic stability. Since tailoring the processing conditions to obtain specific polymorphs is a common practice in many industrial applications, such as oil fractionation, we need to know how varying dynamic thermal treatments affect the polymorphic crystallization, transformation, and mixing behavior of TAG systems. However, the trend that these will follow over time can only be determined through their study in most stable forms. Because of this, both approaches should be considered during the characterization of mixture systems.

It is interesting to note that, despite the importance presumed for the molecular compound system POP/PPO in palm oil and related lipid systems, the mixing interactions thereof with a third component have not been examined yet. The same regarding the POP/OPO system, which plays a part in the structuring of lipid materials such as palm- and lard-based margarine. Moreover, the increase in melting point, solid fat content, and hardness reported for blends of POP- and OPO-rich fat fractions by Sibbald et al. (2016) suggested the potential of molecular compound crystals as partial replacers of *trans* and saturated fats. Aiming to increase our knowledge on the mixing interactions ruling the physical properties of diverse edible fats and oils, the present chapter analyzes the mixing behavior of unsaturated TAGs, either pure or a combination of them able to form molecular compound, and the fully saturated PPP. Palmitic acid-based TAGs may be part of tailored hardstock used for lipid structuring. Thus, their solid phase behavior with unsaturated molecules is relevant regarding the fine-tuning of oleic acid content in healthier functional lipid blends. In addition, PPP is a common high-melting

component of natural lipids. This means that plays a key role as initiator of the crystallization in many complex lipids and their blends and, therefore, on the development of the crystal network structure. Moreover, the solidification properties of lower-melting components and the composition of the different phases obtained during fractional crystallization processes are strongly determined by the crystalline and phase behavior displayed by lipid components at the earliest stages of crystallization.

4.2. PHASE BEHAVIOR OF MIXTURE SYSTEMS

The DSC and X-ray diffraction study contained in the present chapter covers the binary systems PPP/OPO, PPP/POP, and PPP/PPO, and the ternary systems PPP/POP/OPO and PPP/POP/PPO. It is worth noting that one of the objectives was to assess how promoting molecular compound formation in ternary mixtures affects the mixing properties of unsaturated and fully saturated components with respect to binary systems. For this reason, the ratio of POP/OPO and POP/PPO in three-component mixtures was kept at a constant 1:1 relation in all the compositions examined. As mentioned in Chapter 2, POP/OPO and POP/PPO in the ternary mixtures will be indicated by their respective molecular compounds to simplify the nomenclature. This means that, for example, the 50PPP/25POP/25OPO mixture will be referred to as 50PPP/50$MC_{POP/OPO}$.

The mixture systems were examined according to the aforementioned approaches: i) after a long-term thermodynamic stabilization process to favor the occurrence of most stable polymorphs; and ii) during thermal treatments consisting of cooling from the melt below the crystallization temperature and subsequent reheating.

Regarding mixtures subjected to thermodynamic stabilization, the thermal incubation parameters used for each system are shown in Table 4.1. It also includes the reference melting points used to set the specific temperature conditions of the incubation process. In order to construct the stable phase diagrams of the systems, the thermal and structural behavior of the stabilized mixtures was evaluated during a heating treatment at 2 °C·min^{-1} until complete melting. Except in the case of PPP/POP mixtures, for which only specific compositions of interest were examined, the diagrams were based on the data obtained for mixtures at 5-10% molar mass concentration intervals.

Table 4.1. Conditions applied during the thermodynamic stabilization of mixture systems including PPP.

Thermodynamic stabilization process		
Mixture system	**First stage**	**Second stage**
PPP/OPO	7 days at 40 °C	4 months at 12 °C
PPP/POP	7 days at 40 °C	6 months at 27 °C
PPP/PPO	5 days at 40 °C	6 months at 27 °C
PPP/$MC_{POP/OPO}$	7 days at 40 °C	6 months at 27 °C
PPP/$MC_{POP/PPO}$	5 days at 40 °C	6 months at 27 °C

Melting point of mixture components (°C)					
PPP[1]	**POP**[2]	**PPO**[2]	**OPO**[3]	**$MC_{POP/PPO}$**[2]	**$MC_{POP/OPO}$**[3]
65.8	36.2	35.6	21.9	31.2	32.0

[1]Kellens & Reynaers (1992b); [2]Minato et al. (1997a); [3]Minato et al. (1997b)

The thermal treatments applied during the study of the kinetic phase behavior of the systems consisted of cooling from the melt and next reheating at rates from 2 to 15 °C·min^{-1}. The specific thermal protocol and the compositions evaluated varied according to the system under study. It should be noted that the polymorphic and mixing behavior of PPP/POP mixtures during dynamic thermal treatments has been thoroughly described in previous studies (Gibon et al., 1986; Kerridge, 1952; Lu et al., 2019; Smith et al., 2005). For this reason, the kinetic phase behavior of this system is not investigated in this thesis.

In mixture systems, the complicated polymorphic behavior may lead to the occurrence of superimposed and broad DSC peaks, which hinder an accurate determination of the onset temperature of the events displayed by the thermograms. For this reason, unless otherwise indicated, T_{top} will be provided in this chapter to define DSC signals.

In relation to X-ray diffraction experiments, Table 4.2 summarizes the crystallographic data reported in the literature for the different components of the mixtures under study. The long- and short spacing values provided were used as a reference to carry out the polymorphic identification of the samples during the different thermal processing conditions.

Table 4.2. Long- (LS) and short spacing (SS) values and chain-length structure (CLS) of main polymorphic forms described in previous work for PPP, POP, PPO, $MC_{POP/OPO}$, and $MC_{POP/PPO}$.

	LS (nm)	SS (nm)	CLS		LS (nm)	SS (nm)	CLS
PPP[1]				**POP[5]**			
α	4.6	0.41	Double	α	4.7	0.42	Double
β'	4.2	0.42, 0.38	Double	γ	6.5	0.47, 0.45, 0.39, 0.36	Triple
β	4.1	0.46, 0.39, 0.37	Double	δ	6.3	0.43, 0.41, 0.38	Triple
PPO[2]				β'_2	4.2	0.44, 0.42, 0.40	Double
α_2	4.98 → 3.9	0.41	Double	β'_1	4.2	0.43, 0.41, 0.40	Double
α_1	7.8	0.41	Triple	β_2	6.1	0.46, 0.41, 0.39, 0.38, 0.37	Triple
β'_2	4.2	0.41, 0.38	Double	β_1	6.1	0.46, 0.41, 0.39, 0.37, 0.36	Triple
β'_1	6.7	0.41, 0.38	Triple	**$MC_{POP/OPO}$[3]**			
OPO[3,4]				α	4.7	n.d.	Double
α	5.3	0.42	Double	β	4.2	n.d.	Double
β'	4.4	0.43, 0.40	Double	**$MC_{POP/PPO}$[6]**			
β_2	5.6 (2.8)	0.46	n.d.	α	4.6	0.43, 0.42	Double
β_1	6.7	0.46, 0.38, 0.37	Triple	β'	4.2	0.43, 0.39	Double
				β	4.1	0.46, 0.40, 0.38	Double

n.d.: not determined. [1]Kellens et al. (1990); [2]Mizobe et al. (2013); [3]Minato et al. (1997b); [4]Bayés-García et al. (2011); [5]Sato et al. (1989); [6]Minato et al. (1997a).

4.2.1. PPP/OPO binary system

4.2.1.1. *Phase behavior after a thermal stabilization stage*

The mixing phase behavior of PPP/OPO mixtures was examined after a thermodynamic stabilization process consisting of a week at 40 °C, followed by four months at 12 °C. The laboratory-scale XRD patterns obtained at 0 °C for all the compositions confirmed their polymorphic stability (Figure 4.1A).

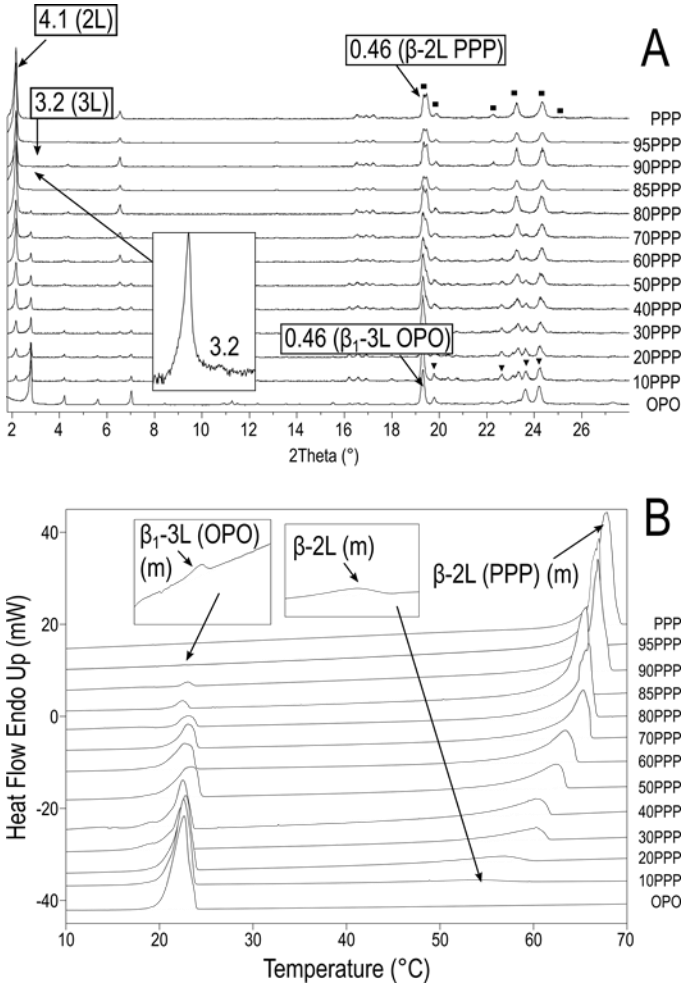

Figure 4.1. PPP/OPO system. (A) Laboratory-scale XRD patterns of stabilized PPP/OPO mixtures obtained at 0 °C. ■: WAXD peaks of β-2L (PPP); ▼: WAXD peaks of β_1-3L (OPO). *d*-spacing values are given in nm. (B) DSC thermograms of stabilized PPP/OPO mixtures heated at 2 °C·min^{-1}. (m): melting. Adapted with permission from Macridachis et al. (2021). Copyright (2021) American Chemical Society.

The SAXD reflection at 4.1 nm was ascribed to the stable β-2L (PPP) form through the corresponding WAXD peaks at 0.46, 0.45, 0.40, 0.38, 0.37, and 0.36 nm (denoted by ■). The triple chain-length structure peak at 3.2 nm (002 reflection) was assigned to the stable β_1-3L form of OPO (WAXD peaks at 0.46, 0.45, 0.39, 0.38, and 0.37 nm, denoted by ▼ in pure OPO sample).

The DSC data obtained when heating the stabilized PPP/OPO mixtures from 0 to 80 °C at a rate of 2 °C·min^{-1} (Figure 4.1B) agreed with XRD data. Single endothermic signals were detected in pure PPP (67.8 °C) and OPO (22.4 °C), whereas the thermal profile of the mixtures showed the successive melting of the stable eutectic phases formed by both TAGs. In agreement with previous work on binary mixtures of mixed-acid TAGs (Minato et al., 1996; Zhang et al., 2007, 2009), the occurrence of phase separation in PPP/OPO mixtures is comprehensible by considering that the efficient lateral packing of these TAGs is prevented by steric hindrance between the straight palmitic acid chains of PPP and the bent oleic acid moieties of OPO.

The PPP/OPO binary phase diagram constructed from the peak temperatures of the endothermic events detected by DSC is depicted in Figure 4.2.

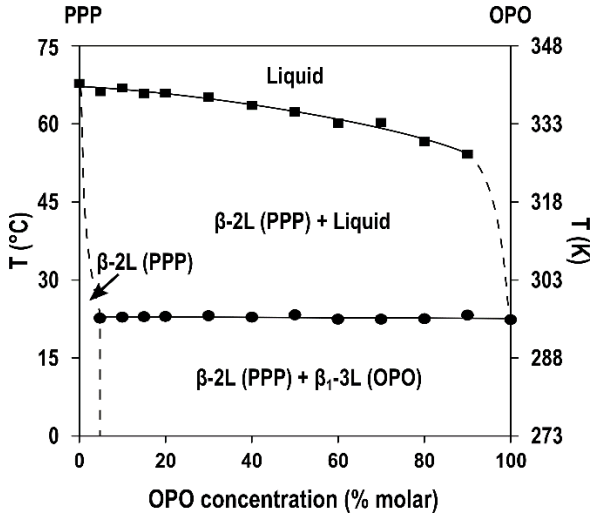

Figure 4.2. Stable binary phase diagram of PPP/OPO mixtures constructed from DSC data obtained when heated at 2 °C·min^{-1}. Adapted with permission from Macridachis et al. (2021). Copyright (2021) American Chemical Society.

As illustrated, the melting temperature of β_1-3L (OPO) remained practically constant at around 22-23 °C for the full set of samples. Further detail in melting data can be found in Table 4.3. By contrast, melting peaks ascribed to β-2L showed lower peak top temperature and more

asymmetric shape towards the pure OPO sample due to the solvent-like behavior of the already molten mixed-acid TAG. The great asymmetry of the eutectic point became clear through the DSC curve of the 10PPP/90OPO composition, in which the weak melting peak of β-2L (PPP) (~16 $J.g^{-1}$) was still identified at 54.2 °C, far above that of β_1-3L (OPO) (see the corresponding enlarged image in Figure 4.1B).

In PPP-rich mixtures, the presence of β_1-3L (OPO) was not confirmed by XRD at the 95PPP/5OPO composition. However, the endothermic phenomenon at 22.8 °C detected in the corresponding DSC thermogram indicated a solubility limit of OPO in PPP below 5%.

Table 4.3. Melting temperatures (°C) of PPP and OPO in stabilized PPP/OPO mixtures heated from 0 to 80 °C at 2 °C·min^{-1}.

Polymorph	PPP	95PPP	90PPP	85PPP	80PPP	70PPP	60PPP
β_1-3L (OPO)	-	22.8 ± 1.1	22.9 ± 0.5	22.9 ± 0.7	23.0 ± 0.5	23.1 ± 0.4	22.9 ± 0.6
β-2L (PPP)	67.8 ± 0.3	66.2 ± 0.9	66.9 ± 0.9	65.8 ± 0.9	65.9 ± 0.6	65.1 ± 0.6	63.5 ± 0.5

Polymorph	50PPP	40PPP	30PPP	20PPP	10PPP	OPO
β_1-3L (OPO)	23.3 ± 0.6	22.4 ± 0.7	22.4 ± 0.6	22.5 ± 0.7	23.3 ± 1.9	22.4 ± 0.7
β-2L (PPP)	62.4 ± 1.1	60.2 ± 1.0	60.2 ± 0.5	56.6 ± 0.6	54.2 ± 0.9	-

4.2.1.2. *Kinetic phase behavior*

The intensity of the cooling and heating treatments applied in actual industrial processes determine the polymorphic crystallization, transformation, and melting behavior of TAGs contained in complex fats. To avoid or promote specific properties in end products, the polymorphic occurrence and mixing interactions of TAGs in the metastable state under varying processing conditions should be known in advance.

DSC and laboratory-scale XRD were used to examine the crystallization and polymorphic transformation behavior of PPP/OPO mixtures during a thermal processing consisting of cooling from the melt to -80 °C at 2 °C·min^{-1}, holding for 1 minute at this temperature, and reheating at the same rate until complete melting. Thermal and diffraction data obtained for selected PPP/OPO mixtures rich in PPP during the process are depicted in Figure 4.3.

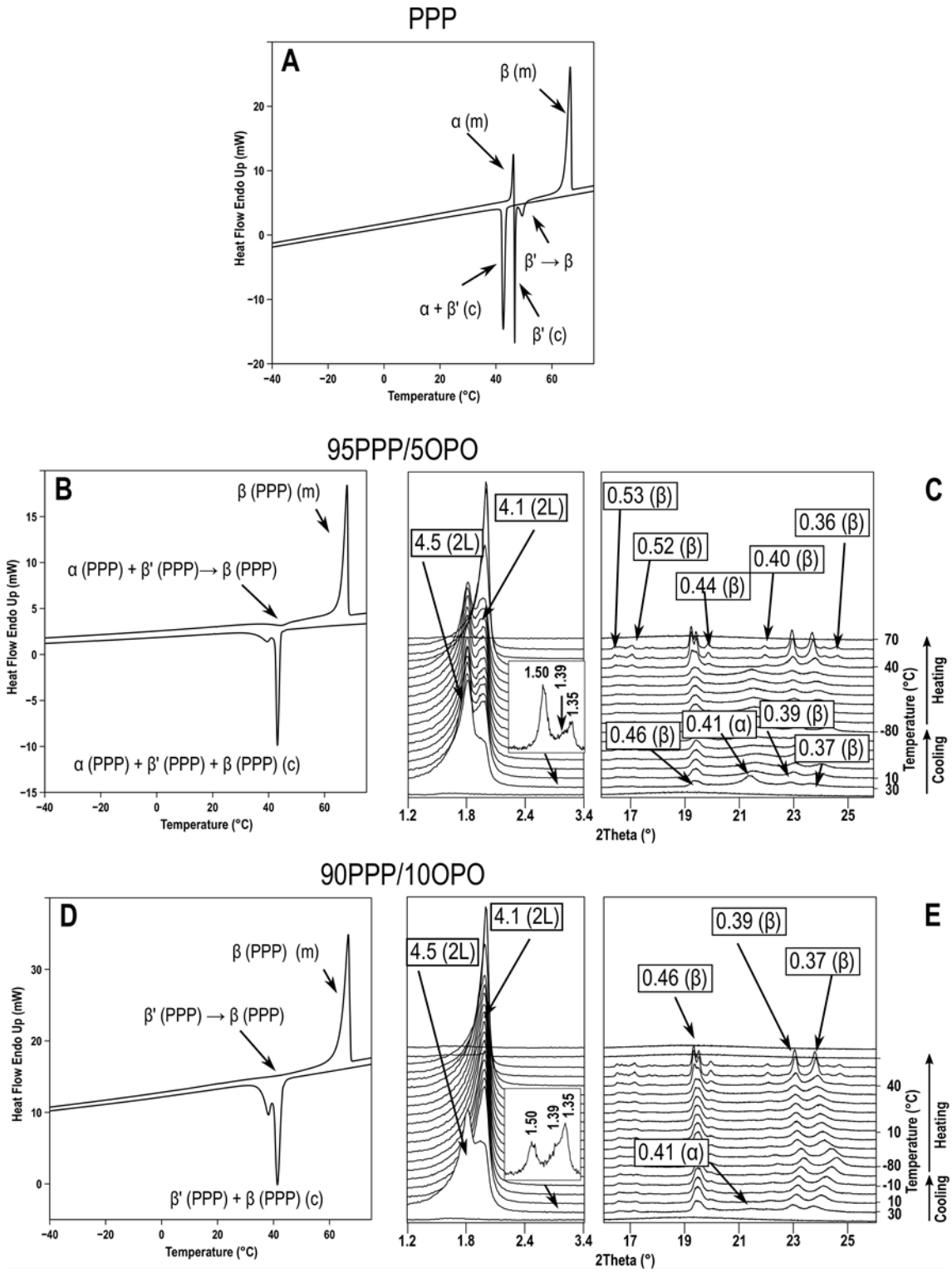

Figure 4.3. Experimental data obtained for pure PPP and PPP-rich mixtures when cooled to -80 °C and subsequently heated at 2 °C·min^{-1}. (A) DSC data of pure PPP; (B, C) DSC and XRD data of the 95PPP/5OPO mixture; and (D, E) DSC and XRD data of the 90PPP/10OPO mixture. (c): crystallization; (m): melting. *d*-spacing values are given in nm.

In contrast with the α + β' crystallization shown by pure PPP (see corresponding XRD patterns in Figure 3.1 of Chapter 3), the double crystallization peak displayed by the 95PPP/5OPO composition during cooling (T_{top} of 42.3 and 38.6 °C) was mainly due to the concurrent occurrence of α-2L (SAXD and WAXD peaks at 4.5 and 0.41 nm, respectively, in XRD patterns at 30 °C) and β-2L (reflections at 4.1, 0.46, 0.39, and 0.37 nm) forms of PPP. However, the three peaks detected at 1.50, 1.39, and 1.35 nm (003 reflections of peaks at 4.5, 4.2, and 4.1 nm) indicated that also some β' was formed. During reheating, the exothermic peak detected at 42.9 °C in DSC corresponded to a α + β' → β transition before the complete melting of the sample at 66.4 °C. Similar behavior was observed in the 90PPP/10OPO mixture, although in this case α-2L peaks vanished from XRD patterns when reaching 10 °C in the cooling process and the exothermic event observed by DSC during reheating was attributed to the β'-2L → β-2L transformation. The absence of further DSC or XRD signals indicated that the mixed-acid TAG was solubilized in PPP.

The immiscible behavior became patent in the 80PPP/20OPO mixture (see experimental data in Figures 4.4A and 4.4B), which during cooling showed an additional polymorphic event attributed to OPO after the β'-2L (PPP) + β-2L (PPP) crystallization. Due to the low amount of the mixed-acid TAG in this mixture, the changes in XRD patterns could only be monitored through SAXD data. Reflections with *d*-spacing values of 6.4 and 3.2 nm detected at -10 °C indicated that the irregular DSC peak occurring from 4 to -16 °C was due to the β_1-3L (OPO) crystallization. In addition, the barely noticed peak at 2.1 nm (002 reflection of the peak at 4.2 nm) associated with β'-2L (PPP) increased in intensity at sub-zero temperatures. Thus, probably some β'-2L (OPO) (with a close long spacing value of 4.3 nm) also crystallized. The same behavior was concluded from the DSC and XRD data of the 70PPP/30OPO composition (Figures 4.4C and 4.4D). In this mixture, WAXD peaks of β'-2L (PPP) (0.42 and 0.38 nm) and β-2L (PPP) (0.46, 0.39, and 0.37 nm) were clearly differentiated at 30 °C. In addition, the next β'-2L (OPO) crystallization was more clearly seen through the strengthening of the SAXD peak at 4.2 nm and the broadening of the WAXD peak at 0.42 nm below -10 °C.

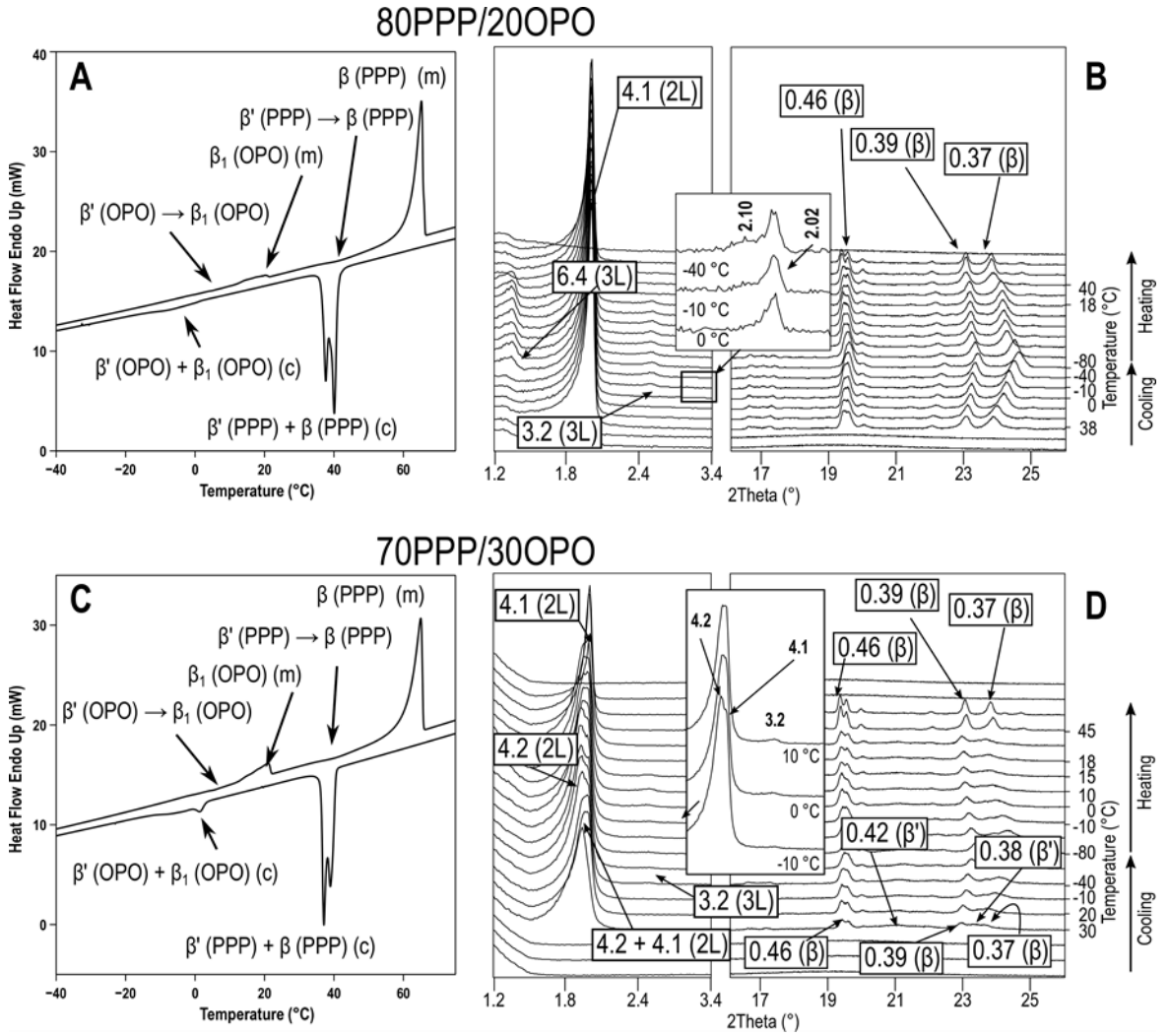

Figure 4.4. DSC thermograms and laboratory-scale XRD patterns of (A, B) 80PPP/20OPO and (C, D) 70PPP/30OPO mixtures when cooled and subsequently heated at 2 °C·min^{-1}. *d*-spacing values are given in nm. (c): crystallization; (m): melting.

During reheating processes, the first exothermic peak observed by DSC in these mixtures near 5 °C corresponded to the solid-state β'-2L (OPO) → β_1-3L (OPO) transformation. This was confirmed through the weakening of the reflection at 4.2 nm and the slight strengthening of that at 3.2 nm in XRD patterns of the 70PPP/30OPO composition between 0-10 °C (see amplified image in Figure 4.4D). The subsequent melting of β_1-3L (OPO) above 20 °C (vanishing of the corresponding SAXD reflections at around 18 °C in XRD patterns) was then followed by the transformation (β'-2L → β-2L) and final melting of PPP.

Figure 4.5 depicts the DSC and XRD data obtained during the thermal processing of the 50PPP/50OPO composition. The initial double crystallization peak with T_{top} of 31.7 and 17.8 °C

evidenced a noticeable decrease in T_c of PPP at increasing amount of liquid OPO in the mixtures. Moreover, the higher relative intensity of β'-2L (PPP) reflections at 20 °C during cooling evidenced a promoted crystallization of this form before that of β-2L (PPP). The subsequent crystallization of OPO (DSC peak at 3.2 °C) led to substantial changes in XRD patterns at -10 °C. The stronger WAXD reflection at 0.42 nm and the new ones at 0.44 and 0.39 nm, together with the SAXD peak at 4.3 nm, were indicative of the β'-2L (OPO) crystallization. Then, the increase in intensity of the typical β WAXD peak at 0.46 nm was attributed to the occurrence of both β_1-3L (OPO) and β_2 (OPO) through small angle peaks at 3.1 (6.4) and 2.8 nm (002 reflection of the peak at 5.6 nm), respectively.

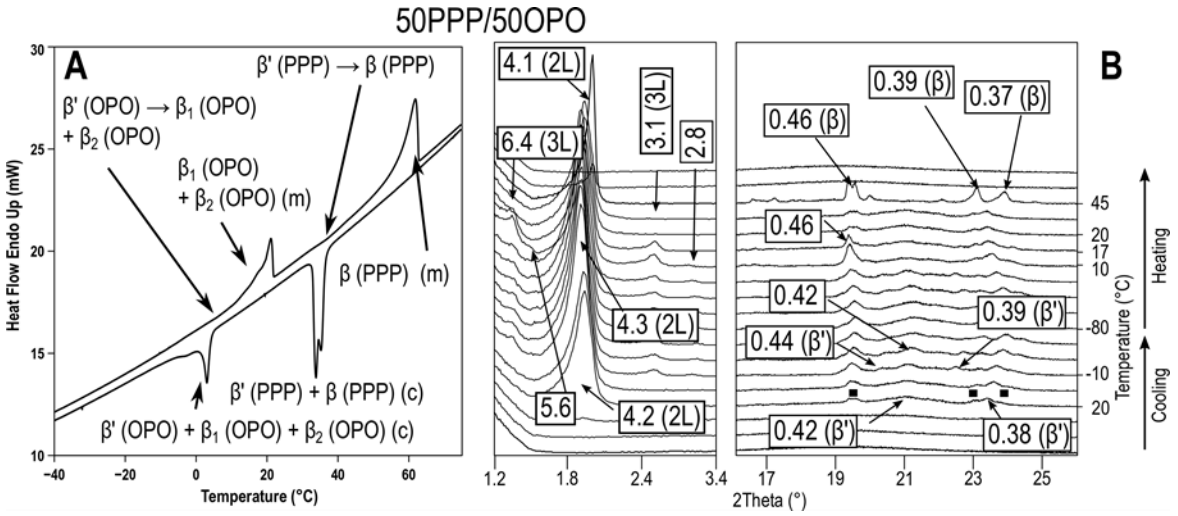

Figure 4.5. DSC thermogram (A) and laboratory-scale XRD patterns (B) of the 50PPP/50OPO mixture cooled and subsequently heated at 2 °C·min^{-1}. *d*-spacing values are given in nm. ■: WAXD peaks of β-2L (PPP). (c): crystallization; (m): melting.

When reheating, the β'-2L (OPO) → β_1-3L (OPO) + β_2 (OPO) transformation (exothermic peak at around 6 °C) became patent in XRD patterns at 10 °C through a simultaneous vanishing of WAXD peaks at 0.44 and 0.39 nm and increase in intensity of small-angle reflections at 6.4 and 5.6 nm. Then, OPO showed a complicated melting behavior (a first weak and two more intense overlapped DSC peaks between 12 and 22 °C) before the final β'-2L (PPP) → β-2L (PPP) transformation and β-2L (PPP) melting. According to the vanishing of β_2 (OPO) and β_1-3L (OPO) reflections from XRD patterns when reaching 17 and 20 °C, respectively, this phenomenon corresponded to the successive melting of these forms.

The overall behavior of PPP/OPO mixtures when OPO was the predominant TAG may be clarified through the DSC and XRD data obtained for the 30PPP/70OPO and 10PPP/90OPO compositions (Figure 4.6).

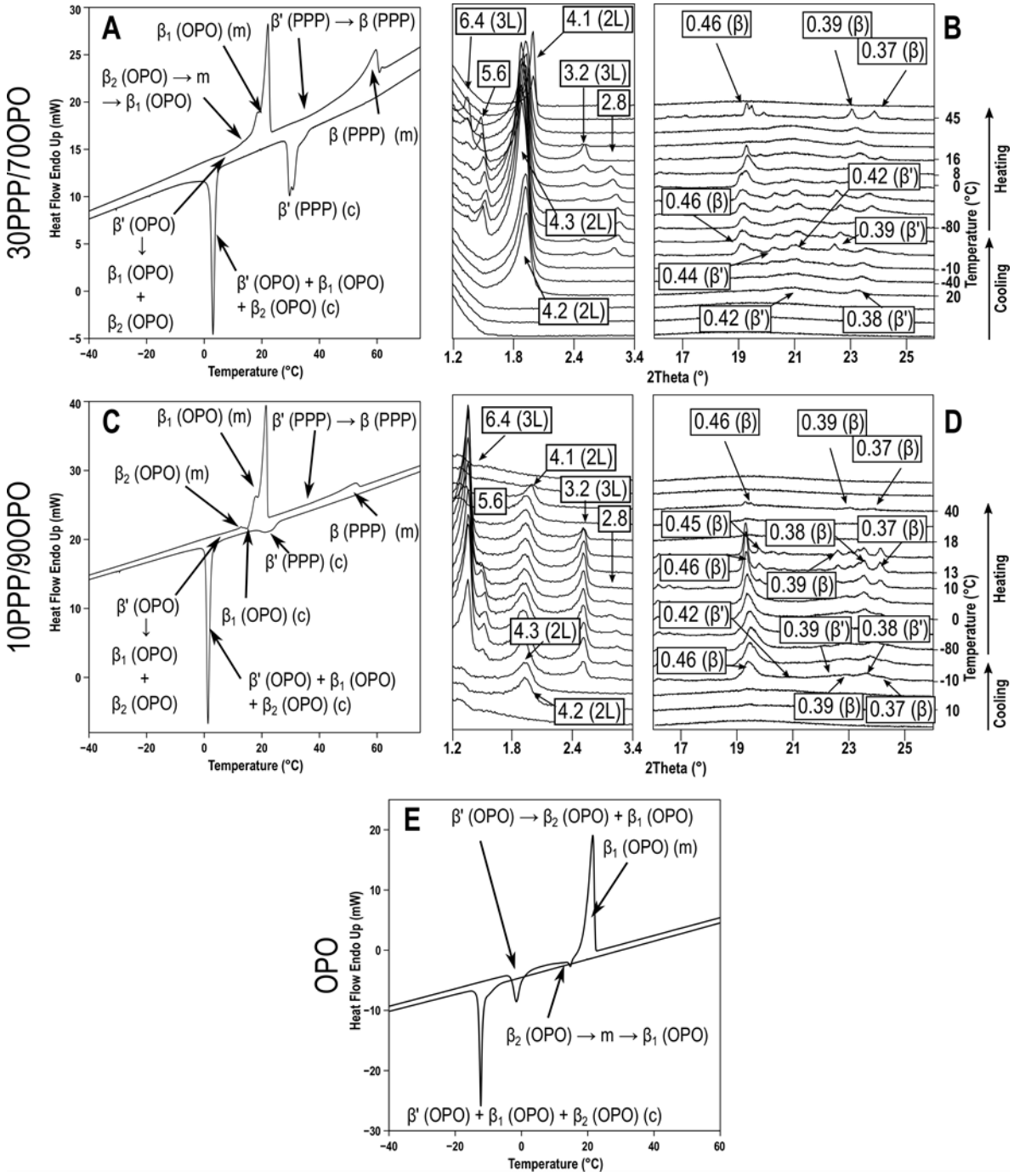

Figure 4.6. DSC thermograms and laboratory-scale XRD patterns of (A, B) 30PPP/70OPO and (C, D) 10PPP/90OPO mixtures when cooled and subsequently heated at 2 °C·min^{-1}. (E) Depicts the thermal behavior of pure OPO at similar conditions. *d*-spacing values are given in nm. (c): crystallization; (m): melting.

According to XRD data, no β-2L (PPP) crystallized in OPO-rich mixtures during cooling and the occurrence of β'-2L (PPP) was followed by that of β'-2L, β_2, and β_1-3L forms of OPO. During reheating, the first polymorphic event observed in DSC at around 6-7 °C corresponded again to the β'-2L (OPO) → β_1-3L (OPO) + β_2 (OPO) transformation. Then, the strengthening of reflections at 6.4 and 3.2 nm after vanishing of those at 5.6 and 2.8 nm at increasing temperature (see XRD patterns of the 30PPP/7OPO composition between 8 and 16 °C) confirmed a β_2 (OPO) → β_1-3L (OPO) transformation. In the 10PPP/90OPO mixture, this related to endothermic and exothermic peaks detected by DSC at 12.7 and 14.8 °C, respectively. The corresponding XRD patterns showed that all OPO was in the stable β_1-3L form at 13 °C, the melting of which led to a double endothermic peak in DSC (T_{top} of 17.6 and 21.7 °C). Thus, in mixtures at higher OPO content, the first overlapped peak probably also corresponded to β_2 (OPO) melting and the remaining ones to β_1-3L (OPO) melting. No double melting peak of β_1-3L (OPO) was observed in the pure OPO sample after the β'-2L → β_1-3L + β_2 transition and the next melt-mediated β_2 → β_1 transformation (Figure 4.6E. See corresponding XRD patterns in Figure 3.6 of Chapter 3). The reason for its occurrence is unclear but it could be related to the occurrence of some inhomogeneity in the sample pan during the recrystallization of the β'-2L (PPO) melt. As in previous compositions, XRD patterns of the 30PPP/70OPO and 10PPP/90OPO above 40 °C confirmed that once all OPO was molten, β'-2L (PPP) transformed into β-2 (PPP) before complete melting.

The overall behavior described in this section is illustrated in Figure 4.7. The distinct polymorphic forms of PPP and OPO obtained during the cooling process at almost the whole range of compositions confirmed the eutectic behavior of the PPP/OPO system also in the metastable state. However, the conditions applied resulted in a solubility of OPO in PPP of around 10-20%, a higher value than that estimated in most stable forms.

Both TAGs showed the concurrent crystallization of diverse polymorphs when cooling at 2 °C·min^{-1}, which was clearly influenced by the ratio of components in the mixtures. In PPP, the occurrence of α was prevented when more than 10% OPO was present. Moreover, β-2L (PPP) predominated in PPP-rich mixtures, whereas β'-2L (PPP) was promoted towards the pure OPO sample. As to the mixed acid TAG, β_1-3L (OPO) and β'-2L (OPO) occurred at all compositions, but the crystallization of β_2 (OPO) was prevented when the PPP content exceeded that of OPO.

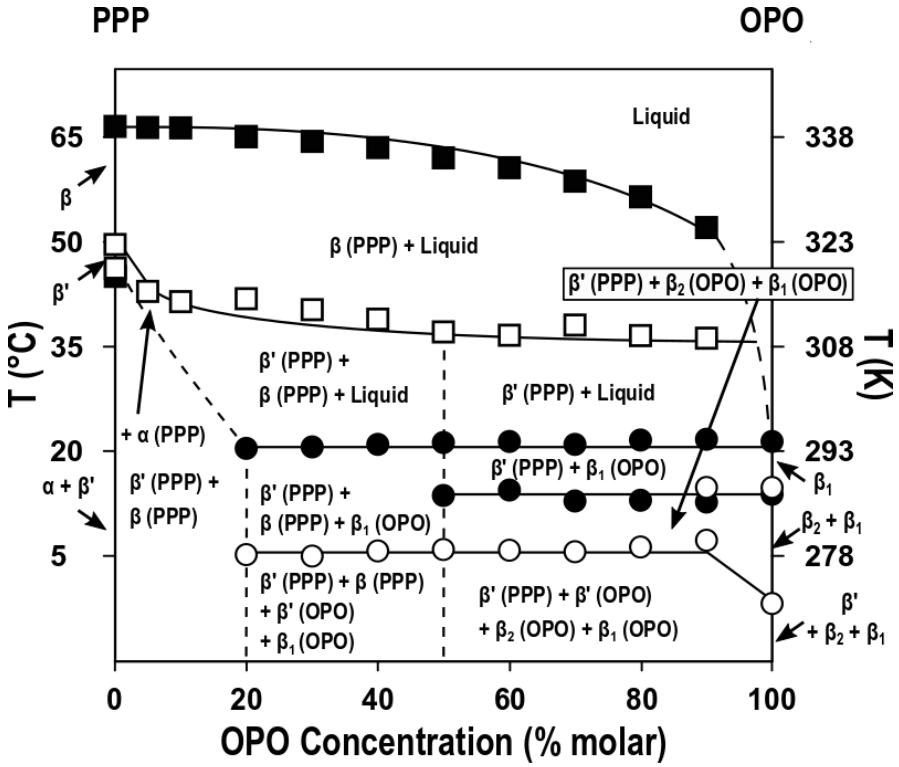

Figure 4.7. Phase behavior observed for PPP/OPO mixtures when heated at 2 °C·min^{-1} after a melt cooling process at the same rate. Delimited areas correspond to polymorphic domains between transitions experimentally determined. Empty symbols: exothermic; filled symbols: endothermic.

Detailed DSC data obtained during the heating treatment of PPP/OPO mixtures at 2 °C·min^{-1} is depicted in Table 4.4. The ratio of TAGs and the polymorphic occurrence during the previous cooling process influenced the transformation behavior, which can be summarized as follows:

(i) In mixtures with a PPP content above 80%, metastable forms of PPP, including small amounts of solubilized OPO, transformed into β-2L (PPP) via the solid-state before complete melting.

(ii) For PPP concentrations between 80 and 60%, the first β'-2L (OPO) → β_1-3L (OPO) transformation and subsequent β_1-3L (OPO) melting was followed by the β'-2L (PPP) to β-2L (PPP) transition and β-2L (PPP) melting.

(iii) In mixtures at lower PPP concentration, the presence of β_2 (OPO) crystals at the beginning of the heating process favored the occurrence of β'-2L (OPO) → β_1-3L (OPO) + β_2 (OPO), and β_2 (OPO) → melt → β_1-3L (OPO) transformations before the final melting of OPO and the further transformation of PPP.

(iv) OPO led to a decrease in the transformation and melting temperatures of β'-2L (PPP) and β-2L (PPP) of up to 5 and 10 °C, respectively, from the pure PPP sample to the 10PPP/90OPO composition. The transformation and melting temperatures of OPO polymorphs remained almost unaltered along the mixtures. However, it became clear that just the presence of 10% PPP content in the mixtures caused an increase in the transition temperature of β'-2L (OPO) with respect to the pure OPO sample.

Aiming to shed some light on the influence of faster thermal treatments on the polymorphic and mixing behavior of the PPP/OPO system, additional DSC and SR-XRD experiments were carried out on the equimolecular composition during a cooling process at 15 °C·min^{-1} and a subsequent heating treatment at the same rate. Phase behavior of eutectic nature was still detected at these conditions, but the crystallization and transformation behavior differed from that of the 50PPP/50OPO mixture processed at 2 °C·min^{-1}. The polymorphic events observed during both treatments are outlined in Figure 4.8. The DSC and SR-XRD data corresponding to the thermal treatment at the highest rate are shown in Figure 4.9.

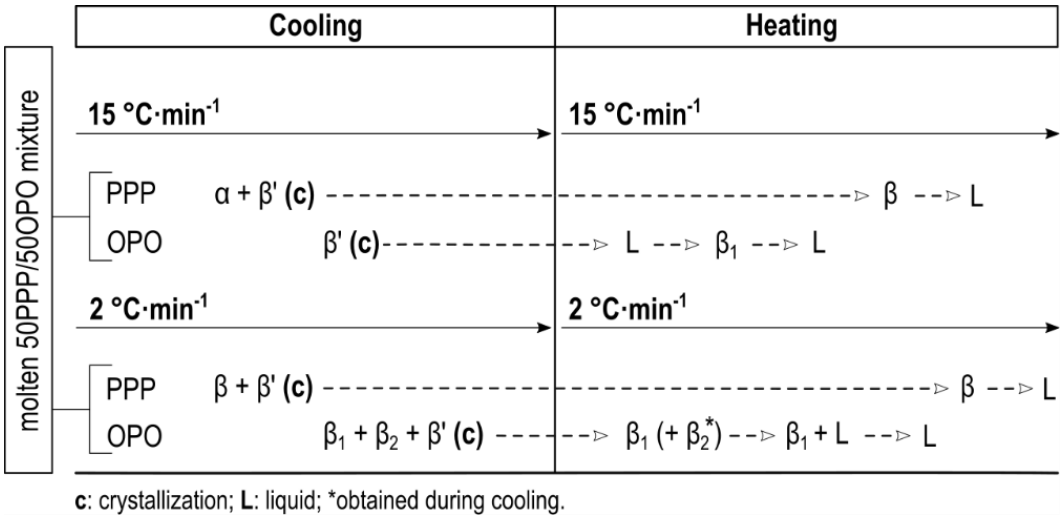

Figure 4.8. Scheme of the polymorphic behavior of the 50PPP/50OPO mixture under different thermal treatments. Adapted with permission from Macridachis et al. (2021). Copyright (2021) American Chemical Society.

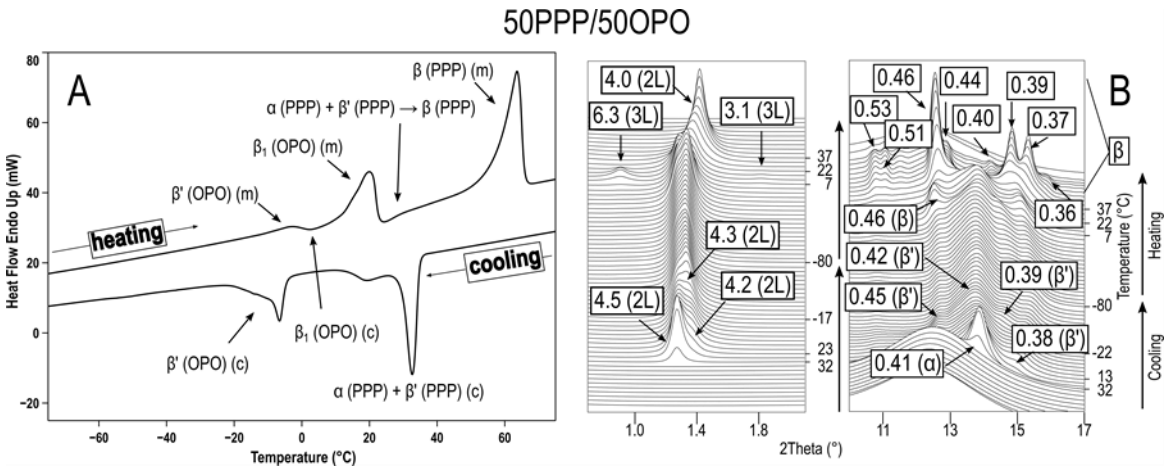

Figure 4.9. DSC thermogram (A) and SR-XRD patterns (B) of the 50PPP/50OPO mixture when cooled to -80 °C at 15 °C·min^{-1} and subsequently heated at the same rate. (c): crystallization; (m): melting. *d*-spacing values are given in nm. Adapted with permission from Macridachis et al. (2021). Copyright (2021) American Chemical Society.

Under fast cooling conditions, the first DSC peak with a shoulder observed at 32 °C was due to the crystallization of α-2L (PPP) (SAXD and WAXD peaks at 4.5 and 0.41 nm) and β' 2L (PPP) (peaks at 4.2, 0.45, 0.42, and 0.38 nm). At decreasing temperature, SAXD reflections at 4.3 and 0.39 nm confirmed that OPO occurred in the β'-2L form (DSC peak at -8 °C). As in pure TAGs, polymorphs of lower stability were favored by a faster cooling process. In Chapter 3, pure OPO cooled at the same rate of 15 °C·min^{-1} showed a main crystallization peak associated with α-2L below -20 °C. The large increase in crystallization temperature undergone by OPO in the presence of PPP likely influenced the favored occurrence of β'-2L (OPO) before α-2L (OPO) even at such high cooling rate. Thus, the mixing properties in least stable α forms could not be clarified under the thermal treatment applied.

During reheating at 15 °C·min^{-1}, β'-2L forms of PPP and OPO behaved in a eutectic manner during polymorphic transformation. The melt-mediated process observed by DSC at -2 °C was related to the vanishing of β'-2L (OPO) reflections from SR-XRD patterns at around 7 °C and the occurrence of new SAXD and WAXD peaks at 6.4 and 0.46 nm, respectively. All together indicated a β'-2L (OPO) → melt → β_1-3L (OPO) transformation. Stable OPO melted shortly after (~23 °C) and metastable forms of PPP (α and β') transformed into β (strong characteristic WAXD peaks of a triclinic subcell and new SAXD reflection at 4.0 nm) before complete melting.

Table 4.4. DSC temperatures (°C) of main polymorphic events occurring in PPP/OPO mixtures when heated at 2 °C·min^{-1} after a melt cooling process at the same rate.

PPP/OPO ratio	Heating at 2 °C·min^{-1}						
	a (m)	*β′ (PPP) (c)*	*β′ (PPP) → β (PPP)*	*β (PPP) (m)*			
PPP	46.3 ± 0.8	46.8 ± 0.8	49.5 ± 0.9	66.6 ± 0.9			
	a (PPP) + β′ (PPP) → β (PPP)		*β (PPP) (m)*				
95/10	42.9 ± 1.3		66.4 ± 0.4				
	β′ (PPP) → β (PPP)		*β (PPP) (m)*				
90/10	41.5 ± 0.5		66.4 ± 0.8				
	β′ (OPO) → β$_1$ (OPO)	*β$_1$ (OPO) (m)*	*β′ (PPP) → β (PPP)*	*β (PPP) (m)*			
80/20	5.2 ± 0.7	20.4 ± 0.5	41.9 ± 1.3	65.1 ± 0.5			
70/30	5.0 ± 1.0	20.6 ± 0.8	40.3 ± 0.3	64.4 ± 1.3			
60/40	5.7 ± 0.6	21.0 ± 0.9	38.9 ± 0.9	63.5 ± 1.0			
	β′ (OPO) → β$_2$ (OPO) + β$_1$ (OPO)		*β$_2$ (OPO) → m → β$_1$ (OPO)*		*β$_1$ (OPO) (m)*	*β′ (PPP) → β (PPP)*	*β (PPP) (m)*
50/50	5.9 ± 1.0		13.7 ± 0.2		21.3 ± 0.6	37.1 ± 0.8	62.1 ± 0.7
40/60	5.8 ± 0.3		14.5 ± 0.4		21.4 ± 0.4	36.7 ± 0.9	60.7 ± 0.5
30/70	5.6 ± 0.8		12.9 ± 0.6		21.0 ± 0.4	38.1 ± 1.3	58.7 ± 1.0
20/80	6.3 ± 0.3		13.0 ± 0.2		21.6 ± 0.3	36.6 ± 0.3	56.5 ± 0.4
	β′ (OPO) → β$_2$ (OPO) + β$_1$ (OPO)		*β$_2$ (OPO) (m)*	*β$_1$ (OPO) (c)*	*β$_1$ (OPO) (m)*	*β′ (PPP) → β (PPP)*	*β (PPP) (m)*
10/90	7.0 ± 1.0		12.7 ± 0.4	14.8 ± 0.2	21.7 ± 0.7	36.2 ± 2.3	52.1 ± 0.3
	β′ (OPO) → β$_2$ (OPO) + β$_1$ (OPO)		*β$_2$ (OPO) (m)*	*β$_1$ (OPO) (c)*	*β$_1$ (OPO) (m)*		
OPO	1.2 ± 1.0		n.d.	14.8 ± 0.4	21.4 ± 0.9		

n.d.: not determined. (c): crystallization; (m): melting.

4.2.2. PPP/POP binary system

4.2.2.1. *Phase behavior after a thermal stabilization stage*

The phase behavior of PPP/POP mixtures in stable forms after a two-week thermodynamic stabilization process was previously evaluated by Minato et al. (1996). The authors confirmed the eutectic nature of the system and solubility values of POP and PPP in each other of at around 40-50% and below 10%, respectively. In the present study, the mixing behavior of PPP/POP mixtures at specific concentration intervals was reexamined after six months of thermal incubation at 27 °C in order to more precisely analyze the solubility limits of the binary system.

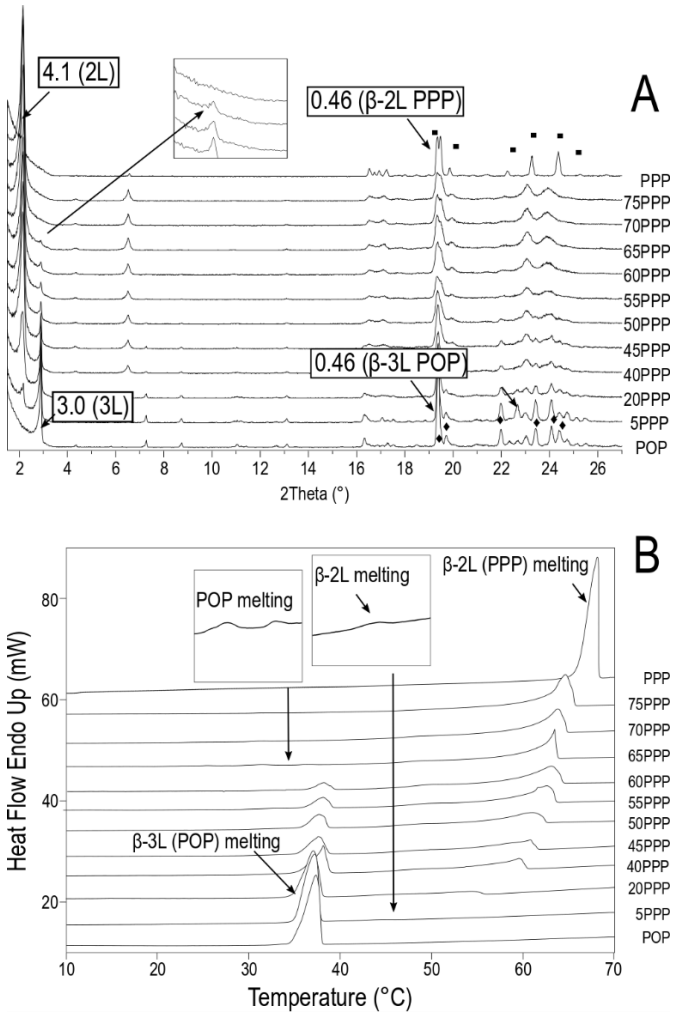

Figure 4.10. PPP/POP system. (A) Laboratory-scale XRD patterns of stabilized PPP/POP mixtures obtained at 10 °C. ■: WAXD peaks of β-2L (PPP); ◆: wide-angle XRD peaks of β-3L (POP). *d*-spacing values are given in nm. (B) DSC thermograms of stabilized PPP/POP mixtures heated at 2 °C·min^{-1}. Reprinted with permission from Macridachis et al. (2021). Copyright (2021) American Chemical Society.

Diffraction patterns of thermodynamically stabilized PPP/POP mixtures obtained at 10 °C confirmed the presence of β-2L (PPP) at all compositions (■ in Figure 4.10A). As to the pure POP sample, the small-angle peak at 3.0 nm (002 reflection) and wide-angle peaks at 0.46, 0.45, 0.40, 0.38, 0.37, and 0.36 nm (denoted by ♦) indicated the presence of the stable β_1-3L (POP) form. However, the increased intensity of a peak at 0.39 nm in the 5PPP/95POP composition (pointed by an arrow) suggested the presence of β_2-3L (POP) (Bayés-García et al., 2013b; Sato et al., 1989) and evidenced that, even after 6 months, not all POP in the mixtures was in the most stable polymorph. This seems to be due to the complicated stabilization shown by symmetric saturated-*cis*-unsaturated components in binary mixtures of TAGs (Koyano et al., 1992; Minato et al., 1997a, 1997b; Takeuchi et al., 2002a). For simplification, POP β forms are referred to as β-3L (POP).

The distinct polymorphism and melting behavior displayed by the components of the mixtures during their heating treatment (clarified in Figure 4.10B) agreed with published data, as shown by the phase diagram depicted in Figure 4.11.

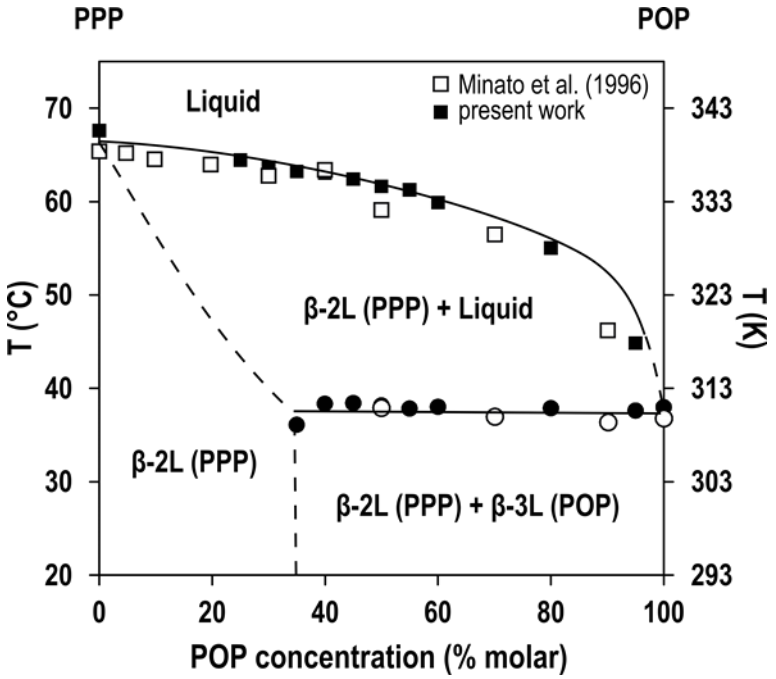

Figure 4.11. Binary phase diagram of incubated PPP/POP mixtures constructed from DSC data obtained when heating at 2 °C·min^{-1}. Reprinted with permission from Macridachis et al. (2021). Copyright (2021) American Chemical Society. Empty symbols correspond to previous data from Minato et al. (1996). Copyright (1996) John Wiley & Sons.

In our case, however, the 60PPP/40POP composition showed a DSC endothermic event associated with POP melting at around 38 °C (see detailed DSC data in Table 4.5). Furthermore, a weak signal consisting of a double endothermic peak (T_{top} of 31 and 36 °C) was still detected in the 65PPP/35POP mixture. Despite this, no evident changes were observed in β-3L (POP) diffraction peaks during the thermal processing before its complete melting (data not shown). Probably, some metastable POP was still present at such high concentration level of PPP, resulting in the first DSC endothermic peak before the melting of β-3L (POP) crystals. Consequently, the amount of POP that showed to be able to integrate into the crystalline phase of PPP was reduced to 30-35% in the present study, which could be explained in part by the longer time allowed for the mixtures to stabilize. We also confirmed a solubility limit of PPP in POP below 5%.

Table 4.5. Melting temperatures (°C) of PPP and POP in stabilized PPP/POP mixtures heated from 10 to 80 °C at 2 °C·min^{-1}.

Polymorph	**PPP**	**75PPP**	**70PPP**	**65PPP**	**60PPP**	**55PPP**
β-3L (POP)	-	-	-	36.1 ± 0.5	38.3 ± 0.3	38.4 ± 0.7
β-2L (PPP)	67.6 ± 0.4	64.4 ± 0.7	63.7 ± 0.6	63.2 ± 0.4	63.1 ± 0.5	62.4 ± 0.7
Polymorph	**50PPP**	**45PPP**	**40PPP**	**20PPP**	**5PPP**	**POP**
β-3L (POP)	38.2 ± 0.4	37.8 ± 0.4	38.0 ± 0.8	37.9 ± 0.9	37.6 ± 0.3	38.0 ± 0.5
β-2L (PPP)	61.6 ± 0.8	61.3 ± 0.4	59.9 ± 0.2	55.0 ± 0.7	44.8 ± 0.5	-

4.2.3. PPP/PPO binary system

4.2.3.1. *Phase behavior after a thermal stabilization stage*

PPP/PPO mixtures were held for 5 days at 40 °C and for 6 months at 27 °C before their analysis. Figure 4.12 depicts the diffraction patterns of stabilized PPP/PPO mixtures measured at 10 °C and the DSC thermograms obtained when the same were heated at 2 °C·min^{-1}.

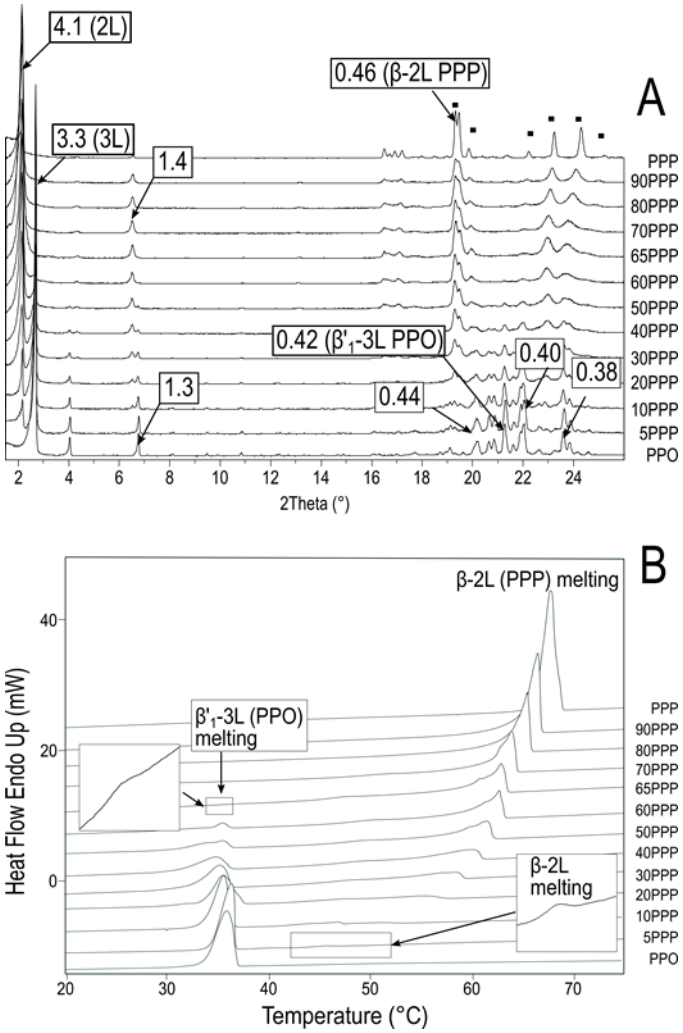

Figure 4.12. PPP/PPO system. (A) Laboratory-scale XRD patterns of stabilized PPP/PPO mixtures obtained at 10 °C. ■: WAXD peaks of β-2L (PPP). *d*-spacing values are given in nm. (B) DSC thermograms of stabilized PPP/PPO mixtures heated at a rate of 2 °C·min^{-1}. Reproduced from Macridachis et al. (2022) with permission from the PCCP Owner Societies.

The single DSC endothermic peaks exhibited by pure PPP and PPO samples at 67.9 and 36.1 °C, respectively, were ascribed to the melting of their stable polymorphs. β-2L (PPP)

showed the SAXD peak at 4.1 nm and WAXD peaks at 0.46, 0.45, 0.40, 0.38, 0.37, and 0.36 nm (denoted by ■ in Figure 4.12A). As to PPO, WAXD peaks at 0.44, 0.42, 0.40, and 0.38 nm of an orthorhombic subcell structure, together that at 3.3 nm (002 reflection of the peak at 6.7 nm) in the SAXD region, indicated the presence of β'_1-3L.

The melting behavior from the 90PPP/10PPO to the 70PPP/30PPO mixture was governed by the trisaturated TAG, and no thermal or XRD signals associated with PPO were detected. Then, at the 65PPP/35PPO composition, the DSC melting peak of β-2L (PPP) at 63.2 °C was preceded by a low-energy one at 34 °C. This temperature corresponded to the melting of β'_1-3L (PPO), according to the SAXD data (presence of 002 and 005 reflections at 3.3 and 1.3 nm, respectively). In this system, the low molecular compatibility between monoacid saturated and mixed-acid saturated-unsaturated TAGs led to a limited solubility of PPO in solid PPP of about 30-35%. One may notice that this value is similar to that estimated before for the symmetric POP.

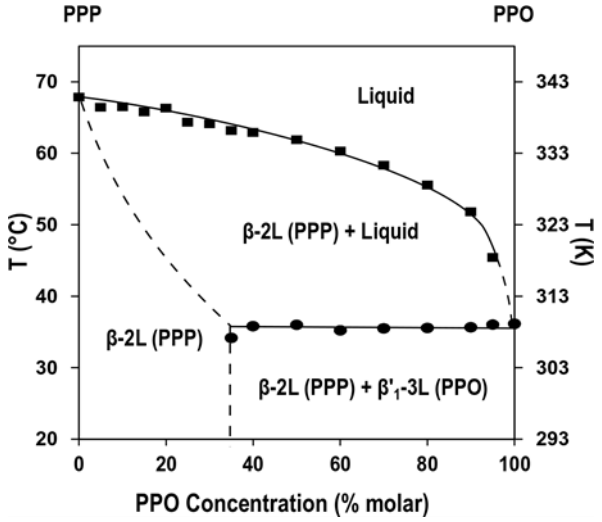

Figure 4.13. Binary phase diagram of incubated PPP/PPO mixtures constructed from DSC data obtained when heating at 2 °C·min^{-1}. Reproduced from Macridachis et al. (2022) with permission from the PCCP Owner Societies.

The mixtures with PPO content beyond the solubility limit were composed by a β-2L (PPP) phase containing solubilized PPO and a β'_1-3L (PPO) one, with the latter exhibiting more intense and well-defined DSC and XRD signals as the content of mixed-acid TAG increased in the samples. As illustrated in the phase diagram of Figure 4.13, PPO showed a steady melting temperature at around 35-36 °C in the mixtures (see detailed melting data in Table 4.6), whereas the liquid curve defined by β phases rich in PPP towards the PPO sample showed the typical

negative slope followed by high-melting components in eutectic systems. In the heating thermograms, the reduction in the melting temperature of β-2L at increasing PPO content was accompanied by the ever-decreasing symmetric shape of the corresponding DSC peaks. This behavior continued until the 5PPP/95PPO composition. The weak β-2L melting peak (T_{top} of 45.4 °C) still detected several degrees above that of β'_1-3L (PPO) suggested the presence of a very asymmetric eutectic composition in the PPP/PPO diagram.

Table 4.6. DSC melting temperatures (°C) of PPP and PPO when stabilized PPP/PPO mixtures were heated from 10 to 80 °C at 2 °C·min^{-1}.

Polymorph	**PPP**	**95PPP**	**90PPP**	**85PPP**	**80PPP**	**75PPP**	**70PPP**	**65PPP**
β'-3L (PPO)	-	-	-	-	-	-	-	34.1 ± 0.5
β-2L (PPP)	67.9 ± 0.7	66.4 ± 1.1	66.5 ± 0.7	65.8 ± 1.2	66.3 ± 2.0	64.3 ± 0.4	64.1 ± 0.7	63.2 ± 0.4
Polymorph	**60PPP**	**50PPP**	**40PPP**	**30PPP**	**20PPP**	**10PPP**	**5PPP**	**PPO**
β'-3L (PPO)	35.8 ± 0.6	36.0 ± 1.0	35.2 ± 0.6	35.5 ± 0.8	35.5 ± 0.3	35.6 ± 0.6	36.0 ± 0.3	36.1 ± 1.3
β-2L (PPP)	62.9 ± 0.5	61.9 ± 0.8	60.3 ± 0.9	58.3 ± 0.6	55.5 ± 0.4	51.8 ± 0.6	45.4 ± 0.4	-

4.2.3.2. *Kinetic phase behavior*

Results on PPP/OPO mixtures evaluated under kinetic conditions allowed us to confirm eutectic behavior in metastable β' phases. The kinetic phase behavior of PPP/PPO mixtures was examined by DSC and X-ray diffraction techniques during the application of a similar thermal treatment. Thus, the mixtures were first cooled from the melt to -30 °C at 2 °C·min^{-1} and then reheated at the same rate.

Figure 4.14A depicts the DSC cooling and heating thermograms obtained for pure PPP and the 90PPP/10PPO composition at the above conditions. The exothermic events displayed by these samples upon cooling were confirmed by XRD (Figure 4.14B. See diffraction data corresponding to pure PPP in Figure 3.1 of Chapter 3) as a concurrent crystallization of α-2L (small- and wide-angle peaks at 4.5 and 0.41 nm, respectively) and β'-2L (peaks at 4.2, 0.45, 0.43, 0.42 and 0.38 nm) forms of PPP. This composition was a solid solution rich in PPP, since no DSC events or XRD reflections attributed to PPO were detected. During reheating, the melt-mediated α-2L → β'-2L transformation and further β'-2L to β-2L solid transition shown by pure PPP before complete melting, in the mixture turned into a solid-state transformation of the two metastable forms into β-2L (single DSC exothermic peak at 44.1 °C and occurrence of characteristic β peaks in XRD pattern at 45 °C).

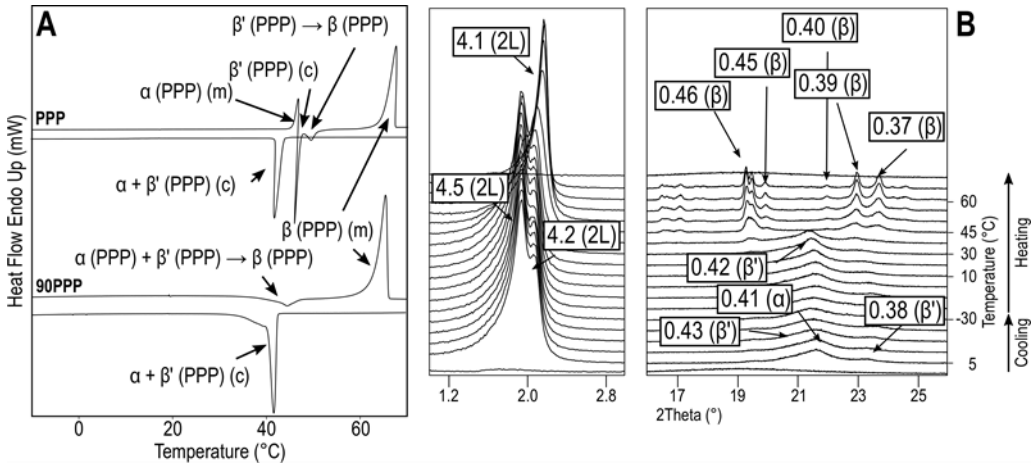

Figure 4.14. (A) DSC thermograms obtained for pure PPP and the 90PPP/10PPO mixture when cooled and subsequently heated at 2 °C·min^{-1}. (B) laboratory-scale XRD data corresponding to the 90PPP/10PPO mixture. (c): crystallization; (m): melting. *d*-spacing values are given in nm.

Phase separation occurred in mixtures at increasing PPO content, which led to a more complex crystallization and phase transformation behavior. This is exemplified by the thermal signals of the 70PPP/30PPO, 50PPP/50PPO, and 30PPP/70PPO blends of Figure 4.15A, which are clarified by the SR-XRD data obtained for the equimolecular mixture (Figure 4.15B).

α-2L (PPP) and β'-2L (PPP) were also obtained at these compositions on cooling but XRD reflections of the least stable form vanished at decreasing temperature until no α was detected in the samples. Although the occurrence of α-2L (PPP) was not confirmed by XRD in the 30PPP/70PPO mixture (Figure 4.15C), the corresponding DSC curve suggested an equivalent behavior. The next crystallization of β'_2-2L (PPO) (DSC peak at about 20 °C) was not evident in WAXD patterns, but the SAXD peak at 4.2 nm increased in intensity and shifted subtly to a lower angle (see amplified image * in Figure 4.15B).

Detailed DSC data obtained during the next reheating of these compositions can be found in Table 4.7. β'_2-2L (PPO) melted at 30-31 °C without further transformation into the stable β'_1-3L (PPO). Its corresponding XRD reflections vanished at around 35 °C (pointed by white arrows in patterns of the 50PPP/50PPO and 30PPP/70PPO compositions) and those occurring at 0.46, 0.39, and 0.38 nm several degrees above evidenced the next β'-2L (PPP) to β-2L (PPP) transition. According to the endothermic peaks at about 40 °C in mixtures with PPP ≤50%, a high PPO content favored the occurrence of this transformation through the melt. Despite this, a weak exothermic signal was still visible in the 50PPP/50PPO composition between β'_2-2L (PPO) and β'-2L (PPP) melting (indicated by a white arrow in Figure 4.15A). Since only a decrease in

intensity of β' reflections was detected by SR-XRD (see amplified image ** in Figure 4.15B), this event could be due to the recrystallization of some PPP demixed from the PPO phase after melting or that was already present in the mixture in a less stable form.

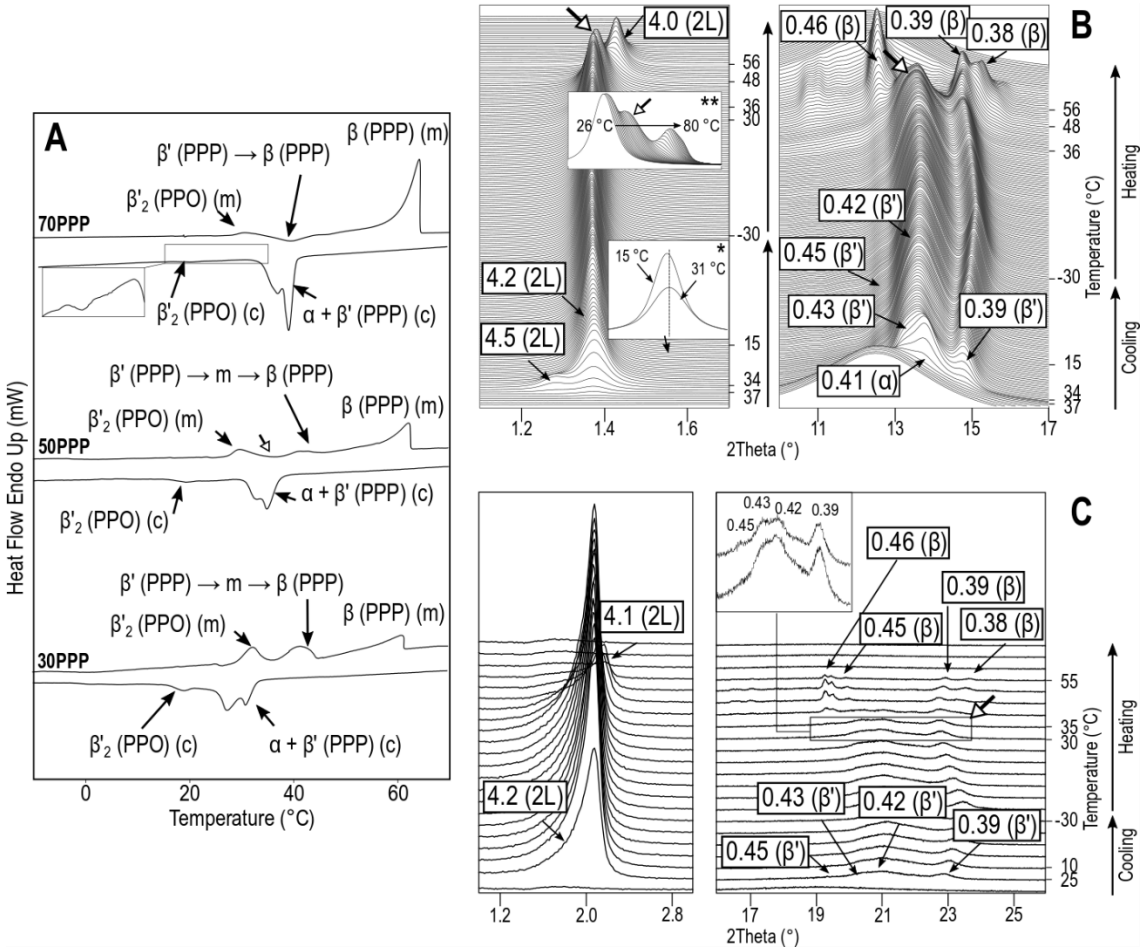

Figure 4.15. (A) DSC thermograms obtained for PPP/PPO mixtures with 70, 50, and 30% PPP when cooled at subsequently heated at 2 °C·min^{-1}. (B) SR-XRD data corresponding to the 50PPP/50PPO mixture. (C) Laboratory-scale XRD patterns obtained for the 30PPP/70PPO composition. (c): crystallization; (m): melting. *d*-spacing values are given in nm.

Table 4.7. DSC temperatures (°C) of main polymorphic events occurring in PPP/PPO mixtures when heated at 2 °C·min^{-1} soon after a melt cooling process at the same rate.

PPP/PPO ratio	Heating at 2 °C·min^{-1}						
	a (m)	*β′ (PPP) (c)*	*β′ (PPP) → β (PPP)*	*β (PPP) (m)*			
PPP	46.3 ± 0.8	46.8 ± 0.8	49.5 ± 0.9	66.6 ± 0.9			
	a (PPP) + β′ (PPP) → β (PPP)		*β (PPP) (m)*				
90/10	44.5 ± 0.4		65.6 ± 0.6				
	β′$_2$ (PPO) (m)		*β′ (PPP) → β (PPP)*	*β (PPP) (m)*			
80/20	31.2 ± 0.8		41.6 ± 0.3	65.0 ± 0.4			
70/30	30.9 ± 0.5		39.5 ± 1.2	63.9 ± 0.6			
60/40	30.5 ± 1.1		39.0 ± 0.7	62.7 ± 0.9			
	β′$_2$ (PPO) (m)		*β′ (PPP) → m → β (PPP)*	*β (PPP) (m)*			
50/50	30.6 ± 0.8		42.4 ± 0.4	61.7 ± 0.6			
40/60	30.4 ± 0.6		40.5 ± 0.4	60.0 ± 0.4			
30/70	30.3 ± 0.6		39.3 ± 0.6	57.6 ± 0.8			
20/80	31.2 ± 0.7		39.4 ± 0.4	55.3 ± 0.4			
	a$_1$ (PPO) (m)	*β′$_2$ (PPO) (c)*	*β′$_2$ (PPO) → m → β′$_1$ (PPO) → m*		*β′ (PPP) → m → β (PPP)*		*β (PPP) (m)*
10/90	18.8 ± 0.3	19.7 ± 0.4	31.4 ± 0.3		41.5 ± 0.6		49.6 ± 0.5
	a$_2$ (PPO) → m → a$_1$ (PPO)		*a$_1$ (PPO) (m)*	*β′$_2$ (PPO) + β′$_1$ (PPO) (c)*	*β′$_2$ (PPO) (m)*	*β′$_1$ (PPO) (c)*	*β′$_1$ (PPO) (m)*
PPO	15.0 ± 0.4		18.6 ± 0.3	19.1 ± 0.3	27.7 ± 0.5	28.5 ± 0.5	31.3 ± 0.4

(c): crystallization; (m): melting.

Figure 4.16 shows the DSC and XRD data obtained during the thermal treatment of the 10PPP/90PPO composition. The increased PPO content (see XRD patterns corresponding to the pure TAG in Figure 3.8 of Chapter 3) favored the additional presence of a small amount of α_1-3L (PPO) crystals in the mixture at the end of the cooling process (SAXD and WAXD peaks at 3.9 and 0.41 nm, respectively). Upon heating, the α_1-3L (PPO) → β'_2-2L (PPO) transformation resulted in the melt-mediated process observed at around 19 °C in DSC and the vanishing of α diffraction peaks at 25 °C. The following exothermic event at around 26 °C led to a slight shifting of the small-angle reflection of β'_2-2L (PPO) towards a higher *d*-spacing (see the enlarged image). This could be indicative of subtle changes in molecular ordering rather than a polymorphic transformation of PPO. The next endothermic peak at 31 °C corresponded to the sequence of events β'_2-2L (PPO) → melt → β'_1-3L (PPO) (new small-angle peak with *d*-spacing value of 3.4 nm at 35 °C) → melt, after which only β'-2L (PPP) was detected by XRD. Although the weak PPP diffraction peaks and the amount of liquid did not allow a proper clarification, the last endothermic event detected after β'-2L (PPP) melting suggested that probably some β-2L (PPP) formed before the end of the process.

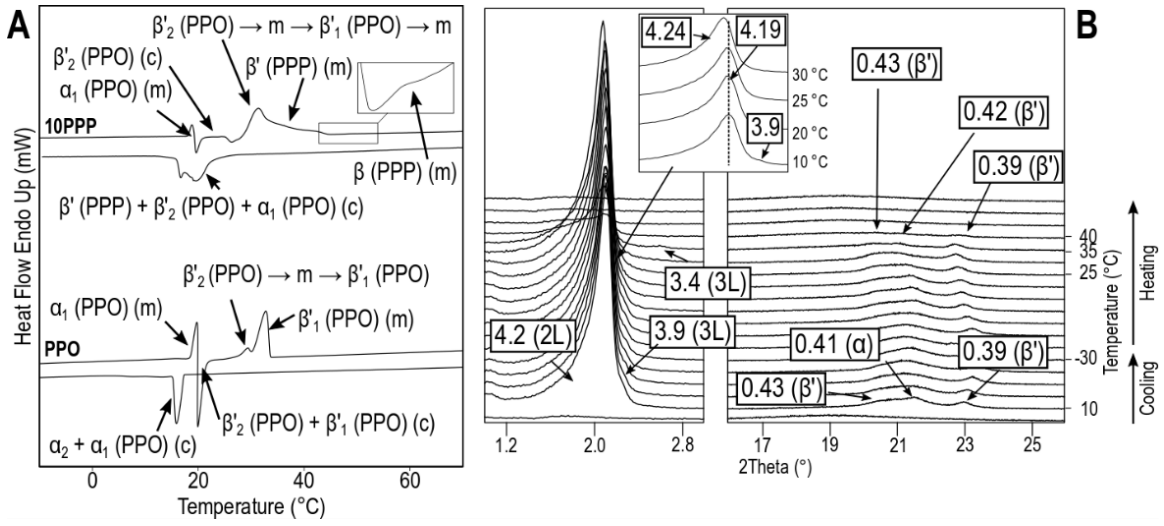

Figure 4.16. (A) DSC thermograms obtained for pure PPO and the 10PPP/90PPO mixture when cooled and subsequently heated at 2 °C·min^{-1}. (B) Laboratory-scale XRD data corresponding to the 10PPP/90PPO mixture. (c): crystallization; (m): melting. *d*-spacing values are given in nm.

The polymorphic and kinetic phase behavior of PPP/PPO mixtures described in this section is depicted in Figure 4.17.

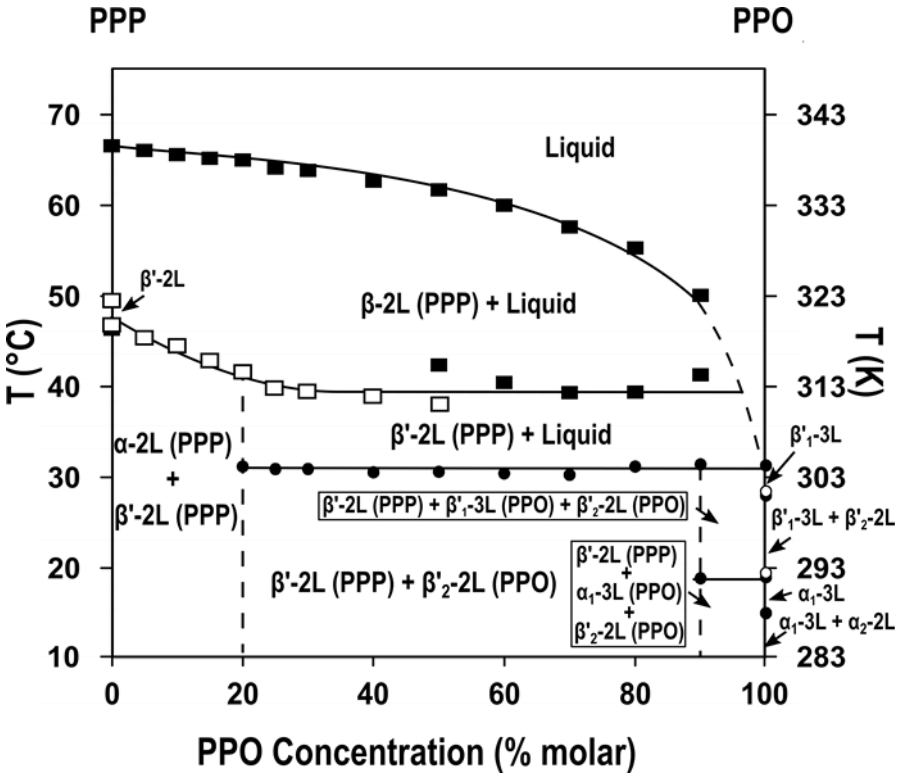

Figure 4.17. Phase behavior observed for PPP/PPO mixtures when heated at 2 °C·min^{-1} after a melt cooling process at the same rate. Delimited areas correspond to polymorphic domains between transitions experimentally determined. Empty symbols: exothermic; filled symbols: endothermic. Reproduced from Macridachis et al. (2022) with permission from the PCCP Owner Societies.

In summary:

(i) The phase behavior of eutectic nature determined for PPP/PPO mixtures in most stable forms was also confirmed in metastable forms obtained during a cooling process at 2 °C·min^{-1}.

(ii) During crystallization, α-2L (PPP) and β'-2L (PPP) incorporating small amounts of PPO occurred in mixtures with PPP above 80%. However, immiscible behavior occurred along almost all compositions. Thus, the kinetic conditions applied led to a lower solubility of PPO in PPP in metastable β' phases than in stable β ones obtained after 6 months of thermodynamic stabilization.

(iii) The polymorphic occurrence detected between 80PPP/20PPO and 20PPP/80PPO was simplified with respect to compositions at the extremes. Also, the stability of the forms obtained increased: the concurrent crystallization of α-2L and β'-2L in pure PPP, and α_2-2L and α-3L in pure PPO, turned into two β'-2L phases behaving in a eutectic manner in the mixtures.

(iv) Regarding reheating processes, two main points can be highlighted. The β to β' transition of PPP was promoted via melt-mediation when PPO accounted for ≥50% in the mixtures. As to PPO, its β'-2L form melted at a considerable higher temperature in the presence of more than 10% PPP. X-ray scattering confirmed as well that the next recrystallization in β_1-3L (PPO) was avoided.

Figure 4.18 shows additional DSC and SR-XRD data obtained when cooling the 50PPP/50PPO mixture at a higher rate of 15 °C·min^{-1}. The occurrence of less stable α-2L (PPP) and α_1-3L (PPO) forms confirmed eutectic behavior also at these conditions. The first melt-mediated transformation when reheating at 2 °C·min^{-1} corresponded to the α_1-3L (PPO) → β'_2-2L (PPO) transition (vanishing of the diffraction peak at 3.9 nm at the expense of those at 4.1 and 0.39 nm). Since α-2L (PPP) reflections were still detected above 32 °C, the next endothermic peak around this temperature was ascribed to β'_2-2L (PPO) melting. However, the disappearance of α peaks and the stronger reflections at 4.2 and 0.39 nm when reaching 36 °C suggested that the α-2L (PPP) → β'-2L (PPP) transformation started at a close temperature, probably favored by the presence of liquid PPO. For the same reason, this event seemed to be obscured in the heating curve, and only the thermal signals of the succeeding β'-2L (PPP) → β-2L (PPP) melt-mediated transformation and β-2L (PPP) melting could be observed.

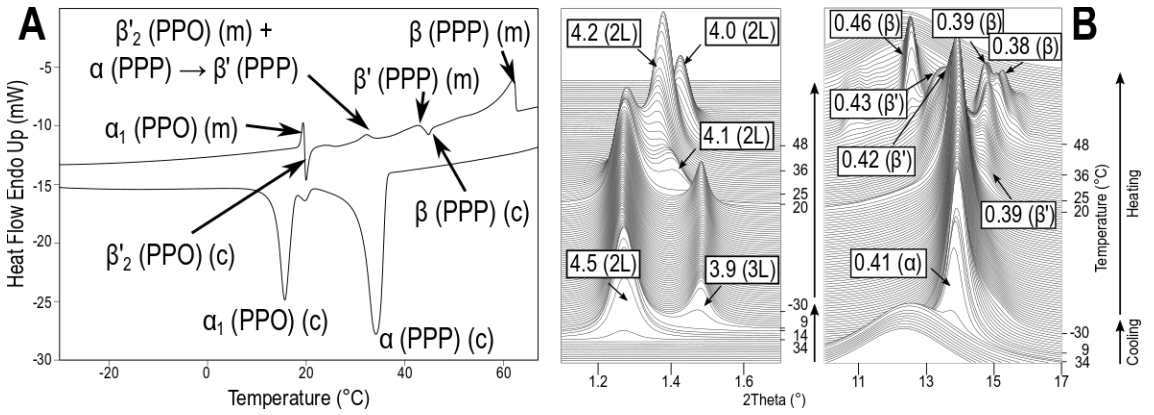

Figure 4.18. 50PPP/50PPO mixture. (A) DSC thermogram and (B) SR-XRD patterns obtained when cooled at 15 °C·min^{-1} and reheated at 2 °C·min^{-1}. (c): crystallization; (m): melting. *d*-spacing values are given in nm.

The results obtained for PPP/PPO mixtures in this study contrast with the complex polymorphism and mixing behavior reported for PPP/PPO mixtures quenched from the melt at 25 °C·min^{-1} to -40 °C and reheated at 5 °C·min^{-1} (Gibon & Durant, 1985). It was found that sub-α solid solutions were formed in mixtures with PPO above 30%, which during reheating sequentially transformed into α and β' solid solutions before phase separation and occurrence of β'-2L and β'-3L crystals. After the melting of the β'-3L crystals likely attributed to PPO, β'-2L transformed into β-2L before complete melting of the mixtures.

The divergent behavior found in our study is explained by the much different rate applied during the cooling treatment, which has a direct impact on the degree of supercooling. Studies aiming to model the kinetic separation of TAG phases formed by melt cooling have, in turn, pointed to a crucial role of supercooling and the excess Gibbs free energy on phase development (Los & Flöter, 1999; Los et al., 2002). Thus, increasing the degree of supercooling by applying faster cooling rates often improves miscibility, whereas large excess free energy is expected to induce kinetic phase separation. Nevertheless, the influence of the latter may be reduced if a sufficient degree of supercooling is achieved. This explains the prevalent occurrence of solid solutions in PPP/PPO mixtures cooled at 25 °C·min^{-1}, despite the great excess free energy expected from the presence of oleic and palmitic acid chains. The more irregular crystal packing resulting from a higher degree of supercooling probably facilitated the accommodation of TAGs which otherwise would be expected to segregate. However, the eutectic tendency of the system was evident during polymorphic transformation.

The influence of supercooling has been reported in other binary systems. The single α phase obtained during rapid chilling of SSS/PPP mixtures turned into two heterogeneous phases rich in either SSS or PPP when cooling rates below 20 °C·min^{-1} were applied (Himawan et al., 2007; Lutton, 1955; MacNaughtan et al., 2006). PPP/POP mixtures subjected to varying dynamic thermal treatments also showed a separation of TAGs in the metastable state at higher cooling rates (Gibon et al., 1986; Lu et al., 2019; Minato et al., 1996). This has implications in the functionality of lipid-based products and the performance of lipid fractionation processes, in which the efficient separation of desired phases may be hindered by solid solution formation.

The similar long spacing values of β'-2L forms of PPP, POP, and PPO complicates the differentiation of eutectic and more or less homogeneous miscible phases of these components by X-ray scattering (Sato, 2012). In our case, the clear distinct DSC peaks and the evolution of the intensity of XRD reflections observed during thermal treatments indicated that one of the β' phases was mainly composed by PPP and the other by PPO. However, strong mixing interactions occurring between them may be responsible for increase in melting temperature underwent by β'_2-2L (PPO) in the mixtures, which exceeded 30 °C at all compositions. The closer melting point of this form to that of stable β'_1-3L (PPO) may have contributed to the prevented occurrence of this form in mixtures with a PPP content above 10%.

4.2.4. Mixtures of PPP and the POP/OPO molecular compound system

4.2.4.1. *Phase behavior after a thermal stabilization stage*

PPP/$MC_{POP/OPO}$ mixtures were analyzed after a thermodynamic stabilization procedure consisting of 7 days at 40 °C and 6 months at 27 °C. Figure 4.19 shows the laboratory-scale XRD patterns of the mixtures obtained at 10 °C after the incubation time and the DSC thermograms obtained when heating the mixtures at 2 °C·min^{-1}.

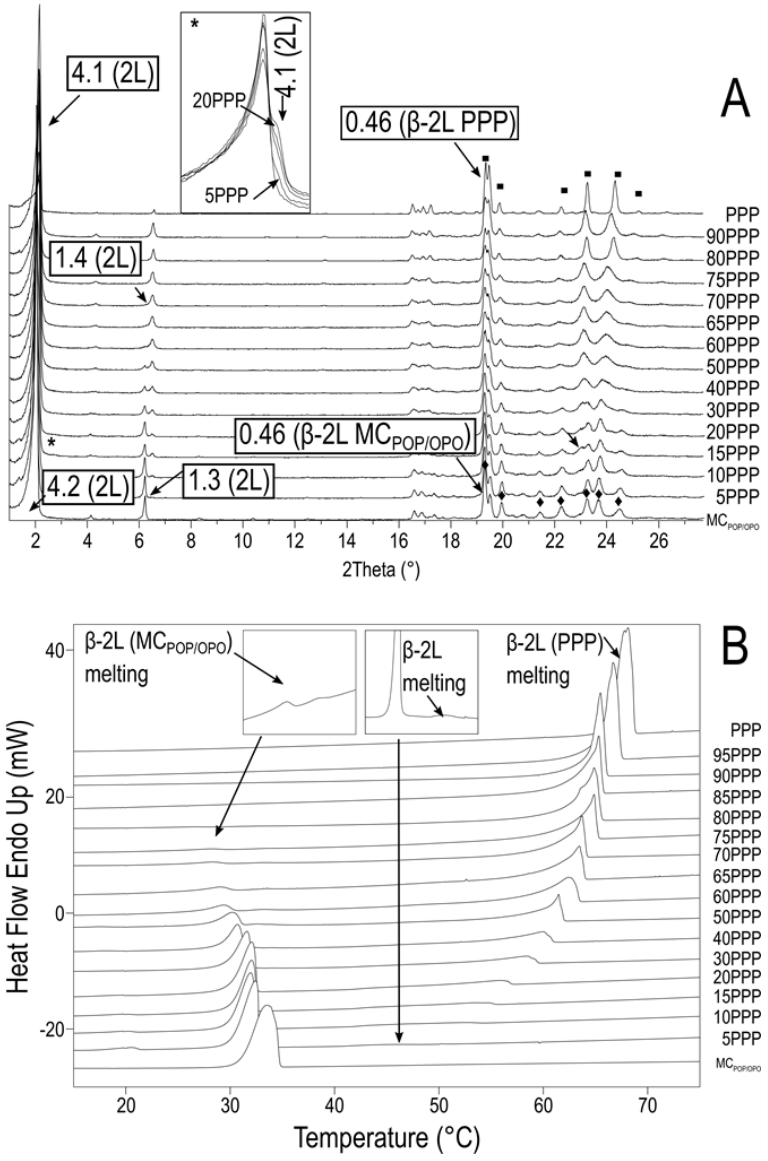

Figure 4.19. Laboratory-scale XRD patterns of stabilized PPP/$MC_{POP/OPO}$ mixtures obtained at 10 °C. ■: WAXD peaks of β-2L (PPP); ◆: WAXD peaks of β-2L ($MC_{POP/OPO}$). *d*-spacing values are given in nm. Adapted with permission from Macridachis et al. (2021). Copyright (2021) American Chemical Society.

Structural similarities between stable β-2L forms of PPP and $MC_{POP/OPO}$ hindered the differentiation of both polymorphs by WAXD data in mixtures with one of the components at a very low concentration. In the same manner, the overlapping of SAXD peaks (*d*-spacing values of 4.2 and 4.1 nm) prevented the accurate detection of low-intensity peaks. To deliver a more precise data analysis, 003 reflections in the SAXD region were also used to support our observations. In the pure $MC_{POP/OPO}$ sample, the SAXD peak at 4.2 nm and its 003 reflection at 1.4 nm were associated with the most stable β-2L ($MC_{POP/OPO}$) through WAXD peaks at 0.46, 0.44, 0.41, 0.40, 0.38, 0.37 and 0.36 nm, ♦). This is in agreement with previous work on POP/OPO mixtures (Minato et al., 1997b; Nakanishi et al., 2018). The DSC heating curve of $MC_{POP/OPO}$ heated at 2 °C·min^{-1} also indicated the presence of a single form through the endothermic event occurring at around 33 °C.

At the low addition of 5% PPP, the melting peak of β-2L ($MC_{POP/OPO}$) was followed by a second one at around 50 °C (see the enlarged image in Figure 4.19B). No discernible changes were observed in the WAXD pattern at 10 °C. However, a low-intensity shoulder appeared on the SAXD peak at 4.2 nm (see the enlarged image in Figure 4.19A). Furthermore, a new low-intense one showed up at 1.3 nm, very close to the β-2L ($MC_{POP/OPO}$) 003 reflection at 1.4 nm. In the pure PPP, this reflection was associated with β-2L (PPP), together with its characteristic β wide-angle peaks (■) and the single 001 reflection at 4.1 nm. Except for the pure $MC_{POP/OPO}$ sample, the former peaks were detected in XRD patterns at all the mixtures, evidencing the immiscible nature of PPP and $MC_{POP/OPO}$.

At the 15PPP/85$MC_{POP/OPO}$ composition, a WAXD peak related to PPP emerged near that of $MC_{POP/OPO}$ at 0.38 nm (pointed by an arrow). Simultaneously, the weak shoulder detected at low concentrations of PPP increased its intensity, exhibiting a clear *d*-spacing of 4.1 nm at 20% PPP. A further increase in the PPP content caused a broadening in diffraction peaks due to the overlapping of the reflections of both polymorphic forms in the diffraction patterns, more noticeable in those at higher angles. Furthermore, close peaks at *d*-spacing around 0.38 nm became a wider single one, making both polymorphs indistinguishable in mixtures at 40% PPP and above. From this mixture on, again the concurrent presence of both polymorphic forms could only be confirmed by SAXD data.

Detailed DSC data regarding the melting behavior of the mixtures can be found in Table 4.8. β-2L ($MC_{POP/OPO}$) melted at temperatures slightly lower in the mixtures than in the pure

$MC_{POP/OPO}$ sample, as shown by the corresponding DSC curves. In mixtures with up to 50% PPP, this temperature remained above 30 °C but dropped to 29°C at increasing PPP content. In the 65PPP/35$MC_{POP/OPO}$ mixture, a weak peak at 1.4 nm, associated with β-2L ($MC_{POP/OPO}$), was still detected in SAXD patterns, although the signal seemed to be lost in mixtures of 70%-75% PPP. Despite this, we concluded that some non-solubilized $MC_{POP/OPO}$ was still present at the 75PPP/25$MC_{POP/OPO}$ composition, according to the subtle endothermic peak still noticeable in the corresponding DSC thermogram in a similar temperature range to that of other samples.

A substantial increase in the melting temperature of β-2L (PPP) from the mixture at 5% PPP towards the equimolecular composition was clearly noticed (difference of ~15 °C). Although not so markedly due to the decrease in the amount of liquid media surrounding β-2L (PPP) crystals, this tendency continued until reaching the pure PPP sample. As a result, the corresponding phase diagram (Figure 4.20) evidenced a similar behavior of the liquidus line compared to that depicted by PPP/OPO, PPP/PPO, and PPP/POP binary systems.

Table 4.8. Melting temperatures (°C) of PPP and $MC_{POP/OPO}$ when stabilized PPP/$MC_{POP/OPO}$ mixtures were heated from 10 to 80 °C at 2 °C·min^{-1}.

Polymorph	**PPP**	**95PPP**	**90PPP**	**85PPP**	**80PPP**	**75PPP**
β-2L (MC)	-	-	-	-	-	28.2 ± 0.4
β-2L (PPP)	67.5 ± 0.6	66.8 ± 0.9	65.6 ± 0.7	65.6 ± 1.1	65.3 ± 1.3	64.5 ± 0.6
Polymorph	**70PPP**	**65PPP**	**60PPP**	**50PPP**	**40PPP**	**30PPP**
β-2L (MC)	28.6 ± 1.2	29.2 ± 1.1	29.4 ± 0.5	30.3 ± 0.3	30.9 ± 0.6	31.7 ± 1.0
β-2L (PPP)	64.2 ± 1.2	63.7 ± 1.1	62.6 ± 0.5	61.6 ± 0.6	60.2 ± 0.6	58.3 ± 1.0
Polymorph	**20PPP**	**15PPP**	**10PPP**	**5PPP**	**$MC_{POP/OPO}$**	
β-2L (MC)	32.1 ± 0.7	31.8 ± 0.8	31.9 ± 0.5	32.2 ± 0.8	33.3 ± 0.3	
β-2L (PPP)	55.7 ± 0.5	54.2 ± 0.6	51.4 ± 0.4	44.9 ± 1.1	-	

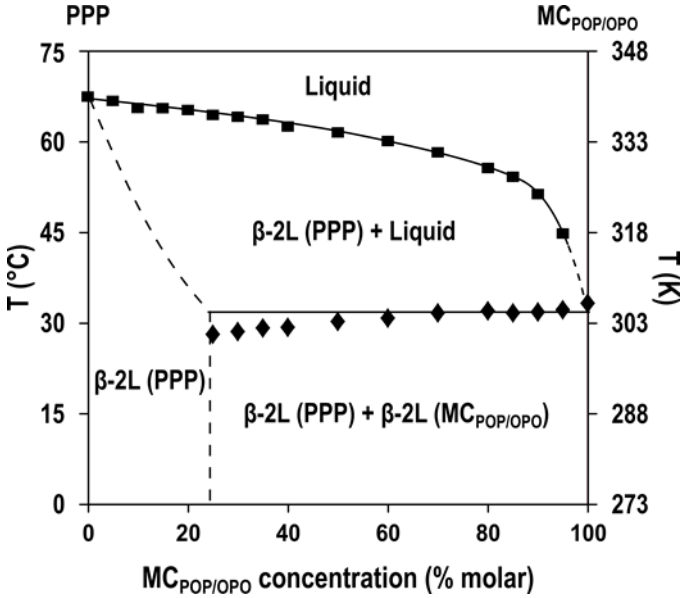

Figure 4.20. Phase diagram of incubated PPP/$MC_{POP/OPO}$ mixtures constructed from DSC data obtained when heating at a rate of 2 °C·min^{-1}. Reprinted with permission from Macridachis et al. (2021). Copyright (2021) American Chemical Society.

In summary, mixtures of PPP with POP and OPO at a concentration ratio allowing the formation of a stable molecular compound showed eutectic phase behavior after six months of thermal incubation. Moreover, according to DSC and X-ray diffraction data, PPP exhibited no solubility in $MC_{POP/OPO}$. By contrast, up to 20-25% of the latter was able to integrate into the crystalline phase of β-2L (PPP), a value that lies between the solubility limits estimated for its pure component OPO and POP (<5% and 35%, respectively).

4.2.4.2. *Kinetic phase behavior*

DSC and SR-XRD experiments were conducted on the 50PPP/50$MC_{POP/OPO}$ mixture to examine the polymorphic occurrence and miscibility properties of the PPP/$MC_{POP/OPO}$ system under metastable conditions. The thermal treatments applied consisted of cooling from the melt to -30 °C at different rates (15 and 2 °C·min^{-1}) and subsequently heating at a constant rate of 2 °C·min^{-1}. The results are shown in Figure 4.21.

When cooling at 15 °C·min^{-1}, two main DSC signals were observed at 33 and 10 °C (Figure 4.21A). According to SR-XRD data (Figure 4.21B), the first α-2L (PPP) crystallization (SAXD and WAXD peaks at 4.5 and 0.41 nm, respectively) was then followed by the occurrence of β-2L ($MC_{POP/OPO}$) form (SAXD peak at 4.2 nm and WAXD peaks at 0.46 and 0.38 nm). The

molecular arrangement of $MC_{POP/OPO}$ in the stable β-2L form seemed to be favored by the presence of the trisaturated TAG since predominant α-2L ($MC_{POP/OPO}$) crystals would be expected under the fast cooling conditions applied (Minato et al., 1997b). The direct crystallization of $MC_{POP/OPO}$ in the stable form was also favored by the fact that this molecular compound does not pack in metastable β' crystals. Thus, the phase behavior of the mixture in α forms could not be assessed under the applied conditions.

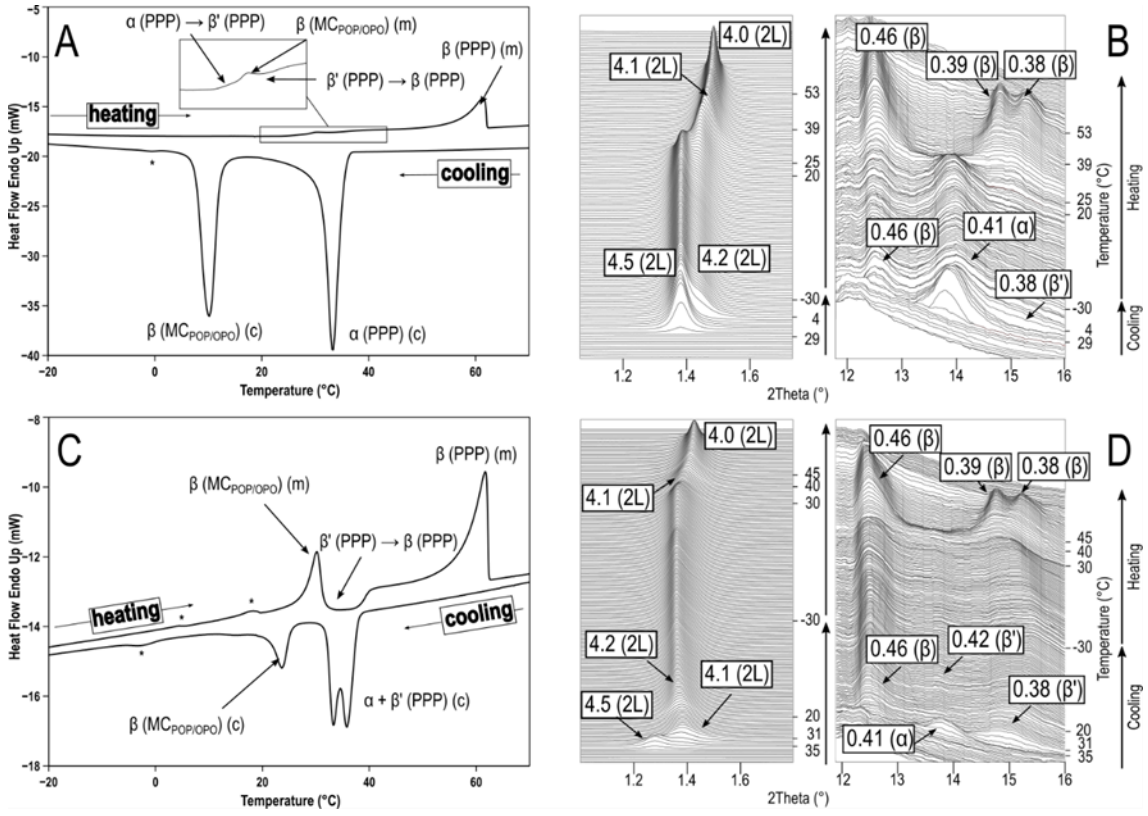

Figure 4.21. DSC and SR-XRD data of the 50PPP/50$MC_{POP/OPO}$ mixture when subjected to different thermal treatments consisting of melt-cooling to -30 °C and reheating until complete melting. (A, B) Cooling at 15 °C·min^{-1} and heating at 2 °C·min^{-1}; (C, D) cooling and heating at 2 °C·min^{-1}. (c): crystallization; (m): melting. *d*-spacing values are given in nm.

During reheating at 2 °C·min^{-1}, no polymorphic events were discerned by DSC until the endothermic peak seen at around 30 °C. However, SR-XRD patterns between 20 and 25 °C showed an increase in the intensity of SAXD and WAXD signals at 4.1 and 0.38 nm, respectively, at the expense of those associated with α-2L (PPP). Thus, it became clear that the α-2L (PPP) → β'-2L (PPP) transformation was the first one to occur. The endothermic event was then ascribed to the subsequent melting of β ($MC_{POP/OPO}$) crystals. Since the characteristic β peak at 0.46 nm did not completely disappear in diffraction patterns until the end of the heating

treatment, we concluded that the further β'-2L (PPP) → β-2L (PPP) transformation (better defined β-like WAXD peaks before final melting) initiated at a close temperature, likely promoted by the presence of molten mixed-acid TAGs in the mixture.

As expected from the prompt formation of β-2L ($MC_{POP/OPO}$) upon fast cooling, except for the favored occurrence of β'-2L (PPP) crystals and the short-life α-2L (PPP) reflections in SR-XRD patterns, the polymorphic and mixing behavior of the 50PPPP/50$MC_{POP/OPO}$ mixture cooled at 2 °C·min^{-1} resulted very similar (see corresponding experimental data in Figures 4.21C and 4.21D and a summary of the polymorphic events occurring under the different thermal conditions in Figure 4.22). It should be highlighted that in both treatments, the DSC thermograms suggested the occurrence of additional polymorphic events not identified by SR-XRD (indicated by *). According to a previous study on equimolecular POP/OPO mixtures subjected to different cooling and heating treatments (Nakanishi et al., 2018), small amounts of POP and OPO probably crystallized separately during cooling. The transition of the crystalline forms of these TAGs to β-2L ($MC_{POP/OPO}$) could explain the two melt-mediated processes detected at 4 and 18 °C in the heating curve of the 50PPP/50$MC_{POP/OPO}$ mixture cooled at 2 °C·min^{-1}.

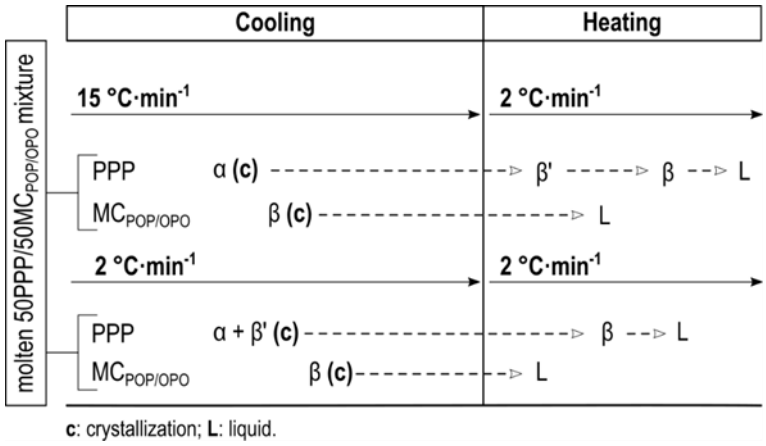

Figure 4.22. Scheme of the main polymorphic events identified in the 50PPP/50$MC_{POP/OPO}$ mixture under different thermal treatments. (c): crystallization; (L): liquid. Reprinted with permission from Macridachis et al. (2021). Copyright (2021) American Chemical Society.

4.2.5. Mixtures of PPP and the POP/PPO molecular compound system

4.2.5.1. *Phase behavior after a thermal stabilization stage*

Figure 4.23A depicts laboratory-scale XRD patterns obtained at 10 °C of thermodynamically stabilized PPP/$MC_{POP/PPO}$ mixtures. DSC thermograms obtained when heating the mixtures at a rate of 2 °C·min^{-1} are depicted in Figure 4.23B.

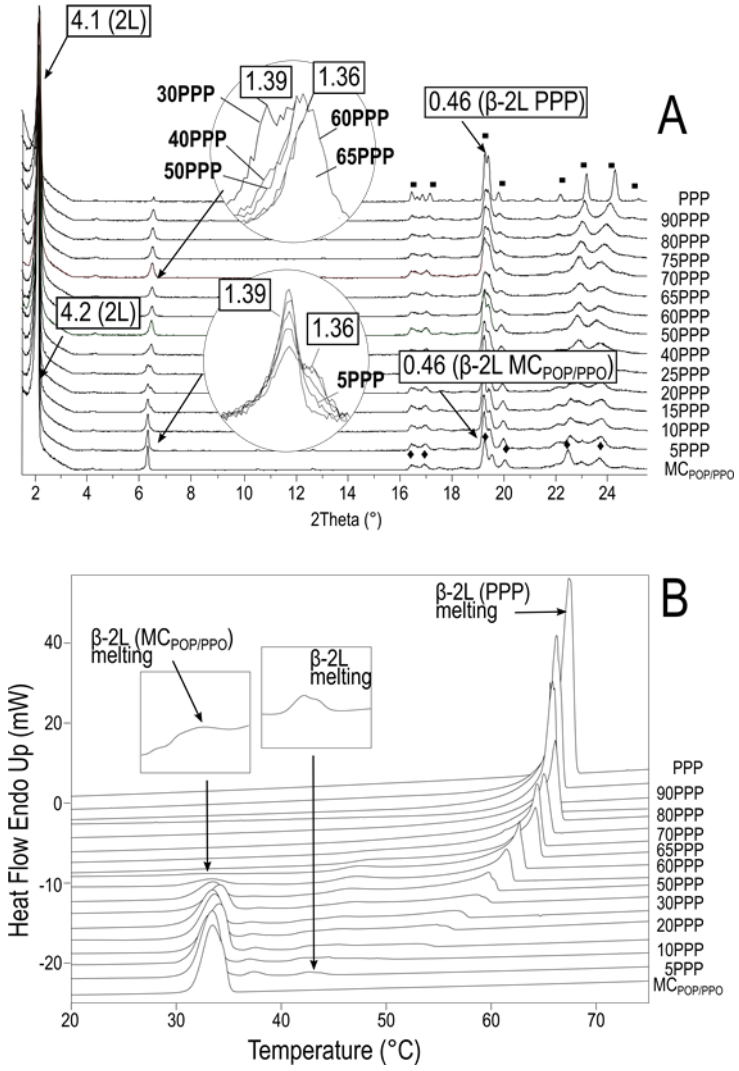

Figure 4.23. PPP/$MC_{POP/PPO}$ system. (A) Laboratory-scale XRD patterns of stabilized PPP/$MC_{POP/PPO}$ mixtures obtained at 10 °C. ■: WAXD peaks of β-2L (PPP); ◆: WAXD peaks of β-2L ($MC_{POP/PPO}$). *d*-spacing values are given in nm. (B) DSC thermograms of stabilized PPP/$MC_{POP/PPO}$ mixtures heated at a rate of 2 °C·min^{-1}. Reproduced from Macridachis et al. (2022) with permission from the PCCP Owner Societies.

The presence of PPP in the stable β-2L form could be confirmed by the small-angle peak at 4.1 nm and its characteristic wide-angle XRD peaks (denoted by ■). As for the pure $MC_{POP/PPO}$ mixture, diffraction peaks at 4.2 nm (003 reflection at 1.39 nm) in the SAXD region and 0.46, 0.44, 0.39, and 0.37 nm in the WAXD region (♦) indicated the occurrence of β-2L ($MC_{POP/PPO}$). In the mixtures, SAXD peaks at 1.36 (003 reflection of peak at 4.1 nm) and 1.39 nm (003 reflection of peak at 4.2 nm) eased the differentiation of the structurally similar β-2L forms of both components when concurrently present.

From pure PPP to the 65PPP/35$MC_{POP/PPO}$ composition, single endothermic peaks above 60 °C were observed in the heating curves, in agreement with the sole identification of β-2L (PPP) form in the corresponding XRD patterns. Neither for the 60PPP/40$MC_{POP/PPO}$ mixture could the presence of the mixed-acid component be detected by this technique. However, the subtle endothermic peak observed at 33 °C in its corresponding DSC thermogram (see amplified image in Figure 4.23B) long before β-2L (PPP) melting was probably attributed to the melting of β-2L ($MC_{POP/PPO}$). This was supported by the occurrence of endothermic signals at a similar temperature in the mixtures towards pure $MC_{POP/PPO}$. Accordingly, up to 35-40% $MC_{POP/PPO}$ dissolved in the solid phase of PPP during thermodynamic stabilization.

Then, the heating curves of mixtures at increasing $MC_{POP/PPO}$ content were characterized by the presence of two main endothermic events corresponding to the successive melting of β-2L ($MC_{POP/PPO}$) and β-2L (PPP). The melting of β-2L (PPP) crystals containing small amounts of mixed-acid components several degrees above $MC_{POP/PPO}$ even at the 5PPP/95$MC_{POP/PPO}$ composition, evidenced the same asymmetry in the eutectic point shown by the mixture systems previously discussed. It should be noted that a weak endothermic signal was also detected in the mixtures at around 37 °C, soon after β-2L ($MC_{POP/PPO}$) melting, but no additional SAXD or WAXD reflections corresponding to different polymorphic forms were detected for any of the mixtures during the heating treatment (data not shown).

The thermal data obtained during when heating PPP/$MC_{POP/PPO}$ mixtures at 5% molar mass intervals (detailed in Table 4.9) were used to construct the phase diagram of Figure 4.24. Overall, the mixing behavior shown by the blends after 6 months of thermodynamic stabilization resembled that described for stabilized PPP/PPO and PPP/POP mixtures in the present study. $MC_{POP/PPO}$ behaved as a single TAG component in the eutectic region of the diagram and formed solid solutions in the region rich in PPP. This would be aligned with the behavior described

before for PPP/$MC_{POP/OPO}$ mixtures, with the major difference between the systems being the amount of mixed-acid component solubilized in PPP. The value was lower for $MC_{POP/OPO}$ (20-25%) than for $MC_{POP/PPO}$ (35-40%), which might be attributed to the greater instability introduced in the PPP crystal lattice by the presence of two oleic acid moieties in OPO.

Table 4.9. Melting temperatures (°C) of PPP and $MC_{POP/PPO}$ in stabilized PPP/$MC_{POP/PPO}$ mixtures heated from 0 to 80 °C at 2 °C·min^{-1}.

Polymorph	**PPP**	**95PPP**	**90PPP**	**85PPP**	**80PPP**	**75PPP**	**70PPP**
β-2L (MC)	-	-	-	-	-	-	-
β-2L (PPP)	67.5 ± 0.6	66.4 ± 0.6	66.0 ± 0.5	65.7 ± 0.5	65.6 ± 1.5	65.0 ± 0.6	64.7 ± 1.0
Polymorph	**65PPP**	**60PPP**	**55PPP**	**50PPP**	**45PPP**	**40PPP**	**35PPP**
β-2L (MC)	-	32.8 ± 0.4	33.4 ± 1.2	33.2 ± 0.5	33.3 ± 0.2	33.7 ± 0.4	33.1 ± 0.3
β-2L (PPP)	63.4 ± 0.9	62.7 ± 0.4	62.0 ± 0.5	61.4 ± 0.8	60.4 ± 0.6	59.7 ± 0.4	58.2 ± 0.3
Polymorph	**30PPP**	**25PPP**	**20PPP**	**15PPP**	**10PPP**	**5PPP**	**$MC_{POP/PPO}$**
β-2L (MC)	33.6 ± 0.7	33.5 ± 0.6	33.6 ± 0.5	33.6 ± 0.8	33.2 ± 0.8	33.6 ± 0.6	33.6 ± 0.4
β-2L (PPP)	58.2 ± 0.6	56.4 ± 0.6	54.5 ± 0.8	52.9 ± 0.7	49.6 ± 1.0	43.7 ± 0.6	-

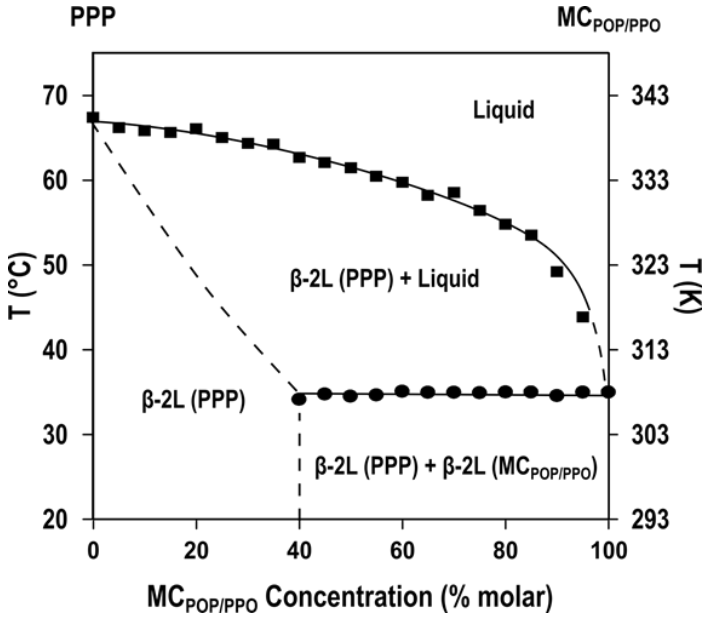

Figure 4.24. Phase diagram of incubated PPP/$MC_{POP/PPO}$ mixtures constructed from DSC data obtained when heating at a rate of 2 °C·min^{-1}. Reproduced from Macridachis et al. (2022) with permission from the PCCP Owner Societies.

4.2.5.2. *Kinetic phase behavior*

In a similar manner to previous mixture systems contained in this chapter, DSC and X-ray diffraction techniques were used to evaluate the polymorphic and phase behavior of PPP/$MC_{POP/PPO}$ mixtures during cooling and subsequent heating processes at 2 °C·min^{-1}.

Main traits of mixtures very rich in PPP can be explained through experimental data obtained for the 80PPP/20$MC_{POP/PPO}$ composition depicted in Figure 4.25.

α and β' solid solution phases rich in PPP occurred during cooling, which in the next heating treatment, and in contrast with the sequence of transformations α-2L → melt → β'-2L → β-2L identified for pure PPP, transited to β through the solid state (DSC exothermic peak at around 40 °C). At decreasing PPP content, mixtures were characterized by the eutectic phases formed by PPP and $MC_{POP/PPO}$ in the metastable state. As in PPP/PPO mixtures, the thermal conditions applied during kinetic experiments resulted in a lower miscibility of the components in the β' phase than in the stable β phase obtained after six months of thermodynamic stabilization.

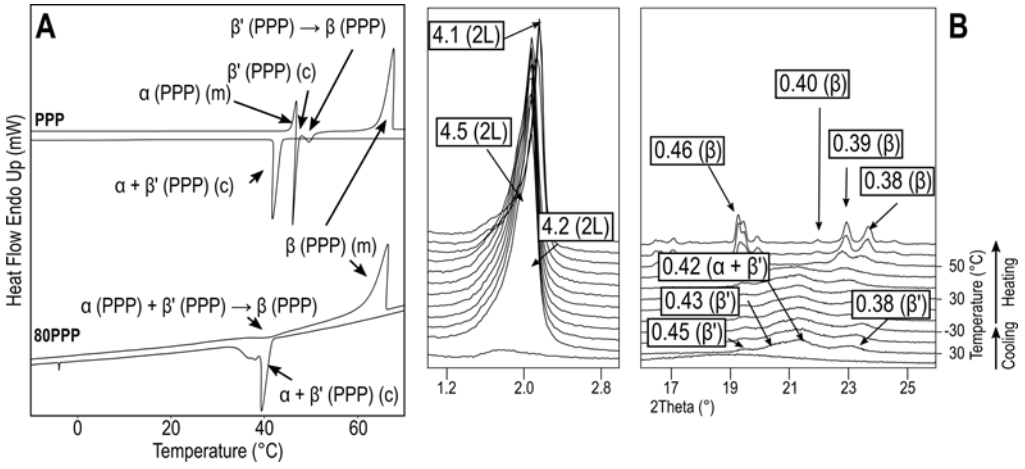

Figure 4.25. (A) DSC thermograms obtained for pure PPP and the 80PPP/20$MC_{POP/PPO}$ mixture when cooled and subsequently heated at 2 °C·min^{-1}. (B) Laboratory-scale XRD data corresponding to the 80PPP/20$MC_{POP/PPO}$ mixture. (c): crystallization; (m): melting. *d*-spacing values are given in nm.

DSC curves and diffraction data of the 70PPP/30$MC_{POP/PPO}$, 50PPP/50$MC_{POP/PPO}$, and 30PPP/70$MC_{POP/PPO}$ compositions in Figure 4.26A exemplify the overall behavior displayed by the mixtures when increasing the $MC_{POP/PPO}$ content up to 80%. α-2L (PPP) and β'-2L (PPP) initially occurred in these mixtures during cooling but the α reflection at 4.5 nm vanished at decreasing temperature and all PPP was in the form of β'-2L crystals at the end of the process (see SR-XRD patterns of the 70PPP/30$MC_{POP/PPO}$ in Figure 4.26B). The second exothermic

event (clearly noticed in the 30PPP/70MC$_{POP/PPO}$ composition at around 21 °C) was ascribed to the crystallization of β'-2L (MC$_{POP/PPO}$). No changes were detected in WAXD peaks due to the similar structure of the distinct β' forms, but a strong new signal with a *d*-spacing very close to that of β'-2L (PPP) at 4.2 nm appeared in the SAXD region (see the enlarged image in SR-XRD patterns of the 50PPP/50MC$_{POP/PPO}$ composition in Figure 4.26C). The last crystallization peak detected at around 8 °C was not identified by XRD in mixtures with high PPP content. However, SR-XRD patterns of the 10PPP/90MC$_{POP/PPO}$ composition at 10 °C (see Figure 4.27) allowed to assign this event to the α-2L (MC$_{POP/PPO}$) crystallization through the WAXD peak at 0.41 nm and the SAXD peak at 5.1 nm which, in agreement with previous work (Minato et al., 1997a), showed a final *d*-spacing value of 4.6 nm at decreasing temperature.

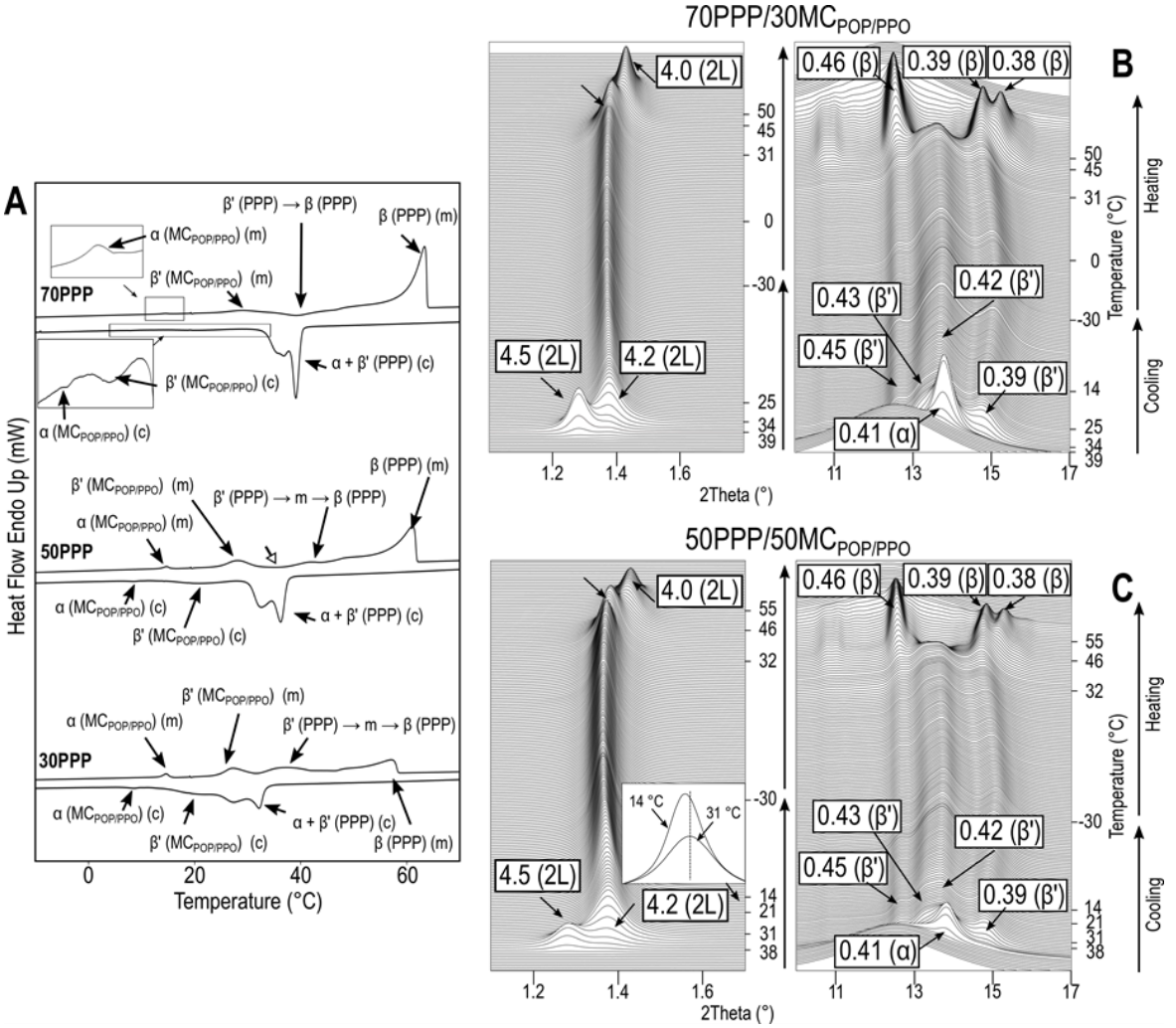

Figure 4.26. (A) DSC data of PPP/MC$_{POP/PPO}$ mixtures with 70, 50, and 30% PPP cooled and reheated at 2 °C·min^{-1}. (B) SR-XRD data corresponding to the 70PPP/30MC$_{POP/PPO}$ mixture. (C) SR-XRD data corresponding to the 50PPP/50MC$_{POP/PPO}$ mixture. (c): crystallization; (m): melting. *d*-spacing values are given in nm.

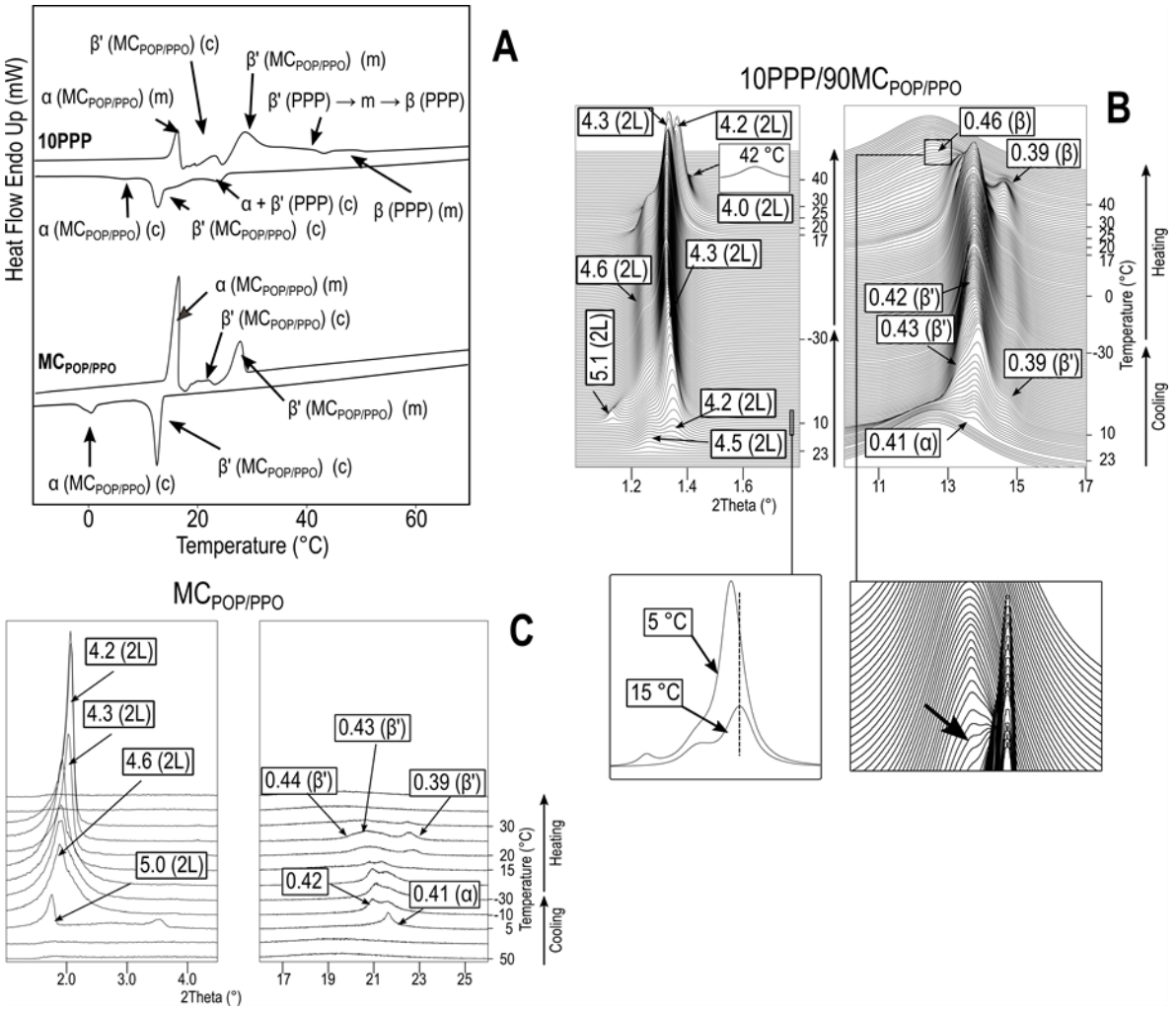

Figure 4.27. (A) DSC thermograms obtained for pure $MC_{POP/PPO}$ and the 10PPP/90$MC_{POP/PPO}$ composition when cooled at subsequently heated at 2 °C·min^{-1}. (B) SR-XRD data corresponding to the 10PPP/90$MC_{POP/PPO}$ mixture. (C) Laboratory-scale XRD data corresponding to the pure $MC_{POP/PPO}$ sample. (c): crystallization; (m): melting. *d*-spacing values are given in nm.

Therefore, it was assumed that the first DSC endothermic peak at around 15 °C in mixtures with 70 to 30% PPP content (Figure 4.26A) during reheating was associated with the α-2L ($MC_{POP/PPO}$) melting. However, the weak thermal signals and the absence of clear diffraction data did not allow to confirm whether or not some additional β'-2L ($MC_{POP/PPO}$) formed next. Afterward, β'-2L ($MC_{POP/PPO}$) melted without further recrystallization in stable β-2L ($MC_{POP/PPO}$) form at any of the compositions (endothermic peaks at around 29 °C). In SR-XRD patterns of 70PPP/30$MC_{POP/PPO}$ and 50PPP/50$MC_{POP/PPO}$ compositions (Figures 4.26B and 4.26C, respectively), β' reflections weakened due to the single presence of β'-2L (PPP) crystals (pointed by arrows). Its corresponding reflections vanished several degrees above, and new ones associated with β-2L (PPP) emerged at around 45 °C (WAXD peaks at 0.46, 0.39, and 0.38 nm).

In the case of the 70PPP/30$MC_{POP/PPO}$ mixture, the β'-2L (PPP) to β-2L (PPP) transition was observed at 36.4 °C in the heating curve. The DSC melting peaks shown by the 50PPP/50$MC_{POP/PPO}$ and 30PPP/70$MC_{POP/PPO}$ mixtures at 40 and 37 °C, respectively, evidenced melt-mediated β' to β transitions of PPP in mixtures rich in $MC_{POP/PPO}$. A barely noticeable crystallization event was still detected in the 50PPP/50$MC_{POP/PPO}$ mixture between β'-2L ($MC_{POP/PPO}$) and β'-2L (PPP) melting (pointed by a white arrow in the corresponding thermogram). Although likely related with the transformation of some metastable PPP, its nature could not be clarified by SR-XRD data.

The 10PPP/90$MC_{POP/PPO}$ mixture behaved similarly during the thermal processing. However, on heating two additional exothermic events occurred after the α-2L ($MC_{POP/PPO}$) melting at around 16 °C (Figure 4.27A). The increase in intensity of the small-angle reflection at 4.3 nm and typical β' wide-angle reflections at 17 °C (Figure 4.27B) confirmed the first one as the β'-2L ($MC_{POP/PPO}$) recrystallization. The second event (T_{top} of 24.2 °C) corresponded with the shifting of the β'-2L ($MC_{POP/PPO}$) small-angle reflection towards a *d*-spacing value of 4.2 nm, more similar to that observed for this form in mixtures with higher PPP content. This decrease in *d*-spacing value of β'-2L ($MC_{POP/PPO}$) was also confirmed for the pure $MC_{POP/PPO}$ sample (corresponding DSC and XRD data are included in Figure 4.27). This could be attributed to a more compact arrangement of POP and PPO molecules in the molecular compound favored during the heating treatment. The subsequent melting of β'-2L ($MC_{POP/PPO}$) at 28 °C was finally followed by the β'-2L (PPP) → β-2L (PPP) transformation (new weak reflections at 4.0 and 0.46 nm when reaching 40 °C) before complete melting at 48.9 °C.

The DSC and diffraction data obtained during thermal processes was used to illustrate the kinetic phase behavior of PPP/$MC_{POP/PPO}$ mixtures in Figure 4.28. Detailed DSC data on the polymorphic transitions depicted are included in Table 4.10. Despite some particularities, we can state that the overall behavior of PPP/$MC_{POP/PPO}$ mixtures was nor very different from that displayed by mixtures of PPP and pure PPO:

(i) During cooling at 2 °C·min^{-1}, α crystals predominantly formed in pure component samples, whereas β' ones were promoted in the mixtures. However, SR-XRD confirmed the formation of short life α-2L (PPP) crystals at almost all compositions.

Also, DSC thermograms showed the prevalent occurrence of small amounts of α-2L ($MC_{POP/PPO}$).

(ii) Metastable solid solution phases rich in the monoacid TAG formed in mixtures with PPP content above 75% and eutectic phases occurred in the remaining compositions. Thus, the miscibility gap increased with respect to thermodynamically stabilized PPP/$MC_{POP/PPO}$ mixtures. $MC_{POP/PPO}$ acting as a single component in the system led to equivalent eutectic properties to those of a two-component system.

(iii) Regarding heating treatments, $MC_{POP/PPO}$ did not vary its transformation pathways or sequence of transformations. α-2L and β'-2L forms melted sequentially and even though not confirmed for all compositions, a melt-mediated transformation presumably occurred in between. Not in the pure $MC_{POP/PPO}$ sample nor in the mixtures the stable β-2L was obtained under the conditions applied.

(iv) In PPP, the β' → β transformation through the melt was promoted when the content of mixed-acid TAGs in the mixture accounted for ≥50%, in a similar manner to the PPP/PPO system.

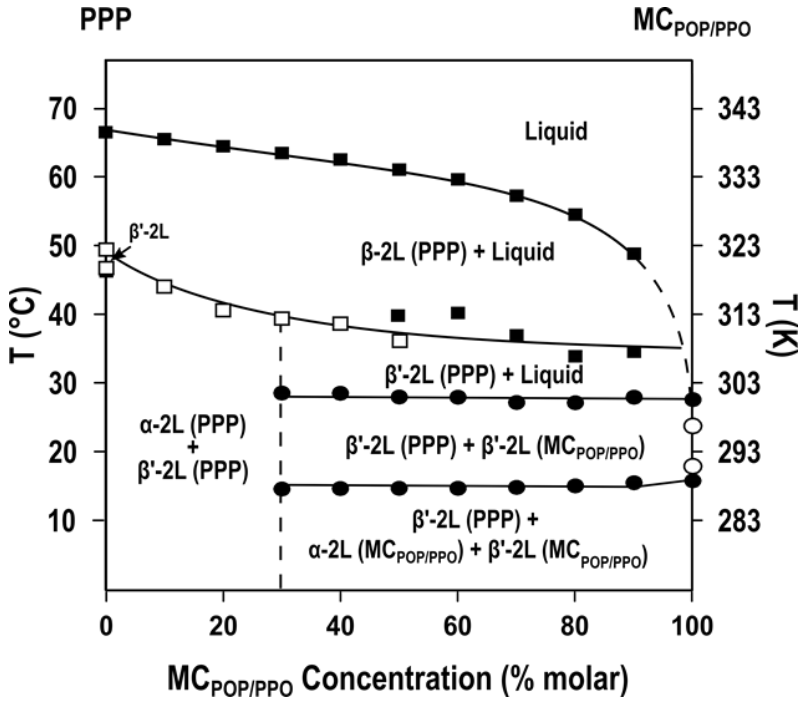

Figure 4.28. Phase behavior observed for PPP/$MC_{POP/PPO}$ mixtures when heated at 2 °C·min^{-1} after a melt cooling process at the same rate. Delimited areas correspond to polymorphic domains between transitions experimentally determined. Empty symbols: exothermic; filled symbols: endothermic. Reproduced from Macridachis et al. (2022) with permission from the PCCP Owner Societies.

Table 4.10. DSC temperatures (°C) of main polymorphic events occurring in PPP/$MC_{POP/PPO}$ mixtures when heated at 2 °C·min^{-1} soon after a melt cooling process at the same rate.

PPP/$MC_{POP/PPO}$ ratio	Heating at 2 °C·min^{-1}					
	a (m)	*β′ (PPP) (c)*	*β′ (PPP) → β (PPP)*	*β (PPP) (m)*		
PPP	46.3 ± 0.8	46.8 ± 0.8	49.5 ± 0.9	66.6 ± 0.9		
	a (PPP) + β′ (PPP) → β (PPP)		*β (PPP) (m)*			
90/10	44.1 ± 0.3		65.5 ± 0.5			
80/20	40.6 ± 0.3		64.5 ± 03			
	a ($MC_{POP/PPO}$) (m)		*β′ ($MC_{POP/PPO}$) (m)*	*β′ (PPP) → β (PPP)*	*β (PPP) (m)*	
70/30	14.6 ± 0.3		28.6 ± 1.1	39.4 ± 0.6	63.5 ± 0.6	
60/40	14.7 ± 0.3		28.5 ± 0.4	38.7 ± 0.4	62.6 ± 0.4	
	a ($MC_{POP/PPO}$) (m)		*β′ ($MC_{POP/PPO}$) (m)*	*β′ (PPP) → m → β (PPP)*	*β (PPP) (m)*	
50/50	14.7 ± 0.5		28.0 ± 0.3	39.8 ± 0.2	61.1 ± 0.5	
40/60	14.7 ± 0.3		28.0 ± 0.4	40.3 ± 0.4	59.7 ± 0.3	
30/70	14.9 ± 0.3		27.2 ± 0.6	37.0 ± 0.9	57.3 ± 0.5	
20/80	15.1 ± 0.4		27.2 ± 0.5	34.0 ± 0.5	54.6 ± 0.7	
	a ($MC_{POP/PPO}$) → m → β′ ($MC_{POP/PPO}$)		*β′ ($MC_{POP/PPO}$) (m)*	*β′ (PPP) → m → β (PPP)*	*β (PPP) (m)*	
10/90	15.5 ± 0.5		28.0 ± 0.5	34.6 ± 1.2	48.9 ± 0.6	
	a ($MC_{POP/PPO}$) (m)		*β′ ($MC_{POP/PPO}$) (c)*	*β′ ($MC_{POP/PPO}$) (m)*		
$MC_{POP/PPO}$	16.0 ± 0.6		18.1 ± 0.4	27.6 ± 0.9		
			23.6 ± 0.4			

(c): crystallization; (m): melting.

Following the same scheme as in the previous mixture systems, we also examined the polymorphic behavior of the 50PPP/50$MC_{POP/PPO}$ composition when rapidly cooled at 15 °C·min^{-1}. The corresponding DSC and SR-XRD data are shown in Figure 4.29.

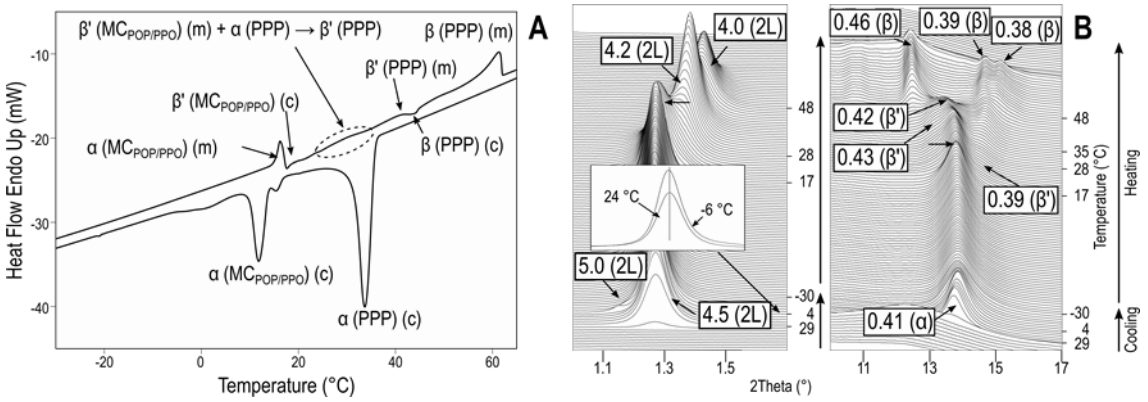

Figure 4.29. 50PPP/50$MC_{POP/PPO}$ mixture. (A) DSC thermogram and (B) SR-XRD patterns obtained when cooled at 15 °C·min^{-1} and reheated at 2 °C·min^{-1}. (c): crystallization; (m): melting. *d*-spacing values are given in nm.

The two exothermic events (T_{top} of 34 and 12 °C) and the single SR-WAXD reflection at 0.41 nm detected on cooling confirmed eutectic behavior for the PPP/$MC_{POP/PPO}$ system in least stable α forms. During the process, the α-2L ($MC_{POP/PPO}$) small-angle peak at 5.0 nm shifted towards that of α-2L (PPP) at 4.5 nm, becoming indistinguishable at 4 °C and below. During our previous study of the 50PPP/50$MC_{POP/OPO}$ mixture subjected to the same cooling conditions, it was observed that the POP/OPO fraction crystallized directly in β-2L ($MC_{POP/OPO}$). We may assume a more difficult molecular arrangement of POP and PPO in the form of a molecular compound, which eases the occurrence of a less stable form. This is comprehensible by considering two characteristics relative to $MC_{POP/PPO}$ formation mentioned in the introduction section: i) the stable "tuning fork" conformation of the glycerol group in PPO must evolve to a "chair" conformation before packing with POP; and ii) since in $MC_{POP/PPO}$ palmitic and oleic acid chains will be concurrently present in one leaflet, the steric effect during its formation will be presumably higher than in $MC_{POP/OPO}$.

The first melt-mediated process when reheating at 2 °C·min^{-1} corresponded to an α → β' transformation according to the weakening of α diffraction peaks at 17 °C (pointed by arrows in SR-SAXD and -WAXD patterns), and new subtle ones occurring at 0.43 and 0.39 nm in the wide-angle region. Given the lower melting point of its α-2L form, this initial event was related to $MC_{POP/PPO}$. The further melt-mediated α-2L (PPP) → β'-2L (PPP) transformation led to the

strengthening of these reflections above 28 °C and resulted in a complex DSC signal between 25 and 35 °C likely due to the upcoming β'-2L ($MC_{POP/PPO}$) melting. Afterward, the melt-mediated process and the predominant β-like diffraction peaks detected at around 45 °C indicated the β'-2L (PPP) to β-2L (PPP) transition before complete melting.

4.2.6. Summary of mixtures of PPP and oleic-rich mixed-acid triacylglycerols

The occurrence of complete miscibility, eutectic behavior with partial miscibility, or molecular compound formation in TAG mixtures rely on the stabilizing or destabilizing effect of the molecular interactions occurring between components. These interactions involve the main body of aliphatic chains, methyl end stacking, and glycerol conformation (Larsson et al., 2006). Thus, the phase behavior displayed by mixtures including PPP and mixed-acid saturated-unsaturated components can be explained on this basis.

The molecular models described in previous work for OPO, POP, PPO, PPP/$MC_{POP/OPO}$, and PPP/$MC_{POP/PPO}$ (Minato et al., 1997c) are depicted in Figure 4.30.

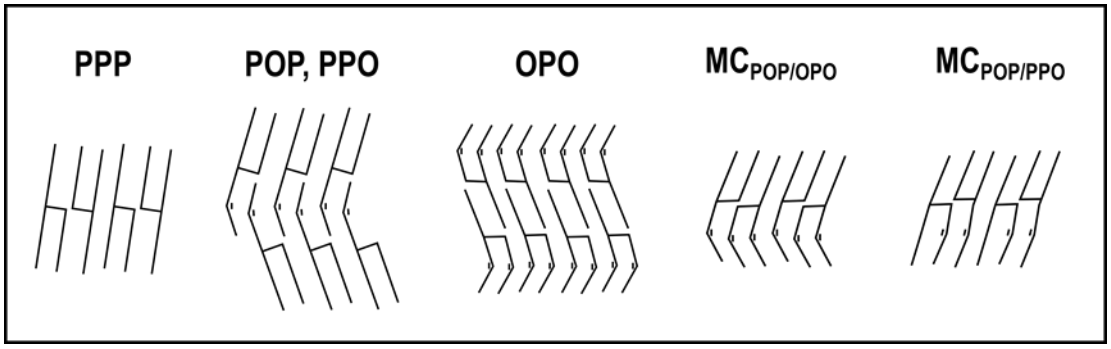

Figure 4.30. Structural models of TAGs and molecular compounds included in the present study.

The formation of molecular compound structures integrating PPP in the mixture systems is highly unlikely. The great steric hindrance between palmitoyl and oleoyl chains of PPP and mixed-acid TAGs, respectively, would prevent from the close packing of these TAGs in a stoichiometric manner. It is generally accepted that to form of a molecular compound, TAGs must meet two requirements: i) the presence of at least two chemically different component fatty acids; and ii) a specific distribution thereof at *sn*- positions of the glycerol group. Eventually, this will allow structural changes that favor affinitive interactions in lamellar leaflets (saturated-saturated, unsaturated-unsaturated), a compatible configuration of adjacent glycerol groups, and

reductions in chain-length mismatch causing disruptions at methyl end regions. For example, in $MC_{POP/PPO}$, the presence of palmitoyl and oleoyl chains in the same leaflet may cause some degree of instability. However, the structure is presumably stabilized by a parallel direction of glycerol groups and a reduced difference in length of fatty acids when PPO changes its glycerol group from a "tuning-fork" to a "chair" configuration (Zhang et al., 2007).

Stable molecular compounds reported on mixtures of TAGs containing *cis* and *trans* fatty acids include POP/OPO, POP/PPO, SOS/OSO, SOS/SSO, and PEP/EPE (with E being elaidic acid) systems (Koyano et al., 1992; Minato et al., 1997a, 1997b; Takeuchi et al., 2002a; Zhang et al., 2020). Moreover, work on the kinetic phase behavior of the binary mixtures PSP/PPS and LSL/LLS suggested that fully saturated TAGs accomplishing the mentioned criteria may also lead to molecular compound formation under some experimental conditions (Boodhoo et al., 2009a; Bouzidi et al., 2010). Accordingly, from a structural perspective, the occurrence of a molecular compound including PPP seems also improbable.

The formation of solid solutions at all concentration ratios in mixtures including PPP and mixed-acid TAGs results equally unlikely. It is well known that close melting temperatures and a high degree of isomorphism between crystal structures are required for different TAG molecules to be able to exchange crystallographic positions at all concentration ratios without disrupting molecular packing upon crystallization (Wesdorp et al., 2013). For this reason, complete miscibility may occur in loosely packed metastable polymorphs but is rare under stable conditions. In our case, the bent configuration of oleic fatty acid moieties in the molecular structure of mixed-acid TAGs is critical in the significant incompatibility shown by oleic-rich components and PPP.

The mixing properties displayed by the mixture systems included in the present chapter agree with previous work on mixtures of monoacid trisaturated and mixed-acid saturated-unsaturated TAGs (Costa et al., 2011; Minato et al., 1996; Wesdorp et al., 2013). Stabilized PPP/OPO, PPP/POP, and PPP/PPO systems showed eutectic behavior with limited solubility of the oleic-rich TAGs in the crystalline phase of PPP. The low solubility value of PPP in the oleic-rich components could not be delimited in the corresponding phase diagrams. In $PPP/MC_{POP/OPO}$ and $PPP/MCP_{POP/PPO}$, the molecular compound systems behaved as a single component, resulting in mixing properties of equivalent nature.

The similar composition of the mixed-acid components within the mixtures led to a similar shape of the stable phase diagrams. Melting points of the low-melting components remained practically constant at all compositions, whereas the liquidus line defined by the melting of β-2L (PPP) phases (including different amounts of solubilized mixed-acid TAGs) showed an increasingly accused negative slope towards the lower melting side of the diagrams. DSC and XRD data confirmed that β-2L (PPP) melted at higher temperature than most stable forms of OPO, POP, PPO, $MC_{POP/OPO}$, and $MC_{POP/PPO}$ even at low PPP concentrations of 5% and 10%. The high difference in melting points at these compositions, which exceeded 10 °C, suggested eutectic points lying at a concentration range very near to 0% PPP. This led to highly asymmetric eutectic diagrams, often referred to as monotectic.

The characteristic behavior of the liquidus curve in all the mixture systems is explained by the great difference in melting temperature, above 30 °C, between stable forms of PPP and the mixed-acid saturated-unsaturated components (values found in the present study are shown in Table 4.11). From the kinetic experiments carried out on binary mixtures of LLL with SSS, PPP, and MMM, Takeuchi et al. (2003) concluded that a lower difference in the length of fatty acids (LLL/MMM), and thus lower difference in melting temperature, favored more symmetric eutectic points. However, in agreement with Kerridge (1952), increasing the difference (LLL/SSS) tended to shift the eutectic composition towards mixtures richer in the lower-melting TAG. The same was observed in binary mixtures of mixed-acid saturated-unsaturated TAGs by Bayés-García et al. (2015). Stabilized binary mixtures of OPO and POO, with close melting properties, showed a symmetric eutectic point in the corresponding phase diagram. The enlarged difference in melting point due to the additional palmitic acid in PPO resulted in highly asymmetric eutectic diagrams in PPO/OPO and PPO/POO systems after long incubation time.

We already mentioned that the loose molecular packing of α forms may ease total compatibility in some TAG mixtures. However, the higher density of packing at increasing polymorphic stability restricts complete miscibility in the β form to TAGs with very isomorphic crystal structures. Since eutectic behavior prevails in most TAG mixture systems, defining the extent of partial miscibility regions and the factors involved takes on particular importance in applications addressed to fine-tuning the properties of lipidic materials. The solubility values determined for pure OPO, POP, PPO, and their equimolecular mixtures in solid PPP under stable conditions are shown in Table 4.11.

Table 4.11. Melting temperature (T_m) and solubility of mixed-acid saturated-unsaturated TAGs in β-2L (PPP) crystals found in the present study.

	Stable form	T_m (°C)	Solubility in PPP
PPP	β-2L	67.9	------
OPO	β_1-3L	22.4	< 5%
POP	β_1-3L	38.0	30-35%
PPO	β'_1-3L	36.1	30-35%
$MC_{POP/OPO}$	β-2L	33.3	20-25%
$MC_{POP/PPO}$	β-2L	33.6	35-40%

Less than 5% OPO dissolved in PPP in the PPP/OPO system, which was characterized by the occurrence of eutectic β_1-3L (OPO) and β-2L (PPP) phases at all compositions. This result might be compared to a recent report on PPP/POO mixtures (Lu et al., 2019). After a crystallization process at a rate of 2 °C·min^{-1}, DSC melting peak properties (characteristic temperatures and enthalpy) and the predicted melting Gibbs free energy of the binary mixtures were used to describe the mixing phase behavior during a heating treatment at a rate of 2 °C·min^{-1}. The resulting phase diagram evidenced a eutectic behavior with partial solid solution at POO concentration up to 10-20%, in agreement with the estimated for tempered PPP/POO mixtures (Gibon & Durant, 1985). With close melting properties, it seems that the *sn-* position of palmitic acid in the TAG molecule may have a certain influence in the miscibility properties exhibited by OPO and POO in PPP. This positive relationship between a greater extent of partial solid solutions and the asymmetry of TAG molecules has been previously reported in some binary systems including monoacid and mixed-acid trisaturated TAGs (Knoester et al., 1972).

Up to 30-35% of POP, also exhibiting a stable β form with triple chain-length structure, was incorporated in the β crystalline phase of PPP. Equivalent solubility limit was estimated for its asymmetric counterpart PPO. The ordered crystal lattice of a pure component is disturbed by the integration of another one with different size and geometry. In turn, this leads to a positive excess Gibbs free energy. The different outcome of POP and PPO with respect to OPO may be explained by differences of the disturbing effect of the bent oleic acid chains on the regular zigzag configuration of palmitic acid in the PPP crystal lattice (Wesdorp et al., 2013). In PPP/OPO mixtures, the resulting excess Gibbs free energy of mixing may be high enough to prevent the formation of PPP/OPO mixed crystals even at a very low content of the diunsaturated TAG. The substitution of one oleic moiety by a palmitic one in POP and PPO increases thermal stability and reduces the number of bent sites due to unsaturation. This results

in a lower steric hindrance in the binary systems including monounsaturated TAGs, which may ease the integration of POP and PPO in solid PPP.

In PPP/$MC_{POP/OPO}$ mixtures, up to 20−25% of the mixed-acid components were solubilized in solid PPP. Therefore, as illustrated in Figure 4.31, it is assumed that, after stabilization, the saturated−unsaturated mixed-acid TAGs were probably embedded closely packed in the crystal lattice of PPP. This would be facilitated by the strong specific interactions occurring between POP and OPO molecules, which also showed to be unaffected by solute−solvent interactions in the presence of up to 98% *n*-dodecane (Ikeda et al., 2010). The great disruptive effect of OPO on the crystal packing of PPP may be partly alleviated by a reduction in the excess Gibbs free energy of mixing when forming a molecular compound with POP. However, the total amount solubilized of the latter TAG decreases by cause of OPO. As a result, the solubility value of $MC_{POP/OPO}$ lied halfway those of pure OPO and POP.

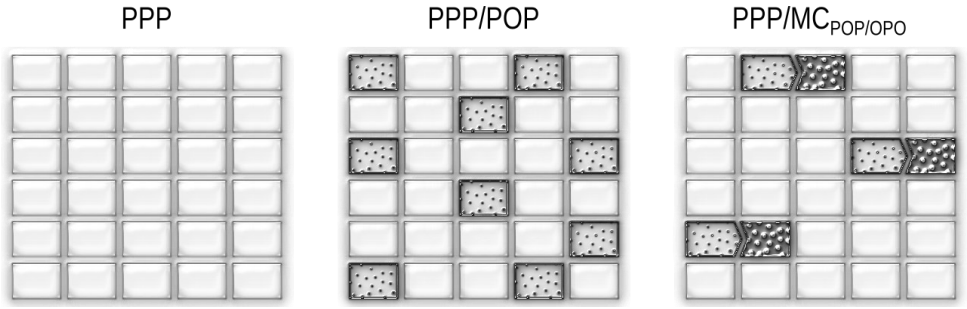

Figure 4.31. Schematic representation of PPP-rich solid solution phases. Reprinted with permission from Macridachis et al. (2021). Copyright (2021) American Chemical Society.

As in the pure TAG components, the increased content of palmitic acid led to a higher solubility of the POP/PPO molecular compound system in PPP of around 35-40%. One may notice that this value exceeded that shown by its pure TAG components. However, the difference was sufficiently low to consider solubility values of POP, PPO and $MC_{POP/PPO}$ of the same order of magnitude.

By considering the overall results obtained for binary and ternary systems, we may conclude that the miscibility gaps in these systems were primarily defined by the total oleic acid content of the mixed-acid components. A minor or almost inexistent effect is exerted by their symmetry (PPP/POP, PPP/PPO) and polymorphic structures under stable conditions (triple structures in pure mixed-acid TAGs and double in molecular compounds).

In agreement with the prevalent eutectic phases displayed after thermodynamic stabilization, the kinetic experiments carried out on PPP/OPO, PPP/PPO, PPP/$MC_{POP/OPO}$, and PPP/$MC_{POP/PPO}$ evidenced independent polymorphic crystallization and transformation of PPP and the mixed-acid components.

In PPP/OPO mixtures, cooling treatments at 2 °C·min^{-1} favored the dissolution of about 10-20% OPO in PPP. However, the overall behavior was ruled by eutectic phases of both TAGs exhibiting different polymorphs. In 50PPP/50OPO and 50PPP/50$MC_{POP/OPO}$ mixtures, PPP promoted the crystallization of the mixed acid components at a higher temperature (increase up to 10 °C) and in more stable forms (β' before α in OPO and β before α forms in $MC_{POP/OPO}$) compared to the pure mixed-acid components during cooling at 15 °C·min^{-1} (Bayés-García et al., 2011a; Minato et al., 1997b). Accordingly, the mixing behavior in the α polymorph could not be clarified for these mixtures at the conditions applied in the present study.

As to PPP/PPO mixtures cooled at 2 °C·min^{-1}, α forms predominated in the pure components at the end of the process but the crystallized mass of the blends was entirely formed by eutectic β' phases. PPP/$MC_{POP/PPO}$ mixtures also showed the favored occurrence of distinct β' forms, even though some α-2L ($MC_{POP/PPO}$) also occurred at almost all compositions according to DSC data. This behavior relates to actual industrial processes regarding palm oil fractionation, in which the occurrence of large clusters formed by uniform, spherical β' crystals is preferred during filtration steps (Basiron, 2005; Kellens et al., 2007). A β form has been identified in palm oil (Deroanne et al., 1977) but its relatively high stability in β'-2L crystals is well known (Braipson-Danthine & Gibon, 2007; Yap et al., 1989). Such property is responsible for its suitability as a β' promoting hard stock (Wassell, 2014). Since the higher melting phase of palm oil is mainly PPP and POP, both with stable β forms, this β' tendency has been related to specific interactions between these components during crystallization from the melt (Smith, 2001). In the present study, we highlight the additional importance of mixing interactions including PPO. We confirmed that during reheating treatments β'-2L forms of PPO and $MC_{POP/PPO}$ melted without further transformation into most stable forms. According to the results on mixtures subjected to thermal incubation, the stabilization of this components eventually occurs. However, kinetic experiments suggested that the presence of PPP may make them less prone to undergo the polymorphic transformation to the most stable form, especially in the case of PPO.

In addition to the above, assays on equimolecular PPP/PPO and PPP/$MC_{POP/PPO}$ mixtures cooled at 15 °C·min^{-1} evidenced the α immiscibility of these systems.

A recent report suggested that $MC_{PPP/POP}$, $MC_{POP/PPO}$, and $MC_{PPP/POP/PPO}$ may occur in PPP/POP/PPO mixtures with POO as diluent (West & Rousseau, 2020). However, the specifics about structure and stoichiometric properties remain unclarified. Such behavior was not confirmed under the experimental conditions used in our study. Furthermore, the two structurally similar β' phases formed in both PPP/PPO and PPP/$MC_{POP/PPO}$ systems were hardly differentiated even by SR-XRD. Some degree of mutual solubility of components is assumed but the thermal curves obtained during cooling and heating processes suggested that one was mainly formed by mixed-acid TAGs and the other by PPP. In this connection, PPO and POP/PPO ($MC_{POP/PPO}$) showed lower solubility limits in PPP under metastable conditions (10 and 20%, respectively) than in the more densely packed stable β phases. This outcome resulted from the specific thermal treatment applied and shows that a wide range of cooling and heating conditions needs to be tested to clarify the kinetic influence on the mixing properties of TAG systems.

The binary and ternary mixtures examined in the present study served as model systems to clarify the impact of a third component on the phase behavior displayed by two-TAG component mixtures. Research on multi-component TAG mixtures is needed for a better understanding of the specific molecular interactions occurring in complex lipids. This is of practical industrial value in applications such as oil separation and crystal engineering for specific food, cosmetic, and pharmaceutical applications.

Under stable conditions, the increasing solubility of the sequence OPO → $MC_{POP/OPO}$ → POP in the stable crystalline phase of PPP showed how the physical properties of lipid blends may vary due to intermolecular interactions resulting from the presence of an additional TAG. Results suggested the incorporation of molecular compound crystals in mixtures of fully saturated and saturated-unsaturated TAGs as a worthy to explore strategy for the development of tunable oleic-rich TAG-based agents for fat structuring. Specifically, the results indicated that molecular compound formation could be useful to prevent liquid phases containing oleic-rich TAGs, such as OPO, from oiling out in fat hardstock. In order to validate this statement, further

research on ternary mixtures that cover a wider range of chemically different TAGs should be carried out.

The results of the present study can be specially linked to actual oil fractionation processes, since the solidification and mixing properties of TAGs contained in high-melting fractions, such as PPP, influence the crystallization behavior of lower-melting components. Previous work showed how the seeding effect of PPP in oleic-rich mixtures may be enhanced by the formation of mixed crystals with POP (Vereecken et al., 2009, 2010b). Our data confirmed similar degree of solid solubility in PPP/PPO and PPP/POP mixtures under stable conditions. It was also found that POP and PPO forming molecular compound behaved as a single TAG component in blends with PPP. Thus, $MC_{POP/PPO}$ led to a eutectic diagram and favored the incorporation of equal amounts of the unsaturated components into PPP-rich solid solution phases. This implies an important role of PPO at the earliest stages of crystallization of lipids when present as a major component. For example, PPP, POP, and PPO, together with the lower-melting POO are main components of palm oil (Basiron, 2005; Smith, 2001). The dry fractionation of lipids entails a fractional crystallization from the melt induced by a cooling treatment at controlled conditions. These, together with the mixing interactions stablished by the different molecules determine the efficient separation of phases with a desired composition. As a relevant example, the enrichment of palm oil stearin fractions in monounsaturated asymmetric TAGs during this kind of processes has been previously highlighted (Deffense, 1985; Smith, 2001). The crystallization and mixing properties reported for PPP/PPO and PPP/$MC_{POP/PPO}$ systems in the present study likely play an important part in this behavior.

4.3. CHAPTER CONCLUSIONS

In the present chapter, we examined the phase behavior of binary and ternary blends of palmitic- and oleic-rich TAGs contained in industrially relevant lipid sources. So far, no studies on ternary mixtures including PPP and mixed-acid saturated-unsaturated TAGs in most stable polymorphs had been conducted. In addition, no high-resolution identification techniques, such as SR-XRD, were used to monitor the complex polymorphic behavior under the influence of dynamic thermal treatments.

Phase diagrams constructed for PPP/OPO, PPP/POP, PPP/PPO, PPP/$MC_{POP/OPO}$ and PPP/$MC_{POP/PPO}$ systems after several months of thermodynamic stabilization evidenced equivalent mixing behavior. Immiscible phases occurred at almost all concentration ratios and large differences in melting points of the components led to highly asymmetric eutectic compositions. In this sense, steric hindrance between saturated and unsaturated fatty acid chains was the main responsible of the outcome. The major difference within the mixture systems lied on the ability of the mixed-acid components to integrate in the crystalline phase of PPP. The extension of the miscibility regions around the pure PPP component were determined by the total amount of oleic acid in the system. This was linked to the decrease in positive excess free energy of mixing when reducing the number of bent unsaturated fatty acid moieties.

In the binary systems, the solubility of OPO was considerably lower than that of POP. As to the PPP/$MC_{POP/OPO}$ system, the total amount of mixed-acid TAGs solubilized in PPP lied between those of the pure mixed-acid TAGs. However, POP-OPO interactions favored the equimolecular solubility of the unsaturated components. In PPP/$MC_{POP/PPO}$ mixtures, the solubility of $MC_{POP/PPO}$ was slightly higher than that of pure POP or PPO in the binary mixtures.

The polymorphic and mixing properties of the mixture systems in the metastable state were examined under the influence of dynamic thermal treatments at varying rates of cooling and heating. The eutectic behavior with partial miscibility displayed by stabilized mixtures was also confirmed in less stable forms. Overall, the blending favored the crystal packing of TAGs in distinct β' forms during cooling processes at intermediate rates. By applying fast cooling rates, we determined α immiscibility in PPP/PPO and PPP/$MC_{POP/PPO}$ systems. No α forms of OPO and $MC_{POP/OPO}$ were identified under the thermal treatments applied, but the high oleic acid

content suggests a probable immiscible behavior of PPP/OPO and PPP/$MC_{POP/OPO}$ mixtures also in the α polymorph.

During reheating treatments, the polymorphic transformation behavior was not substantially modified with respect to the pure component in the latter mixture systems. However, PPO and $MC_{POP/PPO}$ favored melt-mediated β' to β transitions in PPP. In addition, β'-2L of PPO did not transit to β'-3L in the presence of PPP, whereas β'-2L of $MC_{POP/PPO}$ did not transform into β in the mixtures or the pure component sample. A higher degree of intersolubility of the components in these systems likely influenced these results. From the overall crystalline and mixing properties of blends including PPP, POP, and PPO under metastable and stable conditions, it can be inferred a key contribution of mixing interactions between these TAGs to two aspects regarding palm oil and related lipid systems: the great β' stability and the phase development behavior during crystallization processes.

From the results obtained, we may anticipate an important role of ternary on diverse aspects regarding lipid industry applications. For example, the phase development during the fractional crystallization of natural fats and oils, the physical properties of lipid blends in which molecular compound formation may be promoted, or the development of TAG-based tailored functional lipids enriched in specific oleic-rich components. This justifies the need of further studies on the polymorphic and phase behavior of three or more components mixture systems.

CHAPTER 5

PHASE BEHAVIOR OF 1,2,3-TRILAUROYL-GLYCEROL AND OLEIC-RICH TRIACYLGLYCEROLS FORMING MOLECULAR COMPOUND

5.1. INTRODUCTION

Lauric oils represent a group of edible lipids particularly rich in lauric, myristic, and capric acids. Palm kernel and coconut oils are the most industrially relevant, whereas other produced at a smaller scale include those from babassu, tucum, and cuphea (Gunstone et al., 2007). All of them stand out for their high content in trisaturated TAGs in comparison with other vegetable lipid sources. Thus, components such as LLL, CLL, LLM, or CCL represent ~90% and ~60% of total TAG content in coconut and palm kernel oils, respectively (Marikkar et al., 2013; Timms, 2003). Despite LLL being the major TAG present, the high content of mixed-acid TAGs favors their great stability in β'-2L.

The high content in content in medium-chain saturated fatty acids (with a number of carbon atoms between 6 and 12) of lauric oils makes them interesting in food applications. These have been linked to beneficial effects on human health, such as antimicrobial protection or lower adipose tissue deposition with respect to long-chain saturated fatty acids (Man & Manaf, 2006). Lauric oils are usually fractionated, hydrogenated, interesterified, and/or blended to yield a wide variety of products with improved properties (Timms, 2003). Their edible applications include the development of margarine, spreads, pastry, and baked products (Canapi et al., 2005; Eskin & List, 2017). In confectionery, cocoa butter substitutes (CBS) based on lauric fats have applications in the development of compound coatings. These are used to enrobe snacks, biscuits or bakery products when chocolate is not suitable in terms of economic feasibility, processing conditions, or functional properties desired in end products (Talbot, 2009a). In this sense, lauric-CBS provide good oxidative stability, quick solidification, excellent gloss, and a steep melting profile (Shukla, 2005; Smith, 2012).

Due to differences in molecular size and degree on unsaturation of the components, mixtures of lauric and non-lauric lipids tend to eutectic behavior. This was observed in blends of palm kernel oil and its hard fraction with palm oil or palm stearin (Liu et al., 2019; Norlida et al., 1996; Timms, 1984). Blends of coconut oil and palm stearin also show incompatibility (Liu et al., 2018). Eutectic formation results in a lower hardness and a depression in melting point, which may be advantageous to provide melt-away properties in specific products such as candy centers or fat fillings (Hartel et al., 2018; Rahim et al., 1998). It is also valuable to provide a quicker melting to table margarines (Silva et al., 2021; Wassell & Young, 2007). However, the functionality of many

end products may be compromised by eutectic formation, with chocolate being the most industrially relevant example. CB (rich in POS, SOS, and POP) and lauric-CBS are immiscible at almost all ratios in β-3L and β'-2L forms, respectively (Gordon et al., 1979). This limits the incorporation of CB into CBS to a maximum of 5%, which results in poor chocolate-like properties (Talbot, 2009b).

According to the above, mixing interactions between lauric and non-lauric lipids may play a key role in the functionality of foodstuffs. Despite this, studies on model TAG mixtures addressed to unveil the mixing interactions governing the behavior of blends with such configuration were overlooked for a long time. Yoshikawa et al. (2020) examined the polymorphic and mixing behavior of blends including LLL and SOS. The aim was to provide a molecular insight into the incompatible properties of lauric-CBS and CB under metastable conditions and in most stable polymorphs. More recently, the same authors found that the crystallization of β-2L ($MC_{SOS/OSO}$) promoted the direct crystallization of β-2L (LLL) without the need of tempering in ternary mixtures of LLL, SOS, and OSO (Yoshikawa et al., 2022). Promoting these interactions was suggested as a viable option to solve the problem of fat blooming in compound coatings based on lauric-CBS, which is in part due to the β' to β transitions undergone by TAGs containing lauric acid.

The purpose of this chapter is to go further on the characterization of the eutectic properties of LLL and TAG components containing oleic acid. Improving our knowledge about the mixing behavior of LLL and TAGs differing in fatty acid constituents, degree of unsaturation, or polymorphism may help understanding the physical behavior of more complex fat systems including similar molecular species. It is also of practical value for designing fat structuring strategies that improve the functionality of food products.

Concretely, this study reports on the polymorphic and mixing behavior of mixtures including LLL and the monounsaturated POP and PPO. The importance of the latter in edible lipids such as lard, or palm and olive oils was already stated in previous chapters. Following the same approach as in Chapter 4, LLL/POP, LLL/PPO, and LLL/POP/PPO mixtures (with POP/PPO at an equimolecular ratio) were examined after long-time stabilization and during the application of dynamic thermal treatments.

5.2. PHASE BEHAVIOR OF MIXTURE SYSTEMS

To study the phase behavior of LLL/POP, LLL/PPO, and LLL/$MC_{POP/PPO}$ mixtures in most stable forms, these were subjected first to a thermal incubation process to induce the thermodynamic stability. The specific conditions used during the process are detailed in Table 5.1. After the incubation, DSC and laboratory-scale XRD were used to evaluate the thermal and polymorphic behavior of the mixtures during a heating treatment at 2 °C·min^{-1}. Unless otherwise indicated, T_{top} is used to define the temperature of DSC events in this chapter.

Table 5.1. Conditions applied during the thermodynamic stabilization of mixture systems including LLL.

Thermodynamic stabilization process					
Mixture system	**First stage**		**Second stage**		
LLL/POP	5 days at 37 °C		9 months at 27 °C		
LLL/PPO	5 days at 37 °C		9 months at 27 °C		
LLL/$MC_{POP/PPO}$	5 days at 37 °C		6 to 12 months at 27 °C		
Melting temperature of mixture components (°C)					
LLL[1]	**POP[2]**	**PPO[2]**	**OPO[3]**	**$MC_{POP/PPO}$[2]**	**$MC_{POP/OPO}$[3]**
46.5	36.2	35.6	21.9	31.2	32.0

[1]Small (1986); [2]Minato et al. (1997a); [3]Minato et al. (1997b)

To monitor the crystallization, transformation, and mixing behavior in the metastable state, mixture systems were also examined during a thermal treatment consisting of fast cooling from the melt to -30 °C at 25 °C·min^{-1}, holding for 1 minute at this temperature, and reheating at 5 °C·min^{-1}. The high cooling rate used was intended to favor the crystallization of the samples in the α polymorph. So far, the phase behavior of mixtures including LLL in least stable forms has not been examined. Under such cooling conditions, the polymorphic characterization could be achieved by SR-XRD. The identification of the polymorphs was based on the typical XRD patterns previously described in Chapters 3 and 4 (see Tables 3.2 and 4.2).

5.2.1. LLL/POP binary system

5.2.1.1. *Phase behavior after a thermal stabilization stage*

Figure 5.1A shows the XRD patterns of LLL/POP mixtures taken at 10 °C after 9 months of thermodynamic stabilization. The DSC thermograms obtained when heating the mixtures from 0 °C to complete melting at 2 °C·min^{-1} are shown in Figure 5.1B.

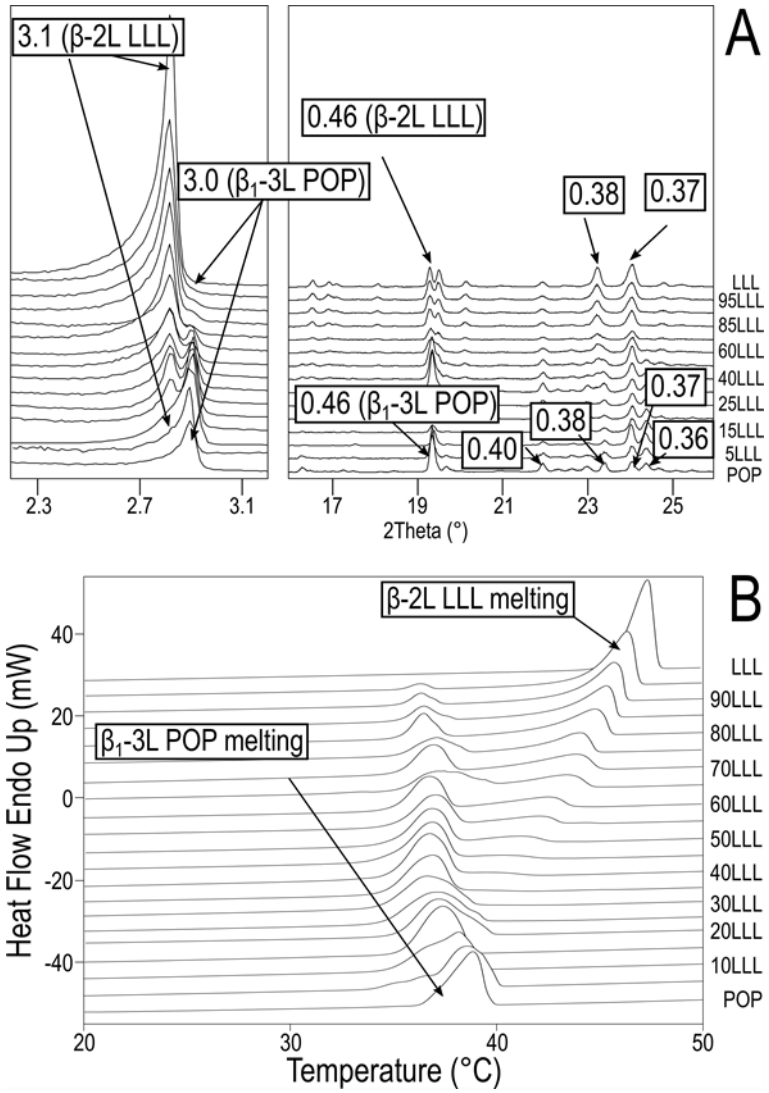

Figure 5.1. LLL/POP system. (A) Laboratory-scale XRD patterns of stabilized LLL/POP mixtures obtained at 10 °C. *d*-spacing values are given in nm. (B) DSC thermograms of stabilized LLL/POP mixtures heated at 2 °C·min^{-1}.

The polymorphic stability was confirmed at all compositions. The SAXD peak at 3.1 nm and WAXD peaks at 0.46, 0.38, and 0.37 nm were attributed to β-2L (LLL). Diffraction peaks at 3.0 (002 reflection), 0.46, 0.40, 0.38, 0.37, and 0.36 nm indicated the presence of β_1-3L (POP). According to XRD and DSC data, the overall behavior was ruled by the immiscibility of both TAGs. The presence of thermal and diffraction signals attributed to POP at the 95LLL/5POP composition denoted the poor integration of the mixed-acid TAG into the solid phase of LLL. In turn, the eutectic phases still identified in the 5LLL/95POP blend evidenced the great insolubility of LLL in the mixed-acid TAG.

To illustrate the thermal behavior of the mixtures during the heating process, melting temperatures determined by DSC were used to construct the phase diagram of Figure 5.2. Detailed melting data is summarized in Table 5.2.

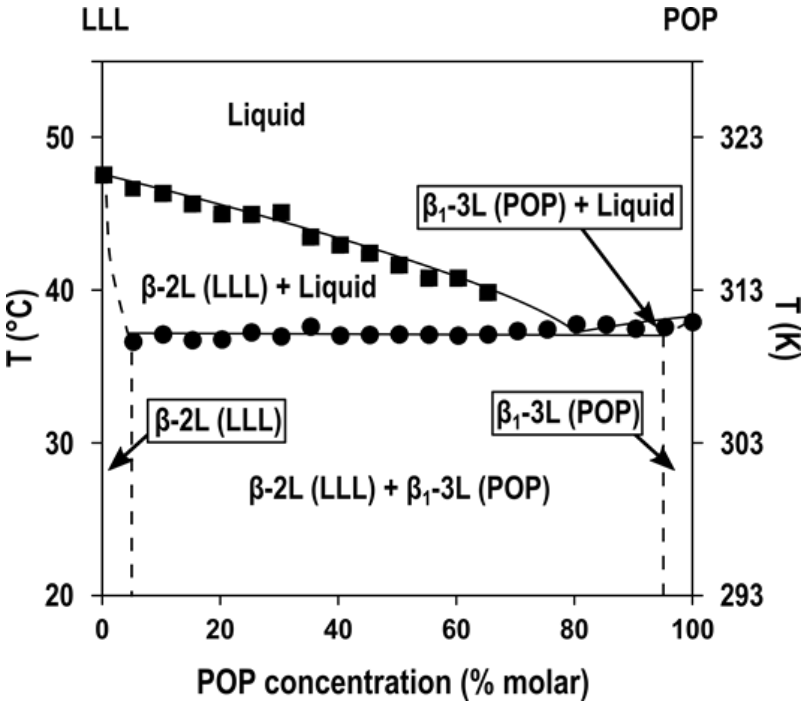

Figure 5.2. Phase diagram of incubated LLL/POP mixtures heated at 2 °C·min^{-1}.

Table 5.2. Melting behavior (°C) of stabilized LLL/POP mixtures heated at 2 °C·min^{-1}.

Polymorph	LLL	95LLL	90LLL	85LLL	80LLL	75LLL	70LLL
β_1-3L (POP)	-	36.4 ± 0.5	36.9 ± 0.8	36.5 ± 0.7	36.6 ± 0.6	37.0 ± 0.3	36.7 ± 0.5
β-2L (LLL)	47.3 ± 0.8	46.4 ± 0.4	46.1 ± 0.8	45.4 ± 0.5	44.8 ± 0.3	44.7 ± 1.6	44.8 ± 0.5
Polymorph	65LLL	60LLL	55LLL	50LLL	45LLL	40LLL	35LLL
β_1-3L (POP)	37.4 ± 0.3	36.8 ± 0.6	36.8 ± 0.6	36.9 ± 0.5	36.9 ± 0.8	36.8 ± 0.3	36.8 ± 0.6
β-2L (LLL)	43.3 ± 0.5	42.7 ± 0.4	42.2 ± 0.5	41.4 ± 0.3	40.6 ± 0.4	40.6 ± 0.4	39.6 ± 0.5
Polymorph	30LLL	25LLL	20LLL	15LLL	10LLL	5LLL	POP
β_1-3L (POP)	36.9 ± 0.3	37.1 ± 0.9	37.2 ± 0.8	37.5 ± 1.0	37.3 ± 0.9	37.4 ± 0.7	37.9 ± 0.7
β-2L (LLL)	n. d.	-	-	-	-	-	-

n. d.: not determined.

From the 95LLL/5POP to the 35LLL/65POP composition, the initial melting of β_1-3L (POP) at around 36-37 °C was followed by that of β-2L (LLL), which shifted to lower temperatures as the POP content increased. At LLL content in the blends of 30% and below, the melting peak of β-2L (LLL) was masked by that of β-3L (POP) in the corresponding heating thermograms (see Figure 5.1). In addition to this, the close long spacing values exhibited by β-2L (LLL) and β_1-3L (POP) made difficult to determine an accurate eutectic point by XRD. However, the trend shown by the liquidus curve suggested that the same was at a composition close to 20% LLL or below. During the heating of the 10LLL/90POP mixture, the corresponding SAXD patterns showed the earlier vanishing of the β-2L (LLL) reflection at 3.1 nm (data not shown). Based on this, we assumed that the eutectic composition in LLL/POP mixtures may include around a 20-10% LLL content.

5.2.1.2. *Kinetic phase behavior*

The polymorphic behavior of LLL/POP mixtures was examined by DSC and SR-XRD when cooled from the melt to -30 °C at 25 °C·min^{-1} and reheated at 5 °C·min^{-1}. The overall crystallization and transformation behavior will be described through the results obtained for selected compositions. The experimental data obtained for mixtures at 90, 80, and 60% LLL content is depicted in Figure 5.3. Results corresponding to mixtures at 40, 20, and 5% LLL content are shown in Figure 5.4.

During cooling, the crystallization behavior of the blends was governed by the formation of solid solutions (ss) and crystalline phases associated with the major TAG present.

In the 90LLL/10POP mixture, the DSC peak detected at around 4 °C resulted in a complex polymorphic crystallization. SAXD patterns at around -1 °C showed that a peak at 3.3 nm occurred first and other at 3.6 and 4.1 nm followed (see Figure 5.3A). In WAXD patterns, peaks at 0.44, 0.41, and 0.38 nm became visible. By considering the characteristic reflections of LLL and POP polymorphs, we concluded that β'-2L (LLL) (reflections at 3.3, 0.44, and 0.39 nm), α-2L (LLL) (3.6 and 0.41 nm), and a solid solution of LLL and POP in α were formed (peaks at 4.1 and 0.41 nm). The formation of α (ss) was concluded from the characteristic long spacing value, which differed from those typical of α-2L (LLL) and α-2L (POP). A similar polymorphism was detected at 80% LLL content but the occurrence of α (ss) was promoted as the LLL content decreased. Thus, this was the only form identified in the 60LLL/40POP mixture. When POP predominated in the blends (Figure 5.4), distinct crystalline phases were again obtained on cooling. As shown by SR-XRD patterns of the 20LLL/80POP mixture (Figure 5.4B), the crystallization of α (ss) was preceded by the occurrence of α-2L (POP) (SAXD peak at 4.6 nm and WAXD peak at 0.41 nm detected at around -6 °C). One may notice that α (ss) showed an increased long spacing value of 4.3 nm. This evidenced the changes occurring in the arrangement of the lamellar structure of solid solutions by cause of the LLL/POP ratio. Towards pure POP, the amount of α-2L (POP) increased at the expense of α (ss) until being the only form detected by SR-XRD data in the 5LLL/95POP mixture (see Figure 5.4C).

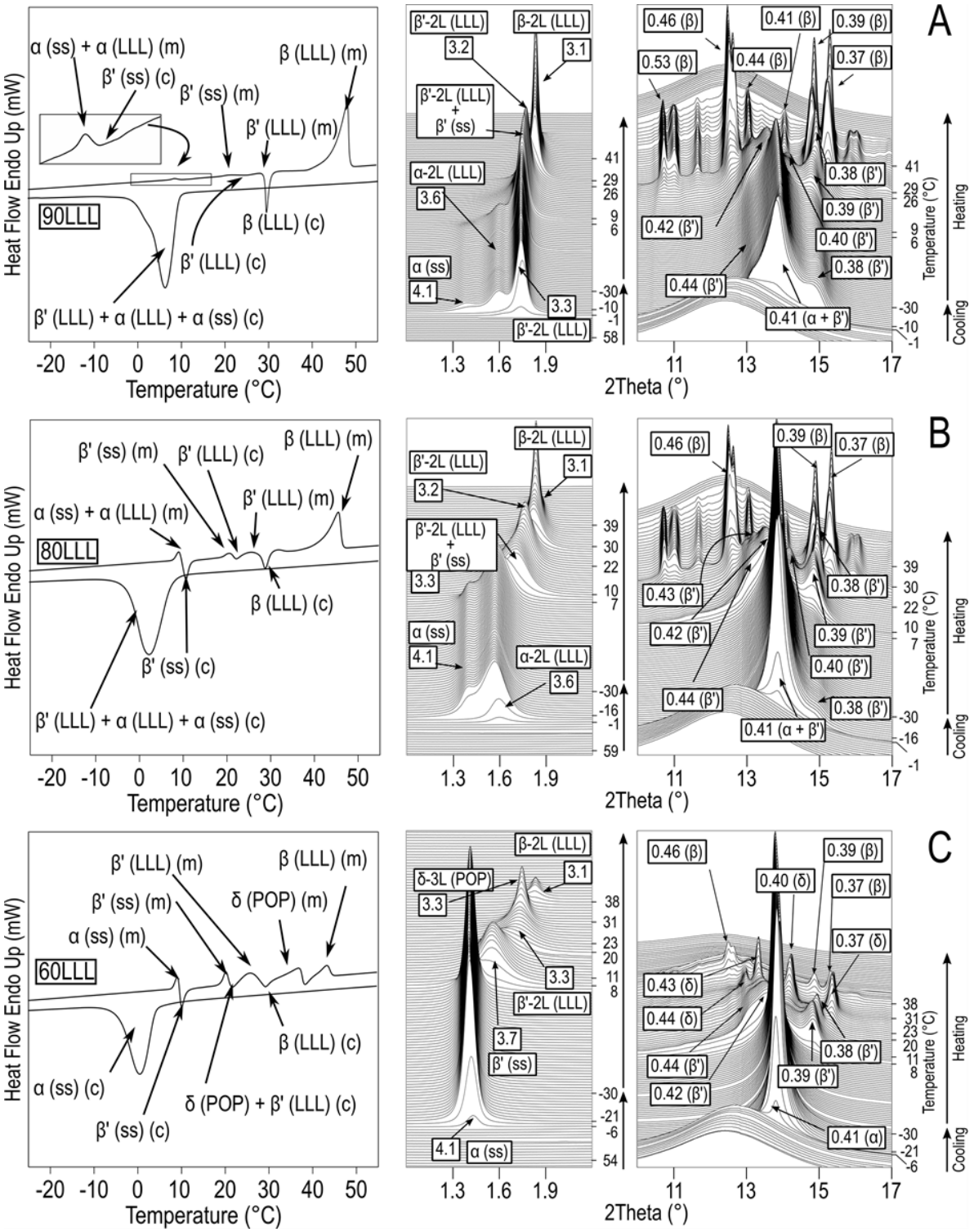

Figure 5.3. DSC (left) and SR-XRD data (right) of (A) 90LLL/10POP, (B) 80LLL/20POP, and (C) 60LLL/40POP mixtures cooled at 25 °C·min^{-1} and reheated at 5 °C·min^{-1}. (c): crystallization; (m): melting. *d*-spacing values are given in nm.

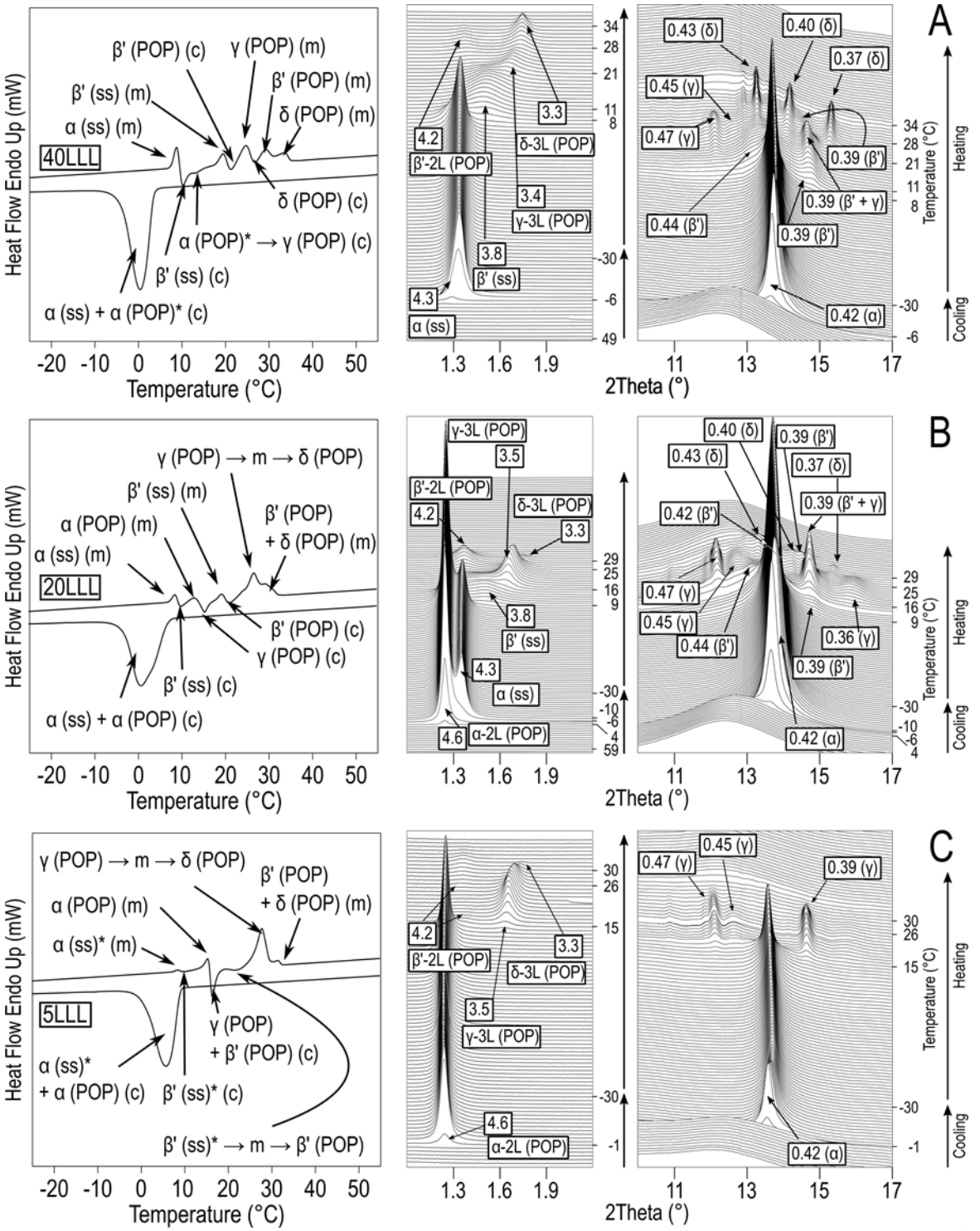

Figure 5.4. DSC (left) and SR-XRD data (right) of (A) 40LLL/60POP, (B) 20LLL/80POP, and (C) 5LLL/95POP mixtures cooled at 25 °C·min^{-1} and reheated at 5 °C·min^{-1}. *Not detected by SR-XRD. (c): crystallization; (m): melting. *d*-spacing values are given in nm.

During the reheating process at 5 °C·min^{-1}, a similar behavior was observed at 90-80% LLL content. However, the polymorphic events were more clearly discerned in the experimental data of the 80LLL/20POP mixture (see Figure 5.3B). The first melt-mediated transformation (endothermic and exothermic peaks at around 8 and 9 °C, respectively) observed by DSC was related to the vanishing peaks at 4.1 and 3.6 nm and the growth of a new one at 3.3 nm in the corresponding SAXD patterns at around 7 °C. In parallel, β' reflections at 0.43, 0.42, and 0.39 nm arose in WAXD patterns. Thus, α (ss) and α-2L (LLL) melted and β' (ss) crystallized next. The second one (DSC peaks at 19 and 21 °C) was linked to the sharpening and shifting of the SAXD peak to 3.2 nm. In addition, WAXD patterns at around 22 °C indicated changes in the β' subcell: a peak grew at 0.40 nm and that at 0.39 nm strengthened and moved to 0.38 nm. This resulted from the melting of β' (ss) and the next formation of β'-2L (LLL). Later on, this form transformed via melt-mediation into β-2L (LLL), which lead to melting and crystallization peaks in the DSC curve at around 21 and 25 °C, respectively. Accordingly, a SAXD peak at 3.1 nm and WAXD peaks at 0.46, 0.39, and 0.37 nm arose in SR-XRD patterns. The sharpening and subtle shifting of β WAXD reflections suggested an increase in the crystallinity of β-2L (LLL). In Chapter 3, it was already noted that this behavior could also relate to a transition into a more stable β form ($\beta_2 \rightarrow \beta_1$) (Allais et al., 2003). However, as before, we will refer to β-2L (LLL) for simplicity. In the heating thermogram, the melting of this form led to a single endothermic event at 47.5 °C.

Melt-mediated α (ss) → β' (ss) transformations also occurred at decreasing LLL content but differences were detected in later transition stages. In the 60LLL/40POP mixture (see Figure 5.3C), the melting of β' (ss) (long spacing value of 3.7 nm) at 20 °C was followed by crystallization of β'-2L (LLL) and δ-3L (POP) at around 22 °C. The POP form was identified by the sharp SAXD peak at 3.3 nm (002 reflection) and WAXD peaks at 0.43, 0.40, and 0.37 nm emerging in patterns at a close temperature. Then, β'-2L (LLL) reflections faded a few degrees above, in accordance with the DSC melting peak spotted at 25.5 °C. The next crystallization of β-2L (LLL) was slowed down by the presence of POP, and related SR-XRD peaks were only seen after δ-3L (POP) was gone (DSC melting peak at 36.4 °C).

When heating POP-rich blends, α-2L (POP) obtained on cooling transformed via-melt mediation into γ-3L (POP) soon after the α (ss) → β' (ss) transition. In the 20LLL/80POP mixture (see corresponding experimental data in Figure 5.4B), this led to endothermic and exothermic events at 13 and 15 °C in the heating thermogram. In SR-XRD patterns of this blend

and that with 40% LLL content (Figure 5.4A), typical γ WAXD peaks at 0.47, 0.45, and 0.39 nm and SAXD peak at 3.5 nm (002 reflection) developed above 16 °C. Then, β' (ss) melted and a new form with long spacing value of 4.2 nm was detected at both compositions. This resulted in the DSC endothermic and exothermic peaks observed in the mixtures at around 19 and 21 °C, respectively. The weak WAXD peaks detected at 0.44, 0.42, and 0.39 nm in the 20LLL/80POP blend at a close temperature (Figure 5.4B) allowed us to assign the SAXD reflection to β'-2L (POP). However, it was not clarified whether this form corresponded to β'_2 or β'_1 of POP. According to these results, the occurrence of β'-2L (POP) from β' (ss) was favored over β'-2L (LLL) in POP-rich blends, whereas the opposite occurred in LLL-rich ones. After the β'-2L (POP) crystallization, the heating thermogram of the 40LLL/60POP mixture (Figure 5.4A) showed a melt-mediated transformation and two consecutive melting events (temperature range from 24 to 34 °C). The first was due to the γ-3L (POP) → δ-3L (POP) transformation. In the corresponding SR-XRD patterns, the SAXD peak at 3.4 nm shifted to 3.3 nm and WAXD peaks at 0.43, 0.40, and 0.37 nm developed from those of γ. According to WAXD patterns, β'-2L (POP) melted next and δ-3L (POP) followed (DSC peaks at around 29 and 33 °C). Despite the higher thermodynamic stability of β', its earlier melting may have resulted from POP-LLL interactions. At decreasing LLL content, the melting of these forms led to a single identifiable DSC peak after the melting of γ-3L (POP) (see DSC data corresponding to the 20LLL/80POP mixture in Figure 5.4B).

As during the cooling process, only polymorphic events related to POP were discerned by SR-XRD when heating the 5LLL/95POP mixture (α-2L → γ-3L + β'-2L → δ-3L + β'-2L) (see Figure 5.4C). However, signals associated with α (ss) → β' (ss) → β'-2L (POP) transitions were still visible in the corresponding heating thermogram.

The polymorphic behavior observed for LLL/POP mixtures under kinetic conditions is illustrated in Figure 5.5. The thermal data corresponding to the main transformation and melting events during the heating process are gathered in Table 5.3. In summary:

i) During cooling, the great incompatibility of LLL and POP led to the formation of diverse crystalline phases at almost all LLL/POP ratios. In mixtures at the extremes, the crystallization was governed by the occurrence of α (ss) and metastable forms of

the major TAG present. A similar content of TAGs in the blends favored the formation of a single solid solution phase.

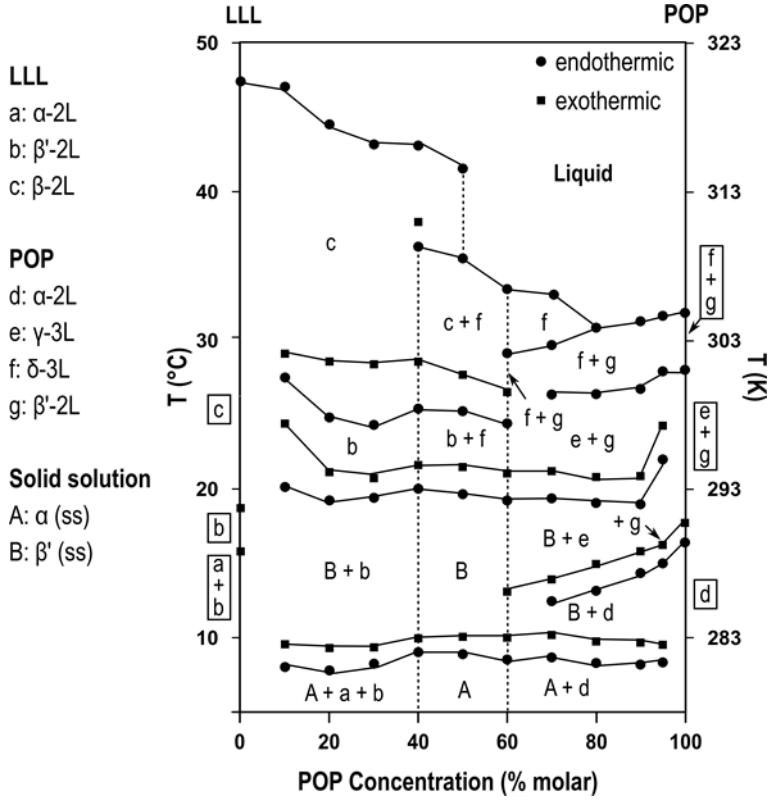

Figure 5.5. Phase behavior observed for LLL/POP mixtures heated at 5 °C·min^{-1} after cooling at 25 °C·min^{-1}. Delimited areas correspond to polymorphic domains between transitions experimentally determined.

ii) The transformation behavior of the blends on heating was determined by the polymorphic behavior displayed during cooling. In LLL-rich mixtures, β' (ss) was formed after the melting of α (ss) and α-2L (LLL). When PPO predominated, α (ss) and α-2L (POP) transformed separately into β' (ss) and β'-2L (POP), respectively, via melt-mediation.

iii) The melting of β' (ss) always led to a separation of the components. However, the next polymorphic occurrence depended on the ratio of TAGs. When LLL predominated, only β'-2L (LLL) was formed, which underwent a melt-mediated transition to β-2L (LLL) before complete melting. Mixtures at compositions close to pure POP showed that β'-2L (POP) crystallized from the melt of β' (ss), whereas the

formation of LLL crystals was prevented. At a similar LLL and POP content, β'-2L (LLL) and δ-3L (POP) arose after the melting of β' (ss). This defined the depression occurring in the liquidus line from LLL-rich mixtures (governed by the melting of β-2L of LLL) to POP-rich mixtures (melting of δ-3L and β'-2L of POP).

Table 5.3. DSC temperatures (°C) of main polymorphic events occurring in LLL/POP mixtures heated at 5 °C·min^{-1} soon after cooling at 25 °C·min^{-1}.

LLL/POP ratio	Heating at 5 °C·min^{-1}								
	a → β′	*β′ → β*	*β (m)*						
LLL	15.8 ± 0.6	18.8 ± 0.6	47.5 ± 0.8						
	a (ss) + a (LLL$_2$) (m)	*β′ (ss) (c)*	*β′ (ss) (m)*	*β′ (LLL$_2$) (c)*	*β′ (LLL$_2$) (m)*	*β (LLL$_2$) (c)*	*β (LLL$_2$) (m)*		
90/10	8.1 ± 1.7	9.6 ± 1.0	20.2 ± 0.4	24.5 ± 1.4	27.5 ± 0.5	29.2 ± 0.8	47.1 ± 0.5		
80/20	7.8 ± 1.2	9.4 ± 1.4	19.3 ± 0.8	21.2 ± 0.5	24.9 ± 0.8	28.6 ± 0.9	44.6 ± 0.7		
70/30	8.3 ± 0.3	9.4 ± 0.4	19.5 ± 0.4	20.8 ± 0.4	24.4 ± 0.3	28.4 ± 1.1	43.2 ± 0.6		
	a (ss) (m)	*β′ (ss) (c)*	*β′ (ss) (m)*	*β′ (LLL$_2$) + δ (POP) (c)*	*β′ (LLL$_2$) (m)*	*β (LLL$_2$) (c)*	*δ (POP) (m)*	*β (LLL$_2$) (m)*	
60/40	9.1 ± 0.4	10.0 ± 0.4	20.1 ± 0.4	21.7 ± 0.6	25.5 ± 0.7	28.6 ± 1.4	36.4 ± 1.1	43.1 ± 0.6	
50/50	8.9 ± 1.5	10.1 ± 1.9	19.7 ± 1.6	21.5 ± 2.0	25.3 ± 2.1	27.7 ± 1.9	35.6 ± 1.7	41.6 ± 1.5	
	a (ss) (m)	*β′ (ss) (c)*	*γ (POP) (c)*[1]	*β′ (ss) (m)*	*β′ (POP) (c)*	*γ (POP) (m)*	*δ (POP) (c)*	*β′ (POP) (m)*	*δ (POP) (m)*
40/60	8.6 ± 0.5	10.0 ± 0.4	13.2 ± 1.0	19.3 ± 0.5	21.4 ± 0.4	24.5 ± 0.4	26.6 ± 0.2	29.2 ± 0.5	33.5 ± 0.6
	a (ss) (m)	*β′ (ss) (c)*	*a (POP) (m)*	*γ (POP) (c)*	*β′ (ss) (m)*	*β′ (POP) (c)*	*γ (POP) → m → δ (POP)*	*β′ (POP) (m)*	*δ (POP) (m)*
30/70	8.7 ± 0.6	10.2 ± 0.4	12.5 ± 0.9	14.0 ± 0.9	19.4 ± 0.6	21.3 ± 0.6	26.4 ± 0.6	29.6 ± 0.7	33.1 ± 1.6
	a (ss) (m)	*β′ (ss) (c)*	*a (POP) (m)*	*γ (POP) (c)*	*β′ (ss) (m)*	*β′ (POP) (c)*	*γ (POP) → m → δ (POP)*	*β′ (POP) + δ (POP) (m)*	
30/70	8.7 ± 0.6	10.2 ± 0.4	12.5 ± 0.9	14.0 ± 0.9	19.4 ± 0.6	21.3 ± 0.6	26.4 ± 0.6	29.6 ± 0.7	
20/80	8.3 ± 0.2	9.8 ± 0.2	13.2 ± 1.1	15.0 ± 0.7	19.1 ± 0.2	20.9 ± 0.3	26.4 ± 0.3	30.8 ± 1.0	
10/90	8.2 ± 0.3	9.7 ± 0.3	14.4 ± 0.3	15.9 ± 0.8	19.0 ± 0.3	20.9 ± 0.3	26.8 ± 0.4	31.2 ± 0.3	
	a (ss) (m)	*β′ (ss) (c)*	*a (POP) (m)*	*γ (POP) + β′ (POP) (c)*	*β′ (ss) (m)*	*β′ (POP) (c)*	*γ (POP) → m → δ (POP)*	*β′ (POP) + δ (POP) (m)*	
5/95	8.4 ± 0.9	9.6 ± 0.9	15.0 ± 0.7	16.3 ± 1.2	19.1 ± 1.0	21.9 ± 0.7	28.0 ± 1.6	31.6 ± 1.0	
	a (m)	*γ + β′ (c)*	*γ → m → δ*	*β′ + δ (m)*					
POP	16.5 ± 0.4	17.8 ± 0.5	28.1 ± 0.3	31.9 ± 0.4					

n. d.: not determined. (ss): solid solution; (c): crystallization; (m): melting. [1]obtained from α (POP) crystals not identified by SR-XRD

5.2.2. LLL/PPO binary system

5.2.2.1. *Phase behavior after a thermal stabilization stage*

Laboratory-scale XRD data obtained at 10 °C for incubated LLL/PPO mixtures (Figure 5.6A) confirmed stable β-2L (LLL) and β'_1-3L (PPO) forms in pure TAG samples and in the mixtures. In addition, the melting behavior monitored when heating the samples at 2 °C·min^{-1} (Figure 5.6B) evidenced identical eutectic behavior to that of LLL/POP mixtures.

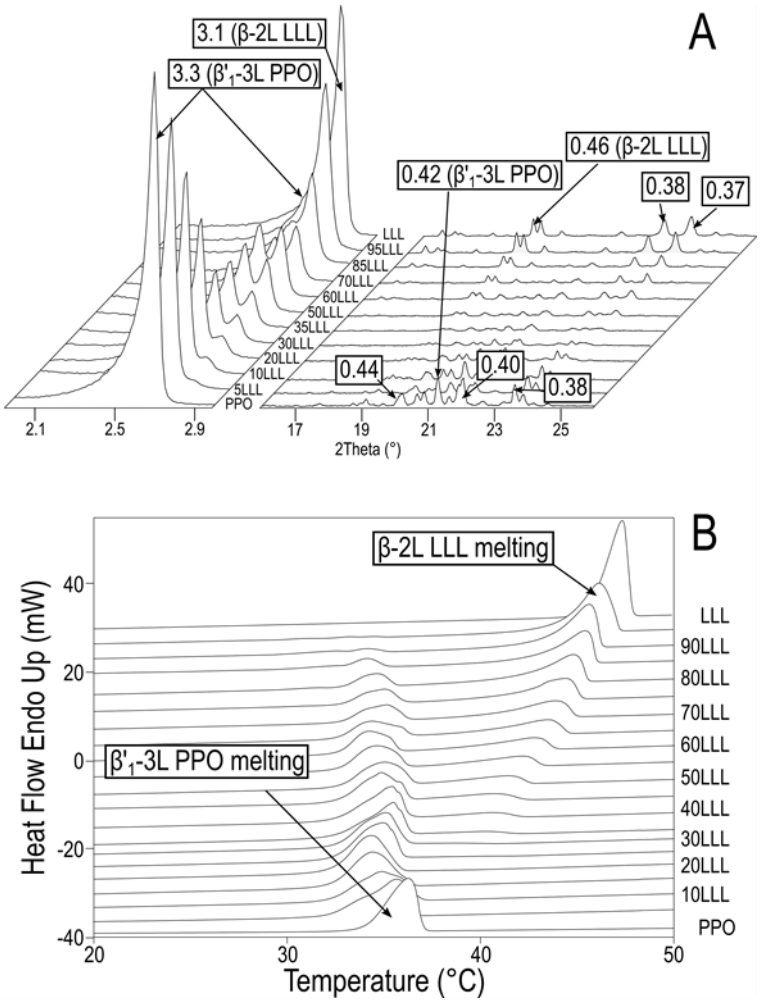

Figure 5.6. LLL/PPO system. (A) Laboratory-scale XRD patterns of stabilized LLL/PPO mixtures obtained at 10 °C. *d*-spacing values are given in nm. (B) DSC thermograms of stabilized LLL/PPO mixtures heated at 2 °C·min^{-1}.

The thermal data obtained during the heating process of the mixtures (see Table 5.4) is summarized in the phase diagram of Figure 5.7. Mixtures in the LLL-rich region showed the successive melting of β'$_1$-3L (PPO) and β-2L (LLL) phases and a solubility of PPO in LLL below 5%. The melting temperature of β-2L (LLL) decreased gradually towards the pure PPO sample until the two main DSC melting peaks became overlapped in mixtures with LLL content below 25%. Thus, the eutectic point could not be determined by DSC. During heating, β'$_1$-3L (PPO) was the only form detected in SAXD patterns of the 10LLL/90PPO mixture before the vanishing of all reflections (data not shown). This led us estimate a eutectic composition with around 20-10% LLL. As in the LLL/POP system, LLL did not dissolve in the mixed-acid TAG at the lowest concentration tested.

Table 5.4. Melting behavior (°C) of stabilized LLL/PPO mixtures when heated at 2 °C·min^{-1}.

Polymorph	LLL	95LLL	90LLL	85LLL	80LLL	75LLL	70LLL
β'$_1$-3L (PPO)	-	34.5 ± 0.3	34.2 ± 0.6	34.2 ± 0.5	34.4 ± 0.6	34.9 ± 0.7	35.1 ± 0.3
β-2L (LLL)	47.3 ± 0.8	46.2 ± 0.4	45.6 ± 0.4	45.5 ± 1.2	44.8 ± 0.9	44.2 ± 0.6	43.8 ± 0.3
Polymorph	65LLL	60LLL	55LLL	50LLL	45LLL	40LLL	35LLL
β'$_1$-3L (PPO)	34.6 ± 0.7	34.5 ± 0.9	34.8 ± 0.6	35.0 ± 0.5	35.2 ± 0.8	35.3 ± 0.4	35.5 ± 0.4
β-2L (LLL)	43.7 ± 0.6	42.9 ± 0.5	42.4 ± 0.8	41.7 ± 0.3	41.2 ± 0.6	40.6 ± 0.3	40.7 ± 0.7
Polymorph	30LLL	25LLL	20LLL	15LLL	10LLL	5LLL	PPO
β'$_1$-3L (PPO)	35.2 ± 0.6	35.0 ± 0.7	34.4 ± 0.9	34.8 ± 0.9	35.0 ± 0.5	35.7 ± 0.6	36.2 ± 0.2
β-2L (LLL)	38.7 ± 0.6	39.3 ± 0.7	-	-	-	-	-

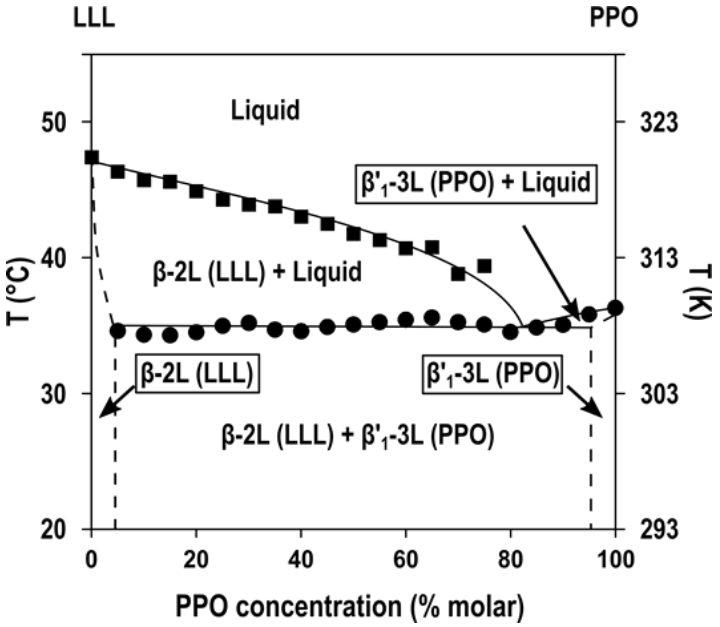

Figure 5.7. Phase diagram of incubated LLL/PPO mixtures heated at 2 °C·min^{-1}.

5.2.2.2. *Kinetic phase behavior*

As in LLL/POP mixtures, the polymorphic behavior of LLL/PPO mixtures cooled and subsequently heated at 25 and 5 °C·min^{-1}, respectively, was governed by crystallization and transformation events involving pure and miscible phases. DSC and SR-XRD data obtained for selected compositions are shown in Figures 5.8 (mixtures with 90, 80, and 60% LLL content) and 5.9 (mixtures with 40, 20, and 5% LLL content).

When cooling the 90LLL/10PPO mixture, β'-2L (LLL), α-2L (LLL), and α (ss) crystallized (DSC peak at 1.8 °C in Figure 5.8A). The formation of α (ss) was assumed from the peak with long spacing value of 3.8 nm arising in the corresponding SAXD patterns at around -1 °C. The same is not characteristic of any of the TAGs present in the mixture. The occurrence of α (ss) increased in the 80LLL/20PPO mixture (see the higher intensity of the corresponding SAXD reflection in Figure 5.8B), whereas the presence of α-2L (LLL) decreased and β'-2L (LLL) was no longer detected. When reducing the LLL content, the inclusion of this TAG in α (ss) was favored, whereas that of PPO, hindered. Thus, when cooling the 60LLL/40PPO mixture (see experimental data in Figure 5.8C), no polymorphs related to LLL occurred and a small fraction of PPO crystallized in α_2-2L before the growth of α (ss). Proof of this was the first reflection at 4.9 nm shown by the corresponding SAXD patterns at around 4-6 °C, which shifted to a *d*-spacing value of 4.2 nm on further cooling. When reaching -21 °C, the peak at 0.37 emerged in WAXD patterns was associated with the sub-α → α transition. Given its absence in blends at increasing LLL content, we assumed that this polymorphic event was exclusively related to α_2-2L (PPO).

A similar polymorphism was detected when cooling PPO-rich mixtures (see Figure 5.9). In these, the sequential crystallization of α forms of PPO and the LLL/PPO solid solution led to discernible exothermic events in the DSC curves. The first one, which was related to the pure TAG, became more energetic and shifted to higher temperatures from the 40LLL/60PPO to the 5LLL/95PPO mixture (DSC peaks at around 5 and 10 °C, respectively). One may also notice that the SAXD peak of α (ss) at 3.9 nm became visibly wider. An explanation is that α_1-3L (PPO), with a characteristic 002 reflection at 3.9 nm, crystallized together with α_2-2L (PPO). This would agree with the prevalent occurrence of both α forms observed in PPO cooled at different rates (see Figure 3.13 in Chapter 3).

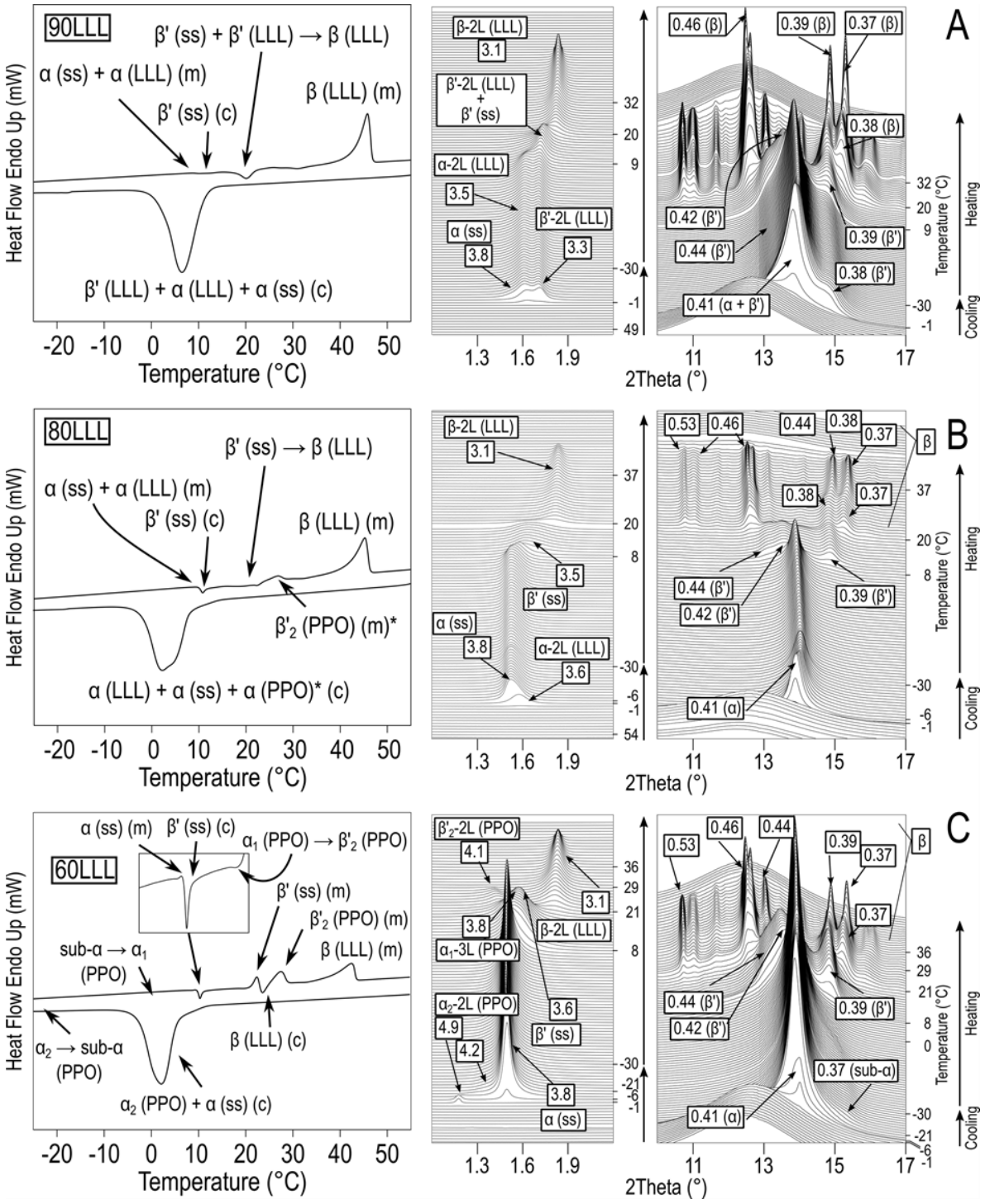

Figure 5.8. DSC (left) and SR-XRD data (right) of (A) 90LLL/10PPO, (B) 80LLL/20PPO, and (C) 60LLL/40PPO mixtures cooled at 25 °C·min^{-1} and reheated at 5 °C·min^{-1}. *Not identified by SR-XRD. (c): crystallization; (m): melting. *d*-spacing values are given in nm.

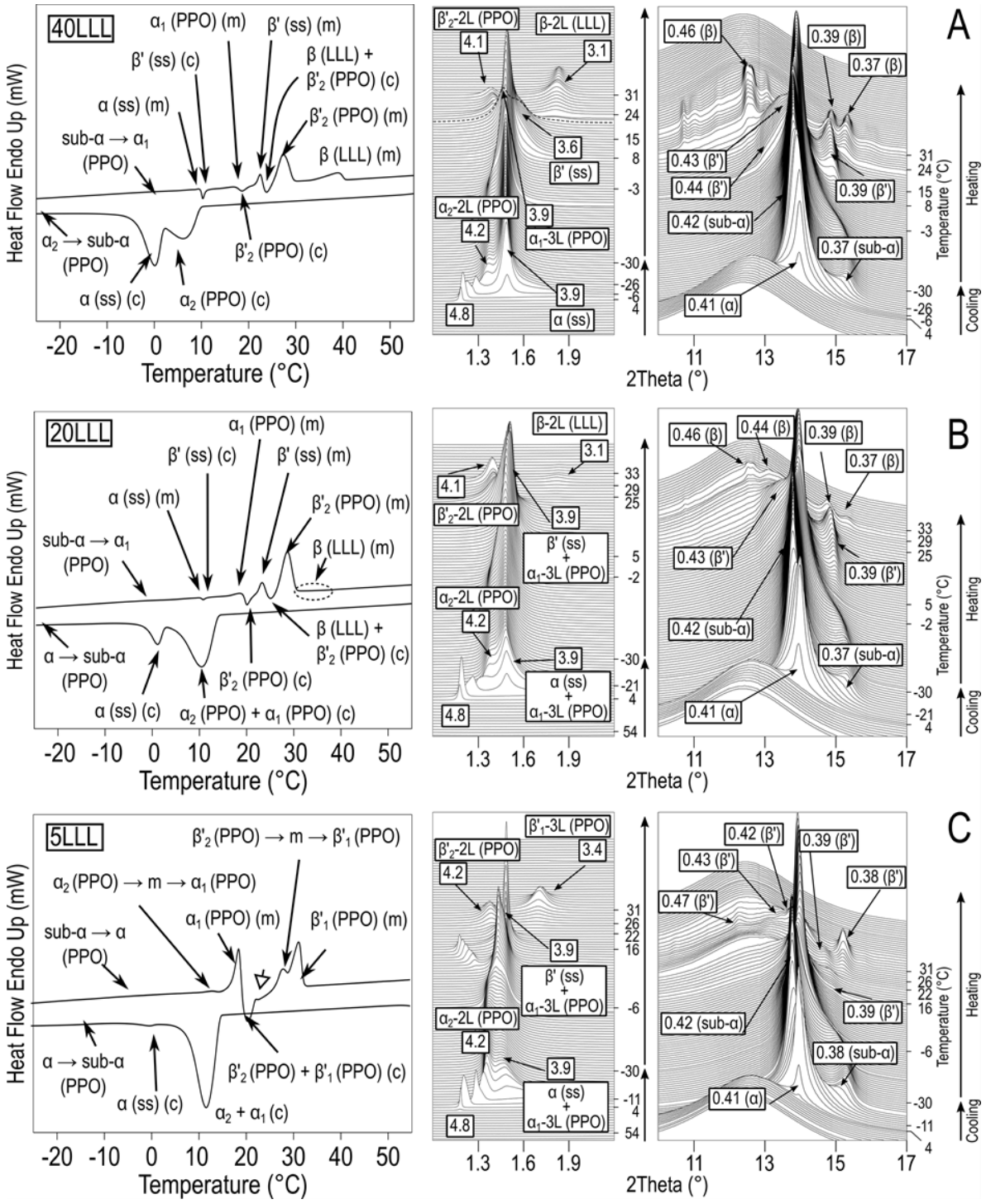

Figure 5.9. DSC (left) and SR-XRD data (right) of (A) 40LLL/60PPO, (B) 20LLL/80PPO, and (C) 5LLL/95PPO mixtures cooled at 25 °C·min^{-1} and reheated at 5 °C·min^{-1}. (c): crystallization; (m): melting. *d*-spacing values are given in nm.

The polymorphic occurrence displayed by the mixtures on cooling determined the transformation behavior when reheating at 5 °C·min^{-1}.

At a 90-80% LLL content (see Figures 5.8A and 5.8B), the consecutive endothermic and exothermic events detected by DSC at around 9 and 12 °C were due to the α (ss) + α-2L (LLL) melting and the next β' (ss) crystallization. In SAXD patterns of the 80LLL/20PPO mixture at around 9 °C, α (ss) and α-2L (LLL) reflections were replaced for a new one at 3.5 nm. In parallel, peaks at 0.44, 0.42, and 0.39 nm increased in intensity in WAXD patterns. The next exothermic event (19-22 °C) was linked to the formation of β-2L (LLL) from β' (ss) (and β'-2L of LLL in the 90LLL/10PPO composition). Finally, β-2L (LLL) melted at around 45-46 °C. It is worth mentioning that, in the 80LLL/20PPO mixture, a melting event not identified by SR-XRD occurred at 26.9 °C. Based on the results at lower LLL content, the same was related to the melting of a small amount of PPO crystals.

The transformation behavior was very similar in mixtures with 60 to 20% LLL content (see Figures 5.8C, 5.9A and 5.9B). According to SR-XRD data at around 0 °C, sub-α (PPO) transited to α_1-3L (PPO) in the first place. At this temperature, sub-α peak at 0.37 nm was no longer present in WAXD patterns and the SAXD peak at 3.9 nm strengthened at expense of that at 4.2 nm. Nevertheless, the first event observed by DSC was the melt-mediated α (ss) → β' (ss) transformation at around 9 °C. Since the long spacing value of β' (ss) resembled that of the preceding α (ss) (3.8-3.9 nm), this form was not distinguished from α_1-3L (PPO) in SAXD patterns. On further heating, α_1-3L (PPO) transformed into β'_2-2L (PPO). DSC endothermic and exothermic events in 40LLL/60PPO and 20LLL/80PPO mixtures between 16 and 19 °C (see Figures 5.9A and 5.9B) showed the melt-mediated nature of this transition. At this point, only β' reflections were seen in the corresponding WAXD patterns and a SAXD reflection at 4.1 nm raised from that at 3.9 nm. Thus, β' (ss) and β'_2-2L (PPO) were concurrently present until the β' (ss) melting, which gave rise to β-2L (LLL) and increased the amount of β'_2-2L (PPO) (see stronger peak at 4.1 nm in SAXD patterns of the 20LLL/80PPO mixture between 25 and 29 °C). Then, β'_2-2L (PPO) melted first and β-2L (LLL) followed. The small amount of LLL crystals in the 20LLL/80PPO mixture led to a barely identifiable β-2L (LLL) melting peak in the corresponding heating thermogram. Moreover, this polymorph no longer occurred at lower LLL content.

At compositions close to pure PPO, distinct sub-α (PPO) → α (PPO) and α_2-2L (PPO) → α_1-3L (PPO) transitions were detected. In the 5LLL/95PPO blend (see experimental data in Figure 5.9C), the second one led to the endothermic event detected at 13.2 °C by DSC. Then, α_1-3L (PPO) melted at around 19 °C and β'_2-2L (PPO) and β'_1-3L (PPO) crystallized. SAXD peaks at 4.2 and 3.4 nm (002 reflection) were together with typical β' WAXD reflections at around this temperature. The overlapped DSC phenomena finally detected corresponded to the melt mediated β'_2-2L (PPO) → β'_1-3L (PPO) transformation (peak at 28.2 °C) and β'_1-3L melting (31.6 °C) (denoted by the increase and decrease in intensity of SAXD peaks at 3.4 and 4.2 nm, respectively). As to solid solution phases, no DSC event due to the α (ss) melting was detected but a subtle one linked to the β' (ss) melting was still visible at around 22 °C (denoted by a white arrow).

The phase behavior observed in LLL/PPO mixtures under the thermal treatments applied is shown in Figure 5.10. Detailed DSC data on the transformation and melting behavior during the reheating process can be found in Table 5.5. As a summary:

i) In the mixture at 90% LLL content, metastable forms of LLL and α (ss) were present at the end of the cooling process. During reheating, successive transformations into α (ss) and β' (ss) took place before the occurrence of β-2L (LLL) and final melting.

ii) Below 80% LLL content, no LLL polymorphs occurred on cooling. The occurrence of α forms of PPO was followed by the crystallization of α (ss) and the next sub-α → α transition of PPO. When reheating, compositions with 20% LLL content and above showed sub-α (PPO) to α_1-3L (PPO) transitions and consecutive melt-mediated α (ss) → β' (ss) and α_1-3L (PPO) → β'_2-2L (PPO) transformations. The next melting of β (ss) was followed by the occurrence of β-2L (LLL). As to mixtures with LLL content below 20%, sub-α (PPO) → α (PPO) transitions occurred and then, α_2-2L (PPO) transformed into α_1-3L (PPO). The next melting of this form led to the crystallization of β'_2-2L (PPO) and stable β'_1-3L (PPO). Later on, the melt-mediated β'_2-2L (PPO) → β'_1-3L (PPO) transformation took place. No β-2L (LLL) crystallized after the α (ss) → melt → β (ss) transformation and β (ss) melting, so PPO governed the final melting stage. One may notice that the liquidus line defined by the blends

showed a minimum close to the 20LLL/80PPO mixture. This agrees with the eutectic composition at 20-10% LLL content estimated for stable LLL/PPO mixtures.

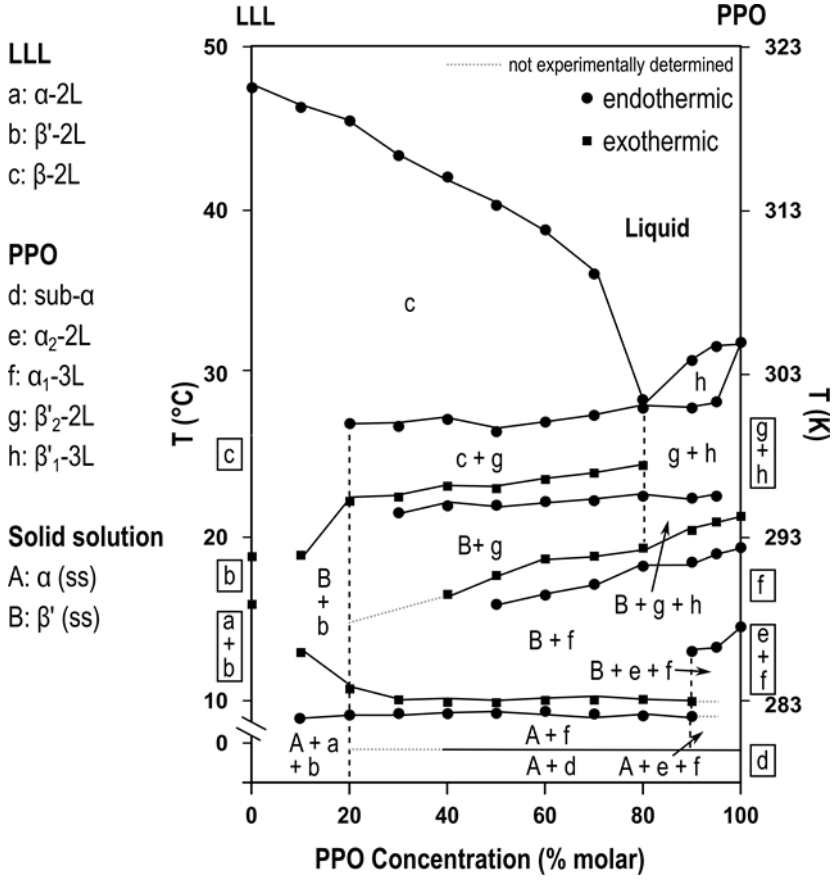

Figure 5.10. Phase behavior observed for LLL/PPO mixtures heated at 5 °C·min^{-1} after cooling at 25 °C·min^{-1}. Delimited areas correspond to polymorphic domains between transitions experimentally determined.

Table 5.5. DSC temperatures (°C) of main polymorphic events occurring in LLL/PPO mixtures heated at 5 °C·min^{-1} soon after cooling at 25 °C·min^{-1}.

LLL/PPO ratio	Heating at 5 °C·min^{-1}								
	a → *β′*	*β′* → *β*	*β (m)*						
LLL	15.8 ± 0.6	18.8 ± 0.6	47.5 ± 0.8						
	a (ss) + a (LLL$_\gamma$) (m)	*β′ (ss) (c)*	*β′ (LLL$_\gamma$) + β′ (ss) → β (LLL$_\gamma$)*			*β (LLL$_\gamma$) (m)*			
90/10	8.9 ± 0.9	12.9 ± 1.7	18.8 ± 3.3			46.3 ± 1.1			
	sub-a (PPO) → a$_1$ (PPO)[1]	*a (ss) + a (LLL$_\gamma$) (m)*	*β′ (ss) (c)*	*a$_1$ (PPO) → β′$_2$ (PPO)*[1]	*β′ (LLL$_\gamma$) + β′ (ss) → β (LLL$_\gamma$)*		*β′$_2$ (PPO)*[1] *(m)*	*β (LLL$_\gamma$) (m)*	
80/20	n. d.	9.1 ± 0.8	10.7 ± 0.7	n. d.	22.2 ± 0.4		26.9 ± 1.0	45.4 ± 1.2	
	sub-a (PPO) → a$_1$ (PPO)[1]	*a (ss) (m)*	*β′ (ss) (c)*	*a$_1$ (PPO) → β′$_2$ (PPO)*[1]	*β′ (ss) (m)*	*β (LLL$_\gamma$) (c)*	*β′$_2$ (PPO)*[1] *(m)*	*β (LLL$_\gamma$) (m)*	
70/30	n. d.	9.2 ± 0.5	10.0 ± 0.3	n. d.	21.4 ± 0.3	22.4 ± 0.4	26.7 ± 0.3	43.3 ± 0.4	
	sub-a (PPO) → a$_1$ (PPO)	*a (ss) (m)*	*β′ (ss) (c)*	*a$_1$ (PPO) (m)*	*β′$_2$ (PPO) (c)*	*β′ (ss) (m)*	*β (LLL$_\gamma$) (c)*	*β′$_2$ (PPO) (m)*	*β (LLL$_\gamma$) (m)*
60/40	n. d.	9.1 ± 0.7	9.8 ± 0.5	n. d.	16.5 ± 0.6	21.9 ± 0.6	23.1 ± 0.7	27.2 ± 0.8	42.0 ± 0.7
50/40	n. d.	9.2 ± 0.2	9.8 ± 0.3	15.8 ± 0.6	17.6 ± 0.3	21.9 ± 0.4	22.9 ± 0.4	26.4 ± 0.5	40.3 ± 0.4
	sub-a (PPO) → a$_1$ (PPO)	*a (ss) (m)*	*β′ (ss) (c)*	*a$_1$ (PPO) (m)*	*β′$_2$ (PPO) (c)*	*β′ (ss) (m)*	*β (LLL$_\gamma$) + β′$_2$ (PPO) (c)*	*β′$_2$ (PPO) (m)*	*β (LLL$_\gamma$) (m)*
40/60	n. d.	9.3 ± 0.3	10.0 ± 0.4	16.4 ± 0.5	18.6 ± 1.4	22.1 ± 0.3	23.5 ± 0.4	27.0 ± 0.5	38.8 ± 1.3
30/70	n. d.	9.1 ± 0.5	10.0 ± 0.5	17.1 ± 0.4	18.8 ± 0.4	22.2 ± 0.5	23.9 ± 0.4	27.4 ± 0.4	36.1 ± 0.7
20/80	n. d.	9.0 ± 0.5	10.0 ± 0.7	18.2 ± 0.8	19.3 ± 0.9	22.5 ± 0.8	24.3 ± 1.3	27.9 ± 1.0	n. d.
	sub-a (PPO) → a (PPO)	*a (ss) (m)*	*β′ (ss) (c)*	*a$_2$ (PPO) → m → a$_1$ (PPO)*	*a$_1$ (PPO) (m)*	*β′$_2$ (PPO) + β′$_1$ (PPO) (c)*	*β′ (ss) (m)*	*β′$_2$ (PPO) → m → β′$_1$ (PPO)*	*β′$_1$ (PPO) (m)*
10/90	n. d.	9.0 ± 0.5	9.9 ± 0.4	13.0 ± 0.5	18.4 ± 0.4	20.4 ± 0.4	22.3 ± 0.5	27.9 ± 0.6	30.8 ± 0.3
5/95	n. d.	n. d.	n. d.	13.2 ± 0.7	18.9 ± 0.8	20.9 ± 0.7	22.5 ± 0.7	28.2 ± 0.9	31.6 ± 0.9
	sub-a → a	*a$_2$ → m → a$_1$*		*a$_1$ (m)*	*β′$_2$ + β′$_1$ (c)*	*β′$_2$ → m → β′$_1$ → m*			
PPO	n. d.	14.4 ± 0.5		19.3 ± 0.5	21.2 ± 0.5	32.0 ± 0.6			

n. d.: not determined. (ss): solid solution; (c): crystallization; (m): melting. [1]Not confirmed by SR-XRD.

5.2.3. Mixtures of LLL and the POP/PPO molecular compound system

5.2.3.1. *Phase behavior after a thermal stabilization stage*

No differences in the phase behavior of LLL/$MC_{POP/PPO}$ mixtures were found after 6 or 12 months of stabilization at 27 °C. Diffraction data of all compositions at 10 °C are shown in Figure 5.11A. The DSC curves obtained when heating the samples at 2 °C·min^{-1} are depicted in Figure 5.11B. See the corresponding melting data in Table 5.6.

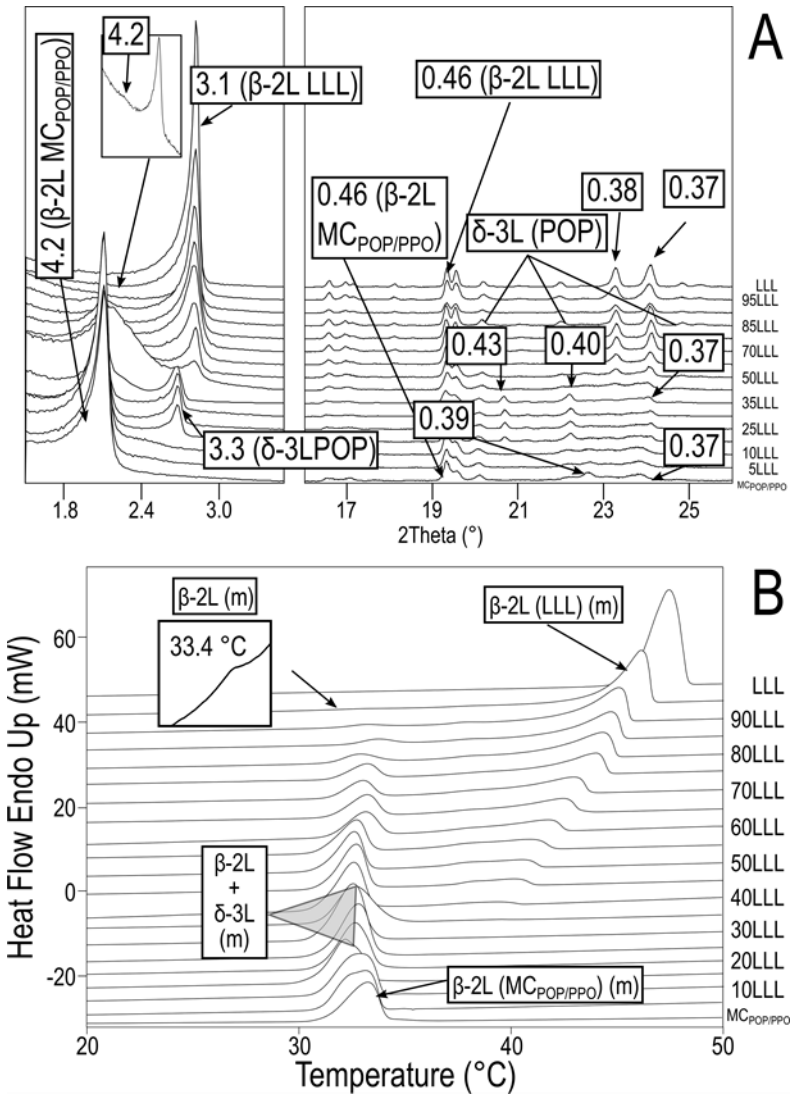

Figure 5.11. LLL/$MC_{POP/PPO}$ mixtures stabilized for one year. (A) Laboratory-scale XRD patterns obtained at 10 °C. *d*-spacing values are given in nm. (B) DSC thermograms obtained when heated at 2 °C·min^{-1}. (m): melting.

Table 5.6. Melting behavior (°C) of incubated LLL/$MC_{POP/PPO}$ mixtures heated at 2 °C·min^{-1}.

Polymorph	LLL	95LLL	90LLL	85LLL	80LLL	75LLL	70LLL
β-2L (ss)	-	33.4 ± 0.6	33.7 ± 1.4	33.3 ± 0.8	32.9 ± 1.4	33.0 ± 0.6	33.3 ± 1.1
β-2L (LLL)	47.3 ± 0.8	46.1 ± 0.6	45.2 ± 0.6	44.7 ± 0.3	44.9 ± 1.3	43.9 ± 0.8	43.3 ± 1.2
Polymorph	65LLL	60LLL	55LLL	50LLL	45LLL	40LLL	
β-2L (ss)	33.0 ± 1.2	33.6 ± 0.6	32.6 ± 0.5	32.8 ± 0.4	32.9 ± 0.5	32.5 ± 0.3	
β-2L (LLL)	42.8 ± 0.7	42.0± 0.9	41.3 ± 0.5	40.8 ± 0.5	40.3 ± 0.4	38.5 ± 1.2	
Polymorph	35LLL	30LLL	25LLL	20LLL	15LLL		
β-2L (ss) + δ-3L (POP)	33.0 ± 0.6	32.6 ± 0.4	32.8 ± 0.5	32.7 ± 0.7	32.5 ± 1.1		
Polymorph	10LLL	5LLL	$MC_{POP/PPO}$				
β-2L (ss)	32.3 ± 1.0	33.5 ± 0.9	-				
β-2L ($MC_{POP/PPO}$)	-	-	33.6 ± 0.7				

Stable forms were confirmed in the pure component samples. In $MC_{POP/PPO}$, the SAXD peak at 4.2 nm and WAXD peaks at 0.46, 0.39, and 0.37 nm showed that all POP and PPO were forming molecular compound. In the mixtures, experimental data showed that not all compositions were in the stable form, and that the polymorphic behavior depended on the ratio of TAGs.

In mixtures with LLL content below 15%, XRD confirmed the only formation of a solid solution in β-2L. By comparison with the great incompatibility observed in incubated LLL/POP and LLL/PPO mixtures, molecular compound formation favored the solubility of LLL in the mixed-acid TAGs.

Mixtures with 95 to 60% LLL content showed two main DSC events during heating. These corresponded to the consecutive melting of β-2L crystals rich in $MC_{POP/PPO}$ (in solid solution with some LLL) and β-2L (LLL). The diffuse SAXD peaks observed at LLL content below 50% indicated great irregularities in the longitudinal packing of TAGs. Then, at 35-15% LLL content, no SAXD peak of β-2L (LLL) (3.1 nm) was detected in XRD patterns, and a new one at 3.3 nm occurred instead. In parallel, peaks of similar intensity arose in WAXD patterns at 0.43, 0.40, and 0.37 nm. These allowed to assign the 002 reflection at 3.3 nm to δ-3L (POP). Based on the behavior observed at LLL content below 15%, we assumed that, in these compositions, most LLL was also solubilized in the β-2L phase rich in mixed-acid TAGs. As illustrated in the diagram of Figure 5.12, the abrupt drop in melting temperature caused by the absence of LLL crystals led to the flattening of the liquidus curve towards pure $MC_{POP/PPO}$. In DSC thermograms, no distinct melting events were discerned for the melting of β-2L (ss) and δ-3L (POP).

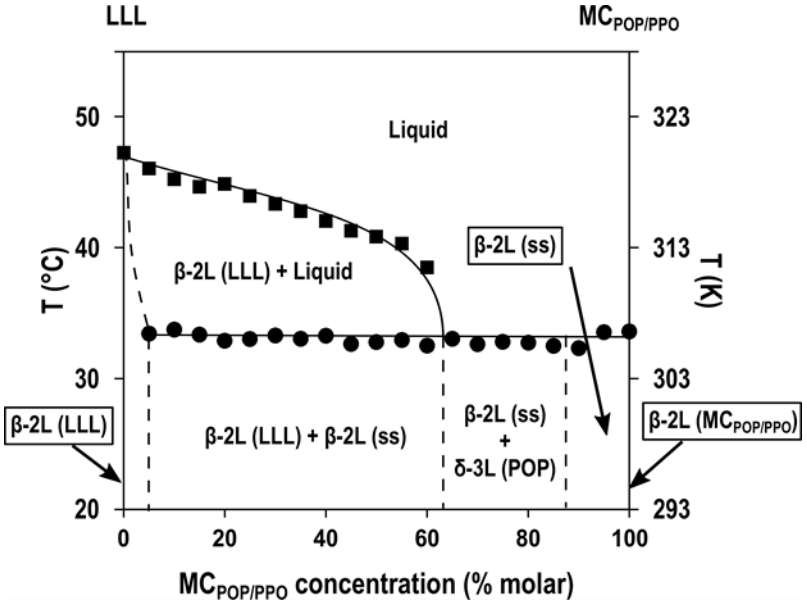

Figure 5.12. Phase diagram of the LLL/$MC_{POP/PPO}$ system after one year of thermodynamic stabilization.

In summary:

i) As in LLL/POP and LLL/PPO mixtures, the phase behavior of LLL/$MC_{POP/PPO}$ mixtures was mostly governed by eutectic interactions. At 40% LLL content and above, the immiscible β-2L forms were primarily attributed to LLL and a phase rich in $MC_{POP/PPO}$.

ii) At LLL content below 40%, LLL formed a solid solution in β-2L with POP and PPO. Below 15%, the 1:1 ratio of POP and PPO ($MC_{POP/PPO}$) was maintained in β-2L (ss). However, a higher LLL content favored the presence of PPO and the excess of POP crystallized in δ-3L.

iii) By considering the behavior of LLL-rich mixtures, one could expect that β-2L (ss) and δ-3L (POP) eventually evolve to $MC_{POP/PPO}$- and LLL-rich β-2L forms. However, it is worth underscoring their long lifespan after one year of incubation. According to results on LLL/POP mixtures, no δ-3L (POP) but β-3L (POP) should occur after such a long incubation time. From this, one may guess that the polymorphism and mixing interactions in such state cause a sufficient reduction in the free energy to delay the stabilization.

5.2.3.2. *Kinetic phase behavior*

The same thermal protocol applied during the kinetic study of LLL/POP and LLL/PPO mixtures, was used to investigate the LLL/$MC_{POP/PPO}$ system. Experimental data obtained for mixtures with 90, 80, and 60% LLL is shown in Figure 5.13. The behavior of mixtures rich in $MC_{POP/PPO}$ is clarified in Figure 5.14.

In LLL-rich mixtures, single exothermic events were detected by DSC on fast cooling (peaks at 2.2 to -2.9 °C from blends with 90 to 60% LLL content). SAXD and WAXD data of the 90LLL/10$MC_{POP/PPO}$ mixture confirmed the crystallization of β'-2L (LLL) (peaks at 3.3, 0.44, and 0.39 nm), α-2L (LLL) (3.6 and 0.41 nm), and α (ss) (4.0 and 0.41 nm). Reducing LLL content promoted the formation of α (ss), which crystallized alone in the 60LLL/40$MC_{POP/PPO}$ mixture (see Figure 5.13C).

The transformation behavior of the blends with higher LLL content when reheating at 5 °C·min^{-1} is described through the experimental of the 80LLL/20$MC_{POP/PPO}$ mixture (Figure 5.13B). α (ss) and α-2L (LLL) melted, and β' (ss) crystallized during the endothermic and exothermic events detected at ~7 and ~9 °C by DSC. Around these temperatures, the corresponding SAXD patterns showed the sequential vanishing of peaks at 4.0 and 3.6 nm. In parallel, a new one ocurred at 3.4 nm and β' reflections (0.44, 0.42, and 0.39 nm) developed in WAXD patterns. The next endothermic and exothermic peaks at around 21 and 22 °C, respectively, corresponded to the melting of β' (ss) (and some β' of LLL) and the next crystallization of β (see characteristic WAXD peaks near 20 °C). This form initially showed a long spacing value of 3.2 nm, which shifted to 3.1 nm on further heating. This led us to concluded that β' (ss) transformed into β (ss), the melting of which (DSC endothermic peak at around 35 °C) was followed by the occurrence of β-2L (LLL) (3.2 → 3.1 nm). This agrees with data on the blend at 60% LLL content (Figure 5.13C). In this, α (ss) → melt → β' (ss) transition was followed by the transformation of β' (ss) into a β (ss) form showing a less sharp SAXD peak with higher *d*-spacing value (reflection at 3.3 nm in related patterns at around 24 °C). One may notice that, at this composition, WAXD peaks at 0.43 and 0.39 nm accompanied β ones after the transition. Thus, some δ-3L (POP) (002 reflection at 3.3 nm) formed together with β (ss). In the DSC curve, the occurrence β-2L (LLL) from β (ss) and the next melting of δ-3L (POP) and β-2L (LLL) led to the broad thermal phenomena ranging from 25 to 45 °C.

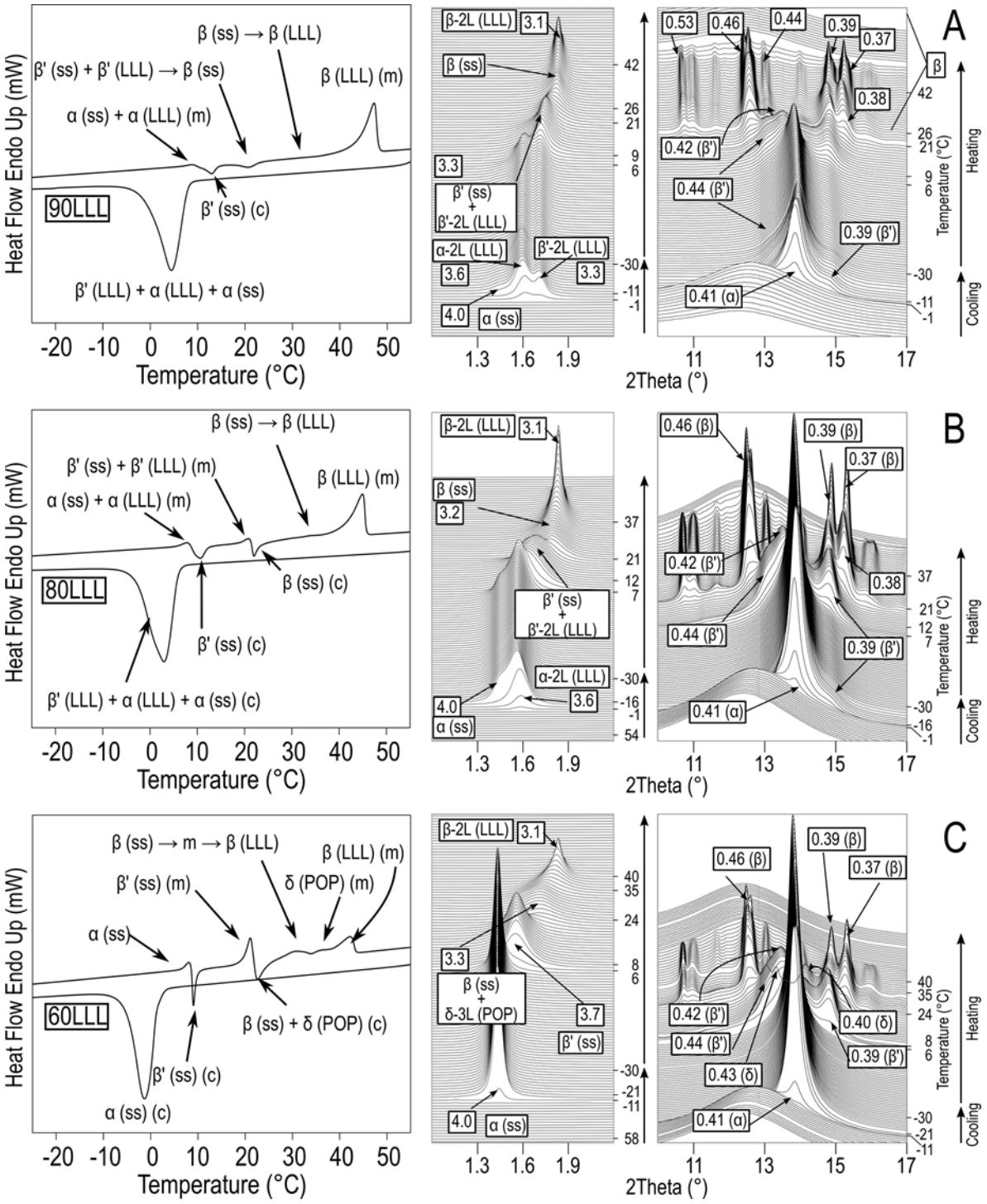

Figure 5.13. DSC (left) and SR-XRD data (right) of (A) 90LLL/10MC$_{POP/PPO}$, (B) 80LLL/20MC$_{POP/PPO}$, and (C) 60LLL/40MC$_{POP/PPO}$ mixtures cooled at 25 °C·min^{-1} and reheated at 5 °C·min^{-1}. (c): crystallization; (m): melting. *d*-spacing values are given in nm.

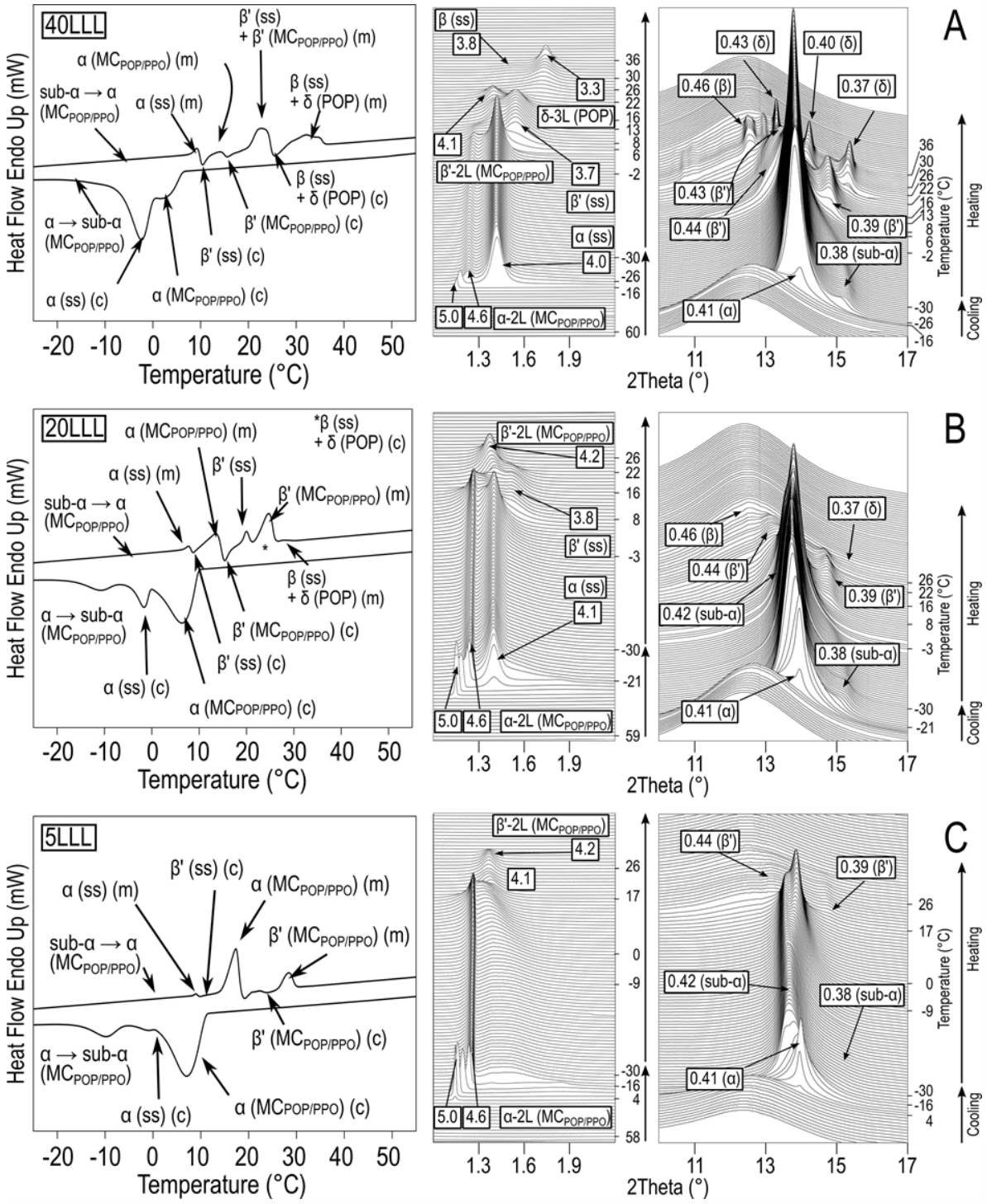

Figure 5.14. DSC (left) and SR-XRD data (right) of (A) 40LLL/60MC$_{POP/PPO}$, (B) 20LLL/80MC$_{POP/PPO}$, and (C) 5LLL/95MC$_{POP/PPO}$ mixtures cooled at 25 °C·min^{-1} and reheated at 5 °C·min^{-1}. (c): crystallization; (m): melting. *d*-spacing values are given in nm.

When cooling $MC_{POP/PPO}$-rich mixtures (Figure 5.14), three main crystallization events were detected by DSC. The first and third ones became more energetic and shifted to higher temperatures in blends with 40 to 5% LLL content (1.8 to 5.1 °C and -12.7 to -11.1 °C, respectively). The second one was barely detected at the lowest LLL concentration, which suggested its connection with a solid solution phase. Accordingly, SR-XRD patterns confirmed that α-2L ($MC_{POP/PPO}$) crystallized first (SAXD peak at 5.0 nm → 4.6 nm and WAXD peak at 0.41 nm). Then, α (ss) occurred (SAXD peak at 4.0-4.1 nm) and the α-2L ($MC_{POP/PPO}$) → sub-α-2L ($MC_{POP/PPO}$) transition followed (peak at 0.38 nm arising in WAXD patterns). The low amount of α (ss) formed in the 5LLL/95$MC_{POP/PPO}$ mixture prevented its detection by SR-XRD (see Figure 5.14C).

When reheating the mixtures with 40 to 20% LLL content at 5 °C·min^{-1} (see experimental data in Figures 5.14A and 5.14B, respectively), sub-α ($MC_{POP/PPO}$) → α-2L ($MC_{POP/PPO}$) transition was only detected by SR-XRD and the first event discernible by DSC was due to the α (ss) → melt → β' (ss) transformation. Then, α-2L ($MC_{POP/PPO}$) melted at around 12-13 °C and β'-2L ($MC_{POP/PPO}$) crystallized. In accordance, peaks at 4.1, 0.44, 0.43, and 0.39 nm grew at a close temperature in the corresponding SR-XRD patterns. On further heating, the broad DSC peak at around 21 °C in the 40LLL/60$MC_{POP/PPO}$ blend (Figure 5.14A) was due to the sequential melting of β' (ss) and β'-2L ($MC_{POP/PPO}$). Then, δ-3L (POP) and β (ss) crystallized at around 23 °C. β (ss) reflections (3.8 and 0.46 nm) vanished earlier from the corresponding SR-XRD patterns, so this form melted before δ-3L (POP) during the last DSC event observed from 25 to 40 °C. The lower fraction of TAGs forming solid solution at decreasing LLL content reduced the amount of δ-3L (POP) and β (ss) obtained from the β' (ss) melt. In the 20LLL/80$MC_{POP/PPO}$ mixture (Figure 5.14B), these forms were barely detected by SR-XRD (WAXD peaks at 0.46 and 0.37 nm before reaching 26 °C) and led to weak DSC signal when melting at around 28 °C. No δ-3L (POP) and β (ss) were detected at lower LLL content.

As in the cooling process, events related to solid solution phases could not be distinguished by SR-XRD when heating the 5LLL/95$MC_{POP/PPO}$ mixture (see Figure 5.14C). However, DSC peaks attributed to α (ss) melting and β' (ss) crystallization were still discernible. Apart from this, the overall transformation behavior was dictated by $MC_{POP/PPO}$. Thus, the α-2L ($MC_{POP/PPO}$) crystals formed during cooling, melted at around 16 °C when reheating. The next formation of β'-2L ($MC_{POP/PPO}$) led to the complex two-step crystallization process observed by DSC from

around 17 to 25 °C. This form finally melted at 27.2 °C without further transformation into stable β-2L ($MC_{POP/PPO}$).

Figure 5.15 depicts the phase behavior of LLL/$MC_{POP/PPO}$ mixtures under kinetic conditions. The DSC data regarding the main events occurring during heating treatments is shown in Table 5.7. In summary:

i) α (ss) including LLL, POP, and PPO crystallized at all compositions. In addition, α-2L (LLL) and β'-2L (LLL) were formed in LLL-rich mixtures, whereas α-2L ($MC_{POP/PPO}$) occurred at 50% LLL content and below. Miscibility was only promoted at a close LLL and $MC_{POP/PPO}$ content.

ii) During reheating, LLL-rich mixtures showed melt-mediated α (ss) + α-2L (LLL) → β' (ss), and β' (ss) + β'-2L (LLL) → β (ss) transformations. After the vanishing of β (ss), β-2L (LLL) occurred.

iii) From 60 to 20% LLL content, β (ss) and δ-3L (POP) crystallized after the β' (ss) melting. When $MC_{POP/PPO}$ predominated, also sub-α ($MC_{POP/PPO}$) → α-2L ($MC_{POP/PPO}$) and α-2L ($MC_{POP/PPO}$) → β'-2L ($MC_{POP/PPO}$) transformations were observed. No β-2L (LLL) was detected once β (ss) was gone in blends with less than 50% LLL content, so δ-3L (POP) defined the last melting stage. According to the liquidus curve depicted in Figure 5.15, increasing the LLL content in the blends favored the melting of these forms at higher temperatures.

iv) Below 20% LLL content, polymorphic transitions regarding solid solution phases were barely detected. In these, the transformation behavior and final melting closely resembled that of the pure $MC_{POP/PPO}$ sample.

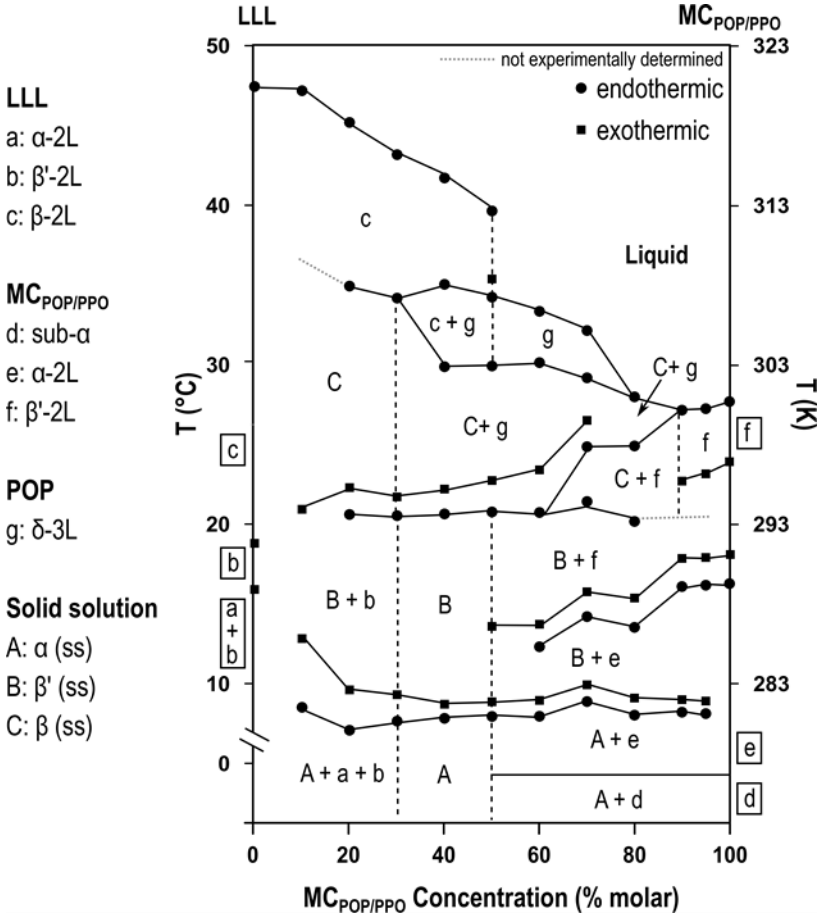

Figure 5.15. Phase behavior observed for LLL/$MC_{POP/PPO}$ mixtures heated at 5 °C·min^{-1} after cooling at 25 °C·min^{-1}. Delimited areas correspond to polymorphic domains between transitions experimentally determined.

Table 5.7. DSC temperatures (°C) of main polymorphic events occurring in LLL/$MC_{POP/PPO}$ mixtures heated at 5 °C·min^{-1} soon after cooling at 25 °C·min^{-1}.

LLL/$MC_{POP/PPO}$ ratio	Heating at 5 °C·min^{-1}									
	a → β′	*β′ → β*	*β (m)*							
LLL	15.8 ± 0.6	18.8 ± 0.6	47.5 ± 0.8							
	a (ss) + a (LLL) (m)	*β′ (ss) (c)*	*β′ (ss) + β′ (LLL) → β (ss)*	*β (ss) → β (LLL)*	*β (LLL) (m)*					
90/10	8.4 ± 0.8	12.8 ± 0.4	20.9 ± 1.4	n. d.	47.2 ± 0.7					
	a (ss) + a (LLL) (m)	*β′ (ss) (c)*	*β′ (ss) + β′ (LLL) (m)*	*β (ss) (c)*	*β (ss) → m → β (LLL)*	*β (LLL) (m)*				
80/20	7.0 ± 2.4	9.5 ± 0.7	20.6 ± 0.7	22.3 ± 1.4	34.9 ± 1.0	45.2 ± 1.0				
	a (ss) (m)	*β′ (ss) (c)*	*β′ (ss) (m)*	*β (ss) (c)*	*β (ss) → m → β (LLL)*	*β (LLL) (m)*				
70/30	7.6 ± 0.6	9.2 ± 0.5	20.5 ± 0.4	21.7 ± 0.5	34.2 ± 0.8	43.2 ± 0.7				
	a (ss) (m)	*β′ (ss) (c)*	*β′ (ss) (m)*	*β (ss) + δ (POP) (c)*	*β (ss) → m → β (LLL)*	*δ (POP) (m)*	*β (LLL) (m)*			
60/40	7.7 ± 0.5	8.6 ± 0.5	20.6 ± 0.7	22.2 ± 0.6	29.9 ± 0.6	35.1 ± 1.3	41.7 ± 0.8			
	sub-a ($MC_{POP/PPO}$) → a ($MC_{POP/PPO}$)	*a (ss) (m)*	*β′ (ss) (c)*	*a ($MC_{POP/PPO}$) (m)*	*β′ ($MC_{POP/PPO}$) (c)*	*β′ (ss) (m)*	*β (ss) + δ (POP) (c)*	*β (ss) → m → β (LLL)*	*δ (POP) (m)*	*β (LLL) (m)*
50/50	n. d.	7.9 ± 0.4	8.8 ± 0.4	n. d.	13.5 ± 0.3	20.7 ± 0.5	22.7 ± 0.5	29.9 ± 0.7	34.2 ± 0.5	39.6 ± 0.4
	sub-a ($MC_{POP/PPO}$) → a ($MC_{POP/PPO}$)	*a (ss) (m)*	*β′ (ss) (c)*	*a ($MC_{POP/PPO}$) (m)*	*β′ ($MC_{POP/PPO}$) (c)*	*β′ (ss) + β′ ($MC_{POP/PPO}$) (m)*	*β (ss) + δ (POP) (c)*	*β (ss) (m)*	*δ (POP) (m)*	
40/60	n. d.	7.9 ± 0.7	8.9 ± 0.9	12.3 ± 0.7	13.7 ± 0.5	20.7 ± 1.4	23.4 ± 0.6	30.1 ± 1.4	33.3 ± 0.4	
	sub-a ($MC_{POP/PPO}$) → a ($MC_{POP/PPO}$)	*a (ss) (m)*	*β′ (ss) (c)*	*a ($MC_{POP/PPO}$) (m)*	*β′ ($MC_{POP/PPO}$) (c)*	*β′ (ss) (m)*	*β′ ($MC_{POP/PPO}$) (m)*	*β (ss) + δ (POP) (c)*	*β (ss) (m)*	*δ (POP) (m)*
30/70	n. d.	8.8 ± 0.5	9.9 ± 0.5	14.1 ± 1.2	15.7 ± 1.1	21.4 ± 0.6	24.8 ± 0.8	26.5 ± 1.1	29.2 ± 2.1	32.1 ± 1.4
	sub-a ($MC_{POP/PPO}$) → a ($MC_{POP/PPO}$)	*a (ss) (m)*	*β′ (ss) (c)*	*a ($MC_{POP/PPO}$) (m)*	*β′ ($MC_{POP/PPO}$) (c)*	*β′ (ss) (m)*	*β (ss) + δ (POP) (c)*	*β′ ($MC_{POP/PPO}$) (m)*	*β (ss) + δ (POP) (m)*	
20/80	n. d.	8.0 ± 1.2	9.0 ± 1.3	13.5 ± 0.7	15.3 ± 0.9	20.1 ± 1.1	n. d.	24.9 ± 1.2	28.0 ± 1.1	
	sub-a ($MC_{POP/PPO}$) → a ($MC_{POP/PPO}$)	*a (ss) (m)*	*β′ (ss) (c)*	*a ($MC_{POP/PPO}$) (m)*	*β′ ($MC_{POP/PPO}$) (c)*	*β′ (ss) (m)*	*β′ ($MC_{POP/PPO}$) (m)*			
10/90	n. d.	8.1 ± 0.9	8.9 ± 1.1	16.0 ± 1.1	17.8 ± 1.2	22.6 ± 1.0	n. d.	27.1 ± 1.2		
5/95	n. d.	8.0 ± 1.7	8.8 ± 2.0	16.1 ± 2.0	17.9 ± 2.2	23.1 ± 1.7	n. d.	27.2 ± 2.1		
	sub-a → a	*a ($MC_{POP/PPO}$) (m)*	*β′ ($MC_{POP/PPO}$) (c)*	*β′ ($MC_{POP/PPO}$) (m)*						
$MC_{POP/PPO}$	n. d.	16.2 ± 0.8	18.1 ± 0.9	23.9 ± 0.9	27.7 ± 0.9					

(ss): solid solution; (c): crystallization; (m): melting; n. d.: not determined

5.2.4. Summary of mixtures of LLL and oleic-rich mixed-acid triacylglycerols

The results on LLL/POP and LLL/PPO mixtures subjected to 9 months of stabilization at 27 °C evidenced identical eutectic behavior. Both systems showed eutectic compositions with around 20-10% LLL content. In addition, no solubility of each TAG in the solid phase of the other was observed at the lowest concentrations tested. It can be assumed that the great incompatibility of the components was related with the steric hindrance between saturated and unsaturated fatty acid chains. In addition, the different length of lauric and palmitic acid moieties of TAG components would also contribute to the phase separation by increasing the instability at methyl end regions.

Regarding the results obtained during dynamic thermal treatments, α (ss) was always obtained in LLL/POP and LLL/PPO mixtures on cooling. However, crystalline phases of the pure components were also formed at almost all ratios. It was already noted that solid solution formation may be kinetically favored at high supercooling conditions. Therefore, in these mixtures, the positive excess free energy of mixing that would prevent the miscibility was partially overcome by the fast cooling treatment applied (25 °C·min^{-1}). Despite this, melt-mediated α (ss) → β' (ss) transitions were always followed by a separation of the mixture components during heating processes. Then, the polymorphic occurrence and transformation behavior that succeeded depended on the major TAG present in the blends.

Our results on LLL/POP and LLL/PPO mixtures relate directly to the functionality of end products as, for example, margarine based on palm oil (rich in POP) and palm kernel oil (rich in LLL). Their blending leads to immiscibility, with a maximum eutectic interaction at around 40% palm kernel oil content (Grimaldi et al., 2001; Norlida et al., 1996). This behavior is valuable to obtain products with butter-like properties like plasticity and a soft mouthfeel (Liu et al., 2019; O'Brien, 2009). The prevalent phase separation shown by LLL/POP mixtures also links to the great incompatibility of CB (rich in POS, SOS, and POP) and lauric-CBS. In line with this, LLL/SOS mixtures aged for two weeks at 25 °C showed a solubility of LLL in SOS below 10%, and of SOS in LLL below 3% (Yoshikawa et al., 2020). Based on the fatty acid composition and distribution, one could expect a similar behavior in LLL/POS mixtures.

In contrast to the binary systems, no polymorphic stability was achieved in LLL/MC$_{POP/PPO}$ mixtures at all ratios after one year of incubation. Solid solutions in β-2L were formed at LLL

content below 15%. The higher solubility of LLL in the mixed-acid TAGs with respect to the binary systems could be due to the double chain-length structure of $MC_{POP/PPO}$. Although no clear explanation can be provided, one may consider that in triple structures of stable POP and PPO, larger voids when including shorter LLL molecules could lead to a greater instability in methyl end regions. The polymorphism observed in mixtures at 35%-15% LLL content indicated that increasing the amount of LLL altered the 1:1 interaction shown by POP and PPO in $MC_{POP/PPO}$. Thus, β-2L (ss) was concurrently present with a δ-3L (POP) at these compositions. During experiments under varying cooling/heating rates, mixtures with 60 to 20% LLL content also showed the occurrence of these forms after the melting of β' (ss). Specifically, in the 40LLL/60$MC_{POP/PPO}$ composition, β (ss) and δ-3L (POP) melted directly without further occurrence of additional polymorphs. By contrast, the same sample subjected to thermodynamic stabilization showed that most LLL was separated into stable β-2L. Despite the low molecular diffusivity in the solid state presumed for the incubated mixtures, an eventual separation of LLL should be also expected at compositions at 35% LLL content and below. The long lifespan of β (ss) and δ-3L (POP) could be due to a narrow difference in the free energy of the system in such state and in most stable forms. This would reduce the driving force for the polymorphic transformation and, therefore, slow the stabilization.

In summary, results on LLL/$MC_{POP/PPO}$ mixtures showed that: i) the solubility of LLL in POP and PPO improved when both TAGs were forming a β-2L structure; and ii) the formation of long-life solid solutions including more than 10% LLL content entailed the separation of part of the POP fraction, which crystallized in δ-3L. However, to which extent the equimolecular ratio of POP and PPO in $MC_{POP/PPO}$ is altered in β (ss) and the specific interactions that trigger this behavior remain unclear. In the future, these issues should be clarified by evaluating the crystalline phase development in LLL/POP/PPO mixtures at varying ratio of mixed-acid TAGs. The engineering of crystalline solid solutions including lauric-based TAGs and unsaturated TAGs with longer saturated fatty acids, such as palmitic or stearic, could be of practical use in diverse lipid structuring applications. For example, in the development of β-stable cocoa butter alternatives (CBA) displaying a higher compatibility with CB than lauric-CBS.

5.3. CHAPTER CONCLUSIONS

We determined the phase behavior of LLL/POP, LLL/PPO, and LLL/$MC_{POP/PPO}$ mixtures after a thermal incubation process to induce the polymorphic stability and under the influence of dynamic thermal treatments based on cooling and subsequent heating processes.

LLL/POP and LLL/PPO binary systems in most stable polymorphs showed identical eutectic behavior. In both cases, the maximum eutectic interaction occurred at around the same LLL content, and no miscibility occurred at the lowest content of each TAG tested. The overall properties were a direct consequence of the different polymorphism, degree of unsaturation, and length of saturated fatty acids exhibited by the components. Even though the miscibility of the components was favored by kinetics during the application of dynamic thermal treatments, the eutectic behavior still prevailed.

In LLL/$MC_{POP/PPO}$ mixtures, one year of thermal incubation was not enough to achieve the polymorphic stability. POP and PPO forming a molecular compound with double chain-length structure favored the formation of β solid solutions including LLL. However, the equimolecular interaction of POP and PPO to form the novel crystalline structure was altered at sufficient levels of LLL, which led to the separation of POP. A similar behavior was determined during experiments under kinetic conditions. Therefore, despite the strong specific interactions associated with TAGs forming molecular compound, different phase behavior and structural arrangement may result from mixing interactions with a third component.

In the future, it would be worthy to unveil the structural factors that favor solid solution formation in mixture systems including LLL. The promotion of three-component solid-solutions including this TAG could be a potential strategy to diversify the applications of lauric oils and their fractions in edible products.

CHAPTER 6

POLYMORPHISM AND CRYSTALLINE BEHAVIOR OF LIPID BLENDS OF COCOA BUTTER AND SHEA BUTTER STEARIN

6.1. INTRODUCTION

Chocolate is a polycrystalline edible material in which fine particles of cocoa solids and sugar are dispersed in a fat phase (Sato, 2001; Timms, 2003). Most typical formulations may include components from the beans of *Theobroma cacao* (CB, cocoa liquor, and cocoa powder), non-cocoa butter vegetable fat, milk solids (milk fat, mil powders), emulsifiers, and/or flavors (Wohlmuth, 2009). The recipe varies among chocolate types, which are standardized by law in most countries. In the European Union, the Directive 2000/36/EC is the legal framework relating to cocoa and chocolate products intended for human consumption.

Only in the European Union, around 3,541,000 tons of chocolate products with an estimated value exceeding €12 billion were produced during 2020 (Eurostat, 2021). Within these, near 15% concerned confections apart from chocolate blocks, bars, slabs, or biscuits. The high popularity and demand for chocolate goods lie in the pleasant flavor provided by cocoa powder and the unique melting profile of CB (Talbot, 2012). It melts quickly at mouth temperature, causing a rapid release of aromatic compounds and a smooth creamy texture. These and other attributes such as a good snap, surface gloss, or bloom resistance rely on the lipid crystals formed within the CB mass (Bayés-García et al., 2015b; Manning & Dimick, 1985; Sato & Koyano, 2001).

The consumption of chocolate and chocolate-type products increases globally year after year (Perez et al., 2022). However, the availability of cacao beans to meet the production demands is not guaranteed. A production restricted to particular geographical areas, complex supply chains, pest outbreaks, or inclement weather, results in fluctuating supply and prices of the beans in the market (Fowler, 2009). This is especially relevant in the production of CB, which shows more diverse industrial applications than cocoa powder (Timms, 2003). Developing CBA that replace CB in foodstuffs is, therefore, one of the current challenges of manufacturers.

CB is mainly a multi-component mixture of TAGs, in which POS, SOS, and POP account for 80-90% of total content. In turn, these determine its characteristic polymorphism and crystalline behavior. Wille & Lutton (1966) identified six polymorphs in CB, which denominated as forms I to VI in order of increasing thermodynamic stability. Among these, Form V or β_2-3L is the most industrially relevant, as it gives rise to the valuable sensory properties of chocolate. Diverse studies have examined the polymorphic crystallization and transformation properties of CB under different approaches. Some of them have focused on the examination of CB in bulk

during the application of thermal treatments under isothermal and non-isothermal conditions (Loisel et al., 1998; van Malssen et al., 1996a, 1999). In this connection, a recent study compared the crystalline behavior of CB in bulk and in emulsion state within lipid bodies of fresh cacao beans during cooling and heating treatments at varying rates (Bayés-García et al., 2019). The effect on the polymorphic occurrence and crystallization kinetics of CB of lipid seed crystals, organic components like limonene, and inorganic minor additives, such as talc particles, has also been investigated (Bayés-García et al., 2022; Hachiya et al., 1989; Rigolle et al., 2016).

Based on their composition, polymorphism, and compatibility with CB, CBA can be classified as CBS, cocoa butter replacers (CBR), and cocoa butter equivalents (CBE) (Lipp & Anklam, 1998). Lauric-based CBS show a great β' stability and poor compatibility with CB. Thus, unless a softening effect is desired (frozen desserts, melt-away candies), CBS normally replace all the CB in formulations (Hartel et al., 2018). CBR are produced by hydrogenation, fractionation, and/or blending oils from soybean, cottonseed, rapeseed, and palm (Talbot, 2009a, 2014). Despite being β'-stable, the presence of stearic, palmitic, and oleic fatty acids allows obtaining compatible blends with up to 25% CB content (Gordon et al., 1979). As to CBE, tropical fats from palm, shea, illipe, kokum, sal, or mango kernel are often used for their production. These are rich in at least one of the major TAGs of CB. Thus, by blending a source of POP (i.e., palm mid fraction), SOS (i.e., kokum butter), and POS (i.e., illipe butter), a β-3L stable product fully compatible with CB can be obtained (Talbot, 2009b). Within CBE, cocoa butter extenders (CBEx) are used for greater economic feasibility and cocoa butter improvers (CBI), rich in SOS, are used to increase the hardness and heat resistance of CB (Timms, 2003).

The six fats used in CBE production can be included in chocolate to a maximum of 5% of the total weight. Otherwise, the products are known as compound chocolates and cannot be legally labeled as "chocolate". Despite this, their tunability is advantageous in the industry for the production of snacks, cakes, and confections with more versatile properties (Norazlina et al., 2021). To design the most functional lipid blend for each specific application, the crystalline behavior of CB and non-CB fats combined at different proportions should be known in advance.

In regard to the above, the present chapter aims to deepen into the polymorphic and physical properties of lipid mixtures based on CB and ShS.

Shea butter, also known as karité butter, is produced from the nuts of *Butyrospermum parkii*, a tree indigenous to the savannah belt of West Africa. Mainly formed by SOS (13-45%), SOO (26-

33%), and OOO (10-20%) (Segman et al., 2012), its fractionation yields a stearin concentrated in SOS (~70%) more suitable for CBE production (Gunstone, 2006). In contrast to CB, the polymorphism of ShS has not been fully detailed by previous work. Ray et al. (2013) combined DSC, XRD, NMR, and microscopy techniques to examine the crystallization behavior of ShS under isothermal and non-isothermal conditions. They confirmed the occurrence of α, γ, β', and β forms with similar subcell to those of SOS. It was also found that DAGs, despite being minor components of ShS, play a key role in the induction times of crystallization and polymorphic transitions.

Studies on blends including shea butter products are also scarce in the scientific literature. Kang et al. (2013) developed a CBE based on 40% palm oil stearin and 60% ShS able to replace up to 30% CB without modifying the crystallization and melting temperature ranges or the solid fat content (SFC). Rodriguez-Negrette et al. (2019) investigated the behavior of blends of CB and whole shea butter in dark chocolate formulations. Shea butter behaved well as CBEx when accounting for up to 30% total fat content. However, it promoted the undesirable β_2-3L (V) to β_1-3L (VI) transition in chocolates after long-time storage. Aiming to assess the feasibility of ShS as CBE, Zeng et al. (2020) studied the melting properties of CB/ShS blends and the effect of different emulsifiers on the occurrence of the β form. The consumer acceptance of chocolate including ShS was also tested through a sensory panel.

So far, fundamental aspects of shea butter products and their blends, such as the polymorphic crystallization, transformation, or microstructural behavior, have been disregarded. In this chapter, we examine the polymorphic behavior of CB, ShS, and selected blends during the application of thermal treatments at varying cooling and heating rates. In addition, we analyze their melting properties in least stable forms and after inducing the occurrence of more stable β crystals. The morphological changes occurring in the fat crystal network of the samples throughout the β phase development under specific isothermal conditions are also unveiled.

6.2. POLYMORPHIC BEHAVIOR UNDER VARYING DYNAMIC THERMAL TREATMENTS

Table 6.1 depicts the crystallographic data of the polymorphic forms identified for POS, SOS, and POP (Arishima et al., 1991; Ghazani & Marangoni, 2018; Lutton, 1951; Sato et al., 1989). Despite their evident common traits, some particularities can be highlighted. For instance, β' forms of POP show double chain-length structure. By contrast, the β' forms of POS may exhibit both double or triple structure and only a β' triple has been identified in SOS. Moreover, no γ form occurs in POS, nor δ in SOS. The mixing interactions of these TAGs result in the distinct behavior of CB, which shows two β' forms with double chain-length structure but no γ or δ forms. The polymorphic and melting data of CB is detailed in Table 6.2. As already stated, the polymorphic properties of ShS were not covered in detail by previous work but one may expect them to be dictated by SOS (Ray et al., 2013; Talbot et al., 2014).

According to the above, the crystalline behavior of CB/ShS blends will be mostly determined by the relative abundance of POS, SOS, and POP within. Given the similar β packing of these TAGs, differences among blends and with respect to the pure fats may be more evident in less stable forms. These precede the stable crystalline phases present in end products, so their characterization is of utmost importance in many industrial processes. Such is the case of the tempering procedure performed during chocolate production to obtain β_2 seed crystals of CB (and blends with CBA). In this, successive cooling and heating treatments are applied to induce crystallization, transformation, and melting events involving unstable forms (Talbot, 2009c). Thus, the properties displayed by these will define parameters such as the temperature ramps or the speed of the thermal treatments.

In this section, we provide an insight into the polymorphic behavior in the metastable state of pure CB, ShS, and mixtures at selected mass ratios. DSC and laboratory-scale XRD techniques were applied to monitor their crystallization and transformation properties under the influence of dynamic thermal treatments. In more detail, molten samples at 70 °C were cooled to -30 °C to induce the crystallization, held at this temperature for one minute, and then reheated until complete melting. Previous chapters already stressed the influence of varying cooling and heating rates on the polymorphic behavior of lipid systems. For this reason, we compared the behavior of the samples during thermal treatments at intermediate and low rates. Specifically, the two

thermal protocols applied consisted of i) cooling to -30 °C and reheating at 2 °C·min^{-1} and ii) cooling to -30 °C and reheating at 0.5 °C·min^{-1}.

Table 6.1. Melting temperature, *d*-spacing values (LS, SS), and chain-length structure (CLS) of main polymorphic forms of POP, SOS, and POS.

	T_m (°C)	LS (nm)	SS (nm)[a]	CLS
POP[1]				
α	15.2	4.65	0.421 (vs)	Double
γ	27.0	6.54	0.474 (s), 0.446 (m), 0.390 (s), 0.358 (w)	Triple
δ	29.2	6.25	0.429 (s), 0.413 (s), 0.383 (s)	Triple
β'_2	30.3	4.24	0.438 (w), 0.423 (s), 0.415 (m), 0.396 (s), 0.383 (w)	Double
β'_1	33.5	4.24	0.445 (w), 0.427 (m), 0.413 (m), 0.396 (s)	Double
β_2	35.1	6.10	0.461 (vs), 0.407 (m), 0.393 (m), 0.382 (m), 0.372 (m), 0.362 (w), 0.355 (w), 0.352 (w)	Triple
β_1	36.7	6.10	0.461 (vs), 0.407 (m), 0.388 (m), 0.382 (m), 0.372 (s), 0.367 (m)	Triple
SOS[1]				
α	23.5	4.83	0.421 (vs)	Double
γ	35.4	7.05	0.472 (s), 0.450 (m), 0.388 (s), 0.363 (w)	Triple
β'	36.5	7.00	0.430 (m), 0.415 (m), 0.402 (s), 0.395 (m), 0.383 (m), 0.370 (s)	Triple
β_2	41.0	6.50	0.458 (vs), 0.400 (m), 0.390 (m), 0.375 (m), 0.367 (m), 0.357 (w)	Triple
β_1	43.0	6.50	0.458 (vs), 0.402 (w), 0.397 (w), 0.385 (w), 0.380 (w), 0.365 (s)	Triple
POS[2,3,4]				
α	19.5	4.76	0.423 (vs)	Double
δ	28.3	7.06	0.463 (m), 0.431 (m), 0.411 (m), 0.389 (s)	Triple
β'_2	29.8	4.40	0.430 (m), 0.408 (s), 0.377 (m)	Double
β'_1	31.6	6.68	0.430 (w), 0.413 (s), 0.385 (s)	Triple
β_3	32.9	6.41	0.461 (vs), 0.398 (m), 0.387 (m), 0.375 (m), 0.366 (m)	Triple
β_2	33.8	6.35	0.460 (vs), 0.397 (m), 0.385 (m), 0.374 (w), 0.369 (w), 0.365 (w)	Triple
β_1	38.7	6.39	0.460 (vs), 0.404 (m), 0.393 (m), 0.386 (m), 0.370 (s)	Triple

[a]vs, s, m, and w represent "very strong", "strong", "medium", and "weak" WAXD reflections. [1]Sato et al. (1989); [2]Lutton (1951); [3]Arishima et al. (1991); [4]Ghazani & Marangoni (2018).

Table 6.2. Melting points and crystallographic data of CB polymorphs determined by Wille & Lutton (1966).

		T_m (°C)	LS (nm)	SS (nm)[a]	CLS
Form	**Equivalence**				
I	Sub-α	17.3	5.45	0.419 (vs), 0.370 (s)	Double
II	α	23.3	4.90	0.424 (vs)	Double
III	β'_2	25.5	4.91	0.492 (vw), 0.462 (w), 0.425 (vs), 0.386 (s)	Double
IV	β'_1	27.5	4.50	0.435 (vs), 0.415 (vs), 0.397 (m), 0.381 (m)	Double
V	β_2	33.8	6.41	0.461 (vs), 0.398 (m), 0.387 (m), 0.375 (m), 0.366 (m)	Triple
VI	β_1	36.3	6.38	0.540 (m), 0.515 (w), 0.458 (vs), 0.398 (s), 0.387 (m), 0.375 (m), 0.367 (w), 0.339 (vw)	Triple

[a]vs, s, m, w, and vw represent "very strong", "strong", "medium", "weak" and "very weak" WAXD reflections.

6.2.1. Cooling and reheating processes at 2 °C·min^{-1}

6.2.1.1. *Pure cocoa butter and shea butter stearin*

The thermal and polymorphic behavior of CB/ShS mixtures may be better understood by considering the properties displayed by the pure fats under the same experimental conditions. Figure 6.1 shows the DSC curve and related XRD patterns acquired during the thermal processing of CB and ShS at 2 °C·min^{-1}. Unless otherwise indicated, the DSC events in this chapter will be defined by their characteristic T_{top}.

Generally, the nomenclature I-VI is used to denote the polymorphic forms of CB. However, we will use the equivalent names with Greek letters to maintain the same naming system as in pure ShS and the mixtures. On cooling pure CB, the first DSC peak detected at T_{onset} of 20.1 °C corresponded to the crystallization of α-2L. Accordingly, peaks at 4.9 and 0.42 nm grew in corresponding SAXD and WAXD patterns at 16 °C. At decreasing temperature, SAXD peaks at 5.4 and 2.7 nm (002 reflection), and the WAXD peak at 0.38 nm, confirmed the second DSC event as the crystallization of sub-α-2L. The peak at 2.7 nm weakened as the temperature approached -30 °C, whereas that at 5.4 nm was shifted until becoming indistinguishable from that at 4.6 nm.

During reheating at 2 °C·min^{-1}, the sub-α peak at 2.7 nm was no longer detected at 0 °C. Assigning specific melting and transition temperatures to the polymorphic forms of CB becomes a difficult task, since these may vary according to the experimental techniques employed, the processing conditions, and even the origin of the lipid sample (Rigolle et al., 2016). As a result, some discrepancies are found in the scientific literature, concretely regarding the melting point of sub-α. Many studies suggested values at around 15-18 °C (Chapman et al., 1971; Huyghebaert & Hendrickx, 1971; Merken & Vaeck, 1980; Wille & Lutton, 1966) but lower temperatures have been reported. van Malssen et al. (1999) estimated a melting range from -8 to 5 °C for sub-α isothermally crystallized at -10 °C and reheated at 2 °C·min^{-1}. However, recent SR-XRD data showed that sub-α formed on cooling at 2 °C·min^{-1}, melted at 13.3 °C when reheated at the same rate (Bayés-García et al., 2019). The endothermic phenomena shown by the heating thermogram in our study showed a T_{onset} of 13.6 °C. Thus, we assumed that the first peak was related to the sub-α melting. However, the behavior of the SAXD peak at 2.7 nm suggested that part of sub-α vanished several degrees below.

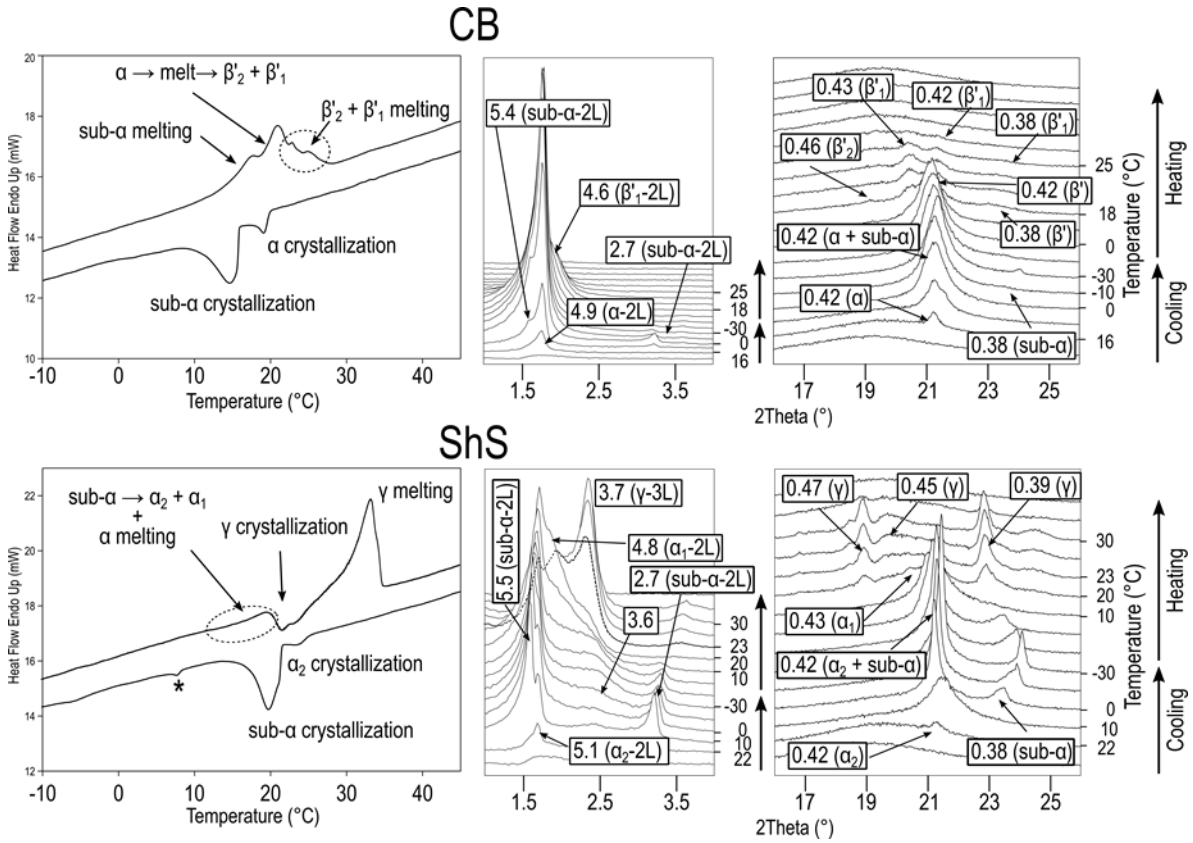

Figure 6.1. DSC thermograms (left) and laboratory-scale XRD patterns (right) obtained for pure CB and ShS cooled and subsequently heated at 2 °C·min^{-1}.

α melted shortly after sub-α (DSC peak at 20.9 °C), which prevented the identification of an intermediate transition by DSC or XRD. What is clear from WAXD peaks detected at 0.43, 0.42, and 0.38 nm when reaching 18 °C is that β' formed next. The peak at 0.46 nm allowed identifying β'$_2$-2L (with long spacing value similar to α-2L), whereas the SAXD peak at 4.6 nm indicated the presence of β'$_1$-2L. Consequently, the last endothermic peaks observed at 22.9 and 24.9 °C by DSC were due to the melting of these forms. The overall transformation shown by CB egreed with that observed in previous studies for CB subjected to similar cooling and heating treatments (Bayés-García et al., 2019, 2022). However, it should be noted that, in contrast with our results, no β'$_1$-2L was observed in these studies after the α-2L transformation. The divergent behavior could be due to the different polymorphic characterization techniques used in the present (laboratory-scale XRD) and in previous work (SR-XRD).

From the resembling polymorphism of POS, SOS, and POP, one might expect similarities regarding the crystallization and transformation behavior of CB and ShS.

As in pure CB, the two main DSC events detected in ShS during cooling (T_{onset} of 25.0 and 21.4 °C) were due to the crystallization of α-2L and sub-α-2L. In XRD patterns at 22 °C, the first one was deduced from the single WAXD peak detected at 0.42 nm (corresponding SAXD reflection at 5.1 nm). The next occurrence of sub-α strengthened the peak at 0.42 nm and caused the growth of one at 0.38 nm in WAXD patterns at 10 °C. In parallel, new SAXD peaks developed at 5.5 and 2.7 nm. No specific WAXD peaks were linked to the broad SAXD reflection detected at around 3.6 nm, which increased in intensity towards -30 °C. Its presence could relate to less ordered crystalline regions formed in lamellar structures due to a difficult packing of saturated and unsaturated fatty acid chains. This behavior was observed during the isothermal crystallization of diverse pure unsaturated TAGs, including SOS (Mykhaylyk et al., 2007; Mykhaylyk & Martin, 2009). The nature of the third DSC peak at around 8 °C (indicated by *) was not clarified either by XRD.

During the next reheating, the first polymorphic changes were detected when reaching 10 °C. The SAXD peak at 2.7 nm decreased in intensity, whereas that at 5.1 nm strengthened and a new one emerged at 4.8 nm. In addition, new reflections became visible at 0.47, 0.45, 0.43, and 0.39 nm in WAXD patterns at 20 °C. Peaks at 0.47, 0.45, and 0.39 nm were associated with the γ form, which at increasing temperature showed a long spacing value of 3.7 nm (002 reflection). The peak at 0.43 nm was related to the SAXD peak at 4.8 nm. This long spacing value agrees with that of α-2L (SOS) determined by Sato et al. (1989). From this, we assumed that two α-2L forms may form in ShS. The same occurs in pure SOS (Baker et al., 2014a; Ueno et al., 1997). For clarity, we will refer to them as α_2 (001 reflection at 5.1 nm) and α_1 (4.8 nm).

Based on the above XRD data, the first endothermic peak detected by DSC at T_{onset} of 16.1 °C was assigned to the sub-α-2L → α_2-2L + α_1-2L transition and the next melting of α forms. However, the behavior of SAXD peaks of α_2-2L and α_1-2L at 10 °C suggested that the transformation of sub-α-2L probably started several degrees below. The next exothermic and endothermic events (peaks at 21.4 and 33.1 °C) corresponded to the crystallization and final melting of γ-3L form.

6.2.1.2. *Blends of cocoa butter and shea butter stearin*

Before going into detail about the polymorphic properties, it is worth making a brief analysis of the thermal behavior displayed by CB/ShS blends when subjected to the same thermal treatments as pure CB and ShS. The DSC thermograms obtained for CB/ShS blends including 95, 80, 70, 50, and 30% of CB content when cooled and reheated at 2 °C·min^{-1} are depicted in Figure 6.2.

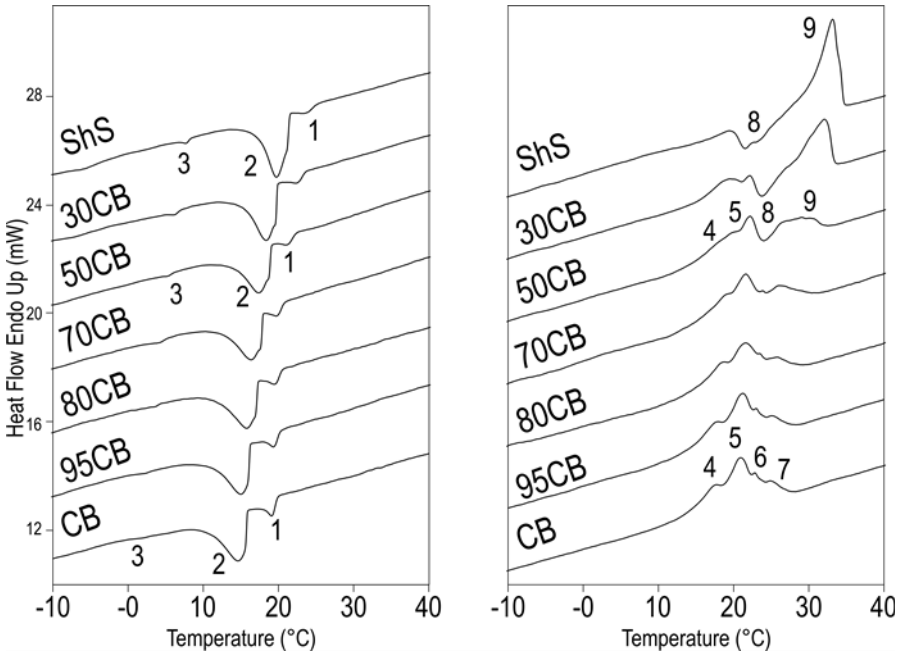

Figure 6.2. DSC cooling (left) and heating thermograms (right) of CB, ShS, and their blends when cooled and subsequently heated at 2 °C·min^{-1}.

The cooling curves of the blends resembled those of the pure fats. Two main crystallization events followed by a third subtle one occurred from 25 to 0 °C. These are denoted as peaks 1, 2, and 3 in the figure. Since almost the whole crystallization process took place before the third event, the onset and end crystallization temperatures of the blends shown in Table 6.3 are based on peaks 1 and 2. The one-way ANOVA showed no significant differences in the behavior of CB and 95CB, 95CB and 80CB, or 80CB and 70CB. However, the initiation and completion of the crystallization shifted notably to higher temperatures as the ShS content increased.

During reheating, the DSC profiles of the blends showed a combination of the thermal signals of the pure fats. Those detected in CB between 15 and 30 °C (denoted as peaks 4, 5, 6, and 7 in Figure 6.2) also occurred in mixtures from 95CB to 70CB. Then, a broadening of the thermal

signals in the 50CB and 30CB mixtures enabled identifying the typical recrystallization and final melting peaks of ShS (peaks 8 and 9). Again, the onset and end temperatures of the whole set of DSC peaks in the blends were higher when increasing the amount of ShS (see Table 6.3).

Table 6.3. Onset and end temperatures (°C) of the global phenomena observed by DSC when CB, ShS, and their blends were cooled and subsequently heated at 2 °C·min^{-1}.

	Cooling		Heating	
	T_{onset}	T_{end}	T_{onset}	T_{end}
CB	20.1 ± 0.6^{a}	9.6 ± 0.6^{a}	13.6 ± 0.3^{a}	27.4 ± 0.2^{a}
95CB	20.3 ± 0.4^{a,b}	10.3 ± 0.4^{a,b}	13.5 ± 0.5^{a}	27.7 ± 0.4^{a}
80CB	20.5 ± 0.4^{b,c}	10.8 ± 0.4^{b,c}	14.5 ± 0.6^{b,c}	28.6 ± 0.5^{b}
70CB	20.8 ± 0.3^{c}	11.7 ± 0.6^{c}	14.9 ± 0.7^{c,d}	29.5 ± 0.6^{c}
50CB	22.4 ± 0.4^{d}	13.3 ± 0.4^{d}	14.1 ± 0.23^{b}	32.2 ± 0.3^{d}
30CB	23.7 ± 0.3^{e}	14.8 ± 0.5^{e}	15.3 ± 0.5^{d}	33.5 ± 0.3^{e}
ShS	25.0 ± 0.6^{f}	16.7 ± 0.4^{f}	16.1 ±0.4^{e}	34.7 ± 0.9^{f}

The same letter within a column indicates that the values are not significantly different ($p > 0.05$, one-way ANOVA, Tukey test).

The similar thermal properties of CB and the 95CB blend are in line with the possibility of including up to 5% ShS content in chocolate without changing the overall properties. Since the behavior of 80CB and 70CB mixtures became also highly similar, we limited the X-ray diffraction study to the blends containing 70% CB content and below.

Figure 6.3 shows the XRD patterns and related DSC data obtained for 70CB, 50CB, and 30CB blends when cooled from the melt to -30 °C and reheated at 2 °C·min^{-1}. Detailed DSC data corresponding to the different polymorphic events detected is gathered in Table 6.4.

In the three blends, XRD data confirmed that the crystallization behavior on cooling was also governed by the initial crystallization of α-2L and the next formation of sub-α-2L.

The DSC curve of the 70CB mixture when reheating at 2 °C·min^{-1} resembled that of pure CB. In consonance, the first two endothermic events (T_{top} of 18.8 and 21.5 °C) were due to sub-α-2L and α-2L melting. The stronger SAXD peak at 5.0 nm detected between 10 and 20 °C was indicative of the sub-α to α transition. At 20-23 °C, typical β' WAXD patterns developed (peaks at 0.43, 0.42, and 0.39 nm). Simultaneously, SAXD peaks at 4.7 and 3.5 nm (002 reflection) grew at the expense of that at 5.0 nm. Therefore, β'-2L and β'-3L crystals formed concurrently from the α melt. Since no β' triple is known for CB, this β'-3L was likely originated from the excess in SOS caused by the addition of ShS. It cannot be ruled out some contribution of POS, for which two distinct β' forms with double and triple structures are known. In line with this, previous

work indicated that β'-3L solid solutions may form in SOS/POS mixtures with at least 30-40% SOS content (Rousset et al., 1998). In the heating thermogram, two DSC events at 23.8 and 26.0 °C indicated the final melting of β'-2L and β'-3L.

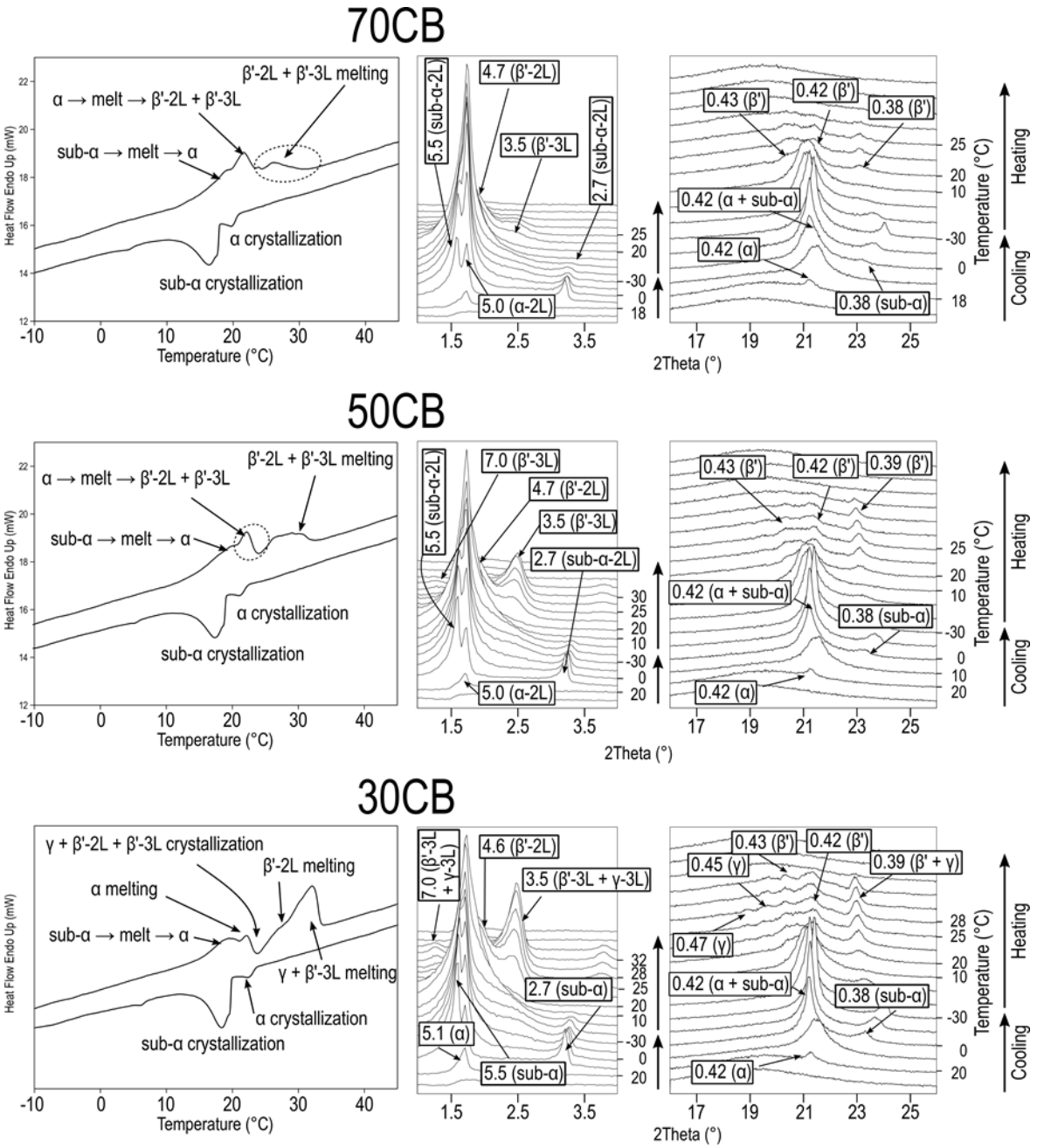

Figure 6.3. DSC thermograms (left) and laboratory-scale XRD patterns (right) obtained for 70CB, 50CB, and 30CB mixtures cooled and subsequently heated at 2 °C·min^{-1}.

Table 6.4. Temperatures (°C) determined by DSC for the main polymorphic events occurring in CB, ShS, and their blends when cooled and subsequently heated at 2 °C·min^{-1}.

Sample		Cooling at 2 °C·min^{-1}		Heating at 2 °C·min^{-1}				
CB		*a-2L (c)*	*sub-a-2L (c)*	*sub-a-2L (m)*	*a-2L → m → β′$_2$-2L + β′$_1$-2L*	*β′$_2$-2L + β′$_1$-2L (m)*		
	T_{onset}	20.1 ± 0.6	15.9 ± 0.4	13.6 ± 0.3	-	-		
	T_{top}	19.3 ± 0.5	14.8 ± 0.3	17.6 ± 0.3	20.9 ± 0.5	22.9 ± 0.3	24.9 ± 0.2	
	T_{end}	17.6 ± 0.6	9.6 ± 0.6	-	-	27.4 ± 0.2		
70CB		*a-2L (c)*	*sub-a-2L (c)*	*sub-a-2L → m → a-2L*	*a-2L → m → β′-2L + β′-3L*	*β′-2L + β′-3L (m)*		
	T_{onset}	20.8 ± 0.3	18.0 ± 0.3	14.9 ± 0.7	-	-		
	T_{top}	19.8 ± 0.3	16.4 ± 0.3	18.8 ± 0.3	21.5 ± 0.3	23.8 ± 0.2	26.0 ± 0.3	
	T_{end}	17.2 ± 0.5	11.7 ± 0.6	-	-	29.5 ± 0.6		
50CB		*a-2L (c)*	*sub-a-2L (c)*	*sub-a-2L → m → a-2L*	*a-2L → m → β′-2L + β′-3L*	*β′-2L + β′-3L (m)*		
	T_{onset}	22.4 ± 0.4	19.1 ± 0.3	14.1 ± 0.2	-	-		
	T_{top}	21.4 ± 0.3	17.5 ± 0.3	18.2 ± 0.9	19.8 ± 1.0	-		
	T_{end}	18.5 ± 0.5	13.3 ± 0.5	-	-	32.2 ± 0.3		
30CB		*a-2L (c)*	*sub-a-2L (c)*	*sub-a-2L → m → a-2L*	*a-2L (m)*	*γ-3L + β′-2L + β′-3L (c)*	*β′-2L (m)*	*γ-3L + β′-3L (m)*
	T_{onset}	23.7 ± 0.3	19.9 ± 0.3	15.3 ± 0.6	-	-	-	-
	T_{top}	22.6 ± 0.5	18.5 ± 0.3	19.2 ± 0.6	22.2 ± 0.3	23.9 ± 0.6	26.8 ± 0.4	32.1 ± 0.4
	T_{end}	20.2 ± 0.6	14.8 ± 0.6	-	-	-	-	33.5 ± 0.4
ShS		*a$_2$-2L (c)*	*sub-a-2L (c)*	*sub-a-2L → a$_2$-2L + a$_1$-2L/ a$_2$-2L + a$_1$-2L (m)*		*γ-3L (c)*	*γ-3L (m)*	
	T_{onset}	25.0 ± 0.6	21.4 ± 0.4	16.1 ± 0.4		-	29.4 ± 0.5	
	T_{top}	23.6 ± 0.3	19.6 ± 0.6	19.5 ± 0.3		21.4 ± 0.3	33.1 ± 0.4	
	T_{end}	21.0 ± 0.4	16.7 ± 0.7	-		-	34.7 ± 0.9	

(-): the peak temperature could not be accurately estimated. (c): crystallization; (m): melting.

A similar sequence of polymorphic events occurred when the 50CB mixture was heated. The sub-α-2L → α-2L transition was succeeded by the melting of α-2L (DSC endothermic peak at 19.8 °C) and next crystallization of β'-2L and β'-3L. In agreement with the increased SOS content in the blend, SAXD patterns indicated a higher β'-3L/β'-2L ratio at this composition. Moreover, the 001 reflection of β'-3L at 7.0 nm was also discerned at this composition. In turn, this led to the unsharpened final melting peak detected by DSC in the range from 24 to 32 °C. Since the SAXD reflection at 4.7 nm was practically gone at 30 °C, β'-2L must have melted first. This would agree with the assumption that β'-2L has a similar nature to β' of CB (containing POS, SOS, and POP) and β'-3L is richer in TAGs containing stearic acid.

The main difference shown by the 30CB mixture with respect to the previous samples was the more complex α transition to more stable polymorphs during heating. WAXD patterns at 25 °C showed that β'-2L and β'-3L reflections (0.43, 0.42, and 0.39 nm) were accompanied by other at 0.47 and 0.45 nm. Thus, some γ may also have formed from the α melt. γ form is characterized by strong sharp WAXD reflections at 0.47 and 0.39 nm and a less intense flatter one at 0.44-0.45 nm (Sato et al., 1989). In this case, the narrow difference in intensity of peaks at 0.47 and 0.45 nm was probably influenced by the major contribution of β' reflections to XRD patterns. Such behavior was also observed in pure SOS (Ueno et al., 1997). The γ-3L form detected in ShS subjected to the same thermal conditions showed a long spacing value of 3.7 nm (002 reflection). In the 30CB blend, the SAXD reflection of γ-3L was masked by that of β'-3L at 3.5 nm.

In the heating thermogram, the β'-3L, β'-2L, and γ-3L crystallization peak at 23.9 °C was followed by two overlapped endothermic phenomena between 27 to 33 °C. The SAXD reflection at 4.6 nm was considerably reduced before reaching 30 °C, so we assumed that β'-2L melted first (DSC peak at 26.8 °C) and γ-3L and β'-3L followed (peak at 32.1 °C).

6.2.2. Cooling and reheating processes at 0.5 °C·min^{-1}

6.2.2.1. *Pure cocoa butter and shea butter stearin*

The polymorphic behavior observed in pure CB and ShS when cooled and heated at a low rate of 0.5 °C·min^{-1} is shown in Figure 6.4. In addition, DSC temperatures corresponding to the main polymorphic events identified are gathered in Table 6.5.

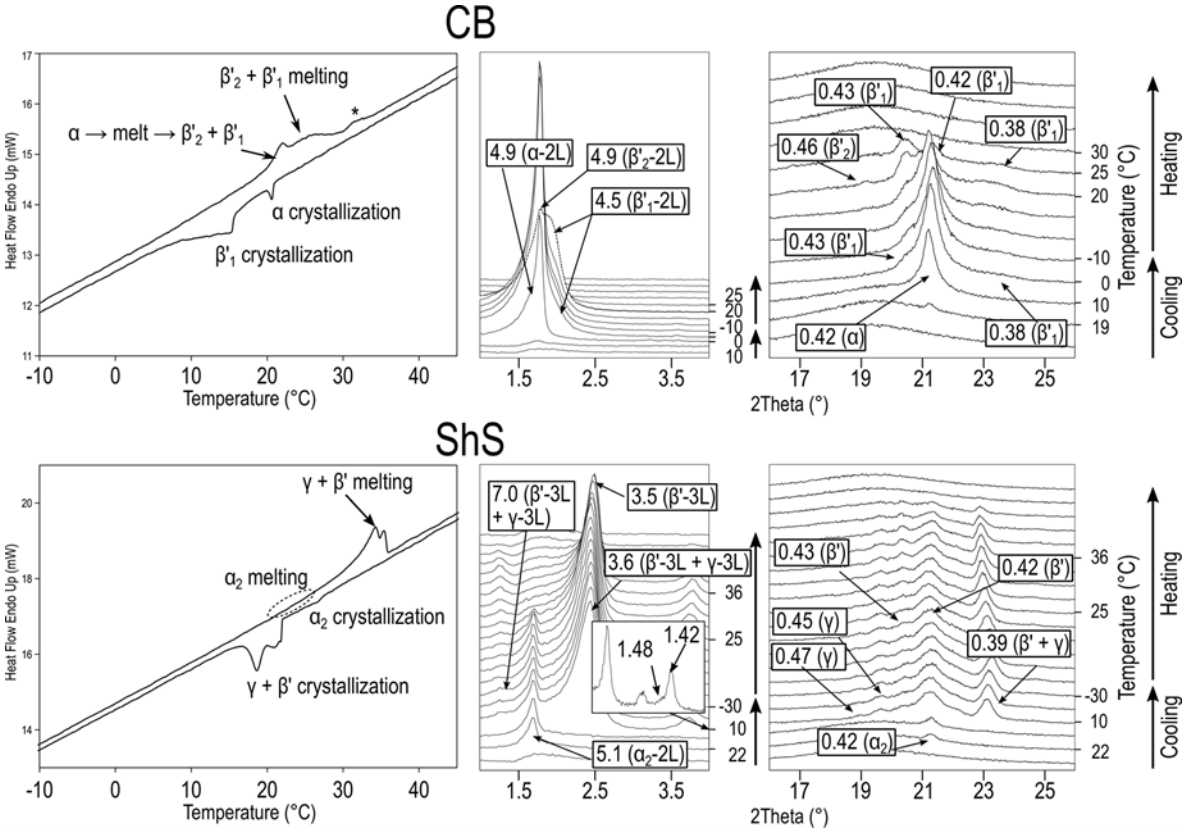

Figure 6.4. DSC thermograms (left) and laboratory-scale XRD patterns (right) obtained for pure CB and ShS cooled and subsequently heated at 0.5 °C·min^{-1}.

As in CB cooled at 2 °C·min^{-1}, two main exothermic events occurred when cooling CB at 0.5 °C·min^{-1}. However, these started at higher temperatures (T_{onset} of 21.2 and 16.1 °C) and led to the formation of more stable forms. No sub-α-2L occurred and some β'$_1$-2L was formed instead after the crystallization of α-2L.

Changes in XRD patterns during slow reheating were first noticed when reaching 20 °C. The peak at 4.5 nm grew at the expense of that at 4.9 nm in the SAXD region and those at 0.43 and 0.38 nm strengthened in the WAXD region. In addition, one showed up at 0.46 nm. Thus, the

sharp peak first seen by DSC at T_{onset} of 20.8 °C must have corresponded to the melt-mediated α-2L → β'_2-2L + β'_1-2L transformation. The overlapped round-shaped signal ending at around 29 °C was due to the next melting of these forms. This is supported by the vanishing of characteristic WAXD peaks at 30 °C. Only liquid was detected above this temperature by XRD, but a DSC event was observed at 32.5 °C (indicated by *). By considering the melting properties of β' forms of CB (see Table 6.2), this could be due to the melting of a more stable form. One may speculate that the slow heating may have provided enough time for the crystallization of some β crystals from the β' melt.

The behavior of ShS was also governed by more stable polymorphic forms when reducing the rate of the thermal treatments from 2 to 0.5 °C·min^{-1}.

On cooling, α_2-2L formed first (DSC peak T_{onset} of 27.5 °C) and β'-3L and γ-3L followed (event ranging from 22 to 18 °C). β'-3L and γ-3L were not distinguished by the main SAXD peaks detected (001 and 002 reflections at 7.0 and 3.6 nm, respectively). Despite this, 005 reflections of γ-3L (1.48 nm) and β'-3L (1.42 nm) evidenced that the second predominated in the crystallized mass. This agrees with the weak γ reflections at 0.47 and 0.45 nm in WAXD patterns. Based on the intensity of XRD peaks in CB and ShS, one may conclude that the formation of β' was favored in ShS. This may relate to a more homogeneous TAG fraction in ShS (containing mainly SOS) than in CB (mixture of POS, POS, and POP). Previous work showed that POP packs more easily in α-2L when crystallizing from the melt than SOS (Koyano et al., 1989). This was explained by the less disturbing effect of shorter saturated fatty acids on interlamellar regions when packing in double chain-length structures. It should be noted that interactions among different TAG species in CB may also hinder to a higher extent their arrangement in densely packed polymorphic forms.

Regarding the reheating process, no DSC signals were seen before the double endothermic event occurring between 32-36 °C. However, α_2-2L was no longer detected in SAXD patterns at 25 °C. Probably, α_2-2L melted near this temperature but the low amount formed upon cooling led to a low energy melting process during reheating. The detrimental effect of low cooling and heating rates on the signal-to-noise ratio of DSC thermal signals also hindered its detection. Even though the vanishing of α_2-2L could have led to the occurrence of more stable forms, this was not confirmed by DSC or XRD. On further heating, the consecutive melting of γ-3L and β'-3L resulted in the two overlapped DSC peaks finally detected at 34.5 and 35.8 °C.

Table 6.5. Temperatures (°C) determined by DSC for the main polymorphic events occurring in CB, ShS, and their blends when cooled and subsequently heated at 0.5 °C·min^{-1}.

Sample		Cooling at 0.5 °C·min^{-1}			Heating at 0.5 °C·min^{-1}			
CB		*a-2L (c)*	*β′$_1$-2L (c)*		*a-2L → m → β′$_2$-2L + β′$_1$-2L*	*β′$_2$-2L + β′$_1$-2L (m)*		
	T_{onset}	21.2 ± 1.0	16.1 ± 1.0		15.4 ± 0.7	-		
	T_{top}	21.0 ± 0.9	15.5 ± 0.8		17.8 ± 0.3	25.5 ± 0.7		
	T_{end}	20.3 ± 0.7	9.8 ± 0.8		-	-		
70CB		*a-2L (c)*	*β′-2L + sub-a-2L (c)*		*sub-a-2L (m)*	*a-2L → m → β′-2L + β′-3L*	*β′-2L+ β′-3L (m)*	
	T_{onset}	22.7 ± 1.2	18.5 ± 1.2			-	22.1 ± 0.9	
	T_{top}	21.9 ± 0.8	17.4 ± 0.7		-	18.0 ± 0.6	-	
	T_{end}	20.8 ± 0.5	13.2 ± 0.9			-	32.9 ± 0.9	
50CB		*a-2L (c)*	*β′-3L + β′-2L + sub-a-2L (c)*		*a-2L → m → β′-2L + β′-3L*	*β′-2L (m)*	*β′-3L (m)*	
	T_{onset}	23.8 ± 0.6	19.2 ± 0.4		-	21.9 ± 0.6	27.8 ± 0.4	
	T_{top}	23.1 ± 0.4	18.2 ± 0.4		18.2 ± 0.8	25.7 ± 0.6	31.8 ± 0.3	
	T_{end}	21.5 ± 0.8	14.2 ± 0.8		-	-	32.9 ± 0.4	
30CB		*a-2L (c)*	*β′-3L + β′-2L + sub-a-2L (c)*		*a-2L → m → γ-3L + β′-2L + β′-3L*	*β′-2L (m)*	*γ-3L + β′-3L (m)*	
	T_{onset}	25.0 ± 0.3	20.0 ± 0.2		-	22.4 ± 0.6	29.4 ± 0.4	
	T_{top}	24.4 ± 0.5	19.0 ± 0.3		17.8 ± 0.3	25.5 ± 0.7	33.1 ± 0.3	
	T_{end}	23.1 ± 0.7	14.4 ± 0.4		-	-	33.9 ± 0.5	
ShS		*a$_2$-2L (c)*	*γ-3L + β′-3L (c)*		*a$_2$-2L (m)*	*γ-3L (m)*	*β′-3L (m)*	
	T_{onset}	27.5 ± 1.08	22.2 ± 0.6	20.5 ± 0.7		31.6 ± 0.6	-	
	T_{top}	26.6 ± 1.1	22.1 ± 0.8	18.9 ± 0.7	-	34.5 ± 0.9	35.8 ± 0.9	
	T_{end}	25.9 ± 1.1	-	17.6 ± 0.8		-	36.2 ± 1.0	

(-): the temperature could not be accurately estimated, or no thermal signal was detected for the polymorphic event. (c): crystallization; (m): melting.

6.2.2.2. *Blends of cocoa butter and shea butter stearin*

Figure 6.5 shows the DSC and XRD data of 70CB, 50CB, and 30CB mixtures cooled from the melt to -30 °C and reheated at 0.5 °C·min^{-1}. The peak parameters of some DSC events were difficult to estimate due to the weakness of the signals obtained (see detailed DSC data on the mixtures in Table 6.5). However, as in the thermal treatments at 2 °C·min^{-1}, these tended to shift to higher temperatures as the ShS content increased.

When cooling the 70CB mixture, the occurrence of α-2L (DSC peak at T_{onset} of 22.7 °C) was followed by the formation of β'-2L and some sub-α-2L form (T_{onset}=18.5 °C). The almost identical cooling curve of the 50CB mixture (peaks at T_{onset} of 23.8 and 19.2 °C) corresponded to a similar phase development during the two-step crystallization process. However, in this case, the β' fraction was related to a mixture of β'-2L and β'-3L crystals (peaks at 4.5 and 3.6 nm in SAXD data at 0 °C). In line with the results obtained for pure CB and ShS, SAXD reflections indicated that the amount of β' formed with respect to α increased from the 70CB to the 50CB mixture. In the 30CB blend, concurrent sub-α-2L, α-2L, β'-2L, and β'-3L forms were also present once the crystallization was completed.

During reheating at 0.5 °C·min^{-1}, the melting of sub-α-2L was not detected by DSC at any composition. However, in the 70CB blend, its reflection at 2.7 nm faded from SAXD patterns between 0 and 10 °C. In 50CB and 30CB mixtures, the same was not present anymore before the heating treatment started. In addition, the evolution of sub-α-2L could not be monitored by its 001 reflection at 5.5 nm since it was masked by that of α at 5.0-5.1 nm. Due to this, we cannot provide a specific melting range for sub-α-2L at this low heating rate. Based on the available data, the melting of this form probably occurred at a temperature far below the melting of α.

DSC endothermic events corresponding to the melting of α-2L were seen at all compositions but their great asymmetry prevented the determination of accurate onset temperature values. In the 70CB mixture, the α-2L melting at 18.0 °C was followed by the crystallization of β'-2L (stronger reflections at 4.6, 0.43, and 0.38 nm in XRD patterns at 20 °C) and a reduced amount of β'-3L (weak SAXD peak at 3.5 nm). The melting of the newly formed β' crystals took place during the broad DSC event occurring between 22 to 33 °C.

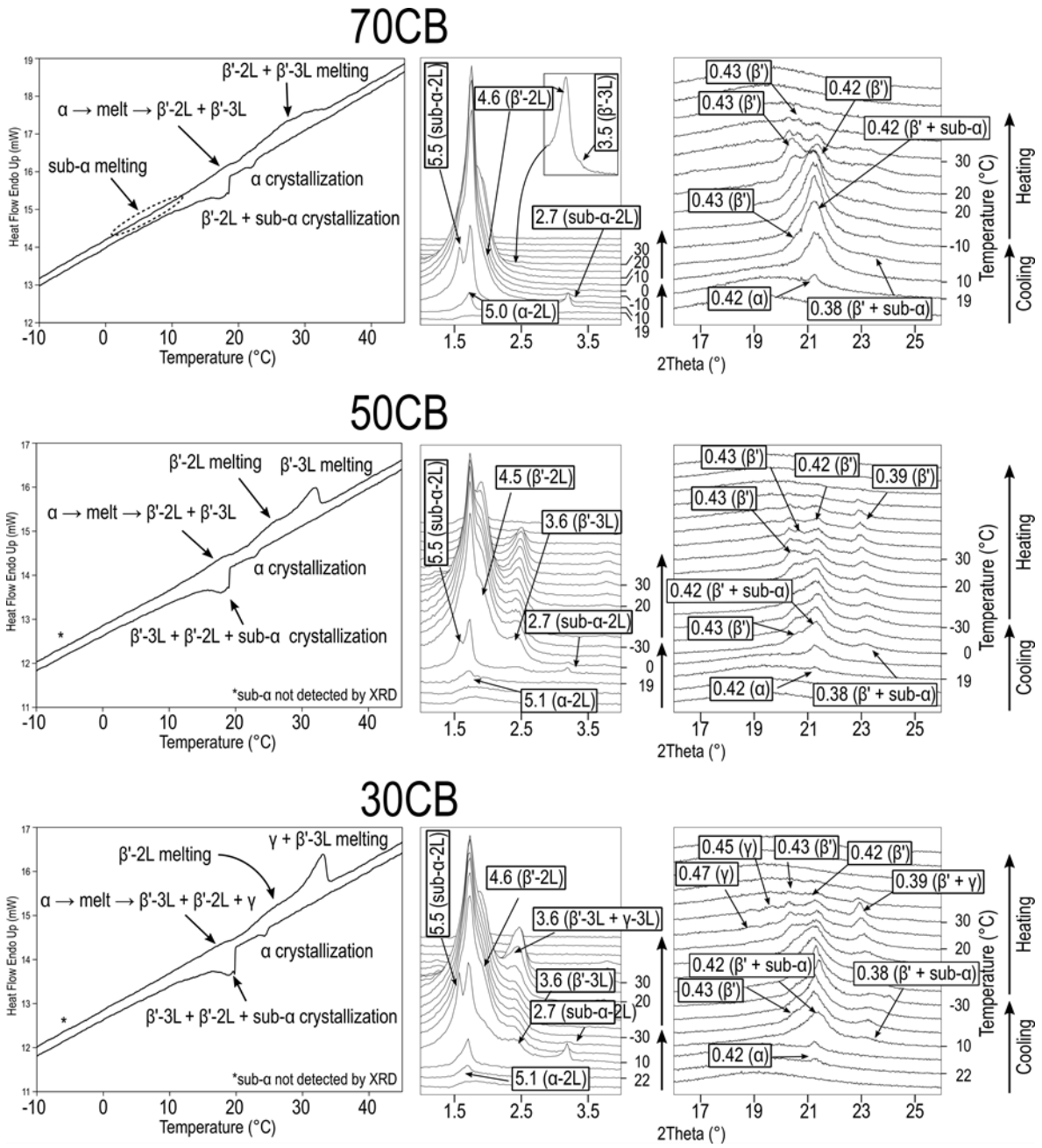

Figure 6.5. DSC thermograms (left) and laboratory-scale XRD patterns (right) obtained for 70CB, 50CB, and 30CB mixtures cooled and subsequently heated at 0.5 °C·min^{-1}.

The melt-mediated transformation of α-2L into β'-2 and β'-3L was also observed in the 50CB mixture. In addition, the more balanced ratio of these forms at this composition allowed a better separation of their respective melting phenomena in the heating thermogram (DSC peaks at 25.7 and 31.8 °C). The corresponding SAXD data showed that, soon after surpassing 20 °C, the

reflection at 4.6 nm (β'-2L) was diminished. The one at 3.6 nm (β'-3L) remained unaltered on further heating until all reflections disappeared from XRD patterns.

In the 30CB mixture, the sharper increase in intensity of the SAXD reflection at 3.6 nm above 20 °C indicated a higher β'-3L crystallization ratio from the α melt. However, WAXD peaks at 0.47 and 0.45 nm confirmed that some γ-3L was formed along with the different β' forms. This form must have contributed to some extent to the strength of the SAXD reflection. The melting behavior succeeding the occurrence of these forms resembled that of the 50CB mixture. This means that β'-2L melted first (DSC peak at 25.5 °C) and γ + β'-3L followed (peak at 33.1 °C). A very low γ-3L/β'-3L ratio may be the reason why, in contrast to pure ShS, the melting of these forms did not result in distinct DSC signals.

Regarding the α-2L → β'-2L + β'-3L transformation in the blends, we may underscore the differences observed between heating treatments at 2 and 0.5 °C·min^{-1}. These were concluded from the intensity of β'-2L and β'-3L reflections in the corresponding SAXD patterns (see Figures 6.3 and 6.5). The presence of CB in the blends favored the α-2L to β'-3L transition with respect to pure ShS. However, the formation of β'-3L was reduced and that of β'-2L was favored at increasing CB content. This stresses again that β'-3L must be primarily formed by SOS molecules. Moreover, independently of the composition, the amount of β'-3L with respect to β'-2L after the α-2L melting was always greater in the samples heated at 2 °C·min^{-1}. This, even though at the beginning of reheating processes at 0.5 °C·min^{-1}, some β'-3L crystals were already present from the previous cooling treatment. We concluded that the lower the heating rate, the more reduced the α-2L → β'-3L transformation ratio. This may be explained by considering the previous assumption that β'-3L is primarily SOS and β'-2L a solid solution of POS, SOS, and POP. After the melting of α, affinitive interactions among the components favor the formation of a single β'-2L phase. However, the higher the ShS content in the blends, the more time may be needed for the excess of SOS molecules to accommodate in the crystal structure. In turn, a higher heating rate will provide less time for this process to be completed and promote alternative polymorphic transformation pathways (Bayés-García et al., 2013b; Sato et al., 2013). This would result in the higher SOS-rich fraction crystallized separately from β'-2L when heating at 2 °C·min^{-1}.

6.2.3. Summary of the polymorphic behavior under kinetic conditions

The crystallization and transformation pathways observed in CB, ShS, and their blends at different cooling and heating rates are summarized in Figure 6.6.

More stable polymorphs crystallized at all compositions when reducing the cooling rate from 2 to 0.5 °C·min^{-1}. In addition, this differed among mixtures depending on their proximity to pure CB and ShS compositions. Sub-α-2L and α-2L were present in all the samples once the treatment at 2 °C·min^{-1} was completed. By lowering the rate, the formation of sub-α-2L was prevented in the pure fats and, that of β', promoted at all compositions. β' showed double chain-length structure when CB dominated the blend, but an excess of SOS favored the additional presence of β'-3L at an ShS content of 50% and above. Likewise, the crystallization temperature was raised in the samples as the amount of ShS increased.

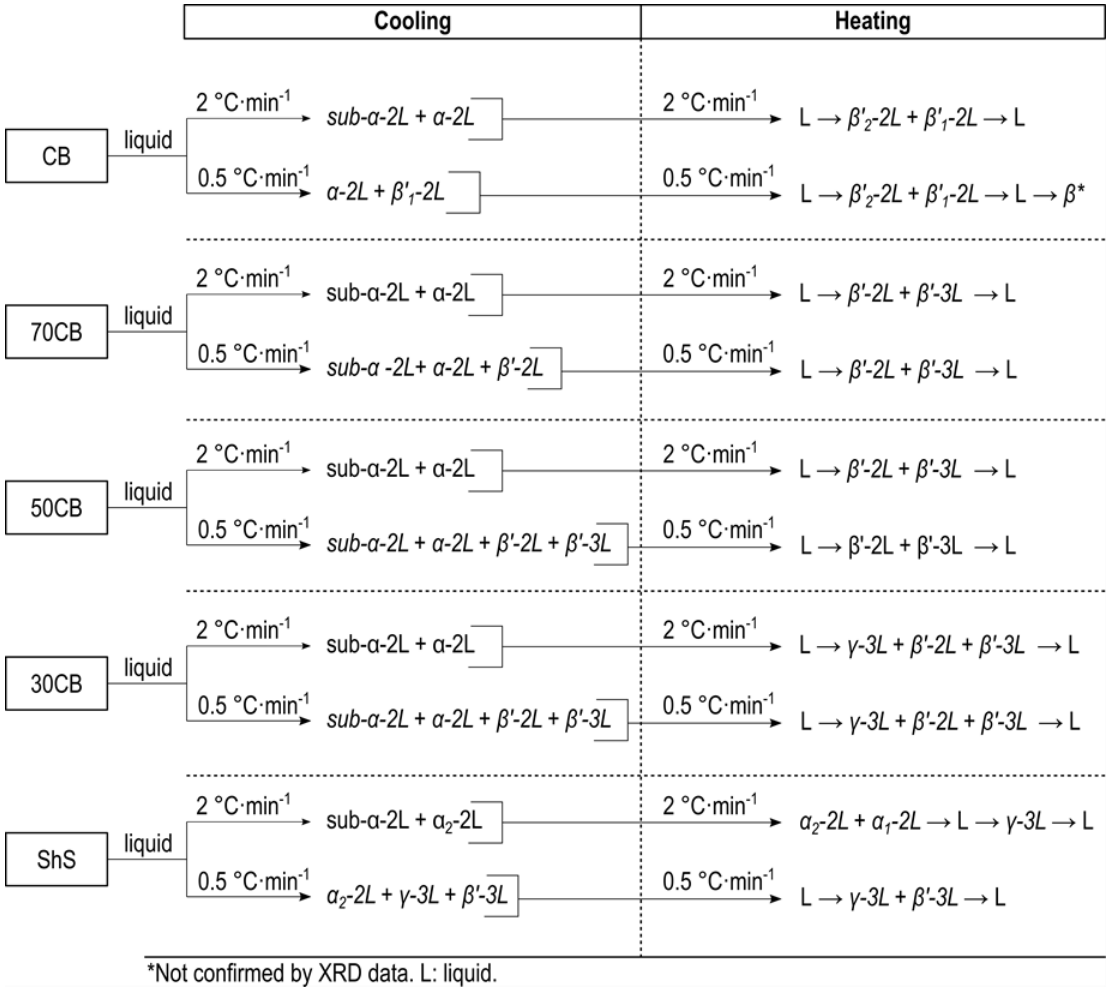

Figure 6.6. Scheme of polymorphic pathways of CB, ShS, and their blends exposed to different thermal treatments.

The polymorphic behavior during heating processes also differed among compositions. However, the differences between samples with the same CB/ShS ratio heated at different rates laid in the transformation ratio rather than in the polymorphic sequence.

No matter the heating rate applied, α-2L transformed via melt-mediation into β'_2-2L and β'_1-2L in pure CB. In the blends, β'-2L and β'-3L were obtained from the α form. Moreover, SAXD data on mixtures heated at 2 and 0.5 °C·min^{-1} revealed that the formation of a β'-2 solid solution of the main TAG was favored before β'-3L phases rich in SOS at the lowest rate. One may notice that also some γ-3L occurred in the 30CB blend, which was due to the low CB/ShS ratio. Moreover, in contrast to the blends, no β'-3L was formed from α-2L in pure ShS heated at 2 °C·min^{-1}. Therefore, the formation of β'-3L was favored over γ-3L in the presence of CB. Such behavior is explained by the increase in POS content and the inability of this TAG to pack in the γ form. Despite γ being characteristic of POP and SOS, mixing interactions of these TAGs and POS do not allow its occurrence in CB.

Even though not confirmed by XRD, the DSC data on pure CB heated at the lowest rate suggested that some β occurred before complete melting. In previous work, the occurrence of this form during heating treatments was only identified by SR-XRD when a very low cooling rate of 0.1 °C·min^{-1} was used (Bayés-García et al., 2019). This difficulty in obtaining β crystals is in line with the need to carry out tempering processes during chocolate production to favor the formation of the desired β_2-3L crystals of CB (Form V). No β crystals were identified for pure ShS or the blends either. Regarding the blends, five polymorphs occurred under the thermal conditions applied. These were, in order of increasing thermal stability, sub-α-2L, α-2L, β'-2L, γ-3L, and β'-3L. However, by considering the polymorphism of the pure component fats, an eventual occurrence of the β form should be expected. The next sections aim to go deeper into the thermal behavior of tempered CB/ShS blends, as well as into the development of the β polymorph during isothermal crystallization.

6.3. EVOLUTION OF THE SOLID FAT CONTENT AS A FUNCTION OF TEMPERATURE

The SFC of a lipid substance refers to its solid/liquid ratio at a specific temperature. It is a key parameter in the industry to assess the quality of lipid-based products, as it relates directly to textural and organoleptic properties. For example, the SFC defines the ease of packaging, spreadability, visual appearance, or oil loss in margarine (Laia et al., 2000; O'Brien, 2009; Silva et al., 2021). In chocolate, the fat phase must have a significant SFC at room conditions but undergo a quick melting near mouth temperature at 37 °C. This triggers the strong flavor release and soft mouth feeling (Hartel et al., 2018). However, the presence of fat crystals beyond this temperature turns its distinctive silky and creamy mouthfeel into an undesirable waxy sensation. This often occurs in low-quality chocolate flavored coatings (Nillson, 1986).

The SFC determination of CB, ShS, and their mixtures was performed according to the ISO 8292-1:2008 standard. Specifically, the samples were subjected to a β-stabilizing thermal protocol and then examined through the direct/parallel method by p-NMR. Further details on the experimental method were included in Chapter 2.

Variations in SFC detected in the temperature range from 10 to 45 °C, are plotted in Figure 6.7 (see detailed values in Table 6.6). The selection of measurement temperatures was based on normal procedures followed in the industry for CB and related lipid materials.

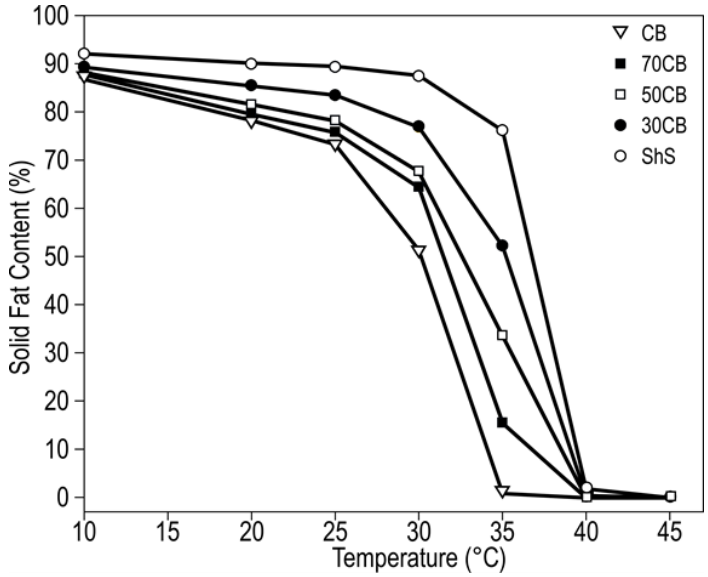

Figure 6.7. SFC profile of CB, ShS, and their blends.

Table 6.6. SFC values of CB, ShS, and their mixtures at selected temperatures.

	SFC (mean % ± standard deviation)				
T (°C)	CB	70CB	50CB	30CB	ShS*
10	86.9 ± 0.1	88.2 ± 0.4	88.4 ± 0.3	89.1 ± 0.0	91.9
20	78.3 ± 0.1	79.5 ± 0.1	81.5 ± 0.4	85.4 ± 0.1	89.9
25	73.2 ± 0.3	75.8 ± 0.1	78.2 ± 0.1	83.4 ± 0.1	89.3
30	51.5 ± 2.1	64.3 ± 0.5	67.6 ± 0.1	76.7 ± 0.7	87.4
35	0.9 ± 0.4	15.4 ± 0.3	33.6 ± 0.6	52.1 ± 0.6	76.0
40	-	-	-	0.7 ± 0.3	1.9
45	-	-	-	-	-

*The values correspond to a single measurement.

All compositions showed nearly 90% solid fat at 10 °C and almost flat melting curves towards 25 °C. This very gradual reduction of SFC at ambient conditions is consistent with the solid properties of CB and ShS. The relatively small differences detected among samples at this stage were magnified at higher temperatures.

The ~73% SFC of CB at 25 °C decreased to ~51% at 30 °C. However, the steepest region in the melting curve lied between 30 and 35 °C. The abrupt falling of SFC to less than 1% in this temperature range agrees with the characteristic sharp melting profile of chocolate. Pure ShS showed a similar phenomenon with onset and end shifted to higher temperatures. The SFC barely varied before reaching 35 °C (~76%) and almost the entire sample melted between this temperature and 40 °C. At this point, near 2% of the fat phase remained in the solid-state.

As could be expected from the above, increasing the amount of ShS in the mixtures led to a greater solid content independently of the measurement temperature. It is worth noting the higher SFC of the mixtures (above 10%) with respect to CB at 30 °C. This was indicative of improved heat-resistant properties, which is an attribute desired in chocolates intended for commercialization in warm tropical and subtropical regions (Suri & Basu, 2021). The melting behavior of nearly the whole fat phase at increasing temperature relied on the CB/ShS ratio. Thus, the steepness in the melting curve of the 70CB mixture at 30-35 °C resembled that of CB. In turn, the highest melting rate of the 30CB blend occurred at the same temperature range than ShS. A less pronounced melting process from 30 to 40 °C was found at an equal CB/ShS ratio.

In summary, the SFC increased, and the melting range shifted towards higher temperatures at increasing ShS content. Such behavior could come with an increase in the hardness of the blends. From this, it is evident that the CB/ShS ratio should be tailored in formulations according to the functional properties desired in end products. For instance, compositions with

around 30% or less ShS would be the most preferred choice for chocolate-like applications. In turn, increasing its content would be suitable for providing a wider melting range to confections.

The compatibility of fats can be more easily visualized by representing the SFC in a diagram of temperature vs. composition. Figure 6.8 shows the isosolid curves of CB/ShS mixtures obtained through the quadratic interpolation method described by Timms (1979) (see Chapter 2).

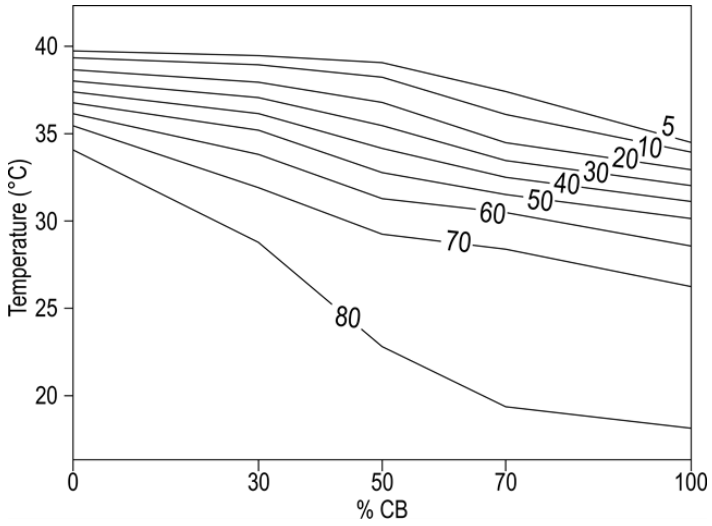

Figure 6.8. Isosolid diagram of CB/ShS mixtures. Numbers in lines indicate the percentage of solid fat.

Despite the fact that some softening due to dilution effects was observed, the isosolid points showed no evident eutectic interaction in the blends examined. It should be noted again that, after the stabilization procedure performed on CB/ShS mixtures before the SFC analysis, β crystals were expected to predominate at all compositions. That said, a high degree of compatibility would agree with the theoretical mixing behavior expected for the POS, SOS, and POP contained in CB (38-40%, 26-31%, and 18-19%, respectively) (Chaiseri & Dimick, 1989) and ShS (7-8%, 70-77%, and ≤1%, respectively) (Gunstone, 2006; Ray et al., 2013; Talbot, 2012).

Thus, complete miscibility was found for POS and SOS in β_2 (Rousset et al., 1998). For mixtures of POS and POP, crystallized from acetone and aged for 6 months at 30 °C, Koyano et al. (1993) delimited a eutectic region in blends with 30 to 60% POS content. Eutectic β phases were also seen in SOS/POP mixtures including 55-80% SOS (Sasaki et al., 2012). The isosolid curves obtained for the ternary system POS/SOS/POP showed eutectic formation at an equivalent mass ratio of POS and POP, and SOS content below 10% (Smith et al., 2013). In

agreement, the ternary diagram of this system in the β_2 polymorph evidenced that the eutectic behavior was mainly governed by POS-POP interactions (Ghazani & Marangoni, 2019b). Miscible phases prevailed when POP content was below 50% and SOS was kept above 20%.

Despite the above, the behavior expected from POS, SOS, and POP interactions present may be altered when further components are involved. An example of convenience is the behavior observed by Rodriguez-Negrette et al. (2019) in mixtures of CB and whole shea butter (with POS, SOS, and POP accounting for 5.2, 38.4, and 0.1% of total TAG content, respectively). They observed the occurrence of softening in the mixtures due to both eutectic interaction and dilution effects. Eutectic formation was confirmed at a CB content in the mixture of 30%. Furthermore, the addition of shea butter caused a continuous decrease in SFC from the pure CB sample to the latter composition. This was linked to a dilution effect of OOO and SOO contained in shea butter (11.2 and 26.3% of total TAG content, respectively). The absence of such strong softening problems in CB/ShS mixtures makes sense since most SOO and OOO separate from the stearin during shea butter fractionation. This also relates to the suitability of ShS for CBI production.

6.4. DEVELOPMENT OF β UNDER ISOTHERMAL CONDITIONS

Polymorphism is one of the factors determining the microstructure of the fat crystals networks formed in lipid systems (Kellens et al., 1991a). In turn, the properties of the networks in terms of crystal size, shape, and distribution influence the physical behavior of final foods (Acevedo & Marangoni, 2015; Metin & Hartel, 2005). Such is the case of the hardness, gloss, or oil binding capacity in products like chocolate, spreads, and shortenings (de Man & Beers, 1987; Dibildox-Alvarado et al., 2004; Widlak & Hartel, 2012). In addition to the polymorphic and mixing behavior of lipid components, the microstructure varies notably with the processing conditions. This was seen in pure CB under the influence of different thermal treatments, the application of shear, or in the presence of additives (Campos et al., 2010; Marangoni & McGauley, 2003; Ramel et al., 2018). Compositional changes in the fat phase when adding CBE at different proportions to CB may also lead to morphological changes of the fat crystal networks developed (Aumpai et al., 2022; Sonwai et al., 2014).

This section examines the evolution of the polymorphic and microstructural properties of CB/ShS blends under static temperature conditions. Since β crystals eventually form the fat

phase of end products containing CB and/or ShS, it is worth clarifying how polymorphic forms of lower stability behave on their transition to β.

Pure CB, ShS, and selected blends were first heated at 70 °C for 30 minutes. The same were then quenched to 22 °C and kept at this temperature for 40 days. The thermal protocol aimed to avoid the direct crystallization of β from the melt due to a "memory effect" (van Malssen et al., 1996b) and favor the direct crystallization of the β' polymorph. During incubation, polymorphic changes in the samples were monitored by laboratory-scale XRD at different days until only β was detected. Variations in their microstructure over this period were tracked by PLM. Some relationships between polymorphism and crystalline morphology were stablished.

Figure 6.9 depicts the XRD diffraction patterns obtained for pure CB and ShS throughout the whole incubation process.

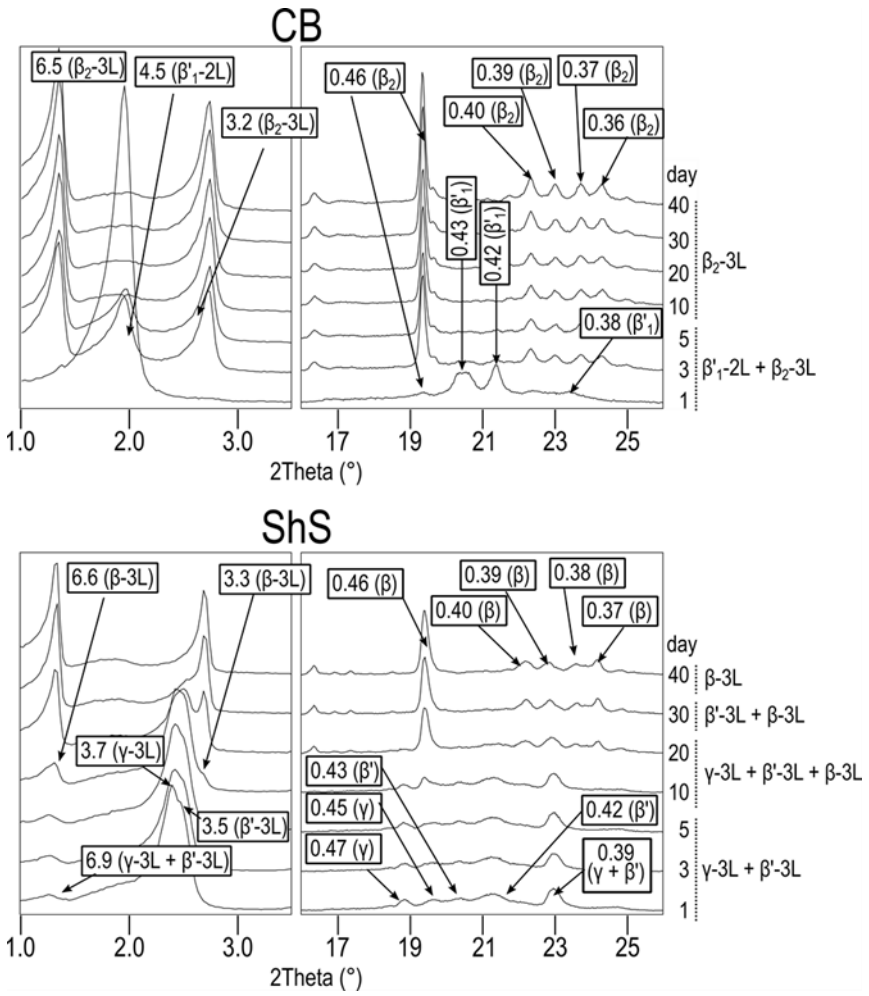

Figure 6.9. XRD patterns of pure CB and ShS crystallized at 22 °C.

In CB, β'_1-2L predominated at day 1 (SAXD peak at 4.5 nm and WAXD peaks at 0.43, 0.42, and 0.39 nm) but some β was also present (weak reflections at 6.5 and 0.46 nm). The direct crystallization of β from the CB melt is highly unlikely (van Malssen et al., 1996b, 1999), so the β'_1-2L to β-3L transition probably started within the first 24 hours. PLM micrographs showed that β'_1-2L developed as a mass of tiny irregular crystals with a certain degree of clustering (Figures 6.10A and 6.10B). The dense branched texture observed at the edge of some of the structures (Figure 6.10C) was due to the growth of β, as it became more evident as time went by. After 3 days, β_2-3L reflections dominated XRD patterns and spherulites (80-140 μm diameter) with a granular center and a more ordered outer region were imaged (Figure 6.10D). Towards day 5, the ongoing structural changes led to variations in the interaction of the light with the sample and the resulting interference colors observed (Figure 6.10E). It should be recalled that no filters were used during the microscopic study. In addition, at this point, feather-like structures, typical of β of CB (Manning & Dimick, 1985), grew around the spherulites. The transition finished before day 10, when only β_2-3L was detected by XRD. At this time, the crystal mass was highly aggregated, but the former structures were still distinguished (Figures 6.10F and 6.10G). No more changes were seen by PLM towards day 40 (Figure 6.10H).

More time was required by ShS for the β development. According to XRD data, concurrent γ-3L and β'-3L forms were present from day 1 to 5. In turn, two different morphologies, consisting of small spherulites and a granular region, were imaged by PLM (see Figures 6.11A-C). Based on previous confocal Raman microscopy data on silica-treated ShS, the granular region could correspond to γ-3L and the small spherulites (maximum diameter ~80 μm) to β'-3L (Ray et al., 2013). After 10 days, feather-like structures started growing due to the transformation of γ-3L and β'-3L into the more stable β-3L form (Figure 6.11D). Over time, these increased in number and size (Figures 6.11E-H) and β-3L reflections strengthened in XRD patterns. The intensity of WAXD peaks at 0.40, 0.39, 0.38, and 0.37 nm evidenced the correspondence of this form with β_2-3L of SOS. γ-3L was no longer present after 20 days of incubation and β'-3L faded between days 30 and 40. At the end of the incubation period, the dense feathery spherulites with highly ordered branches growing from their center (~500 μm diameter) were still surrounded by a vast mass of smaller crystals.

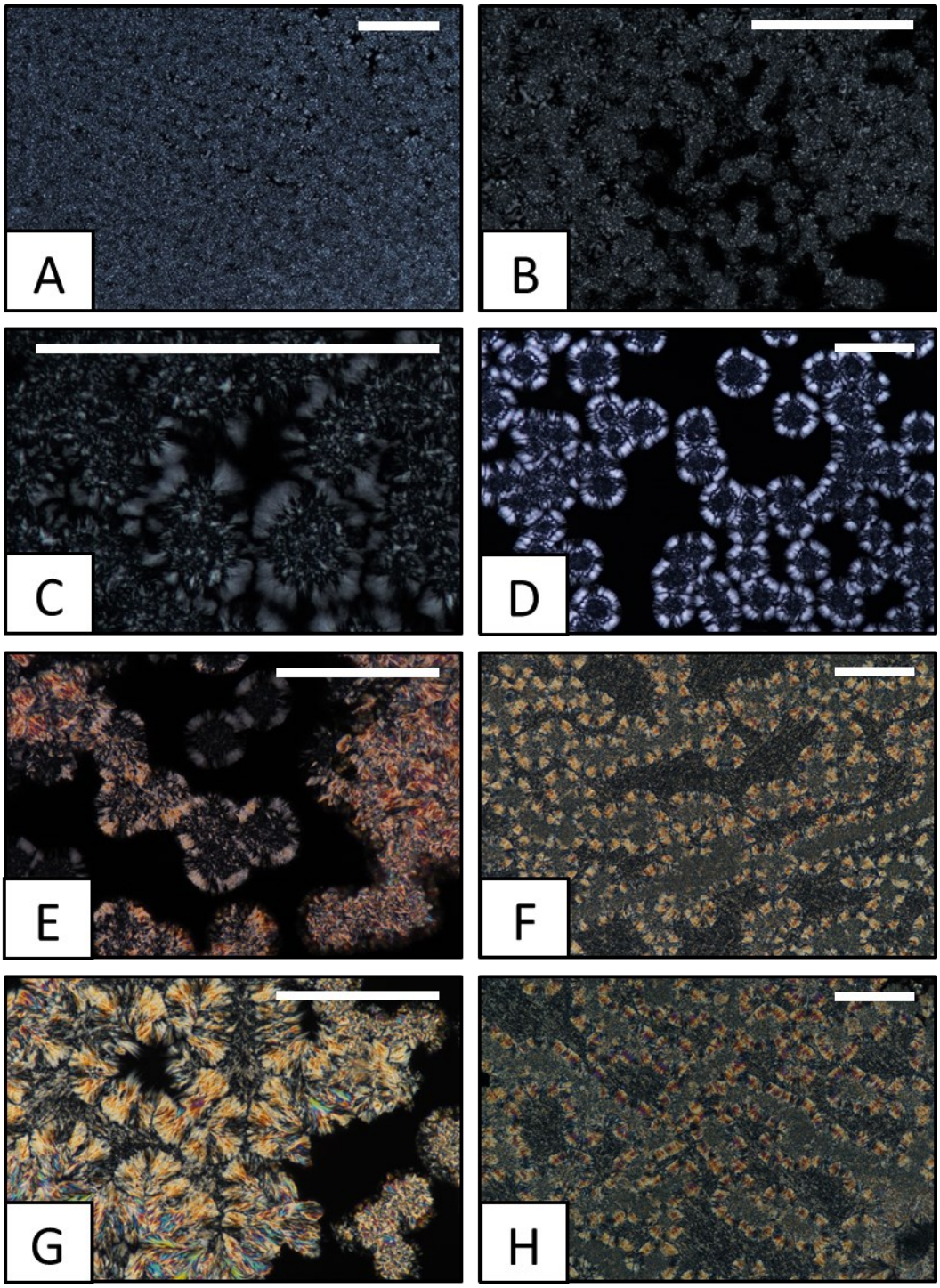

Figure 6.10. PLM micrographs of CB crystallized at 22 °C for (A, B, C) 1 day, (D) 3 days, (E) 5 days, (F, G) 10 days, and (H) 40 days. Scale bar = 250 μm.

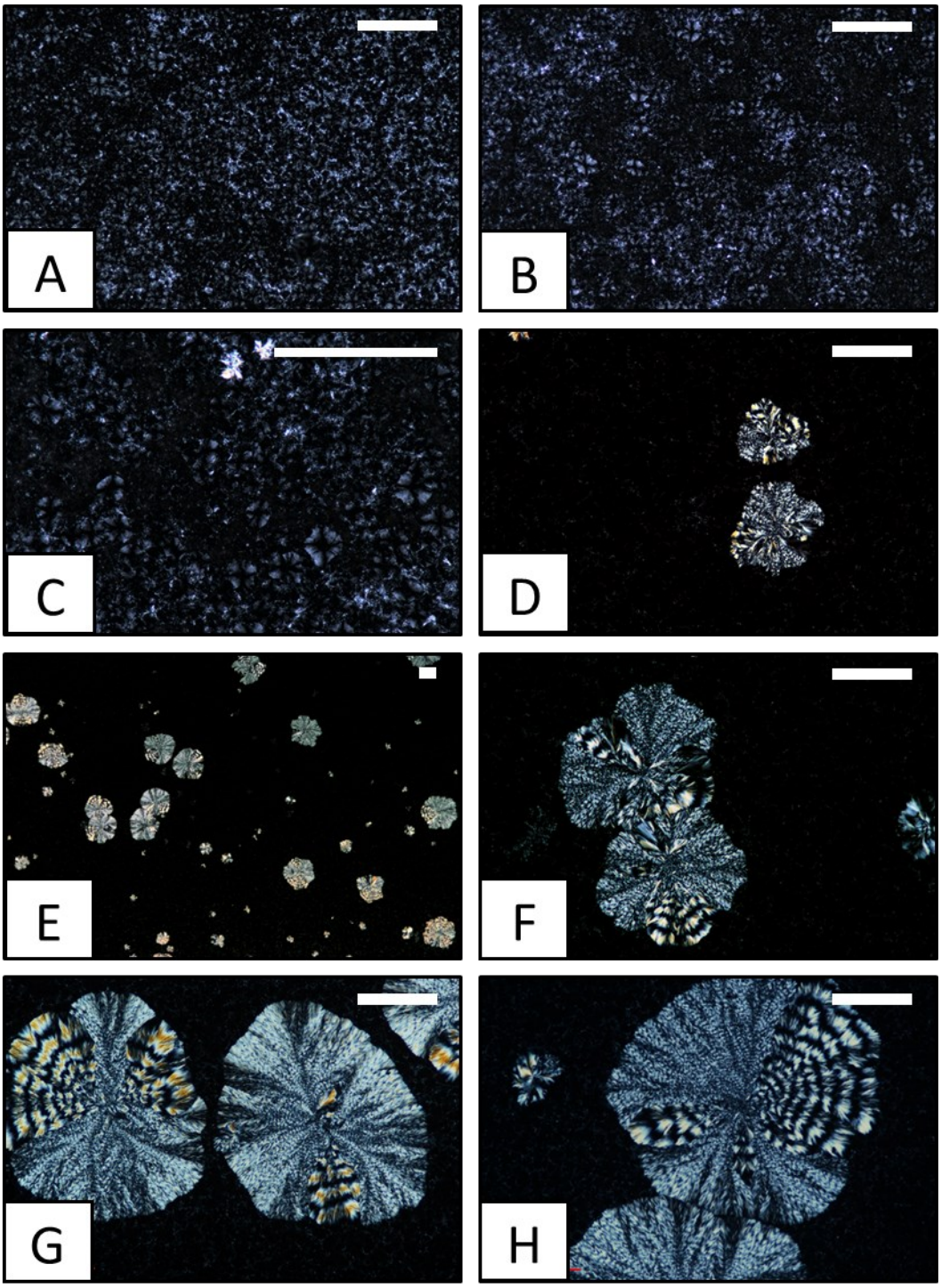

Figure 6.11. PLM micrographs of ShS crystallized at 22 °C for (A, B) 1 day, (C) 5 days, (D) 10 days, (E, F) 20 days, (G) 30 days, and (H) 40 days. Scale bar = 250 μm.

XRD data obtained for the 70CB and 50CB mixtures are shown in Figure 6.12. Both showed β'-2L, β'-3L, and β-3L after 1 day of incubation. As in CB/ShS mixtures crystallized under non-isothermal conditions, β'-3L was promoted before β'-2L at increasing ShS content. In the 70CB mixture, no different morphologies were discerned in the crystalline mass (Figure 6.13A). The bright spherulites within a mass of irregular crystals in the 50CB mixture (Figure 6.14A) resembled those imaged in pure ShS. Thus, we assumed their relationship with β'-3L.

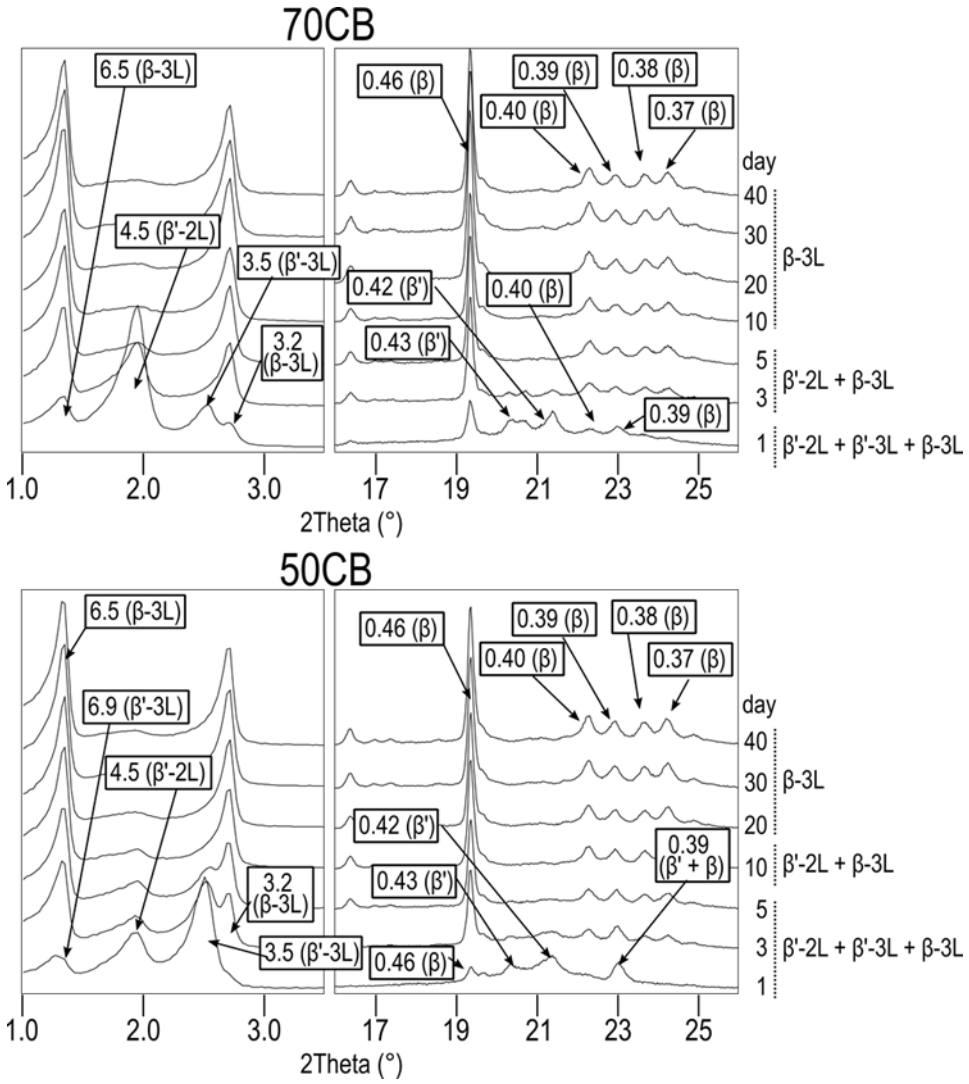

Figure 6.12. XRD patterns of 70CB and 50CB mixtures crystallized at 22 °C.

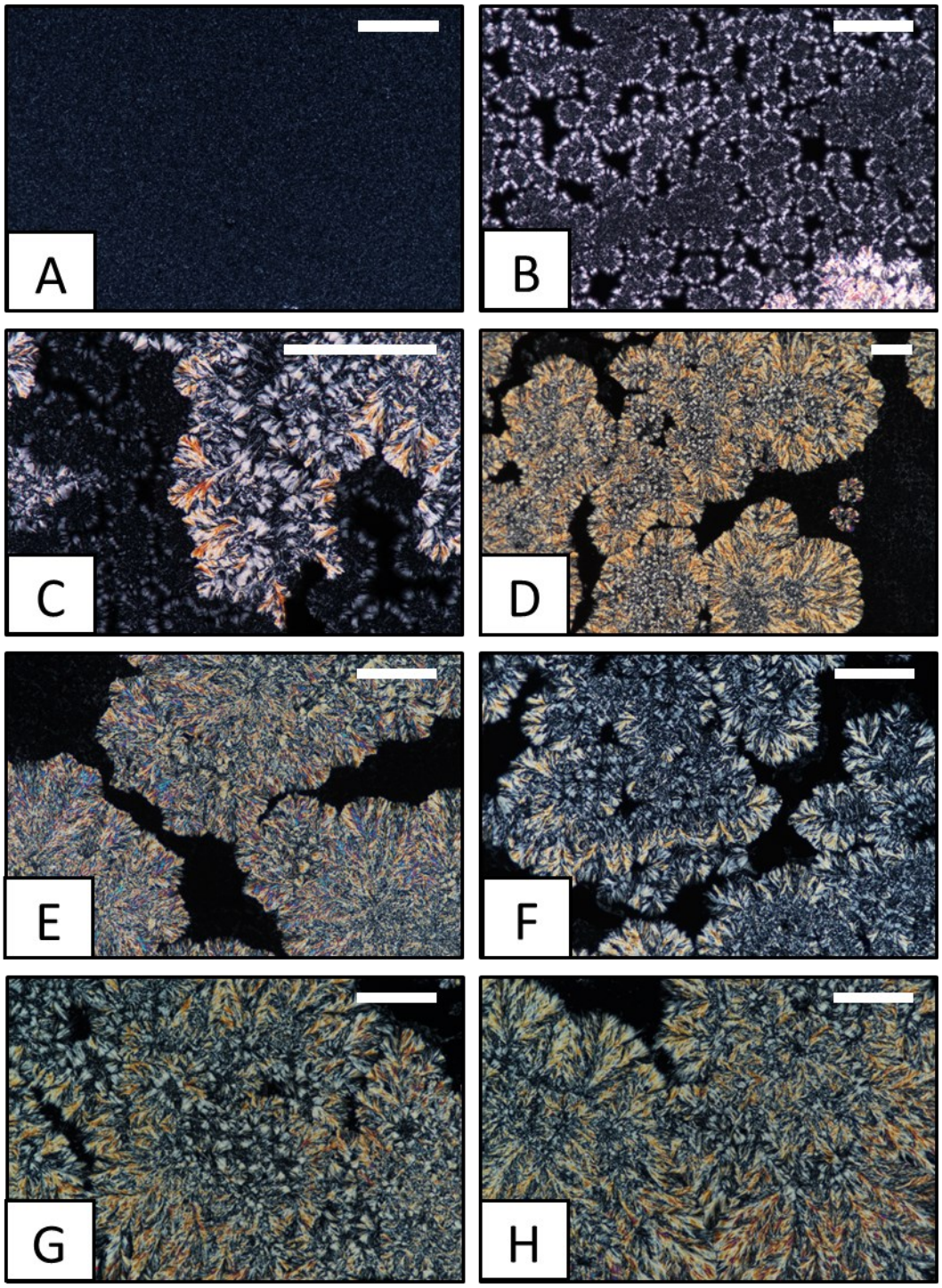

Figure 6.13. PLM micrographs of the 70CB mixture crystallized at 22 °C for (A) 1 day, (B, C) 3 days, (D, E, F) 10 days, (E, F) 20 days, (G) 30 days, and (H) 40 days. Scale bar = 250 μm.

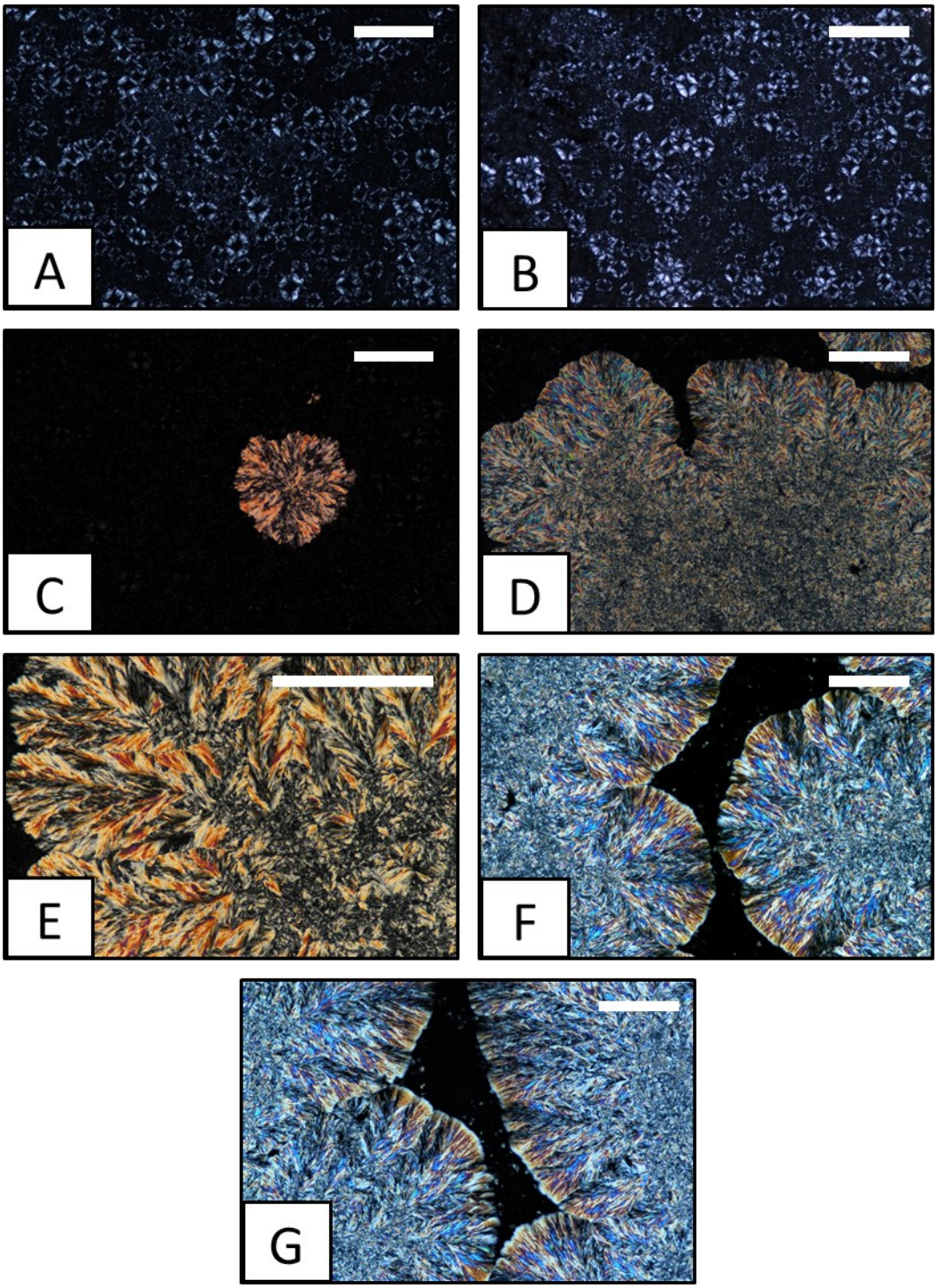

Figure 6.14. PLM micrographs of the 50CB mixture crystallized at 22 °C for (A) 1 day, (B, C) 5 days, (D, E) 10 days, (F) 20 days, and (G) 40 days. Scale bar = 250 μm.

In the 70CB mixture, XRD patterns showed that β'-3L and some β'-2L were consumed in favor of β-3L after 3 days. The microstructural changes during the transition resembled those undergone by pure CB (Figures 6.13B and 6.13C). Granular clusters became surrounded by highly ordered crystallites and large feather-like structures started developing. The completion of the β' → β transformation was confirmed on day 10. Moreover, *d*-spacing values and intensities of the WAXD peaks confirmed β as the solid solution of the major TAGs in the β_2 polymorph. At this time, individual clusters had grown close to each other to form large structures exceeding 1 mm diameter (Figure 6.13D-F). In these, the inner region showed discernible irregular crystallites surrounded by long feather-like structures developed up to 250 μm outward. No additional variations in the microstructure were evident towards day 40 (Figures 6.13G and 6.13H).

The behavior of the 50CB mixture resembled that of the 70CB mixture except for the slower development of the β phase. More concretely, β'-3L was still present at day 5 and the total vanishing of β'-2L was delayed beyond 10 days of incubation. In agreement, more gradual changes in the microstructure were detected by PLM. Micrographs from days 3 to 5 showed the formation of some crystalline aggregates probably due to the β' to β transition (Figures 6.14B and 6.14C). From day 10 to 40, the morphology of the major fraction of the sample was almost identical to that of 70CB mixture once the β phase had developed (Figures 6.14D-G). However, more highly ordered smaller crystallites forming the body of the mass were visible to the naked eye.

In summary, the stabilization of β was hindered from the pure CB to the pure ShS composition. 5-10 days were needed in CB and the 70CB blend, 10-20 days in the 30 CB blend, and more than 30 days in ShS. The wider difference between the incubation temperature and melting point of ShS with respect to CB was the likely cause of this outcome. This behavior agrees with the adjustment of temperature often required when tempering chocolate products including SOS-rich fats (Smith, 2012). It is worth mentioning that, despite the higher point shown by β'-3L during experiments under non-isothermal conditions, it was β'-2L that determined the end of the β' → β transition in the blends isothermally crystallized. The faster vanishing of β'-3L suggested its greater instability when CB was present. By contrast, β'-2L showed a higher shelf-life as the ShS content increased. One may guess that such behavior was

favored by an enrichment of the crystalline structure in SOS molecules. The differences in polymorphism among blends during incubation were accompanied by different microstructures. Samples crystallized in β' changed from a more irregular to a predominantly spherulitic morphology from pure CB to pure ShS. This fact was in part associated with an increase in the β'-3L/β'-2L ratio. The morphological differences among samples were still evident once β was obtained. Feather-like structures were seen at all CB/ShS rations, but these differed in size, density, and distribution. The formation of more regularly shaped crystalline structures towards pure ShS could be in part due to the higher homogeneity of the major TAG fraction. Different microstructures could result from changing the static temperature conditions employed in the present study. However, our results unveiled a clear dependence of the fat crystal network development on fat composition. One may expect that the differences arising from changing the CB/ShS ratio would eventually lead to varying macroscopic properties in final products.

6.5. CHAPTER CONCLUSIONS

The combined use of DSC and laboratory-scale XRD permitted monitoring the polymorphic crystallization, transformation, and melting behavior of CB, ShS, and their blends when subjected to thermal treatments at varying cooling and heating rates. The results evidenced that, during cooling processes, a lower rate favored the crystallization of more stable forms. Also that the polymorphic occurrence in the blends depended on the CB/ShS ratio and was far more diverse than that of the pure fats. During heating treatments, the sequence of polymorphic transitions was not affected by kinetic effects. However, the relative amount of occurring polymorphs was influenced by the heating rate applied.

With regard to the polymorphic behavior, the longitudinal and lateral packing of the crystalline forms of ShS were evidently determined by SOS. In the blends, the main difference observed with respect to the pure fats was the occurrence of β' forms with varying chain-length structures. The triple-layered β', which was linked to the separation of a SOS-rich phase, defined the final stage of melting under the thermal conditions applied. Moreover, the final ratio of β' forms after the transformation of less stable polymorphs was marked by the speed of the heating treatment. This was explained based on the different time provided by the rates applied for the excess of SOS to interact with POS and POP and pack in a double chain-length structure.

The SFC analysis performed after a thermal incubation process showed that the sharp melting displayed by CB at 30-35 °C raised by 5 °C in pure ShS. The thermal properties of the blends were halfway those of the pure fats, which led to flatter and wider melting profiles as the content of CB and ShS became closer in the blends. In addition, the solid properties were generally improved at all temperatures from the pure CB to the pure ShS composition. Such behavior was associated with the great compatibility in the β polymorph of the major TAGs present.

In line with the above, the XRD study on CB/ShS blends crystallized under isothermal conditions evidenced complete miscibility in β_2. During the development of this form, the polymorphic and microstructural behavior differed among compositions. The slower maturation of β from pure CB to pure ShS was a result of the increased stability of the preceding β' crystals. In addition, PLM revealed varying crystalline morphologies by cause of the CB/ShS ratio, in which the polymorphic occurrence seemed to play a relevant role. At all compositions, the β

microstructure was characterized by the growth of typical feather-like crystalline structures but these became more predominant and highly ordered as the ShS content increased.

By considering the properties observed in terms of SFC, melting profile, and β crystals development, CB/ShS blends with ShS content around 30% and below would present the highest potential application in CBA. Specially, the introduction of ShS might be useful to improve the heat-resistant properties of chocolate-type products. It would be worthy to explore in more detail the crystalline and physical behavior CB/ShS mixtures around the mentioned composition both alone and within end products.

In the present study, we deepened into the varying polymorphic, microstructural, and melting properties of CB/ShS blends as a function of composition and thermal processing. Controlling the physical behavior of lipid-based products is essential for the industrial manufacture of foods with specific traits. In this sense, external factors such as the application of thermal treatments (under dynamic or static conditions) or variations in the composition (physical blending of fats, inclusion of additives) influence the polymorphic, microstructural, and melting behavior of lipid crystals. These eventually determine the functional properties of end products. Therefore, assessing the effect of external influences on the microscopic and macroscopic properties of lipid systems helps tailor the most efficient processing conditions for each application, for example, by adapting the temperature regimes applied or adjusting the formulation of lipid blends.

CHAPTER 7

GENERAL DISCUSSION

The physical properties of fats and oils are determined by the wide variety of lipidic components within, mainly TAGs, and their mixing interactions. For this reason, the investigation of single molecules and their combinations is as relevant as that of whole fats. In this regard, the present thesis focuses on the crystallographic and thermal characterization of lipid mixtures composed of pure triacylglycerols, as well as complex real fats.

Regarding pure TAGs, we evaluated the phase behavior of binary and ternary mixtures consisting of a monoacid saturated TAG and mixed-acid saturated-unsaturated TAGs able to form a molecular compound. The general purpose of this study was to determine how the eutectic behavior of a binary system may be modified by the addition of a third component. This work represents a step forward in the characterization of the mixing interactions that govern the properties of complex lipid systems. Specifically, the mixtures under study included the monoacid saturated TAGs PPP and LLL, and the mixed-acid saturated-unsaturated TAGs POP, OPO, and PPO. The interest in these components lies in their importance in food lipids such as palm and coconut oil.

To study the polymorphic and phase behavior of lipid mixtures, the properties of the individual components should be known in advance. For this reason, the study of binary and ternary mixtures of TAGs was preceded by the characterization of the pure TAGs PPP, LLL, OPO, and PPO (see Chapter 3). DSC and X-ray diffraction were used to analyze their polymorphic crystallization and transformation behavior during thermal treatments consisting of cooling from the melt and reheating at varying rates.

During cooling processes, a general trend was observed for all TAGs. Specifically, lower cooling rates favored the occurrence of more stable forms. For example, α-2L, α-2L together with β' 2L, β'-2L, and β-2L forms crystallized in PPP at the rates of 15, 2, 0.5, and 0.1 °C·min^{-1}, respectively. Additionally, OPO showed α-2L crystals when cooled at 15 °C·min^{-1}, and β'-2L, β_2, and β_1-3L crystals when lower rates were used. This behavior was related to the influence of kinetics on the nucleation rate of the polymorphic forms. The occurrence of more stable forms is assumed to be favored by a greater driving force for crystallization (ΔG in the liquid and in the crystalline state). However, a high degree of Δ*T* minimizes the effect of the driving force and eases the crystallization of less stable forms due to their lower interfacial energy (Himawan et al., 2006; Hondoh et al., 2018). As a result, faster cooling treatments, which increase Δ*T* by decreasing the crystallization temperature, favor the occurrence of less stable forms. In addition

to the effect of thermal treatments, it is worth noting the importance of the intrinsic properties of TAGs in the polymorphic-dependent crystallization. In this sense, the shorter length of the fatty acid moieties in LLL with respect to PPP favored its crystallization in forms of higher stability when subjected to the same thermal treatment. Additionally, it was confirmed the strong tendency of PPO to crystallize in metastable α forms even when using a low cooling rate of 0.5 °C·min^{-1}.

During heating treatments, the rate used affects the sequence and nature of polymorphic transitions. Polymorphic transformations involve overcoming a specific energy barrier, which depends on whether they take place in the solid state or via melt mediation. The barrier is assumed to be larger in solid-state transformations, which means that more time may be needed for its occurrence. Thus, fast heating treatments often lead to melt-mediated transitions due to the lower time available for the transformations to take place. Moreover, the time allowed for the transformations at varying heating rates may also lead to a different sequence of polymorphic transitions for an individual TAG species.

In PPP and LLL, there was no evident influence of the heating rate on the polymorphic transformation sequence or the type of the transitions. Under the studied conditions, the polymorphs obtained during cooling always transformed into the next one in order of increasing stability before complete melting. By contrast, results on OPO showed that rapid heating impeded the formation of the intermediate β_2 form, and only the transition from α-2L to β_1-3L was observed. Such behavior agreed with that reported for TAGs like OPO, POO, POP or SOO evaluated under varying cooling and heating rates (Bayés-García et al., 2011a, 2013b, 2013a, 2016). The occurrence of melt-mediated and solid-state transformations in these TAGs, as well as the occurring polymorphic forms, were strongly influenced by kinetics. In this regard, the wide range of conditions used in our study of PPO confirmed a divergent behavior regarding other mixed-acid saturated-unsaturated TAGs. Different heating rates did not vary the sequence of polymorphic transitions, which prevalently occurred via melt mediation. From this, we concluded that the time needed for melt-mediated transformations to occur was always lower than the time allowed by the heating rate applied for the transition. It also suggests a very high energy barrier to overcome for solid-state transformations to occur in PPO. This might be in part due to a lower flexibility of packing caused by the single oleic acid moiety (Kodali et al., 1984). In addition, PPO transitions involve the sequential change from a double to a triple chain-length structure (mainly α_2-2L → α_1-3L → β'_2-2L → β'_1-3L). This probably implies a higher

energy barrier than in transformations with no change in longitudinal packing of TAGs. These factors contributed to the low influence of varying heating rates on the polymorphic behavior of PPO.

The study of PPP, LLL, OPO, and PPO provided a closer look to the complicated crystalline behavior of TAGs with varying fatty acid composition, degree of unsaturation, and symmetry. Especially in the case of PPO, whose polymorphic properties under the influence of kinetics had been barely explored before.

The TAG mixtures investigated in this thesis were characterized by the presence of either PPP or LLL as the monoacid saturated component. Those including PPP consisted of the binary systems PPP/POP, PPP/OPO, and PPP/PPO, and the ternary systems PPP/POP/OPO (PPP/$MC_{POP/OPO}$) and PPP/POP/PPO ($MC_{POP/PPO}$) (Chapter 4). The mixtures including LLL were the binary systems LLL/POP and LLL/PPO, and the ternary system LLL/POP/PPO (LLL/$MC_{POP/PPO}$) (Chapter 5). For almost all of them, the phase behavior was examined under stable and metastable conditions. Analyzing the phase behavior in most stable polymorphs after an incubation time provides better knowledge about the tendency of the systems over time. In turn, metastability studies permit a closer look at the polymorphic behavior that precedes the formation of stable phases. Occasionally, they also allow identifying mixing states different from those occurring under stable conditions.

The results obtained under stable conditions allow a better comparison of the behavior displayed by the different systems. In this regard, the stable phase diagrams of systems including PPP showed a similar eutectic behavior. This consisted of very asymmetric eutectic compositions and a limited miscibility area in the region of the diagram rich in PPP. The low solid-state miscibility determined in these systems resulted from the steric hindrance between palmitic and oleic acid components. As to the asymmetric eutectic points, it is a typical trait of binary mixtures of components with large differences in melting point. The dissimilarity between systems lied in the miscibility gaps.

Attending the binary mixtures, around 30-35% of POP and PPO dissolved in PPP, whereas the solubility of OPO was below 5%. The difference was linked to the positive excess free energy of mixing expected from the disturbing effect of bent oleic acid chains on the crystal lattice of PPP (Wesdorp et al., 2013). The same would be higher in PPP/OPO mixtures than in PPP/POP

and PPP/PPO mixtures due to the double unsaturation of OPO. As a result, the solubility of OPO in PPP was impeded, whereas that of POP and PPO was tolerated at some degree. Regarding ternary mixtures, around 20-25% $MC_{POP/OPO}$ dissolved in PPP of around 20-25%. Hence, the miscibility did not improve from the PPP/POP to the PPP/$MC_{POP/OPO}$ system. However, the total amount of OPO dissolved in PPP increased with respect to the PPP/OPO system. This could be due to a lower excess free energy of mixing caused by $MC_{POP/OPO}$. Regarding $MC_{POP/PPO}$, it showed a solubility in PPP of around 35-40%, which was slightly above that of pure POP and PPO. In contrast to the triple structures of stable POP (β_1-3L), OPO (β_1-3L), and PPO (β'_1-3L), molecular compounds show double structures like that of PPP (β-2L). One might expect that the structural similarity favors the miscibility to some degree. However, the solubility found for POP and $MC_{POP/OPO}$ in PPP would suggest a low impact of the chain-length structure. From the results obtained, it can be concluded that oleic acid content was the most determinant factor in the final solid-state miscibility displayed by the mixtures.

Regarding mixtures containing LLL, stable LLL/POP and LLL/PPO systems also showed eutectic behavior. As in PPP/POP and PPP/PPO mixtures, the incompatibility of the components was governed by steric hindrance. The phase diagrams determined for incubated LLL/POP and LLL/PPO systems and their counterparts with PPP are shown in Figure 7.1 for comparison. LLL/POP and LLL/PPO mixtures showed a less asymmetric eutectic composition with around 20-10% LLL content. In addition, the solubility of each TAG in the solid phase of the other was below 5%. From the results on mixtures including PPP and LLL, it is concluded that the symmetry of the mixed-acid saturated-unsaturated TAGs in the blends did not cause substantial differences in the overall behavior. However, there was an evident influence of the length of palmitic and lauric fatty acids (12 and 16 carbon atoms, respectively) included in the monoacid TAGs. The shorter lauric acid narrowed the difference in the melting point of the components in LLL/POP and LLL/PPO blends, which favored more symmetric eutectic compositions. The higher insolubility of mixed-acid TAGs in LLL was also related to the molecular size. POP and PPO are expected to induce a greater disruptive effect when incorporated into the regular crystalline phase of smaller LLL molecules. This would prevent the dissolution of mixed-acid TAGs even at the lowest concentration tested.

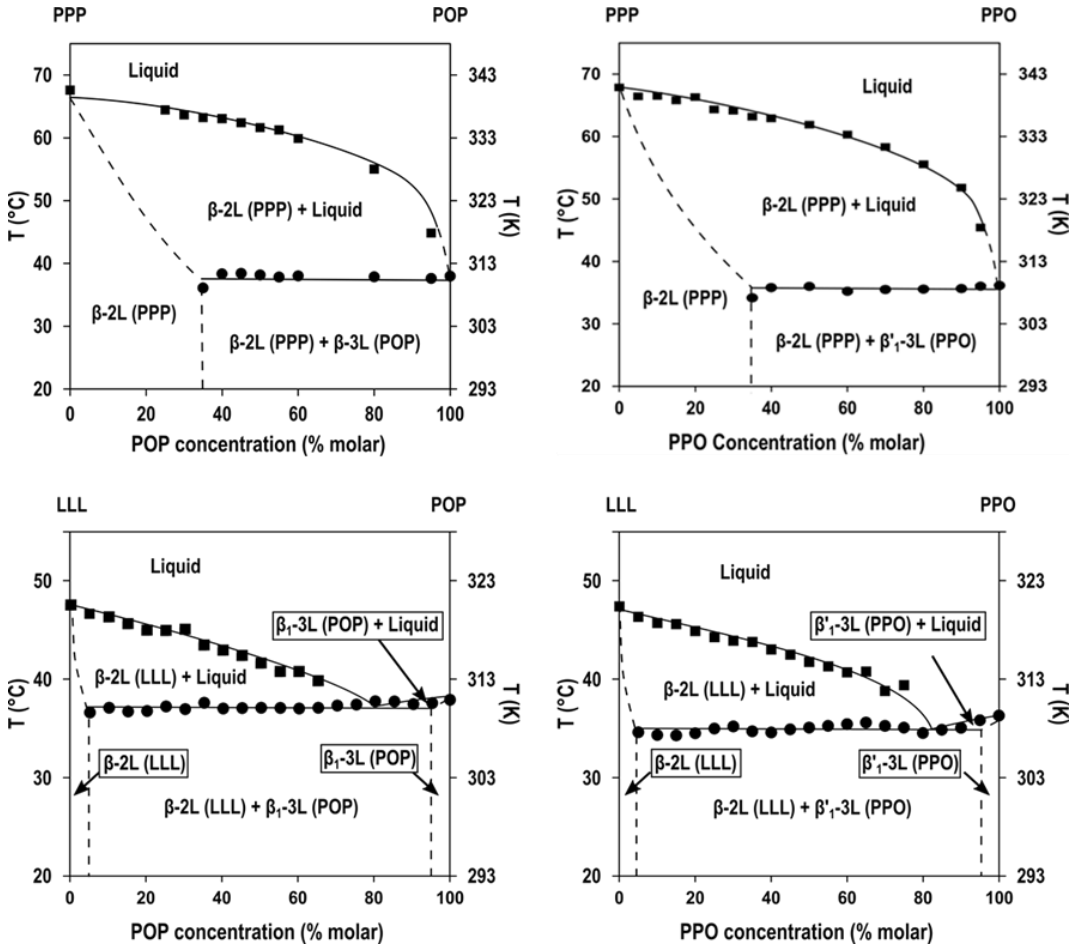

Figure 7.1. Phase diagrams of binary mixtures including PPP (incubation at 40 °C for 5-7 days and 27 °C for 6 months) and LLL (37 °C for 5 days and 27 °C for 9 months).

After one year of thermal incubation, LLL/$MC_{POP/PPO}$ mixtures showed the formation of single solid solutions with up to 15-10% LLL. In addition, mixtures with 15 to 35% LLL content showed the formation of solid solution phases and a metastable phase attributed to POP. Therefore, the miscibility of the system was improved with respect to the binary systems. The reason for the higher dissolution of LLL in the mixed-acid saturated-unsaturated TAGs was not clarified. However, it is reasonable to think of a relationship with the change from triple chain-length structure in their pure forms to a double chain-length structure in the molecular compound. This change might ease the accommodation of LLL molecules to a certain degree. It is also worth contrasting this system with the PPP/$MC_{POP/PPO}$ system. In the latter, $MC_{POP/PPO}$ behaved as a single component over the full range of compositions. In the LLL/$MC_{POP/PPO}$ system, the occurrence of a metastable POP phase above a certain LLL content in the mixtures suggested that POP and PPO were not at a 1:1 ratio in the solid solutions with LLL. As

conclusion, the solubility of LLL at these compositions was favored by a predominant PPO content. This reveals how the mixing interactions between TAGs forming molecular compound may be altered by the addition of a specific third component.

The study of mixtures containing PPP and LLL during cooling and heating treatments at specific rates shed some light on the mixing properties of these systems in the metastable state.

For PPP/OPO, PPP/PPO, and PPP/$MC_{POP/PPO}$ mixtures, eutectic behavior in β' forms with limited solubility of the unsaturated components in PPP was determined. In addition, eutectic α forms were also found in PPP/PPO and PPP/$MC_{POP/PPO}$ mixtures. As to the PPP/$MC_{POP/OPO}$ system, even though the kinetic study only covered the equimolecular mixtures, the eutectic interaction became also evident. Results on these systems also indicated that the polymorphic crystallization and transformation behavior of individual TAGs was influenced by the other components of the mixture. This can be exemplified through the results obtained for PPP/PPO mixtures cooled from the melt and reheated at 2 °C·min^{-1}. In contrast to the predominant α crystals shown by pure PPP and PPO at the end of cooling processes, both showed β'-2L crystals in blends with PPP content from 80 to 20%. Moreover, also the polymorphic sequence and the transformation pathways were affected during heating. Hence, PPP impeded the transformation of β_2'-2L (PPO) into stable β_1'-3L (PPO). In turn, the solid-state β'-2L to β-2L transition of pure PPP occurred through the melt in the presence of PPO.

The kinetic phase behavior of LLL/POP, LLL/PPO, and LLL/$MC_{POP/PPO}$ mixtures was evaluated when cooling at a high rate of 25 °C·min^{-1} and subsequently heating at 5 °C·min^{-1}. Contrary to mixtures systems including PPP, no previous studies had reported on the phase behavior of LLL and unsaturated TAGs in least stable α forms. Thus, such thermal conditions were applied to induce the α crystallization and analyze the behavior of the systems in the widest possible range of polymorphs during heating. On cooling, α (ss) and pure TAGs α forms crystallized in the three mixture systems along a wide range of compositions. When heating the binary mixtures, α (ss) transformed into β' (ss), after which the components separated and pure TAG phases crystallized. In agreement with the results obtained under stable conditions, LLL/$MC_{POP/PPO}$ showed the additional formation of β (ss) and the separate crystallization of a POP fraction. The behavior observed may be linked to that described in this thesis and previous work for mixture systems including PPP. It was found that the fast cooling of PPP/POP and PPP/PPO mixtures at 25 °C·min^{-1} kinetically favored the formation of solid solutions in least

stable forms (Gibon & Durant, 1985). During heating processes, these tended to separate after undergoing several polymorphic transitions. However, our results on the same systems cooled at lower rates (15 and 2 °C·min^{-1}) showed that these components tended to crystallize in an independent manner. Based on this and the incompatibility assumed between fully saturated and saturated-unsaturated TAGs, a higher degree of components separation would also be expected in mixtures including LLL by decreasing the speed of the cooling treatment applied.

The investigation of TAG mixtures in this thesis aimed to extract fundamental knowledge about the interactions taking place in complex fats and their blends. In addition, it was also intended to find potential applicability to the obtained results.

On one hand, the results obtained for mixtures including OPO and $MC_{POP/PPO}$ suggested that promoting molecular compound formation in hard fat-based products may help prevent specific low-melting components from oiling out. On the other hand, it was also concluded that $MC_{POP/PPO}$ behaves as the pure POP and PPO under stable and metastable conditions. This suggests that ternary interactions may prevail over binary ones in complex lipids where these components are concurrently present, such as palm oil. During fats crystallization, the first stage is ruled by the crystallization of high-melting components like PPP and their solid-state miscibility properties. On this stage depends the next crystallization behavior of lower melting TAGs. Based on our results, PPP/POP/PPO interactions are expected to play a part in the early crystallization of palm oil.

Regarding the mixtures including LLL, the results obtained for LLL/POP and LLL/PPO mixtures served as a model case to clarify the eutectic behavior that governs the blends of lauric fats like coconut oil and common fats rich in palmitic and oleic acids, like palm oil or cocoa butter. In LLL/$MC_{POP/PPO}$, the solubility of LLL in the unsaturated components increased with respect to the binary systems. This opens the door to a potential application of this type of interaction to improve the eutectic behavior of mixtures including lauric fats and their fractions. This could be especially interesting to reduce to some extent the incompatibility of mixtures of lauric-based CBS and cocoa butter. However, further research is needed to clarify some aspects left open by this thesis. In the first place, the specific factors involved in the improvement of the components miscibility in LLL/$MC_{POP/PPO}$ mixtures. The results suggested that, above a certain LLL concentration, the formation of a three-component solid solution was favored by the separation of part of the POP fraction. Therefore, in the second place, it would be interesting

to evaluate how varying the POP/PPO ratio may affect the polymorphism and solid-state miscibility of LLL/POP/PPO mixtures.

The physical blending of fats constitutes the basis for developing novel fat-based products or improving the functional properties of the existing ones. In line with this, this thesis also covered the polymorphic and thermal behavior study of binary blends of CB and ShS as a case study of real fats blends. As in the TAG mixtures previously discussed, the study of CB/ShS blends implied the investigation of the pure fat components. The industrial manufacture of lipid materials often involves the crystallization of metastable forms before obtaining the desired stable crystals. Thus, it is relevant to gain an in-depth knowledge of the varying polymorphism of natural fats and their blends. Following this premise, the polymorphic behavior of CB, ShS, and their mixtures was evaluated during the application of dynamic thermal treatments. Their thermal properties were also analyzed through the SFC determination. In addition, their polymorphic and microstructural behavior during the development of the β phase was monitored during a 40-day isothermal crystallization process at 22 °C.

The DSC and XRD measurements performed during the application of dynamic thermal treatments permitted identifying sub-α-2L, α-2L, β'-2L, and β'-3L forms in all CB/ShS blends. β'-2L was associated with a solid solution of POS, SOS, and POP, whereas β'-3L, which is characteristic of ShS, was mainly attributed to SOS. In addition, γ occurred when the ShS content in the blends exceeded 50%. In agreement with our studies on TAG components, during cooling processes, more stable forms crystallized when a lower rate was used. During the next heating, the rate used had a special influence on the ratio of β'-2L and β'-3L formed from the α-2L transformation. Slower heating provided more time for the SOS molecules to incorporate into the β'-2L solid solution of TAGs, thus decreasing the amount of β'-3L formed. Additionally, the thermal data obtained during cooling and heating processes showed that ShS caused an overall increase in the crystallization and final melting temperatures of the blends.

The study of SFC evidenced that increasing the ShS content in the blends caused an overall improvement in their heat resistance. This agreed with the absence of evident eutectic interactions in the isosolid points obtained from the SFC curves, which may be in part related to the ability of the main TAGs in the blends to form a β solid solution. Regarding the melting profiles, these varied according to the CB/ShS ratio in the blend. Thus, for example, the blend

with 70% CB content showed a sharp melting in a temperature range similar to that of CB at 30-35 °C. Then, the melting range shifted towards 35-40 °C as the composition became closer to pure ShS.

The isothermal crystallization study showed that less time was needed for the stabilization of β at increasing CB content in the blends. This was presumably due to the narrower difference in the incubation temperature and the melting temperature of CB with respect to ShS. As to the microstructure, pure fats and mixtures showed different crystal morphologies along the whole stabilization process, which in some cases were linked to a specific polymorphic occurrence. For example, the β form resulted in typical feather-like structures at all compositions. However, the crystals formed became thinner and showed more regularly shaped structures towards pure ShS. The microstructural changes observed at varying CB/ShS ratio would presumably lead to different macroscopic properties of the fat phase in final products.

The main objective of this research was characterizing the fundamental properties of CB, ShS, and their blends in terms of polymorphism, melting behavior, and microstructure. In addition, another objective was to find some applicability to the results generated. In this sense, applications related with the development of chocolate-type food products are of special interest. Three attributes which are desired in the fat phase of chocolates include: i) a sharp melting behavior near mouth temperature at 37 °C; ii) absence of solid fat above this temperature to avoid a waxy mouthfeel; and iii) a rapid development of the β crystals eventually forming the microstructure of the end product. These aspects were considered when comparing the properties displayed by the 70CB/30ShS, 50CB/50ShS, and 30CB/70ShS blends evaluated in this study. It was concluded that compositions with around 30% ShS would present the greatest potential application in the development of heat-resistant chocolate products.

CHAPTER 8

GENERAL CONCLUSIONS

This thesis provides new insights into the polymorphism and crystalline behavior of edible lipids ranging from pure component TAGs and multi-component TAG mixtures to binary blends of complex natural fats. The general conclusions extracted from the research carried out are summarized below.

The DSC and X-ray diffraction study of PPP, LLL, OPO, and PPO subjected to dynamic thermal treatments help characterize the polymorphic behavior of elementary components of natural lipids such as lard or palm, olive, and coconut oils.

Slow thermal treatments favored the crystallization of more stable forms during cooling and the amount of each polymorph obtained after transformations during heating. In turn, fast thermal treatments led to the occurrence of less stable forms during cooling and, occasionally, impeded specific polymorphic transformations during heating. The polymorphic occurrence upon cooling was explained through the effect of supercooling on the polymorphic-dependent nucleation of TAGs. The sequence and nature of the polymorphic transitions on heating resulted from the rate used and the specific energy barrier associated with each type of transformation.

In addition, the differences in polymorphic crystallization and transformation shown by monoacid saturated TAGs were ascribed to the length of the fatty acid moieties. Structural factors also seemed responsible for the divergent behavior of PPO with respect to that described for other mixed-acid saturated-unsaturated TAGs in the literature. Very slow cooling was needed to induce the crystallization of more stable forms. Moreover, no solid-state transitions occurred during heating at any of the rates used. It was assumed that the restricted chain packing caused by the double saturation and the great structural differences among PPO polymorphs may result in high energy barriers for this type of transformation to occur.

The phase behavior of the mixture systems PPP/POP, PPP/PPO, PPP/OPO, LLL/POP, and LLL/PPO, PPP/$MC_{POP/OPO}$, PPP/$MC_{POP/PPO}$, and LLL/$MC_{POP/PPO}$ was examined to gain further understanding of the mixing interactions occurring in natural lipids and their blends.

Eutectic interactions governed the behavior of all the systems under stable and metastable conditions, which was mostly explained by repulsive chain-chain interactions occurring between the components.

The results on incubated binary mixtures showed that the degree of solid-state miscibility in blends of fully saturated and saturated-unsaturated TAGs is primarily ruled by the molecular size and degree of unsaturation of the components. This was reflected in the great immiscibility of systems based on LLL with respect to those including PPP, as well as the varying miscibility ranges in PPP-based systems as a function of the oleic acid content of the unsaturated TAG.

The results on three-component mixtures showed that the miscibility varied to some extent with respect to the binary systems. Again, the degree of unsaturation ruled the behavior of ternary systems including PPP, whereas structural factors, such as the chain length of the polymorphic structures involved, presumably ruled the higher miscibility of LLL/$MC_{POP/PPO}$ mixtures with respect to the binary systems.

It was also found that the binary interactions between TAGs forming molecular compound in ternary systems varied according to the nature of the third component.

On the one hand, $MC_{POP/PPO}$ behaved as the pure POP and PPO in mixtures with PPP in stable and metastable polymorphs. This led us to conclude a presumably relevant role of the solid-state miscibility of PPP, POP, and PPO in the early crystallization of palm oil. In turn, the ternary interactions of these TAGs would be expected to influence the seeding effect exerted by PPP in the crystallization of lower melting components of this fat.

On the other hand, LLL/$MC_{POP/PPO}$ mixtures revealed that the typical 1:1 stoichiometry of TAGs forming molecular compound was altered by ternary interactions allowing the occurrence of solid solutions. The structural factors responsible for such outcome still need further clarification. Nevertheless, the solid-state miscibility observed suggested that promoting these type of interactions could be useful for improving the eutectic behavior resulting from blending lauric and non-lauric fats.

In addition to the above, the results obtained from the wide range of mixture systems evaluated in the present thesis may serve to predict the mixing behavior of diverse TAGs with different fatty acid substituents, such as SSS, SOS, SSO, and OSO.

Finally, to make an approach to a more complex blend of lipids, we characterized the polymorphic behavior, solid fat content, and microstructure of mixtures of CB and ShS.

The crystalline forms identified in the blends resulted from the characteristic polymorphism of the pure fat components, which, in turn, was governed by the main monounsaturated TAGs

present. In addition, their occurrence during cooling and heating processes varied according to the composition of the mixture and the speed of the thermal treatments applied.

A higher ShS content in the blends resulted in an improvement of the heat-resistant properties and a more hindered obtention of β crystals. This behavior was related to the elevated amount of the high-melting SOS in this fat. In addition, evident differences in microstructural development and crystal morphology were observed among the pure fats and the blends.

From the overall results, it was concluded that CB/ShS mixtures in the right proportion could be potentially used in specific confectionery applications, such as the formulation of chocolate-type products with higher physical stability against warm ambient conditions.

Based on the findings from this thesis, the following issues to be developed in the future are proposed:

- It is well known the seeding effect of PPP in the crystallization of fats like palm oil but the specific mechanisms involved are still unclear. Based on the results on POP/POP/PPO mixtures, the simultaneous microstructural and X-ray diffraction investigation of blends of these TAGs by powerful characterization techniques, such as synchrotron radiation microbeam X-ray diffraction, could shed light on this matter.

- Further research on ternary mixtures including LLL at varying POP/PPO ratios may help explain the behavior of molecular compound-forming TAGs in LLL/$MC_{POP/PPO}$ mixtures. It may be also worth analyzing how LLL behaves in ternary mixtures with varying mixed-acid saturated-unsaturated TAGs. Promoting three or more component solid solutions including LLL would be of special interest to mitigate the great incompatibility of blends of lauric-CBS and CB.

- Following on from the study of CB/ShS mixtures initiated in this thesis, it would be interesting to evaluate the performance of specific compositional ratios in actual chocolate preparations. Relevant aspects to be analyzed would be the effect of the fat phase on the thermal profile, visual appearance, texture, and fat bloom stability on the end products. This investigation could also be complemented by sensory evaluation studies.

REFERENCES

Acevedo, N. C., & Marangoni, A. G. (2010). Characterization of the nanoscale in triacylglycerol crystal networks. *Cryst. Growth Des.*, *10*(8), 3327–3333.

Acevedo, N., & Marangoni, A. G. (2015). Nanostructure and microstructure of fats. *Annu. Rev. Food Sci. Technol.*, *6*, 71–96.

Aini, I. N., & Miskandar, M. S. (2007). Utilization of palm oil and palm products in shortenings and margarines. *Eur. J. Lipid Sci. Technol.*, *109*(4), 422–432.

Akita, C., Kawaguchi, T., & Kaneko, F. (2006). Structural study on polymorphism of cis-unsaturated triacylglycerol: Triolein. *J. Phys. Chem. B*, *110*(9), 4346–4353.

Allais, C., Keller, G., Lesieur, P., Ollivon, M., & Artzner, F. (2003). X-ray diffraction / calorimetry coupling. A tool for polymorphism control. *J. Therm. Anal.*, *74*, 723–728.

Arishima, T., Sagi, N., Mori, H., & Sato, K. (1991). Polymorphism of POS . I. Occurrence and polymorphic transformation. *J. Am. Oil Chem. Soc.*, *68*(10), 710–715.

Aronhime, J. S. (1988). Application of thermal analysis (DSC) in the study of polymorphic transformations. *Thermochim. Acta*, *134*(C), 1–14.

Aumpai, K., Tan, C. P., Huang, Q., & Sonwai, S. (2022). Production of cocoa butter equivalent from blending of illipé butter and palm mid-fraction. *Food Chem.*, *384*, 132535.

Badan Ribeiro, A. P., Masuchi, M. H., Miyasaki, E. K., Fontenele Domingues, M. A., Zuliani Stroppa, V. L., Marangoni de Oliveira, G., & Guenter Kieckbusch, T. (2015). Crystallization modifiers in lipid systems. *J. Food Sci. Technol.*, *52*(7), 3925–3946.

Baker, M. R., Bouzidi, L., Garti, N., & Narine, S. S. (2014a). Multi-length-scale elucidation of kinetic and symmetry effects on the behavior of stearic and oleic TAG. I: SOS and SSO. *J. Am. Oil Chem. Soc.*, *91*(4), 559–570.

Baker, M. R., Bouzidi, L., Garti, N., & Narine, S. S. (2014b). Multi-length-scale elucidation of kinetic and symmetry effects on the behavior of stearic and oleic TAG. II: OSO and SOO. *J. Am. Oil Chem. Soc.*, *91*(10), 1685–1694.

Barba, L., Arrighetti, G., & Calligaris, S. (2013). Crystallization and melting properties of extra virgin olive oil studied by synchrotron XRD and DSC. *Eur. J. Lipid Sci. Technol.*, *115*(3), 322–329.

Basiron, Y. (2005). Palm oil. In F. Shahidi (Ed.), *Bailey's industrial oil and fat products* (6th ed., pp. 333–429). John Wiley & Sons: Hoboken, NJ, USA.

Basso, R. C., Paula, A., Ribeiro, B., Helen, M., Antonio, L., Guaraldo, L. A., Oliveira, A., Pavie, L., & Grimaldi, R. (2010). Tripalmitin and monoacylglycerols as modifiers in the crystallisation of palm oil. *Food Chem.*, *122*(4), 1185–1192.

Bayés-García, L., Calvet, T., Cuevas-Diarte, M. À., Ueno, S., & Sato, K. (2011a). In situ synchrotron radiation X-ray diffraction study of crystallization kinetics of polymorphs of 1,3-dioleoyl-2-palmitoyl glycerol (OPO). *CrystEngComm*, *13*, 3592–3599.

Bayés-García, L., Calvet, T., Cuevas-Diarte, M. À., Ueno, S., & Sato, K. (2011b). Heterogeneous microstructures of spherulites of lipid mixtures characterized with synchrotron radiation microbeam X-ray diffraction. *CrystEngComm*, *13*(22), 6694–6705.

Bayés-García, L., Calvet, T., Cuevas-Diarte, M. À., Ueno, S., & Sato, K. (2013a). Crystallization and transformation of polymorphic forms of trioleoyl glycerol and 1,2-dioleoyl-3-rac-linoleoyl glycerol. *J. Phys. Chem. B*, *117*(31), 9170–9181.

Bayés-García, L., Calvet, T., Cuevas-Diarte, M. À., Ueno, S., & Sato, K. (2013b). In situ observation of transformation pathways of polymorphic forms of 1,3-dipalmitoyl-2-oleoyl glycerol (POP) examined with synchrotron radiation X-ray diffraction and DSC. *CrystEngComm*, *15*(2), 302–314.

Bayés-García, L., Calvet, T., Cuevas-Diarte, M. À., Ueno, S., & Sato, K. (2015a). Phase behavior of binary mixture systems of saturated-unsaturated mixed-acid triacylglycerols: Effects of glycerol structures and chain-chain interactions. *J. Phys. Chem. B*, *119*(12), 4417–4427.

Bayés-García, L., Calvet, T., Cuevas-Diarte, M. À., Rovira, E., Ueno, S., & Sato, K. (2015b). New textures of chocolate are formed by polymorphic crystallization and template Effects: Velvet chocolate. *Cryst. Growth Des.*, *15*(8), 4045–4054.

Bayés-García, L., Calvet, T., Cuevas-Diarte, M. À., & Ueno, S. (2016). In situ crystallization and transformation kinetics of polymorphic forms of saturated-unsaturated-unsaturated triacylglycerols: 1-Palmitoyl-2,3-dioleoyl glycerol, 1-stearoyl-2,3-dioleoyl glycerol, and 1-palmitoyl-2-oleoyl-3-linoleoyl glycerol. *Food Res. Int.*, *85*, 244–258.

Bayés-García, L., Calvet, T., Cuevas-Diarte, M. À., & Ueno, S. (2017). From trioleoyl glycerol to extra virgin olive oil through multicomponent triacylglycerol mixtures: Crystallization and polymorphic transformation examined with differential scanning calorimetry and X-ray diffration techniques. *Food Res. Int.*, *99*(June), 476–484.

Bayés-García, L., Calvet, T., & Cuevas-Diarte, M. À. (2018). Effects of dynamic temperature variations on microstructure and polymorphic behavior of lipid systems. In K. Sato (Ed.), *Crystallization of lipids. Fundamentals and applications in food, cosmetics and pharmaceuticals* (pp. 183–210). Wiley-Blackwell: Hoboken, NJ, USA..

Bayés-García, L., Aguilar-Jiménez, M., Calvet, T., Koyano, T., & Sato, K. (2019). Crystallization and melting behavior of cocoa butter in lipid bodies of fresh cacao beans. *Cryst. Growth Des.*, *19*(7), 4127–4137.

Bayés-García, L., Colomer-Llombart, E., Aguilar-Jiménez, M., & Calvet, T. (2021). Polymorphic fingerprint as an approach to authenticate Iberian pig categories. *J. Am. Oil Chem. Soc.*, *98*(11), 1093–1105.

Bayés-García, L., Yoshikawa, S., Aguilar-Jiménez, M., Ishibashi, C., Ueno, S., & Calvet, T. (2022). Heterogeneous nucleation effects of talc particles on polymorphic crystallization of cocoa butter. *Cryst. Growth Des.*, *22*(1), 213–227.

Bennema, P., Hollander, F. F. A., Boerrigther, S. X. M., Grimbergen, R. F. P., van de Streek, J., & Meekes, H. (2001). Morphological connected net-roughening transition theory. In *Crystallization processes in fat and lipid systems and polymorphism of fats and fatty acids* (pp. 99–150). Marcel Dekker: New York, NY, USA.

Bernstein, J. (2002). *Polimorphism in molecular crystals* (pp. 29–49). Oxford University Press Inc: New York, NY, USA.

Bhaggan, K., Smith, K. W., Blecker, C., & Danthine, S. (2018a). Polymorphism and kinetic behavior of binary mixtures of trisaturated triacylglycerols containing palmitic and stearic acid under non-isothermal conditions. *Eur. J. Lipid Sci. Technol.*, *120*(9), 1800072.

Bhaggan, K., Smith, K. W., Blecker, C., & Danthine, S. (2018b). Binary mixtures of tripalmitoylglycerol (PPP) and 1,3-dipalmitoyl-2-stearoyl-sn-glycerol (PSP): Polymorphism and kinetic phase behavior. *Eur. J. Lipid Sci. Technol.*, *120*(3), 1700306.

Boodhoo, M. V., Kutek, T., Filip, V., & Narine, S. S. (2008). The binary phase behavior of 1,3-dimyristoyl-2-stearoyl-sn-glycerol and 1,2-dimyristoyl-3-stearoyl-sn-glycerol. *Chem. Phys. Lipids*, *154*(1), 7–18.

Boodhoo, M. V., Bouzidi, L., & Narine, S. S. (2009a). The binary phase behavior of 1, 3-dipalmitoyl-2-stearoyl-sn-glycerol and 1, 2-dipalmitoyl-3-stearoyl-sn-glycerol. *Chem. Phys. Lipids*, *160*(1), 11–32.

Boodhoo, M. V., Bouzidi, L., & Narine, S. S. (2009b). The binary phase behavior of 1,3-dicaproyl-2-stearoyl-sn-glycerol and 1,2-dicaproyl-3-stearoyl-sn-glycerol. *Chem. Phys. Lipids*, *157*(1), 21–39.

Bots, P., Benning, L. G., Rodriguez-Blanco, J. D., Roncal-Herrero, T., & Shaw, S. (2012). Mechanistic insights into the crystallization of amorphous calcium carbonate (ACC). *Cryst. Growth Des.*, *12*(7), 3806–3814.

Bouzidi, L., Boodhoo, M. V., Kutek, T., Filip, V., & Narine, S. S. (2010). The binary phase behavior of 1,3-dilauroyl-2-stearoyl-sn-glycerol and 1,2-dilauroyl-3-stearoyl-sn-glycerol. *Chem. Phys. Lipids*, *163*(6), 607–629.

Bouzidi, L., & Narine, S. S. (2012a). Relationships between molecular structure and kinetic and thermodynamic controls in lipid systems. Part II: Phase behavior and transformation paths of SSS, PSS and PPS saturated triacylglycerols - Effect of chain length mismatch. *Chem. Phys. Lipids*, *165*(1), 77–88.

Bouzidi, L., & Narine, S. S. (2012b). Relationships between molecular structure and kinetic and thermodynamic controls in lipid systems Part III. Crystallization and phase behavior of 1-palmitoyl-2,3-stearoyl-sn-glycerol (PSS) and tristearoylglycerol (SSS) binary system. *Chem. Phys. Lipids*, *165*(1), 105–119.

Braipson-Danthine, S., & Gibon, V. (2007). Comparative analysis of triacylglycerol composition, melting properties and polymorphic behavior of palm oil and fractions. *Eur.*

J. Lipid Sci. Technol., *109*(4), 359–372.

Callaghan, P. T. (1977). The use of 13C spin relaxation to investigate molecular motion in liquid tristearin. *Chem. Phys. Lipids*, *19*(1), 56–73.

Campos, R., Narine, S. S., & Marangoni, A. G. (2002). Effect of cooling rate on the structure and mechanical properties of milk fat and lard. *Food Res. Int.*, *35*(10), 971–981.

Campos, R. (2005). Experimental methodology. In A. G. Marangoni (Ed.), *Fat crystal networks* (pp. 267–348). Marcel Dekker: New York, NY, USA.

Campos, R., Ollivon, M., & Marangoni, A. G. (2010). Molecular composition dynamics and structure of cocoa butter. *Cryst. Growth Des.*, *10*(1), 205–217.

Canapi, E. C., Agustin, Y. T. V., Moro, E. A., Pedrosa, E., & Bendaño, M. L. J. (2005). Coconut oil. In F. Shahidi (Ed.), *Bailey's industrial oil and fat products* (6th ed., pp. 123–148). John Wiley & Sons: Hoboken, NJ, USA.

Cebula, D. J., McClements, D. J., Povey, M. J. W., & Smith, P. R. (1992). Neutron diffraction studies of liquid and crystalline trilaurin. *J. Am. Oil Chem. Soc.*, *69*(2), 130–136.

Chaiseri, S., & Dimick, P. S. (1989). Lipid and hardness characteristics of cocoa butters from different geographic regions. *J. Am. Oil Chem. Soc.*, *66*(12), 1771–1776.

Chapman, G. M., Akehurst, E. E., & Wright, W. B. (1971). Cocoa butter and confectionery fats. Studies using programmed temperature X-ray diffraction and differential scanning calorimetry. *J. Am. Oil Chem. Soc.*, *48*(12), 824–830.

Chung, S. Y., Kim, Y. M., Kim, J. G., & Kim, Y. J. (2009). Multiphase transformation and Ostwalds rule of stages during crystallization ofametal phosphate. *Nat. Phys.*, *5*(1), 68–73.

Co, E., & Marangoni, A. G. (2020). Fat crystal networks. In F. Shahidi (Ed.), *Bailey's industrial oil and fat products* (7th ed., pp. 161–212). John Wiley & Sons: Hoboken, NJ, USA.

Corkery, R. W., Rousseau, D., Smith, P., Pink, D. A., & Hanna, C. B. (2007). A case for discotic liquid crystals in molten triglycerides. *Langmuir*, *23*(13), 7241–7246.

Costa, M. C., Boros, L. A. D., Souza, J. A., Rolemberg, M. P., Krähenbühl, M. A., & Meirelles, A. J. A. (2011). Solid-liquid equilibrium of binary mixtures containing fatty acids and triacylglycerols. *J. Chem. Eng. Data*, *56*(8), 3277–3284.

Craven, R. J., & Lencki, R. W. (2012). Triacylglycerol polymorphism is a stereochemical phenomenon. *Lipid Technol.*, *24*(9), 204–207.

D'Souza, V., deMan, J. M., & deMan, L. (1990). Short spacings and polymorphic forms of natural and commercial solid fats: A review. *J. Am. Oil Chem. Soc.*, *67*(11), 835–843.

Danthine, S., & Deroanne, C. (2003). Physical and textural characteristics of hydrogenated low-erucic acid rapeseed oil and low-erucic acid rapeseed oil blends. *J. Am. Oil Chem. Soc.*, *80*(2), 109–114.

Danthine, S., Delatte, S., Blecker, C., Smith, K. W., & Bhaggan, K. (2015). Crystallization behaviour of binary fat blends containing shea stearin as hard fat. *Eur. J. Lipid Sci. Technol.*, *117*(11), 1687–1699.

de Jong, S., & van Soest, T. C. (1978). Crystal structures and melting points of saturated triglycerides in the β-2 phase*. *Acta Crystallogr.*, *B34*, 1570–1583.

de Man, J. M., & Beers, A. M. (1987). Fat crystal networks: Structure and rheological properties. *J. Texture Stud.*, *18*(4), 303–318.

de Man, J. M. (1998). Functionality of palm oil in foods. *J. Food Lipids*, *5*(2), 159–170.

de Man, J. M., & de Man, L. (2001). Polymorphism and texture of fats. In N. Widlak, R. Hartel, & S. Narine (Eds.), *Crystallization and solidification properties of lipids* (pp. 225–236). AOCS Press: Champaign, IL, USA..

Deffense, E. (1985). Fractionation of palm oil. *J. Am. Oil Chem. Soc.*, *62*(2), 376–385.

Deroanne, C., Marcoen, J. M., Watelet, J. P., & Severin, M. (1977). La double cristallisation de l'huile de palme Mise en evidence par diffraction des rayons X et analyse calorimetrique differentielle. *J. Therm. Anal.*, *11*(1), 109–119.

Dibildox-Alvarado, E., Rodrigues, J. N., Gioielli, L. A., Toro-Vazquez, J. F., & Marangoni, A. G. (2004). Effects of crystalline microstructure on oil migration in a semisolid fat matrix. *Cryst. Growth Des.*, *4*(4), 731–736.

Directive 200/36/EC. *Cocoa and chocolate products intended for human consumption*. European Parliament, Council of the European Union. Retrieved from: https://eur-lex.europa.eu/legal-content/EN/TXT/PDF/?uri=CELEX:32000L0036&from=EN

Douaire, M., di Bari, V., Norton, J. E., Sullo, A., Lillford, P., & Norton, I. T. (2014). Fat crystallisation at oil-water interfaces. *Adv. Colloid Interface Sci.*, *203*, 1–10.

Elisabettini, P., Desmedt, A., Gibon, V., & Durant, F. (1995). Effect of sorbitan tristearate on the thermal and structural properties of monoacid triglycerides - influence of a "cis" or "trans" double bond. *Fat Sci. Technol.*, *97*(2), 65–69.

Engström, L. (1992). Triglyceride systems forming molecular compounds. *Fat Sci. Technol.*, *94*(5), 173–181.

Eskin, N. A. M., & List, G. R. (2017). Food applications of lipids. In C. C. Akoh (Ed.), *Food lipids. Chemistry, nutrition and biotechnology* (4th ed., pp. 421–452). CRC Press: Boca Raton, FL, USA.

EUROSTAT. Statistical Office of the European Communities (2021). *Main producers of chocolate in the EU*. Retrieved from: https://ec.europa.eu/eurostat/en/web/products-eurostat-news/-/ddn-20200831-1.

Floeter, E., Haeupler, M., & Sato, K. (2018). Molecular interactions and mixing phase behavior of lipid crystals. In K. Sato (Ed.), *Crystallization of lipids. Fundamentals and applications in food,*

cosmetics and pharmaceuticals (pp. 61–104). Wiley-Blackwell: Hoboken, NJ, USA.

Foubert, I., Dewettinck, K., van de Walle, D., Dijkstra, A. J., & Quinn, P. J. (2007). Physical properties: Structural and physical characteristics. In F. D. Gunstone, J. L. Harwood, & A. J. Dijkstra (Eds.), *The lipid handbook* (3rd ed., pp. 471–534). CRC Press: Boca Raton, FL, USA.

Foubert, I., Fredrick, E., Vereecken, J., Sichien, M., & Dewettinck, K. (2008). Stop-and-return DSC method to study fat crystallization. *Thermochim. Acta*, *471*(1–2), 7–13.

Fowler, M. S. (2009). Cocoa beans: From tree to factory. In S. T. Beckett (Ed.), *Industrial chocolate manufacture and use* (4th ed., pp. 10–47). Wiley-Blackwell: Oxford, UK.

Garti, N., Aronhime, J. S., & Sarig, S. (1989). The role of chain length and an emulsifier on the polymorphism of mixtures of triglycerides. *J. Am. Oil Chem. Soc.*, *66*(8), 1085–1089.

Ghazani, S. M., & Marangoni, A. G. (2018). New insights into the β polymorphism of 1,3-palmitoyl-stearoyl-2-oleoyl glycerol. *Cryst. Growth Des.*, *18*(9), 4811–4814.

Ghazani, S. M., & Marangoni, A. G. (2019a). The triclinic polymorphism of cocoa butter is dictated by its major molecular species, 1-palmitoyl, 2-oleoyl, 3-stearoyl glycerol (POS). *Cryst. Growth Des.*, *19*(1), 90–97.

Ghazani, S. M., & Marangoni, A. G. (2019b). The ternary solid state phase behavior of triclinic POP, POS and SOS and its relationship to CB and CBE properties. *Cryst. Growth Des.*, *19*(2), 704–713.

Ghotra, B. S., Dyal, S. D., & Narine, S. S. (2002). Lipid shortenings: A review. *Food Res. Int.*, *35*(10), 1015–1048.

Gibon, V., & Durant, F. (1985). Etude du polymorphisme et de l'intersolubilite de triglycerides palmito-oleiques par diffraction rx de poudres et analyse calorimetrique differentielle. *Bull. Des Sociétés Chim. Belges*, *94*(11–12), 1009–1020.

Gibon, V., Durant, F., & Deroanne, C. (1986). Polymorphism and intersolubility of some palmitic, stearic and oleic triglycerides: PPP, PSP and POP. *J. Am. Oil Chem. Soc.*, *63*(8), 1047–1055.

Gordon, M. H., Padley, F. B., & Timms, R. E. (1979). Factors influencing the use of vegetable fats in chocolate. *Fette, Seifen, Anstrichm.*, *81*(3), 116–121.

Goto, M., Kodali, D. R., Small, D. M., Honda, K., Kozawa, K., & Uchida, T. (1992). Single crystal structure of a mixed-chain triacylglycerol: 1,2-Dipalmitoyl-3-acetyl-sn-glycerol. *Proc. Natl. Acad. Sci. U. S. A.*, *89*(17), 8083–8086.

Gregersen, S. B., Andersen, M. D., Hammershøj, M., & Wiking, L. (2017). Impact of triacylglycerol composition on shear-induced textural changes in highly saturated fats. *Food Chem.*, *215*, 438–446.

Gresti, J., Bugaut, M., Maniongui, C., & Bezard, J. (1993). Composition of molecular species of

triacylglcyerols in bovine milk fat. *J. Dairy Sci.*, *76*(7), 1850–1869.

Grimaldi, R., Aparecida, L., Gonçalves, G., & Gioielli, L. A. (2001). Interactions in interesterified palm and palm kernel oils mixtures. I-Solid fat content and consistency. *Grasas y Aceites*, *52*(6), 349–354.

Gunstone, F. D. (2006). Minor specialty oils. In F. Shahidi (Ed.), *Nutraceuticals and specialty lipids and their co-products* (pp. 91–126). CRC Press: Boca Raton, FL, USA.

Gunstone, F. D., Harwood, J. L., & Dijkstra, A. J. (2007). *The lipid handbook* (F. D. Gunstone, J. L. Harwood, & A. J. Dijkstra (eds.); 3rd ed.). CRC Press; Boca Raton, FL, USA.

Gunstone, F. D. (2013). Composition and properties of edible oils. In W. Hamm, R. J. Hamilton, & G. Calliaw (Eds.), *Edible oil processing* (2nd ed., pp. 1–40). Wiley-Blackwell: Oxford, UK.

Hachiya, I., Koyano, T., & Sato, K. (1989). Seeding effects on solidification behavior of cocoa butter and dark chocolate. II. Physical properties of dark chocolate. *J. Am. Oil Chem. Soc.*, *66*(12), 1763–1770.

Hagemann, J. W., Tallent, W. H., Barve, J. A., Ismail, I. A., & Gunstone, F. D. (1975). Polymorphism in single-acid triglycerides of positional and geometric isomers of octadecenoic acid. *J. Am. Oil Chem. Soc.*, *52*, 204–207.

Hartel, R. W., von Elbe, J. H., & Hofberger, R. (2018). Confectionery science and technology. In *Confectionery science and technology*. Springer international Publishing: Gewerbestrasse, Switzerland .

Helmholdt, R. B., Peschar, R., & Schenk, H. (2002). Structure of C15-, C17- and C19-mono-acid β-triacylglycerols. *Acta Crystallogr. Sect. B*, *B58*, 134–139.

Hernqvist, L. (1984). On the structure of triglycerides in the liquid state and fat crystallization. *Fette, Seifen, Anstrichm.*, *86*(8), 297–300.

Herrera, M. L., Falabella, C., Melgarejo, M., & Añón, M. C. (1998). Isothermal crystallization of hydrogenated sunflower oil: I-nucleation. *J. Am. Oil Chem. Soc.*, *75*(10), 1273–1280.

Hikosaka, M., Sakurai, K., Ohigashi, H., & Keller, A. (1994). Role of transient metastable hexagonal phase in the formation of extended chain single crystals of vinylidene fluoride and trifluoroethylene copolymers. *Jpn. J. Appl. Phys.*, *33*(1R), 214.

Himawan, C., Starov, V. M., & Stapley, A. G. F. (2006). Thermodynamic and kinetic aspects of fat crystallization. *Adv. Colloid Interface Sci.*, *122*(1–3), 3–33.

Himawan, C., MacNaughtan, W., Farhat, I. A., & Stapley, A. G. F. (2007). Polymorphic occurrence and crystallization rates of tristearin/tripalmitin mixtures under non-isothermal conditions. *Eur. J. Lipid Sci. Technol.*, *109*(1), 49–60.

Hoffman, J. D., Davis, G. T., & Lauritzen, J. I., E. (1976). The rate of crystallization of linear polymers with chain folding. In N. B. Hannay (Ed.), *Treatise on solid state chemistry. Volume*

3. Crystalline and noncrystalline solids (pp. 497–614). Plenum Press: New York, NY, USA.

Hondoh, H., Ueno, S., & Sato, K. (2018). Fundamental aspects of crystallization of lipids. In K. Sato (Ed.), *Crystallization of lipids. Fundamentals and applications in food, cosmetics and pharmaceuticals* (pp. 105–142). Wiley-Blackwell: Hoboken, NJ USA.

Huyghebaert, A., & Hendrickx, H. (1971). Polymorphism of cocoa butter, shown by differential scanning calorimetry. *Leb. Und-Technologie*, *4*, 59–63.

Ikeda, E., Ueno, S., Miyamoto, R., & Sato, K. (2010). Phase behavior of a binary mixture of 1,3-dipalmitoyl-2-oleoyl-sn-glycerol and 1,3-dioleoyl-2-palmitoyl-sn-glycerol in n-dodecane solution. *J. Phys. Chem. B*, *114*(34), 10961–10969.

Ikeda-Naito, E., Hondoh, H., Ueno, S., & Sato, K. (2014). Mixing phase behavior of 1,3-dipalmitoyl-2-oleoyl-sn-glycerol (POP) and 1,2-dipalmitoyl-3-oleoyl-rac-glycerol (PPO) in n-dodecane solution. *J. Am. Oil Chem. Soc.*, *91*(11), 1837–1848.

ISO. Internatinal Organization for Standardization (2008). *Animal and vegetable fats and oils - Determination of solid fat content by pulsed NMR - Part 1*: Direct method (ISO standard no 8292-1:2008).

Jensen, L. H., & Mabis, A. J. (1963). Crystal structure of β-tricaprin. *Nature*, *197*, 681–682.

Johansson, D., & Bergenståhl, B. (1995). Sintering of fat crystal networks in oil during post-crystallization processes. *J. Am. Oil Chem. Soc.*, *72*(8), 911–920.

Kang, K. K., Jeon, H., Kim, I. H., & Kim, B. H. (2013). Cocoa butter equivalents prepared by blending fractionated palm stearin and shea stearin. *Food Sci. Biotechnol.*, *22*(2), 347–352.

Kaufmann, N., Andersen, U., & Wiking, L. (2012). The effect of cooling rate and rapeseed oil addition on the melting behaviour, texture and microstructure of anhydrous milk fat. *Int. Dairy J.*, *25*(2), 73–79.

Kellens, M., Meeussen, W., & Reynaers, H. (1990). Crystallization and phase transition studies of tripalmitin. *Chem. Phys. Lipids*, *55*(2), 163–178.

Kellens, M., Meeussen, W., Gehrke, R., & Reynaers, H. (1991a). Synchrotron radiation investigations of the polymorphic transitions of saturated monoacid triglycerides. Part 1: Tripalmitin and tristearin. *Chem. Phys. Lipids*, *58*(1–2), 131–144.

Kellens, M., Meeussen, W., Hammersley, A., & Reynaers, H. (1991b). Synchrotron radiation investigations of the polymorphic transitions in saturated monoacid triglycerides. Part 2: Polymorphism study of a 50:50 mixture of tripalmitin and tristearin during crystallization and melting. *Chem. Phys. Lipids*, *58*(1–2), 145–158.

Kellens, M., Meeussen, W., & Reynaers, H. (1992). Study of the polymorphism and the crystallization kinetics of tripalmitin: A microscopic approach. *J. Am. Oil Chem. Soc.*, *69*(9), 906–911.

Kellens, M., & Reynaers, H. (1992a). Study of the polymorphism of saturated monoacid

triglycerides II: Polymorphic behaviour of a 50/50 mixture of tripalmitin and tristearin. *Fat Sci. Technol.*, *8*(286–293).

Kellens, M., & Reynaers, H. (1992b). Study of the polymorphism of saturated monoacid triglycerides I: Melting and crystallization behavior of tristearin. *Fett-Lipid*, *94*(3), 94–100.

Kellens, M., Gibon, V., Hendrix, M., & De Greyt, W. (2007). Palm oil fractionation. *Eur. J. Lipid Sci. Technol.*, *109*(4), 336–349.

Keller, A., Hikosaka, M., Rastogi, S., Toda, A., Barham, P. J., & Goldbeck-Wood, G. (1994). An approach to the formation and growth of new phases with application to polymer crystallization: Effect of finite size, metastability, and Ostwald's rule of stages. *J. Mater. Sci.*, *29*(10), 2579–2604.

Kerridge, K. (1952). Melting-point diagrams for binary triglyceride systems. *J. Chem. Soc.*, *0*, 4577–4579.

Knoester, M., de Bruyne, P., & van den Tempel, M. (1968). Crystallization of triglycerides at low supercooling. *J. Cryst. Growth*, *3*(4), 776–780.

Knoester, M., De Bruijne, P., & van Den Tempel, M. (1972). The solid-liquid equilibrium of binary mixtures of triglycerides with palmitic and stearic chains. *Chem. Phys. Lipids*, *9*(4), 309–319.

Kodali, D. R., Atkinson, D., Redgrave, T. G., & Small, D. M. (1984). Synthesis and polymorphism of 1,2-dipalmitoyl-3-acyl-sn-glycerols. *J. Am. Oil Chem. Soc.*, *61*(6), 1078–1084.

Kodali, D. R., Atkinson, D., Redgrave, T. G., & Small, D. M. (1987). Structure and polymorphism of 18-carbon fatty acyl triacylglycerols: Effect of unsaturation and substitution in the 2-position. *J. Lipid Res.*, *28*(4), 403–413.

Kodali, D. R., Atkinson, D., & Small, D. M. (1989). Molecular packing of 1,2-dipalmitoyl-3-decanoyl-sn-glycerol (PP10): Bilayer, trilayer and hexalayer structures. *J. Phys. Chem.*, *93*(11), 4683–4691.

Kodali, D. R. (2014). Trans fats: Health, chemistry, functionality, and potential replacement solutions. In D. R. Kodali (Ed.), *Trans fats replacement solutions* (pp. 1–39). AOCS Press: Urbana, IL, USA.

Koyano, T., Hachiya, I., Arishima, T., Sato, K., & Sagi, N. (1989). Polymorphism of POP and SOS. II. Kinetics of melt crystallization. *J. Am. Oil Chem. Soc.*, *66*(5), 675–679.

Koyano, T., Hachiya, I., & Sato, K. (1992). Phase behavior of mixed systems of SOS and OSO. *J. Phys. Chem.*, *96*(25), 10514–10520.

Koyano, T., Kato, Y., Hachiya, I., & Unemura, R. (1993). Crystallization behavior of ternary mixture of POP/POS/SOS. *J. Japan Oil Chem. Soc.*, *42*, 453–457.

Laia, O. M., Ghazalia, H. M., Cho, F., & Chong, C. L. (2000). Physical and textural properties

of an experimental table margarine prepared from lipase-catalysed transesterified palm stearin: Palm kernel olein mixture during storage. *Food Chem.*, *71*(2), 173–179.

Larsson, K. (1964). The crystal structure of the β-form of trilaurin. *Ark. För Kemi*, *23*, 1–15.

Larsson, K. (1966). Classification of glyceride crystal forms. *Acta Chem. scand., 20*(8), 2255–2260.

Larsson, K. (1972). Molecular arrangements in glycerides. *Fette, Seifen, Anstrichm.*, *74*(3), 136–142.

Larsson, K., Quinn, P., Sato, K., & Tiberg, F. (2006). *Lipids: Structure, physical properties and functionality*. The Oily Press: Bridgewater, UK.

Lipp, M., & Anklam, E. (1998). Review of cocoa butter and alternative fats for use in chocolate - Part A. Compositional data. *Food Chem.*, *62*(1), 73–97.

Liu, C., Meng, Z., Cao, P., Jiang, J., Liang, X., Piatko, M., Campbell, S., Lo, S. K., & Liu, Y. (2018). Visualized phase behavior of binary blends of coconut oil and palm stearin. *Food Chem.*, *266*(January), 66–72.

Liu, C., Meng, Z., Chai, X., Liang, X., Piatko, M., Campbell, S., & Liu, Y. (2019). Comparative analysis of graded blends of palm kernel oil, palm kernel stearin and palm stearin. *Food Chem.*, *286*, 636–643.

Loisel, C., Keller, G., Lecq, G., Bourgaux, C., & Ollivon, M. (1998). Phase transitions and polymorphism of cocoa butter. *J. Am. Oil Chem. Soc.*, *75*(4), 425–439.

Los, J., & Flöter, E. (1999). Construction of kinetic phase diagrams. *Phys. Chem. Chem. Phys.*, *1*(18), 4251–4257.

Los, J. H., van Enckevort, W. J. P., Vlieg, E., Flöter, E., & Gandolfo, F. G. (2002). Metastable states in multicomponent liquid-solid systems II : Kinetic phase separation. *J. Phys. Chem. B*, *106*, 7331–7339.

Lu, C., Zhang, B., Zhang, H., Guo, Y., Dang, L., Liu, Z., Shu, Q., & Wang, Z. (2019). Solid–liquid phase equilibrium and phase behaviors for binary mixtures composed of tripalmitoylglycerol (PPP), 1,3-dipalmitoyl-2-oleoyl-glycerol (POP), and 1,2-dioleoyl-3-palmitoyl-glycerol (POO). *Ind. Eng. Chem. Res.*, *58*(23), 10044–10052.

Lusi, M. (2018). A rough guide to molecular solid solution: Design, synthesis and characterization of mixed crystals. *CrystEngComm*, *20*(44), 7042–7052.

Lutton, E. S., Jackson, F. L., & Quimby, O. T. (1948). The polymorphism of the mixed triglycerides of palmitic and stearic acids. *J. Am. Oil Chem. Soc.*, *70*, 2441–2445.

Lutton, E. S. (1951). The polymorphism of the disaturated triglycerides-OSS, OPP, POS,OPS and OSP. *J. Am. Chem. Soc.*, *73*(12), 5595–5598.

Lutton, E. S. (1955). Phase behavior of triglyceride mixtures involving primarily tristearin, 2-oleyldistearin, and triolein. *J. Am. Oil Chem. Soc.*, *32*(2), 49–53.

MacNaughtan, W., Farhat, I. A., & Himawan, C. (2006). A differential scanning calorimetry study of the crystallization kinetics of tristearin-tripalmitin mixtures. *J. Am. Oil Chem. Soc.*, *83*(1), 1–9.

Macridachis, J., Bayés-García, L., & Calvet, T. (2020). An insight into the solid-state miscibility of triacylglycerol crystals. *Molecules*, *25*(19), 4562.

Macridachis, J., Bayés-García, L., & Calvet, T. (2021). Mixing phase behavior of tripalmitin and oleic-rich molecular compound-forming triacylglycerols. *Ind. Eng. Chem. Res.*, *60*(15), 5374–5384.

Macridachis, J., Bayés-García, L., & Calvet, T. (2022). Solid phase behavior of mixture systems based on tripalmitoyl glycerol and monounsaturated triacylglycerols forming a molecular compound. *Phys. Chem. Chem. Phys., 24*, 3749–3760.

Man, Y. B. C., & Manaf, M. A. (2006). Medium-chain triacylglycerols. In F. Shahidi (Ed.), *Nutraceuticals and specialty lipids and their co-products* (pp. 27–56). CRC Press: Boca Raton, FL, USA.

Manning, D. M., & Dimick, P. S. (1985). Crystal morphology of cocoa butter. *Food Microstruct.*, *4*(2), 249–265.

Marangoni, A. G., & Lencki, R. W. (1998). Ternary phase behavior of milk fat fractions. *J. Agric. Food Chem.*, *46*(10), 3879–3884.

Marangoni, A. G., & McGauley, S. E. (2003). Relationship between crystallization behavior and structure in cocoa butter. *Cryst. Growth Des.*, *3*(1), 95–108.

Marangoni, A. G. (2012). *Structure-function analysis of edible fats* (pp. 1–4). AOCS Press: Urbana, IL, USA.

Marangoni, A. G., Acevedo, N., Maleky, F., Co, E., Peyronel, F., Mazzanti, G., Quinn, B., & Pink, D. (2012). Structure and functionality of edible fats. *Soft Matter*, *8*(5), 1275–1300.

Marangoni, A. G., & Wesdorp, L. H. (2013a). Nucleation and crystalline growth kinetics. In A. G. Marangoni & L. H. Wesdorp (Eds.), *Structure and properties of fat crystal networks* (2nd ed., pp. 27–100). CRC Press: Boca Raton, FL, USA.

Marangoni, A. G., & Wesdorp, L. H. (2013b). Crystallography and polymorphism. In A. G. Marangoni & L. H. Wesdorp (Eds.), *Structure and properties of fat crystal networks* (2nd ed., pp. 1–24). CRC Press: Boca Raton, FL, USA.

Marikkar, J. M. N., Saraf, D., & Dzulkifly, M. H. (2013). Effect of fractional crystallyzation on composition and thermal behavior of coconut oil. *Int. J. Food Prop.*, *16*(6), 1284–1292.

Martini, S. (2013). Sonocrystallization of fats. In R. W. Hartel, J. P. Clark, D. Rodrígues-Lázaro, & D. Topping (Eds.), *Springer briefs in food, health and nutrition*. Springer: New York, NY, USA.

Maximo, G. J., Costa, M. C., Coutinho, J. A. P., & Meirelles, A. J. A. (2014). Trends and

demands on soli-liquid equilibrium of lipidic mixtures. *RSC Adv.*, *4*, 31840–31850.

Meng, Z., Liu, Y., Shan, L., Jin, Q., Wang, F., & Wang, X. (2011). Specialty fats from beef tallow and canola oil: Establishment of reaction conditions, characterization of products, and evaluation of crystal stability. *Food Biophys.*, *6*(1), 115–126.

Merken, G. V., & Vaeck, S. V. (1980). Etude du polymorphisme du beurre de cacao par calorimétrie DSC. *Leb. Und-Technologie*, *13*, 314–317.

Metin, S., & Hartel, R. W. (2005). Crystallization of fats and oils. In F. Shahidi (Ed.), *Bailey's industrial oil and fat products* (6th ed., pp. 45–76). Jon Wiley & Sons: Hoboken, NJ, USA.

Minato, A., Ueno, S., Yano, J., Wang, Z. H., Seto, H., Amemiya, Y., & Sato, K. (1996). Synchrotron radiation X-ray diffraction study on phase behavior of PPP-POP binary mixtures. *J. Am. Oil Chem. Soc.*, *73*(11), 1567–1572.

Minato, A., Ueno, S., Smith, K., Amemiya, Y., & Sato, K. (1997a). Thermodynamic and kinetic study on phase behavior of binary mixtures of POP and PPO forming molecular compound systems. *J. Phys. Chem. B*, *101*(18), 3498–3505.

Minato, A., Ueno, S., Yano, J., Smith, K., Seto, H., Amemiya, Y., & Sato, K. (1997b). Thermal and structural properties of sn-1,3-dipalmitoyl-oleoylglycerol and sn-1,3-dioleoyl-2-palmitoylglycerol binary mixtures examined with synchrotron radiation X-ray diffraction. *J. Am. Oil Chem. Soc.*, *74*(10), 1213–1220.

Minato, A., Yano, J., Ueno, S., Smith, K., & Sato, K. (1997c). FT-IR study on microscopic structures and conformations of POP-PPO and POP-OPO molecular compounds. *Chem. Phys. Lipids*, *88*(1), 63–71.

Mizobe, H., Tanaka, T., Hatakeyama, N., Nagai, T., Ichioka, K., Hondoh, H., Ueno, S., & Sato, K. (2013). Structures and binary mixing characteristics of enantiomers of 1-oleoyl-2,3-dipalmitoyl-sn-glycerol (S-OPP) and 1,2-dipalmitoyl-3-oleoyl-sn-glycerol (R-PPO). *J. Am. Oil Chem. Soc.*, *90*(12), 1809–1817.

Moran, D. P. J. (1963). Phase behaviour of some palmito-oleo triglyceride systems. *J. Appl. Chem.*, *13*(2), 91–100.

Mullin, J. W. (2001). *Crystallization* (4th ed., pp. 181–215). Butterworth-Heinemann: Oxford, UK.

Mykhaylyk, O. O., Castelletto, V., Hamley, I. W., & Povey, M. J. W. (2004). Structure and transformation of low-temperature phases of 1,3-distearoyl-2-oleoyl glycerol. *Eur. J. Lipid Sci. Technol.*, *106*(5), 319–324.

Mykhaylyk, O. O., Smith, K. W., Martin, C. M., & Ryan, A. J. (2007). Structural models of metastable phases occurring during the crystallization process of saturated/unsaturated triacylglycerols. *J. Appl. Crystallogr.*, *40*, 297–302.

Mykhaylyk, O. O., & Martin, C. M. (2009). Effect of unsaturated acyl chains on structural

transformations in triacylglycerols. *Eur. J. Lipid Sci. Technol.*, *111*(3), 227–235.

Nagai, T., Kinoshita, T., Kasamatsu, E., Yoshinaga, K., Mizobe, H., Yoshida, A., Itabashi, Y., & Gotoh, N. (2020). Simultaneous quantification of mixed-acid triacylglycerol positional isomers and enantiomers in palm oil and lard by chiral high-performance liquid chromatography coupled with mass spectrometry. *Symmetry*, *12*(9), 1385.

Nagpal, T., Sahu, J. K., Khare, S. K., Bashir, K., & Jan, K. (2021). Trans fatty acids in food: A review on dietary intake, health impact, regulations and alternatives. *J. Food Sci.*, *86*(12), 5159–5174.

Nakanishi, K., Mikiya, Y., Ishiguro, T., & Ueno, S. (2018). Crystallization behavior of molecular compound in binary mixture system of 1,3-dioleoyl-2-palmitoyl-sn-glycerol and 1,3-dipalmitoyl-2-oleoyl-sn-glycerol. *J. Am. Oil Chem. Soc.*, *95*(1), 51–59.

Nakanishi, K., & Ueno, S. (2020). Mixing ratio and cooling rate dependence of molecular compound formation in OPO/POP binary mixture. *Molecules*, *25*(22), 5253.

Narine, S. S., & Marangoni, A. G. (1999). Fractal nature of fat crystal networks. *Phys. Rev. E*, *59*(2), 1908–1920.

Narine, S. S., & Marangoni, A. G. (2005). Microstructure. In A. G. Marangoni (Ed.), *Fat crystal networks* (pp. 179–254). Marcel Dekker: New Yoek, NY, USA.

Nillson, J. (1986). Measuring solid fat content. *Manuf. Confect.*, *5*, 88–91.

Noorzyanna, Y., Marikkar, N., Mustafa, S., & Mat Sahri, M. (2017). Composition and thermal analysis of ternary mixtures of avocado fat:palm stearin:cocoa butter (Avo:PS:CB). *Int. J. Food Prop.*, *20*(2), 465–474.

Norazlina, M. R., Jahurul, M. H. A., Hasmadi, M., Mansoor, A. H., Norliza, J., Patricia, M., Ramlah George, M. R., Noorakmar, A. W., Lee, J. S., & Fan, H. Y. (2021). Trends in blending vegetable fats and oils for cocoa butter alternative application: A review. *Trends Food Sci. Technol.*, *116*, 102–114.

Norlida, H. M., Md. Ali, A. R., & Muhadhir, I. (1996). Blending of palm oil, palm stearin and palm kernel oil in the preparation of table and pastry margarine. *Int. J. Food Sci. Nutr.*, *47*(1), 71–74.

Norris, R. (1977). The physical properties of triacylglcyerols in relation to milkfat. Doctoral thesis, Massey University, Auckland, New Zealand.

O'Brien, R. D. (2009). *Fats and oils. Formulating and processing for applications* (pp. 263–339). CRC: Boca Raton, FL, USA Press.

Ostwald, W. (1897). Studies of the formation and transformation of solid substances. *Zeitschrift Für Phys. Chemie*, *22U*(1), 289–330.

Perez, M., Lopez-Yerena, A., & Vallverdú-Queralt, A. (2022). Traceability, authenticity and sustainability of cocoa and chocolate products: A challenge for the chocolate industry.

Crit. Rev. Food Sci. Nutr., *62*(2), 475–489.

PerkinElmer. (1982). *Instructions Model DSC-4*. Norwalk, CT, USA.

Peyronel, M. F., Acevedo, N. C., & Marangoni, A. G. (2010). Structural and mechanical properties of fats and their implications for food quality. In L. H. Skibsted, J. Risbo, & M. L. Andersen (Eds.), *Chemical deterioration and physical instability of food and beverages* (pp. 216–259). CRC Press: Boca Raton, FL, USA.

Peyronel, F., & Campos, R. (2012). Methods used in the study of physical properties of fats. In A. G. Marangoni (Ed.), *Structure-function analysis of edible fats* (pp. 231–294). AOCS Press: Urbana, IL, USA.

Pink, D. A., Hanna, C. B., Sandt, C., MacDonald, A. J., MacEachern, R., Corkery, R., & Rousseau, D. (2010). Modeling the solid-liquid phase transition in saturated triglycerides. *J. Chem. Phys.*, *132*(5), 254502.

Precht, D., & Frede, E. (1977). Die kristallstruktur der fette I. Molekülanordnungen von gesättingent tryglyceriden und tryglyceridgemischen. *Kieler Milchwirtsch. Forschungsberichte*, *29*, 265–285.

Rahim, M. A. A., Kuen, L. P., Fisal, A., Nazaruddin, R., & Sabariah, S. (1998). Fat interactions and physical changes in 'melt-away alike' chocolate during storage. In S. S. Koseoglu, K. C. Rhee, & R. F. Wilson (Eds.), *Proceedings of conference on oilseed and edible oils processing, Istanbul 1996, Volume 2* (pp. 141–143). AOCS Press: Champaign, IL, USA.

Ramel, P. R., Campos, R., & Marangoni, A. G. (2018). Effects of shear and cooling rate on the crystallization behavior and structure of cocoa butter: Shear applied during the early stages of nucleation. *Cryst. Growth Des.*, *18*(2), 1002–1011.

Ray, J., Smith, K. W., Bhaggan, K., Nagy, Z. K., & Stapley, A. G. F. (2013). Crystallization and polymorphic behavior of shea stearin and the effect of removal of polar components. *Eur. J. Lipid Sci. Technol.*, *115*(10), 1094–1106.

Rigolle, A., Goderis, B., Van Den Abeele, K., & Foubert, I. (2016). Isothermal crystallization behavior of cocoa butter at 17 and 20 °C with and without limonene. *J. Agric. Food Chem.*, *64*(17), 3405–3416.

Rodriguez-Negrette, A. C., Huck-Iriart, C., & Herrera, M. L. (2019). Physical chemical properties of shea/cocoa butter blends and their potential for chocolate manufacture. *J. Am. Oil Chem. Soc.*, *96*(3), 239–248.

Rossell, J. B. (1967). Phase diagrams of triglyceride systems. In R. Paoletti & D. Kritchevsky (Eds.), *Advances in lipid research* (pp. 355–408). Academic Press Inc: London, UK.

Rossell, J. B. (1985). Fractionation of lauric oils. *J. Am. Oil Chem. Soc.*, *62*(2), 385–390.

Rousset, P., & Rappaz, M. (1996). Crystallization kinetics of the pure triacylglycerols glycerol-1,3-dipalmitate-2-oleate, glycerol-1-palmitate-2-oleate-3-stearate, and glycerol-1,3-

distearate-2-oleate. *J. Am. Oil Chem. Soc.*, *73*(8), 1051–1057.

Rousset, P., Rappaz, M., & Minner, E. (1998). Polymorphism and solidification kinetics of the binary system POS-SOS. *J. Am. Oil Chem. Soc.*, *75*(7), 857–864.

Rousset, P. (2002). Modeling crystallization kinetics of triacylglcyerols. In A. G. Marangoni & S. S. Narine (Eds.), *Physical properties of lipids* (pp. 1–36). Marcel Dekker: New York, NY, USA.

Sabariah, S., Ali, A. R. M., & Chong, C. L. (1998). Chemical and physical characteristics of cocoa butter substitutes, milk fat and Malaysian cocoa butter blends. *J. Am. Oil Chem. Soc.*, *75*(8), 905–910.

Sasaki, M., Ueno, S., & Sato, K. (2012). Polymorphism and mixing phase behavior of major triacylglycerols of cocoa butter. In N. Garti & N. R. Widlak (Eds.), *Cocoa butter and related compounds* (pp. 151–172). AOCS Press: Urbana, IL, USA.

Sato, K., & Kuroda, T. (1987). Kinetics of melt crystallization and transformation of tripalmitin polymorphs. *J. Am. Oil Chem. Soc.*, *64*(1), 124–127.

Sato, K., Arishima, T., Wang, Z. H., Okima, K., Sagi, N., & Mori, H. (1989). Polymorphism of POP and SOS. I. Occurrence and polymorphic transformation. *J. Am. Oil Chem. Soc.*, *66*(5), 664–674.

Sato, K. (1999). Solidification and phase transformation behaviour of food fats – a review. *Fett-Lipid*, *101*, 467–474.

Sato, K. (2001a). Molecular aspects in fat polymorphism. In N. R. Widlak, R. W. Hartel, & S. S. Narine (Eds.), *Crystallization and solidification properties of lipids* (pp. 1–16). AOCS Press: Champaign, IL, USA.

Sato, K. (2001b). Crystallization behaviour of fats and lipids — a review. *Chem. Eng. Sci.*, *56*(7), 2255–2265.

Sato, K., Goto, M., Yano, J., Honda, K., Kodali, D. R., & Small, D. M. (2001). Atomic resolution structure analysis of β' polymorph crystal of a triacylglycerol: 1,2-Dipalmitoyl-3-myristoyl-sn-glycerol. *J. Lipid Res.*, *42*(3), 338–345.

Sato, K., & Koyano, T. (2001). Crystallization properties of cocoa butter. In N. Garti & K. Sato (Eds.), *Crystallization processes in fats and lipid systems* (pp. 429–456). Marcel Dekker: New York, NY, USA.

Sato, K., & Ueno, S. (2011). Crystallization, transformation and microstructures of polymorphic fats in colloidal dispersion states. *Curr. Opin. Colloid Interface Sci.*, *16*(5), 384–390.

Sato, K. (2012). Polymorphic properties of palm oil and its major component triacyglycerols. In O.-M. Lai, C.-P. Tan, & C. C. Akoh (Eds.), *Palm oil: Production, processing, characterization, and uses* (pp. 393–429). AOCS Press: Urbana, IL, USA.

Sato, K., Bayés-García, L., Calvet, T., Cuevas-Diarte, M. À., & Satoru, U. (2013). External factors affecting polymorphic crystallization of lipids. *Eur. J. Lipid Sci. Technol.*, *115*, 1224–1238.

Sazaki, G., Kurihara, K., Nakada, T., Miyashita, S., & Komatsu, H. (1996). A novel approach to the solubility measurement of protein crystals by two-beam interferometry. *J. Cryst. Growth*, *169*(2), 355–360.

Seddon, J. M. (1998). Structural studies of liquid crystals by X-ray diffraction. In D. Demus, J. Goodby, G. . Gray, H. W. Spiess, & V. Vill (Eds.), *Handbook of liquid crystals* (pp. 635–679). Wiley-VCH: Weinheim, Germany.

Segman, O., Wiesman, Z., & Yarmolinsky, L. (2012). Methods and technologies related to shea butter chemophysical properties and to the delivery of bioactives in choolate and related products. In *Cocoa butter and related compounds* (pp. 417–442). AOCS Press: Urbana, IL, USA.

Seilert, J., Moorthy, A. S., Kearsley, A. J., & Flöter, E. (2021). Revisiting a model to predict pure triglyceride thermodynamic properties: Parameter optimization and performance. *J. Am. Oil Chem. Soc.*, *98*(8), 837–850.

Shahidi, F., & Senanayake, S. P. J. N. (2006). Nutraceutical and specialty lipids. In F. Shahidi (Ed.), *Nutraceuticals and specialty lipids and their co-products* (pp. 1–26). CRC Press: Boca Raton, FL, USA.

Shukla, V. K. . (2005). Confectionery lipids. In F. Shahidi (Ed.), *Bailey's industrial oil and fat products* (6th ed., pp. 159–174). John Wiley & Sons: Hoboken, NJ, USA.

Sibbald, A. N., Carney, J. R., & Marangoni, A. G. (2016). Enhanced structuring of fat with reduced saturates using mixed molecular compounds. *J. Am. Oil Chem. Soc.*, *93*(11), 1441–1452.

Silva, T. J., Barrera-Arellano, D., & Ribeiro, A. P. B. (2021). Margarines: Historical approach, technological aspects, nutritional profile, and global trends. *Food Res. Int.*, *147*, 110486.

Simpson, T. D., & Hagemann, J. W. (1982). Evidence of two β' phases in tristearin. *J. Am. Oil Chem. Soc.*, *59*(4), 169–171.

Small, D. M. (1984). Lateral chain packing in lipids and membranes. *J. Lipid Res.*, *25*(13), 1490–1500.

Small, D. M. (1986). *The physical chemistry of lipids: From alkanes to phospholipids*. Plenum Press: New York, NY, USA.

Smith, K. W. (2001). Crystallization of palm oil and its fractions. In N. Garti & K. Sato (Eds.), *Crystallization processes in fats and lipid systems* (pp. 357–380). Marcel Dekker: New York, NY, USA.

Smith, K. W., Cain, F. W., & Talbot, G. (2005). Crystallisation of 1,3-dipalmitoyl-2-

oleoylglycerol and tripalmitoylglycerol and their mixtures from acetone. *Eur. J. Lipid Sci. Technol.*, *107*(9), 583–593.

Smith, K. W. (2012). Confectionery fats. In N. Garti & N. R. Widlak (Eds.), *Cocoa butter and related compounds* (pp. 475–496). AOCS Press: Urbana, IL, USA.

Smith, K. W., Bhaggan, K., Talbot, G., & Van Malssen, K. F. (2011). Crystallization of fats: Influence of minor components and additives. *J. Am. Oil Chem. Soc.*, *88*(8), 1085–1101.

Smith, K. W., Bhaggan, K., & Talbot, G. (2013). Phase behavior of symmetrical monounsaturated triacylglycerols. *Eur. J. Lipid Sci. Technol.*, *115*(8), 838–846.

Sonwai, S., Kaphueakngam, P., & Flood, A. (2014). Blending of mango kernel fat and palm oil mid-fraction to obtain cocoa butter equivalent. *J. Food Sci. Technol.*, *51*(10), 2357–2369.

Stewart, D. I., Chong, P. S., & Stapley, A. G. F. (2017). Investigation of the crystallization and melting of the tripalmitin/triolein system via hot stage microscopy, differential scanning calorimetry, and pulsed NMR. *Cryst. Growth Des.*, *17*(6), 3005–3016.

Suri, T., & Basu, S. (2021). Heat resistant chocolate development for subtropical and tropical climates: A review. *Crit. Rev. Food Sci. Nutr.*, 1–20.

Taguchi, K., Toda, A., Hondoh, H., Ueno, S., & Sato, K. (2021). Kinetic study on alpha-form crystallization of mixed-acid triacylglycerols POP, PPO, and their mixture. *Molecules*, *26*(1), 220.

Takagi, T., & Ando, Y. (1995). Stereospecific analysis of monounsaturated triacylglycerols in cocoa butter. *J. Am. Oil Chem. Soc.*, *72*(10), 1203–1206.

Takeguchi, S., Sato, A., Hondoh, H., Aoki, M., Uehara, H., & Ueno, S. (2020). Multiple β forms of saturated monoacid triacylglycerol crystals. *Molecules*, *25*(21), 5086.

Takeuchi, M., Ueno, S., Yano, J., Flöter, E., & Sato, K. (2000). Polymorphic transformation of 1,3-distearoyl-sn-2-linoleoyl-glycerol. *J. Am. Oil Chem. Soc.*, *77*(12), 1243–1250.

Takeuchi, M., Ueno, S., & Sato, K. (2002a). Crystallization kinetics of polymorphic forms of a molecular compound constructed by SOS (1,3-distearoyl-2-oleoyl-sn-glycerol) and SSO (1,2-distearoyl-3-oleoyl-rac-glycerol). *Food Res. Int.*, *35*(10), 919–926.

Takeuchi, M., Ueno, S., Flöter, E., & Sato, K. (2002b). Binary phase behavior of 1,3-distearoyl-2-oleoyl-sn-glycerol (SOS) and 1,3-distearoyl-2-linoleoyl-sn-glycerol (SLS). *J. Am. Oil Chem. Soc.*, *79*(7), 627–632.

Takeuchi, M., Ueno, S., & Sato, K. (2003). Synchrotron radiation SAXS/WAXS study of polymorph-dependent phase behavior of binary mixtures of saturated monoacid triacylglycerols. *Cryst. Growth Des.*, *3*(3), 369–374.

Talbot, G. (2009a). Compound coatings. In G. Talbot (Ed.), *Science and technology of enrobed and filled chocolate, confectionery and bakery products* (pp. 80–100). CRC Pres: Cambridge, UK.

Talbot, G. (2009b). Vegetable fats. In S. T. Beckett (Ed.), *Industrial chocolate manufacture and use*

(4th ed., pp. 415–433). Wiley-Blackwell: Oxford, UK.

Talbot, G. (2009c). Chocolate temper. In S. T. Beckett (Ed.), *Industrial chocolate manufacture and use* (4th ed., pp. 261–275). Wiley-Blackwel: Oxford, UKl.

Talbot, G. (2012). Chocolate and cocoa butter - Structure and composition. In N. Garti & N. R. Widlak (Eds.), *Cocoa butter and related compounds* (pp. 1–34). AOCS Press: Urbana, IL, USA: Urbana, IL, USA.

Talbot, G. (2014). Fats for chocolate and sugar confectionery. In K. K. Rajah (Ed.), *Fats in food technology* (2nd ed., pp. 169–206). Wiley-Blackwell: Oxford, UK.

Talbot, G., Smith, K. W., Bhaggan, K., Ray, J., Nagy, Z., & Stapley, A. (2014). Physical characterisation of silica-treated shea stearin. *Lipid Technol.*, *26*(4), 83–86.

Timms, R. E. (1979). Computer-program to construct isosolid diagrams for fat blends. *Chem. Ind.*, *7*, 257–258.

Timms, R. E. (1984). Phase behaviour of fats and their mixtures. *Prog. Lipid Res.*, *23*, 1–38.

Timms, R. E. (2003). *Confectionery fats handbook. Properties, production and application*. The Oily Press: Bridgewater, UK.

Tran, T., & Rousseau, D. (2016). Influence of shear on fat crystallization. *Food Res. Int.*, *81*, 157–162.

Ueno, S., Minato, A., Seto, H., Amemiya, Y., & Sato, K. (1997). Synchrotron radiation X-ray diffraction study of liquid crystal formation and polymorphic crystallization of SOS (sn-1,3-distearoyl-2-oleoyl glycerol). *J. Phys. Chem. B*, *101*(35), 6847–6854.

Ueno, S., Ristic, R. I., Higaki, K., & Sato, K. (2003). In situ studies of ultrasound-stimulated fat crystallization using synchrotron radiation. *J. Phys. Chem. B*, *107*(21), 4927–4935.

van de Streek, J., Verwer, P., de Gelder, R., & Hollander, F. (1999). Structural analogy between β' triacylglycerols and n-alkanes. Toward the crystal structure of β'-2 p.p+2.p triacylglycerols. *J. Am. Oil Chem. Soc.*, *76*(11), 1333–1341.

van Driessche, A. E. S., Benning, L. G., Rodriguez-Blanco, J. D., Ossorio, M., Bots, P., & García-Ruiz, J. M. (2012). The role and implications of bassanite as a stable precursor phase to gypsum precipitation. *Science*, *336*(6077), 69–72.

van Langevelde, A., van Malssen, K., Driessen, R., Goubitz, K., Hollander, F., Peschar, R., Zwart, P., & Schenk, H. (2000). Structure of CnCn+2Cn-type (n = even) β'-triacylglycerols. *Acta Crystallogr. Sect. B*, *B56*, 1103–1111.

van Malssen, K., Peschar, R., & Schenk, H. (1996a). Real-time X-ray powder diffraction investigations on cocoa butter. I. Temperature-dependent crystallization behavior. *J. Am. Oil Chem. Soc.*, *73*(10), 1209–12015.

van Malssen, K., Peschar, R., Brito, C., & Schenk, H. (1996b). Real-time X-ray powder diffraction investigations on cocoa butter. III. Direct β-crystallization of cocoa butter:

Occurrence of a memory effect. *J. Am. Oil Chem. Soc.*, *73*(10), 1225–1230.

van Malssen, K., van Langevelde, A., Peschar, R., & Schenk, H. (1999). Phase behavior and extended phase scheme of static cocoa butter investigated with real-time X-ray powder diffraction. *J. Am. Oil Chem. Soc.*, *76*(6), 669–676.

Vekilov, P. G. (2010). The two-step mechanism of nucleation of crystals in solution. *Nanoscale*, *2*(11), 2346–2357.

Vereecken, J., Foubert, I., Smith, K. W., & Dewettinck, K. (2009). Effect of SatSatSat and SatOSat on crystallization of model fat blends. *Eur. J. Lipid Sci. Technol.*, *111*(3), 243–258.

Vereecken, J., Foubert, I., Smith, K. W., Sassano, G. J., & Dewettinck, K. (2010a). Crystallization of model fat blends containing symmetric and asymmetric monounsaturated triacylglycerols. *Eur. J. Lipid Sci. Technol.*, *112*(2), 233–245.

Vereecken, J., de Graef, V., Smith, K. W., Wouters, J., & Dewettinck, K. (2010b). Effect of TAG composition on the crystallization behaviour of model fat blends with the same saturated fat content. *Food Res. Int.*, *43*(8), 2057–2067.

Wagh, A., & Martini, S. (2017). Crystallization behavior of fats. Effects of processing conditions. In C. C. Akoh (Ed.), *Food lipids. Chemistry, nutrition and biotechnology* (4th ed., pp. 327–348). CRC Press: Boca Raton, FL, USA.

Walstra, P. (2001). Fat crystal networks. In N. Garti & K. Sato (Eds.), *Crystallization processes in fats and lipid systems* (1st ed., pp. 289–328). Marcel Dekker: New York, NY, USA.

Wassell, P., & Young, N. W. G. (2007). Food applications of trans fatty acid substitutes. *Int. J. Food Sci. Technol.*, *42*(5), 503–517.

Wassell, P. (2014). Bakery fats. In K. K. Rajah (Ed.), *Fats in food technology* (2nd ed., pp. 39–82). Wiley-Blackwell: Oxford, UK.

Watanabe, S., Yoshikawa, S., Arishima, T., & Sato, K. (2018). Polymorphism and mixing phase behavior in ternary mixture systems of SOS-SSO-OSO: Formation of molecular compound crystals. *J. Am. Oil Chem. Soc.*, *95*(4), 447–460.

Watanabe, S., Yoshikawa, S., & Sato, K. (2021). Formation and properties of dark chocolate prepared using fat mixtures of cocoa butter and symmetric/asymmetric stearic-oleic mixed-acid triacylglycerols: Impact of molecular compound crystals. *Food Chem.*, *339*, 127808.

Wesdorp, L. H. (1990). Liquid-multiple solid phase equilibria: Theory and experiments. Doctoral thesis, Delft University of Technology: Delft, Netherlands. .

Wesdorp, L. H., Van Meeteren, J. A., de Jong, S., van der Giessen, R., Overbosch, P., Grootscholten, P. A. M., Struik, M., Royers, E., Don, A., de Loos, T., Peters, C., & Gandasasmita, I. (2013). Liquid–multiple solid phase equilibria in fats. Theory and experiments. In A. G. Marangoni & L. H. Wesdorp (Eds.), *Structure and properties of fat*

crystal networks (2nd ed., pp. 241–418). CRC Press: Boca Raton, FL, USA.

West, R., & Rousseau, D. (2020). Tripalmitin-driven crystallization of palm oil: The role of shear and dispersed particles. *J. Am. Oil Chem. Soc.*, *97*(9), 989–999.

Widlak, N. R., & Hartel, R. W. (2012). Causes and best manufacturing practices to minimize bloom in confections. In *Cocoa butter and related compounds* (pp. 173–194). AOCS Press: Urbana, IL, USA.

Wille, R. L., & Lutton, E. S. (1966). Polymorphism of cocoa butter. *J. Am. Oil Chem. Soc.*, *43*(8), 491–496.

Williams, S. D., Ransom-painter, K. L., & Hartel, R. W. (1997). Mixtures of palm kernel oil with cocoa butter. *J. Am. Oil Chem. Soc.*, *74*(4), 357–366.

Wohlmuth, E. G. (2009). Recipes. In S. T. Beckett (Ed.), *Industrial chocolate manufacture and use* (4th ed., pp. 434–450). Wiley-Blackwell: Oxford, UK.

Yang, D., & Hrymak, A. N. (2011). Crystal morphology of hydrogenated castor oil in the crystallization of oil-in-water emulsions: Part I. Effect of temperature. *Ind. Eng. Chem. Res.*, *50*(20), 11585–11593.

Yano, J., Ueno, S., Sato, K., Arishima, T., Sagi, N., Kaneko, F., & Kobayashi, M. (1993). FT-IR study of polymorphic transformations in SOS, POP and POS. *J. Phys. Chem.*, *97*, 12967–12973.

Yano, J., & Sato, K. (1999). FT-IR studies on polymorphism of fats: Molecular structures and interactions. *Food Res. Int.*, *32*(4), 249–259.

Yap, P. H., de Man, J. M., & de Man, L. (1989). Polymorphism of palm oil and palm oil products. *J. Am. Oil Chem. Soc.*, *66*(5), 693–697.

Yoshikawa, S., Watanabe, S., Yamamoto, Y., & Kaneko, F. (2020). Binary phase behavior of 1,3-distearoyl-2-oleoyl-sn-glycerol (SOS) and trilaurin (LLL). *Molecules*, *25*(22), 5313.

Yoshikawa, S., Watanabe, S., Yamamoto, Y., Kaneko, F., & Sato, K. (2022). Interactive polymorphic crystallization behavior in eutectic triacylglycerol mixtures containing molecular compound crystals. *Cryst. Growth Des.*, *22*(3), 1753–1763.

Zeng, J., Shen, J., Wu, Y., Liu, X., Deng, Z. Y., & Li, J. (2020). Effect of adding shea butter stearin and emulsifiers on the physical properties of cocoa butter. *J. Food Sci.*, *85*(4), 972–979.

Zhang, H., Zhang, L., Sun, X., & Xie, S. (2015). Applications of low-field pulsed nuclear magnetic resonance technique in lipid and food. In F. R. S. Atta-ur-Rahman & M. Iqbal Choudhary (Eds.), *Applications of NMR spectroscopy* (pp. 3–56). Elsevier: Oxford, UK.

Zhang, L., Ueno, S., Miura, S., & Sato, K. (2007). Binary phase behavior of 1,3-dipalmitoyl-2-oleoyl-sn-glycerol and 1,2-dioleoyl-3-palmitoyl-rac-glycerol. *J. Am. Oil Chem. Soc.*, *84*(3), 219–227.

Zhang, L., Ueno, S., Sato, K., Adlof, R. O., & List, G. R. (2009). Thermal and structural properties of binary mixtures of 1,3-distearoyl-2-oleoyl-glycerol (SOS) and 1,2-dioleoyl-3-stearoyl-sn-glycerol (sn-OOS). *J. Therm. Anal. Calorim.*, *98*(1), 105–111.

Zhang, L., Wei, K. J., Chen, J. chun, Xiong, M., Li, X., Hondoh, H., & Ueno, S. (2020). Effect of cis–trans isomerization on the crystallization behavior of triacylglycerols. *Cryst. Growth Des.*, *20*(3), 1655–1664.

Zhou, S. L., Zhang, F. Q., Jin, Q. Z., Liu, Y. F., Shan, L., Zhang, T., Zou, X. Q., & Wang, X. G. (2010). Characterization of palm kernel oil, palm stearin, and palm olein blends in isosolid diagrams. *Eur. J. Lipid Sci. Technol.*, *112*(9), 1041–1047.

Ziegler, G. (2009). Product design and shelf-life issues: Oil migration and fat bloom. In G. Talbot (Ed.), *Science and technology of enrobed and filled chocolate, confectionery and bakery products* (pp. 185–210). CRC Press: Cambridge, UK.

¡Somos los mejores!